

University of Strathclyde

Department of Pure and Applied Chemistry

Novel Semiconductor Photocatalysis – New Indicator Inks and
Standardisation Testing

Mark Alexander Steven M^cGrady MSci

A thesis presented in fulfilment of the requirements for the degree
of Doctor of Philosophy

2012

This thesis is the result of the author's original research. It has been composed by the author and has not been previously submitted for examination which has led to the award of a degree.

The copyright of this thesis belongs to the author under the terms of the United Kingdom Copyright Acts as qualified by University of Strathclyde Regulation 3.50. Due acknowledgement must always be made of the use of any material contained in, or derived from, this thesis.

Signed:

Date:

Acknowledgements

I would like to take this opportunity to firstly thank Professor Andrew Mills for his supervision throughout my PhD. His insight and guidance was always appreciated and his expertise in the field proved invaluable in the experimental work which constitutes this thesis. I would also like to thank the Carnegie Trust for the Universities of Scotland for providing the funding for the project.

Although a PhD is very much the work of an individual, it would be wrong not to take this opportunity to thank all those members of the lab, both past and present, who provided training and assistance during the project. Special thanks must go to Dr Laurence Tetley of the University of Glasgow, who assisted in the acquisition of the SEM images of the paste films described in chapter 5; Dr Pik Leung Tang of the University of Strathclyde, who assisted in the acquisition of the AFM and XRD images of the same films; Dr Jishun Wang, who provided extensive training in the preparation and analysis of the indicator inks; and Dr Matthew Crow, who provided training in the preparation of the paste films.

Finally a huge thank you to all those people who helped in other ways, whether it be moral support, repairing instruments or supplying chemicals, their help is very much appreciated.

Contents

Acknowledgements	ii
Contents.....	iii
Figures.....	vi
Abbreviations and Symbols	xiv
Abstract.....	xvi
1 Introduction.....	1
1.1. SPC – General Mechanism of Action ⁸	2
1.1.1. Semiconductors and Band Theory ⁹⁻¹⁰	2
1.1.2. Semiconductors and Light – SPC ⁸	4
1.2. Suitable Semiconductors – Titanium Dioxide (TiO ₂) ⁸	7
1.3. Titanium Dioxide in SPC: Mechanism for the Removal of Organic Pollutants ⁸	10
1.4. SPC in Environmental Remediation and Other Uses – Commercial Opportunities.....	12
1.5. TiO ₂ Powders and Films	15
1.5.1. Chemical Vapour Deposition (CVD) ^{8,53}	16
1.5.2. Sol-Gel Synthesis ^{8,57}	18
1.6. Assessment of Photocatalytic Activity – Standard Tests.....	20
1.6.1. The Stearic Acid (SA) Test.....	22
1.6.2. The Methylene Blue (MB) Test.....	23
1.6.3. Standard Tests in the Field.....	25
1.7. Indicator Inks	27
1.8. Project Aims.....	30
1.9. References.....	32
2 Experimental	38
2.1. Indicator Inks	38
2.1.1. Preparation of the Photocatalyst Indicator Inks.....	38
2.1.2. Pre-treatment of Activ TM Prior to Activity Measurements Using the Indicator Inks.....	41
2.1.3. Preparation of a Photocatalyst Indicator Ink Film	43
2.1.4. Assessment of the Photocatalytic Activity Using an Indicator Ink.....	44
2.2. The Production of Paste Films and the Measurement of Their Photocatalytic Activities	50
2.2.1. Synthesis of a TiO ₂ Paste for the Preparation of Photocatalyst Films of Varying Activity.....	50
2.2.2. Preparation of a TiO ₂ Paste Film	55
2.2.3. Characterisation of the Annealed Paste Films	58
2.2.3.1. Scanning Electron Microscopy (SEM) ¹⁵⁻¹⁶	58
2.2.3.2. Atomic Force Microscopy (AFM) ¹⁷⁻¹⁹	60
2.2.3.3. X-ray diffraction (XRD) ^{8,17,20-21}	62
2.2.4. The Stearic Acid Test.....	67
2.2.5. The Methylene Blue Test.....	69
2.3. References.....	74
3 Results and Discussion: Characterisation of a Photocatalyst Indicator Ink Based on the Redox Dye 2,6-dichloroindophenol.....	77

3.1. Spectral Properties of the Substrate	78
3.2. The Standard DCIP ink – Reduction and Recovery in Ambient Atmospheric Conditions	79
3.3. The Effect of the Polymer on the Performance of the DCIP Ink – Assessment of Polyvinyl Alcohol (PVA)	87
3.4. The Effect of the Glycerol Level and the use of Other Polyols	91
3.5. The Effect of Light Intensity on the Performance of the DCIP Ink	100
3.6. The Effect of Dye Loading Level on the Performance of the DCIP Ink	103
3.7. The Effect of Spin Speed on the Performance of the DCIP Indicator Ink	106
3.8. The Stability of the DCIP Indicator Ink	108
3.9. The DCIP Indicator Ink in a Felt-Tipped Pen – A Rapid Method for Assessing the Photocatalytic Activity in the Field	110
3.10. Conclusions	113
3.11. References	114
4 Evaluation of New Photocatalyst Indicator Inks	117
4.1. Properties of the Redox Dyes for Photocatalyst Inks Used to Assess the Photocatalytic Activity of Activ™ Self-Cleaning Glass	118
4.2. Indicator Inks Under Anaerobic Conditions – A Comparison of the Rate of Dye Photoreduction	122
4.2.1. Methylene Blue (MB)	122
4.2.2. Resorufin (Rf)	126
4.2.3. Resazurin (Rz)	130
4.2.4. 2,6-dichloroindophenol (DCIP)	135
4.2.5. Comparison of Initial Results Under Anaerobic Conditions – The Elimination of the Rf-based Indicator Ink	137
4.2.6. The Indicator Inks Under Ambient Atmospheric Conditions – The Elimination of the MB-based Indicator Ink	139
4.3. Photocatalyst Inks Under Aerobic Conditions – Rz and DCIP	145
4.4. Conclusions	152
4.5. References	153
5 Characterisation of Sol-Gel TiO ₂ Paste Films and the Measurement of Their Photocatalytic Activities Using Standard and Novel Methods	155
5.1. Characterisation of the Sol-Gel Paste Films	156
5.1.1. Absorbance Spectroscopy	156
5.1.2. Mechanical Stability of Annealed Paste Films	158
5.1.3. Scanning Electron Microscopy (SEM)	160
5.1.4. Atomic Force Microscopy (AFM)	161
5.1.5. X-Ray Diffraction (XRD)	164
5.2. Measurement of Photocatalytic Activity of the Paste Films – Correlation of Standard Tests	170
5.2.1. The Stearic Acid Test	170
5.2.2. The Methylene Blue Test	177
5.3. The Indicator Ink Test	180
5.3.1. The Patent Blue VF Indicator Ink	180
5.3.2. The DCIP Indicator Ink	185
5.4. Correlation of Standard Tests	190
5.4.1. Low Temperature, ‘High Activity’ Paste Films (450 – 850 °C)	190

5.4.2. High Temperature, ‘Low Activity’ Paste Films (800 – 1100 °C).....	192
5.5. Conclusions.....	196
5.6. References.....	198
6 Acidic Photocatalyst Indicator Inks and Reversible Redox Dyes.....	201
6.1. Dye Families and the Dyes Used.....	202
6.2. Thiazines.....	204
6.2.1. Methylene Blue Under Anaerobic Conditions.....	204
6.2.2. The Acidic Methylene Blue Ink Under Ambient Atmospheric Conditions	212
6.2.3. Thionine (Th) and Toluidine Blue (TB).....	216
6.3. Phenazines.....	222
6.4. Oxazines.....	225
6.5. Conclusions.....	228
6.6. References.....	229
Summary.....	231
Further Work.....	234

Figures

Figure 1.1.: A scheme showing the evolution of SPC (as reproduced from [6]).....	1
Figure 1.2.: The orbital arrangement as a molecule is built up from a single atom of an element through to a semiconductor (i.e. many-element molecule). The gap represented by ΔE is referred to as the bandgap of the material	3
Figure 1.3.: The activation of a semiconductor by ultra-bandgap light. The diagram in the top right shows the promotion of an electron (e^- , indicated by a ‘-’ sign) from the valence band into the conduction band through adsorption of a photon of ultra-bandgap light, leaving behind a hole (h^+ , indicated by a ‘+’ sign) in the valence band. The main diagram shows the processes that can then occur in the semiconductor particle following excitation. The h^+/e^- pair can recombine in the semiconductor bulk (process (1)) or migrate to the surface and recombine there (process (2)), both accompanied by the emission of a small amount of thermal energy. Alternatively, however, the h^+/e^- pair can migrate to the surface independently and undergo chemical reactions with adsorbed surface species (process (3)) via charge transfer.....	5
Figure 1.4.: The use of TiO_2 in SPC to destroy an organic pollutant. Note that the ‘+’ sign represents a photogenerated hole, whilst the ‘-’ sign symbolises a photogenerated electron.....	11
Figure 1.5.: The home of the future, as predicted and kindly reproduced from [34].....	15
Figure 1.6.: The basic CVD technique.....	17
Figure 1.7.: The mechanism used in the novel UV dosimeter developed by Mills et al, where D_{ox} and D_{red} represent the oxidised and reduced forms of the dye, respectively .	27
Figure 1.8.: The structures of resazurin (Rz) and its reduced product, resorufin (Rf)....	28
Figure 1.9.: The structures of; (a) 2,6-dichloroindophenol (DCIP), (b) resorufin (Rf) and, (c) methylene blue (MB), and their reduced products.....	30
Figure 2.1.: The arrangement used to ‘clean’ the samples of Activ™. An enclosed box is used into which a slit is cut allowing a hand-held UVC lamp to be held in place in order to irradiate the samples (figures (a) and (b)). Over a period of 50 minutes, a stream of wet air is flown into the sample chamber from an inlet port to the rear (figure (c)) which acts in tandem with the UVC to ‘scour’ the sample surface, thus ensuring reproducibility.....	42
Figure 2.2.: A typical sample of the standard DCIP ink and a Copic felt-tipped marker	44
Figure 2.3.: The sample cell holder used to irradiate indicator ink films on Activ™ self-cleaning glass under various atmospheric conditions	45
Figure 2.4.: The typical positioning of the Activ™ sample under the UVA source in the specially designed cell holder. By adjusting the distance between the sample under test and the lamp, the irradiance could be altered.....	46
Figure 2.5.: The typical change in the absorbance spectrum of the DCIP indicator ink with irradiation time, and (inset) the change in the absorbance at λ_{max} with time.....	48
Figure 2.6.: The diffuse reflectance accessory used in this work with the major components highlighted	50
Figure 2.7.: The major components of the acid digestion bomb.....	53
Figure 2.8.: The generation of a TiO_2 film from paste. Initially a quartz disc is taped down with a layer of Scotch Magic Tape™ (a) and a spatula-tip of paste is applied (b). The paste is then doctor-bladed across the sample surface using the edge of a Pasteur	

pipette (c)-(e), creating the paste film, the opacity of which decreases as it dries due to a reduction in the film thickness	56
Figure 2.9.: The high magnification SEM image of a paste film annealed at 1000 °C ..	60
Figure 2.10.: The AFM images obtained for a paste film annealed at 1100 °C at low magnification (left) and higher magnification (right)	62
Figure 2.11.: The path of two separate x-ray beams of incident angle θ reflected by alternate lattice planes within a crystal, the distance between which is given by the interplanar spacing d . Note the difference in the path length between the two reflected waves is defined by $AB + BC$	63
Figure 2.12.: The as-measured XRD spectra of pure anatase (top) and pure rutile, with the crystal plane reflections as indicated.....	65
Figure 2.13.: The XRD spectrum of an 825 °C paste film annealed on quartz, with the major peaks highlighted. Note that A denotes anatase, whilst R denotes a peak due to rutile	66
Figure 2.14.: The peaks observed due to stearic acid when the film is coated on to a 450 °C paste film, and the subsequent change in the peak shape with irradiation as the stearic acid is photooxidised	69
Figure 2.15.: The absorbance spectrum of a 1×10^{-5} M MB solution after being placed in contact with an 800 °C paste film for 15 minutes. Absorption of the dye by the underlying paste film has decreased the dye's peak absorbance by ca. 0.1 absorbance units.....	71
Figure 3.1.: The UV-Visible absorbance spectra of plain glass (blue trace), Activ™ (pink trace) and quartz (green trace) over the wavelength range 300 – 400 nm. The inset diagram shows the UV-Visible absorbance spectra of all three materials over the wavelength range 200 – 800 nm	79
Figure 3.2.: The structure of DCIP and its reduction mechanism in the indicator ink formulation.....	80
Figure 3.3.: The change in the UV-Visible absorbance spectrum of the standard DCIP ink on Activ™ with increasing UV irradiation time under ambient atmospheric conditions. The green trace shows the initial spectrum obtained for the ink film, whilst the red trace shows the spectrum obtained after 7.5 minutes of UVA irradiation. Spectra were recorded at 30 s intervals.....	81
Figure 3.4.: The variation in the absorbance at λ_{\max} for the DCIP ink with UV irradiation time, based on the data presented in figure 3.3.	82
Figure 3.5.: The variation in the absorbance at λ_{\max} with irradiation time for a DCIP ink cast on plain glass.....	84
Figure 3.6.: The reduction, and subsequent recovery, of a DCIP ink on Activ™ under ambient atmospheric conditions. The recovery was monitored over a period of ca. 40 hours in the dark with spectra being recorded at 1 hour intervals and the absorbance at 629 nm extracted from it.....	85
Figure 3.7.: The shorthand structures of both HEC (left) and PVA	87
Figure 3.8.: The change in spectral shape obtained as a DCIP indicator ink with PVA as the polymer is irradiated on the surface of Activ™. The green trace shows the initial ink spectrum, whilst the red trace shows that obtained after 9 minutes of UVA irradiation. Spectra were recorded at 20 s intervals for 2 minutes, then at 1 minute intervals up to 9 minutes	88

Figure 3.9.: The variation in the absorbance at λ_{\max} with irradiation time for the PVA-based, DCIP ink, extracted from figure 3.8.	89
Figure 3.10.: The variation in the absorbance at λ_{\max} for the PVA-based ink due to reduction and the subsequent recovery observed over 1 hour	90
Figure 3.11.: The variation in the spectral shape obtained for a DCIP ink with nil glycerol when irradiated on the surface of Activ TM . Spectra were recorded at 30 s intervals for 1 minute, at 1 minute intervals up to 5 minutes, then at 5 minute intervals up to 1 hour	92
Figure 3.12.: The variation in the absorbance at λ_{\max} (638 nm) with time for a DCIP ink with no SED present.....	93
Figure 3.13.: The variation in the initial rate of reduction, r_i , with glycerol loading.....	94
Figure 3.14.: The variation in the initial rate of reduction of the DCIP indicator ink with glycerol content over the glycerol loading range of 0 to ca. 0.1 g.....	96
Figure 3.15.: The variation of λ_{\max} with glycerol level.....	98
Figure 3.16.: The variation of the initial rate of reduction, r_i , of the DCIP ink on Activ TM with increasing UV irradiance	101
Figure 3.17.: The variation in the initial rate of DCIP reduction on Activ TM with increasing dye level.....	103
Figure 3.18.: A comparison between the initial ink film traces obtained at 2 mg (blue trace) and 10 mg (pink trace) dye loading levels	105
Figure 3.19.: The variation in zero order t_{50} % for DCIP reduction on Activ TM with increasing dye level.....	106
Figure 3.20.: The variation in r_i with spin speed for the DCIP indicator ink.....	107
Figure 3.21.: The variation in the zero order t_{50} % with increasing spin speed for the DCIP indicator ink	108
Figure 3.22.: The DCIP indicator ink (left) and a similar ink after 1 month at room temperature (right)	109
Figure 3.23.: The type of felt-tipped pen commonly used with a sample of the DCIP ink	111
Figure 3.24.: The photoreduction of the DCIP ink when applied to Activ TM self-cleaning glass and Hydrotec tile using an indicator pen. At 0 minutes (a), the ink is observed to produce a striking blue colour on both the tile and glass surface. After 5 minutes irradiation (b) at a UVI of ca. 7 mW cm ⁻² , the ink is observed to have changed colour on the surface of Activ TM , though is still visible on Hydrotec. Further irradiation up to 1 hour eventually leads to dye photoreduction on the tile surface (c)	112
Figure 4.1.: A plot showing the variation in the dye redox potential for the dyes studied here (a) and the Pourbaix diagram for titanium (b, kindly reproduced from [6]). On the titanium Pourbaix diagram, dashed line 1 corresponds to the variation in the redox potential for the reduction of O ₂ to water, whilst dashed line 2 corresponds to the variation in the redox potential for the reduction of protons to give H ₂	121
Figure 4.2.: The structure of MB and its subsequent reduction reaction	123
Figure 4.3.: The UV-Visible absorbance spectra of MB (1 x 10 ⁻⁵ M) in aqueous solution (pink trace) and when placed in the indicator ink formulation and cast as a film on the surface of Activ TM (blue trace).....	124
Figure 4.4.: The change in the UV-Visible absorbance spectrum of a MB ink with irradiation under N ₂ . The green trace indicates the initial ink spectra, whereas the red trace shows the ink spectra after 1 hour of UVA irradiation. Spectra were recorded at	

30 s intervals for 5 minutes and then at 10 minute intervals from 10 minutes up to 70 minutes.....	125
Figure 4.5.: The change in absorbance at λ_{\max} (608 nm) with irradiation time for a MB ink on Activ™.....	126
Figure 4.6.: The structure of resorufin and its subsequent reduction reaction.....	127
Figure 4.7.: A comparison of the UV-Visible absorption spectra for Rf as a 10^{-5} M aqueous solution (pink trace) and when cast as an ink film on the surface of Activ™.....	128
Figure 4.8.: The change in the UV-Visible absorbance spectrum of an Rf ink with irradiation under N ₂ . The green trace indicates the initial ink spectra, whereas the red trace shows the ink spectra after 2 hours of UVA irradiation. Spectra were recorded at 30 s intervals for 2 minutes, at 1 minute intervals up to 7 minutes, at 10 minutes, and then every 10 minutes up to 2 hours	129
Figure 4.9.: The change in the absorbance at 580 nm due to Rf with UVA irradiation time.....	130
Figure 4.10.: The UV-Visible absorbance spectra of Rz in solution (blue trace) and when cast as an ink film on the surface of Activ™	131
Figure 4.11.: The spectral changes which occur as an Rz ink is irradiated on the surface of Activ™. The green trace shows the initial spectrum of the ink, whereas the red trace shows the spectrum obtained after 50 minutes of UV irradiation. Spectra were recorded at 60 s intervals for 5 minutes, at 10 minutes, and at 10 minute intervals up to 50 minutes	133
Figure 4.12.: The variation in the peak absorbance due to both Rz and Rf with UV irradiation time. The blue trace shows how the Rz peak at 610 nm varies with irradiation time, whereas the pink trace shows that for Rf at 580 nm	134
Figure 4.13.: A comparison between the solution (10^{-5} M, pink trace) and cast ink spectra on Activ™ of DCIP	135
Figure 4.14.: The change in spectral shape for a DCIP ink cast on Activ™ with increasing irradiation time. The green trace shows the initial ink spectrum, whilst the red trace shows that obtained after 80 minutes of UVA irradiation. Spectra were recorded at 1 minute intervals for 7 minutes, at 2 minute intervals up to 15 minutes, at 20 minutes and finally at 10 minute intervals up to 80 minutes	136
Figure 4.15.: The variation in the absorbance at 629 nm with UVA irradiation time for the DCIP ink when irradiated on Activ™.....	137
Figure 4.16.: The variation in the absorbance at 580 nm with UV irradiation time as an Rf-based ink is reduced on the surface of Activ™ under ambient atmospheric conditions	139
Figure 4.17.: The change in the peak absorbance due to Rz (blue trace, 610 nm) and Rf (pink trace, 580 nm) as an Rz ink is irradiated on the surface of Activ™ under anaerobic conditions before being subjected to ambient atmospheric conditions (nil UVA) once the reduction reaction is complete. When monitoring the performance of the ink post-reduction, spectra were recorded every 2 minutes for 1 hour, from which the peak absorbance is extracted	141
Figure 4.18.: The reduction, and subsequent recovery, of a DCIP ink on Activ™. As for Rz above, recovery spectra were recorded at 2 minute intervals for 1 hour.....	142
Figure 4.19.: The reduction, and subsequent recovery, of a MB ink on Activ™. As previously, recovery spectra were recorded at 2 minute intervals for 1 hour	143

Figure 4.20.: The change in spectral shape for a MB ink as it is irradiated under ambient atmospheric conditions. The green trace shows the initial spectrum of the ink, whilst the red trace shows the ink spectrum 1 hour later. Spectra were recorded at 1 minute intervals for 4 minutes, at 2 minute intervals up to 10 minutes, and finally at 10 minute intervals up to 1 hour. The inset diagram shows the change in the peak absorbance due to MB over this 1 hour irradiation period	145
Figure 4.21.: The change in the relative Δ Absorbance (Δ Abs _{rel}) at λ_{\max} with UV irradiation time for the DCIP (blue trace) and Rz (pink trace) inks under ambient atmospheric conditions.....	147
Figure 4.22.: The variation in the reduction profiles for DCIP under various atmospheres.....	148
Figure 4.23.: The variation in the reduction profiles for Rz under various atmospheres	149
Figure 4.24.: A plot of the variation in the t_{50} % for DCIP (blue trace) and Rz (pink trace) inks with varying %O ₂	150
Figure 5.1.: The variation in the UV-Visible absorbance spectra of the paste films with increasing annealing temperature.....	157
Figure 5.2.: The observed opacity of the paste films annealed on quartz at the following temperatures (clockwise from top left); 450, 760, 900 and 1100 °C.....	158
Figure 5.3.: SEM images recorded at higher magnification of paste films annealed at the following temperatures (from left to right); top - 450 °C, 800 °C, 900 °C and bottom – 1000 °C and 1100 °C	161
Figure 5.4.: AFM images recorded at low magnification (sample area 25 μm^2) of the paste films annealed at the following temperatures (from left to right): 450, 825, 900 and 1100 °C.....	162
Figure 5.5.: AFM images recorded at higher magnification (sample area 1 μm^2) of the paste films annealed at the following temperatures (from left to right): 450, 760, 900 and 1100 °C.....	162
Figure 5.6.: The variation in the average particle size, as calculated from the AFM images, with annealing temperature (30 minutes annealing time) for the paste films. The error bars represent the error in the mean particle size at each temperature.....	163
Figure 5.7.: The variation in the XRD pattern obtained for the paste films as the annealing temperature is increased from 450 °C (front, black trace) through to 1100 °C	164
Figure 5.8.: The variation in the amount of anatase TiO ₂ present in the paste film with increasing annealing temperature.....	167
Figure 5.9.: The variation in both the SSA (blue trace) and the average particle size (pink trace) with annealing temperature	168
Figure 5.10.: The variation in the SSA with the % anatase present for the paste films	169
Figure 5.11.: The variation in the infra red absorbance spectrum due to stearic acid with increasing UVA irradiation time on a TiO ₂ paste film annealed at 450 °C.....	171
Figure 5.12.: The variation in the integrated peak area due to stearic acid with UVA irradiation on a paste film annealed at 450 °C	172
Figure 5.13.: The photooxidation of stearic acid on a paste film annealed at 450 °C over 5 runs.....	173
Figure 5.14.: The variation in the zero order rate constant, k_0 , for stearic acid photooxidation with annealing temperature over the range 450-850 °C	174

Figure 5.15.: The variation in the rate of stearic acid photooxidation as a function of the anatase level present in the paste films annealed over the temperature range 450-850 °C	175
Figure 5.16.: The variation in the initial rate of stearic acid removal with annealing temperature over the range 850-1100 °C	176
Figure 5.17.: The change in the spectral shape due to MB as the dye is photomineralised when placed in contact with a 450 °C paste film. The green trace shows the initial MB solution spectrum obtained after being placed in contact with the paste film for 15 minutes, whilst the red trace shows the spectrum due to the dye after 270 minutes of UVA irradiation. Spectra were recorded every 5 minutes for 15 minutes, every 15 minutes up to an hour, at 95 and 105 minutes, and then every 15 minutes until completion.....	178
Figure 5.18.: The variation in the initial rate of photomineralisation of MB with increasing film annealing temperature	179
Figure 5.19.: The structure of patent blue VF and its reduction mechanism	181
Figure 5.20.: The absorbance spectrum of the PB ink cast on a 450 °C paste film, and the change in spectral shape due to irradiation with UVA light. The green trace indicates the initial ink spectrum whilst the red trace shows the ink spectrum following irradiation. Spectra were recorded every 30 s for 5 minutes, and then every 1 minute up to 18 minutes	182
Figure 5.21.: The variation in the absorbance at λ_{\max} for the PB ink with irradiation time on a 450 °C paste film.....	183
Figure 5.22.: The variation in the average zero order rate constant, k_0 , with annealing temperature for PB reduction	184
Figure 5.23.: The diffuse reflectance spectrum of a DCIP ink cast on a 1000 °C paste film, and the subsequent spectral changes which occur upon UVA irradiation. The green trace indicates the initial spectrum of the ink whilst the red trace shows that obtained after reduction has ceased. Spectra were recorded at 1 minute intervals for 5 minutes, at 10 minutes, and finally at 10 minute intervals up to 2 hours.....	186
Figure 5.24.: The variation in the average k_0 for DCIP reduction on paste films over the temperature range 800-900 °C	187
Figure 5.25.: The variation in the average k_0 for DCIP reduction on paste films over the temperature range 1000-1100 °C	187
Figure 5.26.: The variation in both the zero order rate constant, k_0 , for DCIP reduction and the SSA with increasing annealing temperature over the range 800-1100 °C	188
Figure 5.27.: The correlation in the rate of photomineralisation of stearic acid and MB over the temperature range 450-850 °C	191
Figure 5.28.: The correlation between the rate of photomineralisation of stearic acid and photoreduction of PB on paste films annealed over the range 450-800 °C	192
Figure 5.29.: The correlation in the rate of photomineralisation of stearic acid and MB over the temperature range 800-1100 °C	193
Figure 5.30.: The correlation between the rate of photomineralisation of stearic acid and photoreduction of PB on paste films annealed over the range 800-1100 °C	194
Figure 5.31.: The correlation between the rate of photomineralisation of MB and photoreduction of PB on paste films annealed over the range 800-1100 °C	195
Figure 6.1.: The change in spectral shape for a MB ink as it is irradiated under ambient atmospheric conditions. The green trace shows the initial spectrum of the ink, whilst	

the red trace shows the ink spectrum 1 hour later. Spectra were recorded at 1 minute intervals for 4 minutes, at 2 minute intervals up to 10 minutes, and finally at 10 minute intervals up to 1 hour.....	205
Figure 6.2.: The variation in the spectral shape due to MB as it is reduced on the surface of ‘new’ Activ™ under anaerobic conditions. The green trace shows the initial ink spectrum whilst the red trace shows that obtained upon complete reduction. Spectra were recorded every 10 s for 1 minute, then at 30 s intervals up to 5 minutes, and finally after 10 minutes UVA irradiation	206
Figure 6.3.: The variation in the absorbance at λ_{\max} due to MB with irradiation time as the dye is reduced in the indicator ink formulation on ‘new’ Activ™ under anaerobic conditions	207
Figure 6.4.: The variation in the spectral shape of the acidified MB ink with increasing irradiation time under anaerobic conditions. The green trace shows the initial ink spectrum obtained on Activ™ whilst the red trace shows that obtained after complete reduction. Spectra were recorded at 10 s intervals for 1 minute, then at 30 s intervals up to 5 minutes, and finally at 5 minute intervals up to 50 minutes	208
Figure 6.5.: The variation in the absorbance at λ_{\max} due to MB with increasing irradiation time as the acidified ink is reduced on Activ™.....	209
Figure 6.6.: The variation in the absorbance at λ_{\max} for MB with time in the acidified ink formulation as it is initially reduced under anaerobic conditions on Activ™ before being allowed to recover, initially using air from a bench tap, and then when subjected to ambient atmospheric conditions.....	210
Figure 6.7.: The variation in spectral shape of the acidic MB indicator ink as it is reduced on the surface of Activ™ under ambient atmospheric conditions. The green trace shows the initial ink spectrum whilst the red trace shows that after 5 minutes UVA irradiation. Spectra were recorded at 10 s intervals for 1 minute, then at 30 s intervals up to 5 minutes	212
Figure 6.8.: The variation in the absorbance at λ_{\max} of the acidic MB ink with irradiation time under ambient atmospheric conditions	213
Figure 6.9.: The variation in the peak absorbance due to MB as the acidic indicator ink is reduced and then allowed to recover under ambient atmospheric conditions (blue trace). The pink trace shows the variation in the peak absorbance for a ‘neutral’ MB film irradiated under N ₂ and allowed to recover under ambient atmospheric conditions on the old batch of Activ™	215
Figure 6.10.: The structure of Th and its reduction mechanism	216
Figure 6.11.: The structure of, and the reduction mechanism for TB	217
Figure 6.12.: The change in spectral shape which occurs as the acidic Th ink is reduced on Activ™. The green trace shows the initial ink spectrum prior to reduction, whilst the red trace shows that obtained after 25 minutes of UVA irradiation. Spectra were recorded every 10 s for 1 minute, then every 30 s up to 5 minutes, and finally every 5 minutes up to 25 minutes	218
Figure 6.13.: The change in spectral shape which occurs as the acidic TB ink is reduced on Activ™. The green trace shows the initial ink spectrum prior to reduction, whilst the red trace shows that obtained after 2.5 minutes of UVA irradiation. Spectra were recorded at 5 s, 10 s, then every 10 s up to 1 minute, and finally every 30 s up to 2.5 minutes	219

Figure 6.14.: Diagrams showing how potential energy, P(E) varies with redox potential. The diagram on the left, (a), shows what might be anticipated, whilst (b) shows the overlap in parabolas which occurs. The degree of overlap of these parabolas is indicated by x	220
Figure 6.15.: The structure of NR and its subsequent reduction mechanism	222
Figure 6.16.: The structure of SO and its subsequent reduction mechanism.....	223
Figure 6.17.: The variation in the spectra of the acidic SO ink as it is reduced under anaerobic conditions on Activ™. The green trace indicates the initial ink spectrum obtained whilst the red trace shows that observed after 35 minutes. Spectra were recorded at 10 s, 1 minute, then at 1 minute intervals up to 10 minutes, and finally at 5 minute intervals up to 35 minutes	224
Figure 6.18.: The structure of NB and its subsequent reduction mechanism	225
Figure 6.19.: The structure of BCB and its subsequent reduction mechanism.....	226
Figure 6.20.: The variation in the spectral shape of the acidic BCB ink as it is reduced under ambient atmospheric conditions on Activ™. The green trace indicates the initial ink spectrum whilst the red trace shows that following 3 minutes UVA irradiation. Spectra were recorded every 10 s for 1 minute, and then at 30 s intervals up to 3 minutes	227

Abbreviations and Symbols

BCB: Brilliant cresyl blue

DCIP: 2,6-dichloroindophenol

HEC: Hydroxyethyl cellulose

LMB: Leuco-methylene blue

MB: Methylene blue

NB: Nile blue

NR: Neutral red

PB: Patent blue VF

PVA: Polyvinyl alcohol

Rf: Resorufin

Rz: Resazurin

SA: Stearic acid

SO: Safranin O

TB: Toluidine blue

Th: Thionine

%RH: The percentage relative humidity

Abs: The absorbance, derived from a UV-Visible absorbance spectrum or an infrared spectrum

AbsU: Absorbance units, a theoretical unit of absorbance measurement in both UV-Visible and infrared spectroscopy

Δ Abs: The change in absorbance at the peak wavelength over the course of the reaction, calculated from $Abs_t - Abs_{\infty}$, where Abs_t is the peak absorbance at a specific time during the reaction, and Abs_{∞} is the initial peak absorbance

AFM: Atomic force microscopy, a surface analysis technique

$[D]_t$: The concentration of a certain species D at time t. D is chosen here simply since, in most instances, the species concerned is a dye

D_{ox} : The oxidised form of a species D, where again D is chosen since in most instances the species is a dye

D_{red} : The reduced form of a species D, where again D is chosen since in most instances the species is a dye

E_0 : The redox potential for a denoted redox couple, quoted at a certain pH and compared, typically, to the standard hydrogen electrode (SHE)

e^- : An electron

h^+ : A hole, produced in conjunction with an electron when TiO_2 is illuminated with ultra-bandgap light

k: The reaction rate constant

λ_{max} : The wavelength of maximum absorption

pphr: parts per hundred resin

PSH: Photoinduced superhydrophilicity, a process whereby a water droplet, when irradiated on the surface of TiO_2 , diminishes in contact angle due to changes in the degree of hydrophilicity of the surface

r_i : The initial rate of a reaction, typically calculated over the first 20 % of the reaction

SEM: Scanning electron microscopy, a surface analysis technique

SPC: Semiconductor photocatalysis, the process whereby a pollutant is oxidised to mineral acids, CO_2 and H_2O when placed in contact with a suitable semiconductor and irradiated with ultra-bandgap light

SSA: The specific surface area

$t_{50\%}$: The time taken for half the reaction to have occurred

TiO_2 : Titanium dioxide, the photocatalyst of choice in this work

UVA: The region of the electromagnetic spectrum from 320-400 nm

UVI: The UV irradiance, measured in mW cm^{-2}

XRD: X-ray diffraction, a technique used to provide information on a substrate's phase and morphology

Abstract

Since its emergence in the literature nearly 40 years ago, the field of semiconductor photocatalysis, in particular using titanium dioxide, has grown rapidly. Indeed, owing to its self-cleaning and anti-microbial action, to name but two, the technology has now started to find its way into commercial products, including self-cleaning tiles and glasses. In order to test the efficiency of such products, many potential pollutants have been assessed in the research laboratories, ranging from organic to inorganic, solid to gaseous, and even microorganisms. However, such tests are usually highly scientific and very slow, and thus not suitable for use in the field for demonstrations to potential customers. What is needed is a simple, rapid method of assessing the photocatalytic activity which can be accessed by the greater, non-scientific community. This thesis details the development of photocatalyst indicator inks, which work via a novel photoreduction mechanism, and attempts to correlate their performance with other 'standard' tests. In chapter 3, an indicator ink based on the dye 2,6-dichloroindophenol (DCIP) is introduced, and its kinetic performance is examined as a function of the ink components and reaction conditions. The ink's performance is then compared to that of other indicator inks in chapter 4, including that with resazurin as its dye, which is the pioneering technology in this field. In chapter 5, the indicator ink is then assessed alongside the stearic acid and methylene blue tests using films of varying activity produced in-house. The existence of any correlation between them could theoretically allow them to be marketed as a set of standard tests. Finally, in chapter 6, a new series of indicator inks utilising an acidic formulation are introduced. Such formulations allow dyes such as methylene blue, an O₂-sensitive material, to be used, opening the door to a new generation of acidic indicator inks.

1 Introduction

Since the pioneering work of Fujishima and Honda in the early 1970's¹⁻², the field of semiconductor photocatalysis (SPC) has grown rapidly in stature. Typing the words 'semiconductor photocatalysis' into the Google search engine yields 80,000 hits³, whilst the same search string inserted into both the Science Direct and the American Chemical Society publications websites registers 5,427 and 1,739 hits respectively⁴⁻⁵. Indeed, over the 16 year period from 1981-1997 alone, over 2000 papers were published on the topic⁶, a production rate which appears to have been more than sustained, if not improved, since, with one researcher claiming in 2002 that it was of the rate of 'one paper per day'⁷. The reason for such an intense publication record appears to be that, as it has evolved, the term 'semiconductor photocatalysis' has come to cover a wide range of possible reactions, the chief ones suggested by Mills and Le Hunte⁶ and demonstrated in the evolutionary scheme taken from their work in figure 1.1. below.

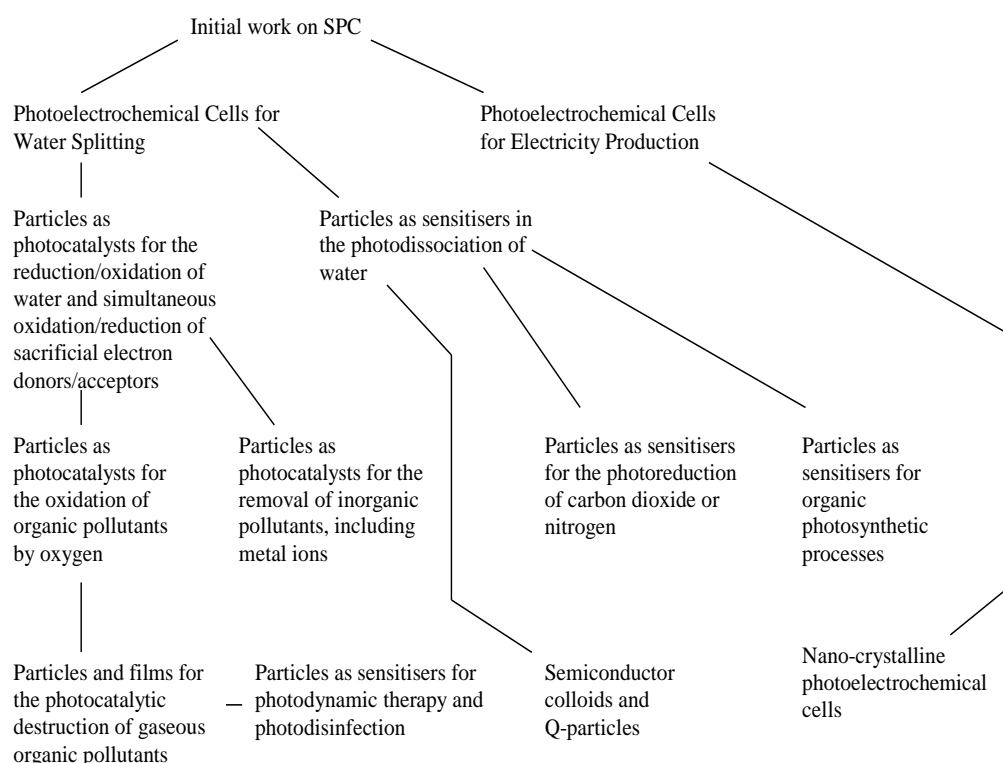


Figure 1.1.: A scheme showing the evolution of SPC (as reproduced from [6])

Whilst all of the research areas listed in figure 1.1. still appear to be filling publication inches, it could be argued that those which are of the greatest interest, particularly in the current eco- and environmentally-friendly world we inhabit, are the use of SPC in water splitting (as a source of alternative energy, particularly hydrogen), the destruction of organic pollutants (gaseous, liquid and solid) and the removal of inorganic pollutants (including metal ions, again solid, liquid and gaseous). With concerns growing in society about the fate of the ozone layer and the legacy which we will leave behind for future generations, there is a high demand for technologies which will help improve the standard of living, aid the environment and reduce waste output: SPC appears to deliver this, be it the removal of toxic pollutants from the air, the cleaning of wastewater streams prior to discharge into our waterways or the removal of debilitating organisms/bacteria from drinking water, to name but 3 applications.

1.1. SPC – General Mechanism of Action⁸

All photosensitised, semiconductor reactions, as indicated in figure 1.1., fall under the general equation⁶ given in equation 1.1.;



where A is an electron acceptor and D an electron donor. In order to fully appreciate how this occurs, it is necessary to take a brief step back into some basic molecular bonding theory.

1.1.1. Semiconductors and Band Theory⁹⁻¹⁰

Since electrons exist within discrete atomic orbitals (i.e. energy levels) in an atom, when these orbitals overlap, as is the case initially in the formation of a diatomic molecule, their overlap creates two new molecular orbitals. One of these generated molecular orbitals is higher in energy than the parent atomic orbitals (referred to as an antibonding orbital) whilst the other is lower in energy (referred to as a bonding orbital).

According to the Aufbau principle, the electrons from the atomic orbitals will move to occupy the molecular orbitals formed in order of increasing energy; hence the bonding orbital will be occupied preferentially.

If the theory is extended to the formation of a molecule with many atoms, as is the case when a molecular solid of an element is formed, so it is that the generated molecular orbitals, despite having their own discrete energies, will come to be so tightly packed together in the energy diagram that they will appear diffuse, with no individual molecular orbitals apparent. Instead, the bonding and antibonding molecular orbitals will resemble two separate bands, as is shown in figure 1.2. The band of bonding molecular orbitals is referred to as the valence band, whilst the band of antibonding molecular orbitals is referred to as the conduction band.

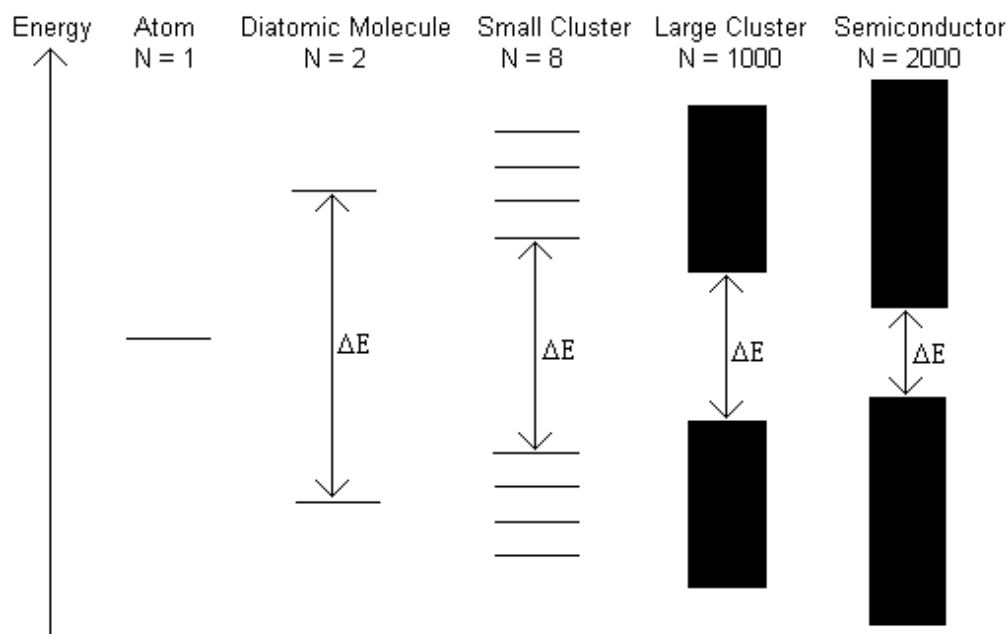


Figure 1.2.: The orbital arrangement as a molecule is built up from a single atom of an element through to a semiconductor (i.e. many-element molecule). The gap represented by ΔE is referred to as the bandgap of the material

The energy difference between the valence and conduction bands is referred to as the bandgap of the material, and represents the minimum energy required to excite an electron from the highest occupied molecular orbital (HOMO) of the valence band to the lowest unoccupied molecular orbital (LUMO) of the conduction band. If the bandgap is too large, no electron promotion can occur, as is the case for insulator materials. Conversely, some materials possess no real bandgap, i.e. the valence and conduction bands are observed to overlap slightly, as is the case in metals. In between these scenarios lie semiconductors, whereby the bandgap lies between those of a conductor and insulator and can be traversed by an electron.

1.1.2. Semiconductors and Light – SPC⁸

Upon irradiation of a semiconductor with ultra-bandgap light, and since wavelength is inversely proportional to energy ($E = h\nu/\lambda$), an electron (e^-) can be excited from the valence band into the conduction band. As a consequence, a positive vacancy is left behind in the valence band, referred to as a ‘hole’ (h^+). This e^-/h^+ pair have several options upon their generation, namely;

1. The e^-/h^+ pair can recombine within the bulk volume of the semiconductor, with the emission of a small amount of thermal energy;
2. The e^-/h^+ pair can migrate to the semiconductor surface and recombine there, again accompanied by the emission of a small amount of thermal energy, or;
3. The e^-/h^+ pair can migrate to the semiconductor surface and be trapped by adsorbed surface species, making them available for chemical reactions (i.e. charge transfer reactions) with said surface species

Such processes are described visually in figure 1.3. The likelihood of such processes occurring depends upon a number of factors, such as; the lifetime of the photogenerated h^+/e^- pair, the energy imparted to them upon excitation, and the apparent rate constant, and hence the likelihood of recombination, compared to that of charge transfer to adsorbed surface species. However, should migration towards the surface occur, it is apparent that the photogenerated species are available to facilitate chemical reactions

using molecules adsorbed on to the semiconductor. Using the general reaction described previously (equation 1.1.), it is apparent that a range of reactions, encompassed by the scheme shown in figure 1.1., can thus be facilitated.

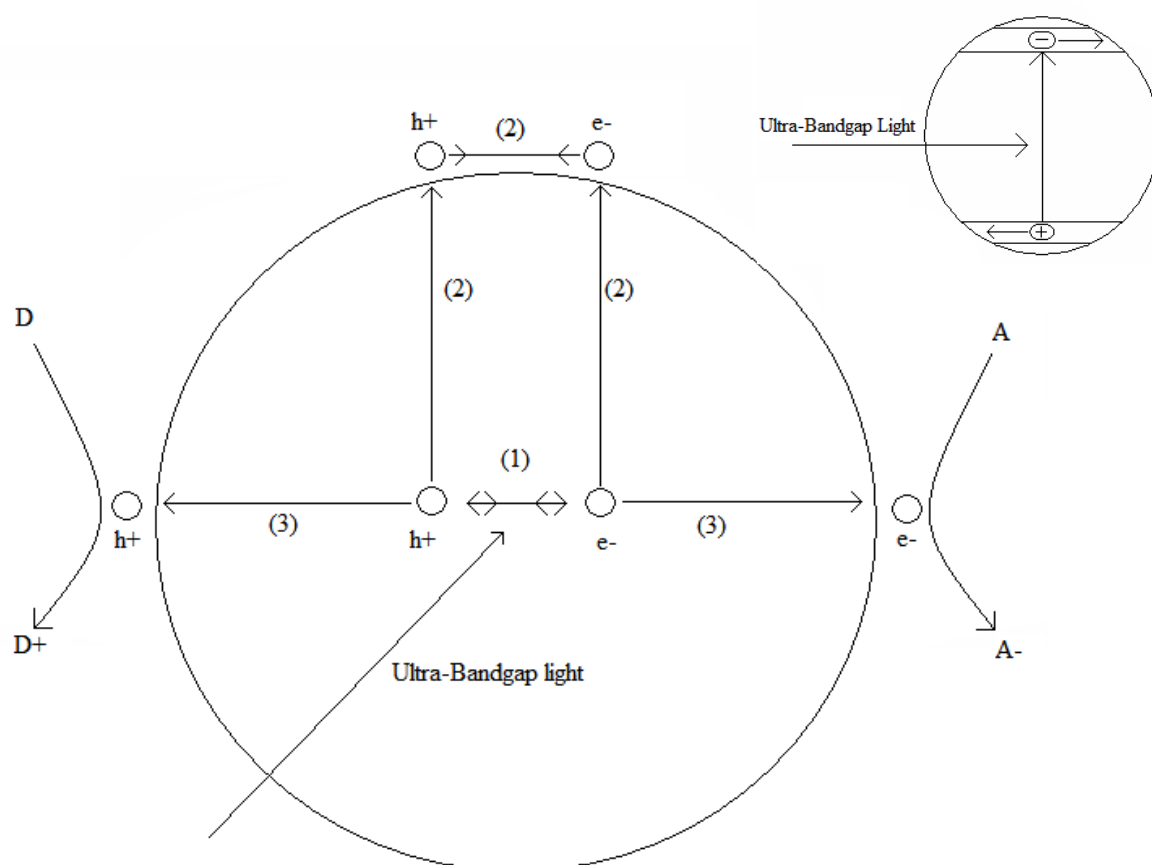


Figure 1.3.: The activation of a semiconductor by ultra-bandgap light. The diagram in the top right shows the promotion of an electron (e^- , indicated by a '-' sign) from the valence band into the conduction band through adsorption of a photon of ultra-bandgap light, leaving behind a hole (h^+ , indicated by a '+' sign) in the valence band. The main diagram shows the processes that can then occur in the semiconductor particle following excitation. The h^+/e^- pair can recombine in the semiconductor bulk (process (1)) or migrate to the surface and recombine there (process (2)), both accompanied by the emission of a small amount of thermal energy. Alternatively, however, the h^+/e^- pair can migrate to the surface independently and undergo chemical reactions with adsorbed surface species (process (3)) via charge transfer

The work of Fujishima and Honda² demonstrated that by connecting a TiO₂ electrode to a Pt electrode and irradiating the system with ultra-bandgap irradiation in the presence of H₂O, it is possible to facilitate the photodissociation of water, i.e. water acts as the electron donor, D, and the evolved H⁺ ions from this reaction act as the electron acceptors, A. Prior to their work on water splitting, however, Fujishima and Honda¹¹ had also investigated the use of SPC in the oxidation of other species. A few years later, the work of Frank and Bard¹²⁻¹³ then demonstrated the use of SPC in the oxidation of both the cyanide anion, CN⁻, and the sulfite ion, SO₃²⁻, two inorganic species which can be found in wastewater discharge. It would appear that these three key papers represent the beginning of the evolution of SPC for use in environmental remediation. In 1983, the work of Pruden and Ollis¹⁴ and Hsiao et al¹⁵ extended the theory further, demonstrating that SPC could be used in the degradation of organic compounds, namely chlorinated hydrocarbons and carbon tetrachloride. Since then, researchers have continued to investigate a range of other organic materials which can be subjected to SPC, including, but not exclusively;

- Hydrocarbons (e.g. hexane¹⁶, ethylene¹⁷ and toluene¹⁸);
- Alcohols (e.g. ethanol¹⁹⁻²⁰ and methanol²⁰);
- Esters (e.g. diethyl phthalate²¹);
- Pesticides and herbicides (e.g. atrazine²² and metolachlor²³), and;
- Acids (e.g. stearic acid²⁴, acetic acid and propionic acid²⁵)

Such a list, however, is nowhere near exhaustive, and is limited to SPC using titanium dioxide (TiO₂) as the photocatalyst. Hoffmann et al list over 130 organic compounds in their review article²⁶ (1995) which they observed as test substrates in the literature, whilst Mills and Le Hunte quoted a figure of over 200 organic substrates in their review article published only 2 years later⁶. It is anticipated that such a list will have grown in the intervening years between these publications and this thesis as more and more researchers come to appreciate the benefits of SPC.

Other methods of environmental remediation currently deployed include incineration, adsorption, absorption and condensation²⁷. However, both adsorption and absorption can generate potentially harmful waste, thus negating any benefits, whilst condensation is relatively inefficient. Incineration is also unfavourable owing to the cost of both the construction and operation of such a system; hence there is certainly a market to develop new, cost-effective techniques to aid in pollutant destruction.

1.2. Suitable Semiconductors – Titanium Dioxide (TiO₂)⁸

Based on the theory presented in figure 1.3., it would be assumed that all semiconductors should be suitable for use in SPC. However, the use of a semiconductor in such a process is dependent upon many factors. Many semiconductors are found to be photocatalytically inactive simply because the likelihood of recombination of the photogenerated h⁺/e⁻ pair is so great; there is no significant proportion of the species which make it to the particle surface to undergo reaction with any surface adsorbed species. In addition, even for those materials where the recombination of the photogenerated species is sufficiently slow, the bandgap of the semiconductor becomes important, since there is a desire to stay away from harmful irradiation sources. Semiconductors whose bandgap energy corresponds to both UVC and, to a lesser extent, UVB wavelengths, are undesirable due to the health issues associated with such light sources. Avoiding such sources would enhance the likelihood of such a technology realising a commercial product. As a result, both the publication record and, subsequently, the emerging industry centred on SPC have focussed on the use of semiconductors with bandgap energies corresponding to visible and UVA-light wavelengths (since, as stated previously, energy is inversely proportional to wavelength). Table 1.1. lists some common semiconductors and their corresponding bandgaps.

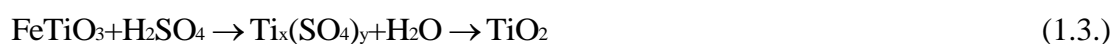
Of all the semiconductors, both natural and synthetically prepared in the laboratory, the one which has attracted the greatest attention for SPC purposes is titanium dioxide (TiO₂). The works of both Fujishima and Honda² and Frank and Bard¹²⁻¹³, despite being for very different SPC applications, both utilised TiO₂ (although Frank and Bard

also examined the use of zinc oxide, cadmium sulphide and tungsten oxide, to name but three) as their semiconductor.

Semiconductor	Bandgap (eV)	Wavelength (nm)
Germanium	0.67	1851
Gallium Arsenide	1.42	873
Cadmium Telluride	1.56	795
Aluminium Arsenide	2.16	574
Titanium Dioxide	3.2	388
Diamond (blue)	5.46-6.4	194-227

Table 1.1.: Some semiconductors and their corresponding bandgaps. The bandgap for each semiconductor is also quoted as the wavelength of electromagnetic irradiation required for excitation

However, the extensive use today of TiO₂ as the semiconductor of choice owes more to its material properties than just simple nostalgia. TiO₂ is biologically and chemically inert, inexpensive, photostable, and very photoactive⁶, so much so that it is now taken to be the benchmark photocatalyst. Outside of photocatalysis, the material is an excellent pigment owing to its high opacity and brightness²⁸, and is revered for its ‘whiteness’; hence, it can be found in a whole host of materials ranging from paper and paint, to toothpaste and even as a food additive (E171)²⁸⁻²⁹. The pigment is typically produced either by the direct oxidation of TiCl₄ (equation 1.2.), or via the reaction of ilmenite (FeTiO₃), a titanium ore, with sulphuric acid³⁰⁻³² (equation 1.3.), i.e.



The material, however, does suffer from two main drawbacks. Firstly, in 2006, the International Agency for Research on Cancer (IARC) classified titanium dioxide dust as a group 2B carcinogen³³, i.e. the material is “possibly carcinogenic to humans”, which is highly undesirable for a material to potentially be used in commercial air purification, water remediation, etc. From a SPC perspective, however, the other main problem in

the use of TiO₂ is that the material, dependent upon the phase present, has a bandgap of ca. 3.0-3.2 eV, which corresponds to wavelengths of ca. 413-387 nm respectively. As a result, UVA light is required to facilitate electronic excitation across the bandgap. Although UVA light is less harmful than both UVB and UVC radiation, visible light photocatalysis is a much more attractive option for commercial products, since TiO₂ can feasibly only absorb a maximum of ca. 5 % of sunlight³⁴. As a result, there is a sustained interest in the development of visible light-activated photocatalysts, through the generation of new semiconductors and the doping of TiO₂ with metal ions to lower its bandgap. An excellent review into visible light-induced SPC has been compiled by Chatterjee and Dasgupta³⁵. However, despite this apparent hindrance, the benefits of TiO₂ far outweigh the negative aspects, hence its rapid emergence as the leading photocatalyst in the field.

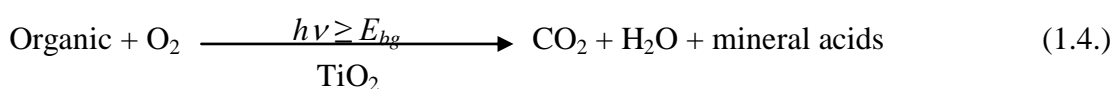
TiO₂, as alluded to above, exists in 3 major phases, namely; anatase, rutile and brookite. Both rutile and anatase have a tetragonal crystal system, whilst brookite is orthorhombic²⁹. In rutile, the Ti centres are surrounded by an octahedron of O atoms, whereas in both brookite and anatase, such octahedra are distorted along their axes³⁶. Whilst most publications list rutile as the most stable form of TiO₂³⁷⁻³⁹, others claim that anatase is more stable by ca. 8-12 kJ/mol³⁶. However, since the ΔG value for the transition between these phases is relatively small (ca. 6 kJ mol⁻¹)³⁹, it comes as no surprise that differing opinions are provided in different sources. All of the literature published on the subject would appear to suggest that anatase is the most photocatalytically active of the three, followed by rutile and then brookite. Such observations are thought to be due to anatase possessing a greater degree of surface hydroxylation and a higher Fermi level. The Fermi level represents the highest energy level occupied by the electrons in a semiconductor at 0 K, and also represents the level wherein the probability of finding an electron is exactly half⁴⁰.

However, depending on the information source, such information can not only be disputed, but indeed contradicted. It is apparent that the activity of any TiO₂ semiconductor is dependent upon many factors, which are discussed in detail later. However, within the literature, Degussa P25, a commercial semiconductor powder, is

taken to be the ‘gold standard’ to which all photocatalysts, both powders and films, commercial and laboratory-prepared, are compared to. Interestingly, Degussa P25 is a mixture of ca. 70 % anatase and 30 % rutile⁶, further emphasising the previous point on the apparent relative activity of the three phases.

1.3. Titanium Dioxide in SPC: Mechanism for the Removal of Organic Pollutants⁸

The general reaction mechanism for SPC, given previously in equation 1.1., can be elaborated further to describe the destruction of most organic substrates, including those listed in section 1.1.2., thus yielding the general equation of TiO₂-mediated SPC as given in equation 1.4.⁴¹;



where E_{bg} is the bandgap of the semiconductor. The processes involved, discussed in general terms in section 1.1., are more fully elaborated here, and represented figuratively in figure 1.4.

Upon irradiation of the semiconductor, the photogenerated h^+/e^- pair can undergo one of the three scenarios listed previously in section 1.1.2. Should the latter of these three scenarios prevail, i.e. the photogenerated species reach the surface with sufficient charge separation such that no recombination occurs, both the h^+ and the e^- will be available for reaction with any materials adsorbed on the semiconductor surface. For the removal of a surface-bound organic substrate, it is believed that the photogenerated hole (redox potential = + 2.53 V⁴²) oxidises a surface titanium hydroxide group to form a radical, i.e. $\text{Ti}^{\text{IV}}\text{OH}^{\cdot+}$. Similar to the photogenerated hole, such a radical is a powerful oxidant, capable of oxidising the adsorbed organic contaminant to CO₂ and H₂O (and mineral acids in some instances).

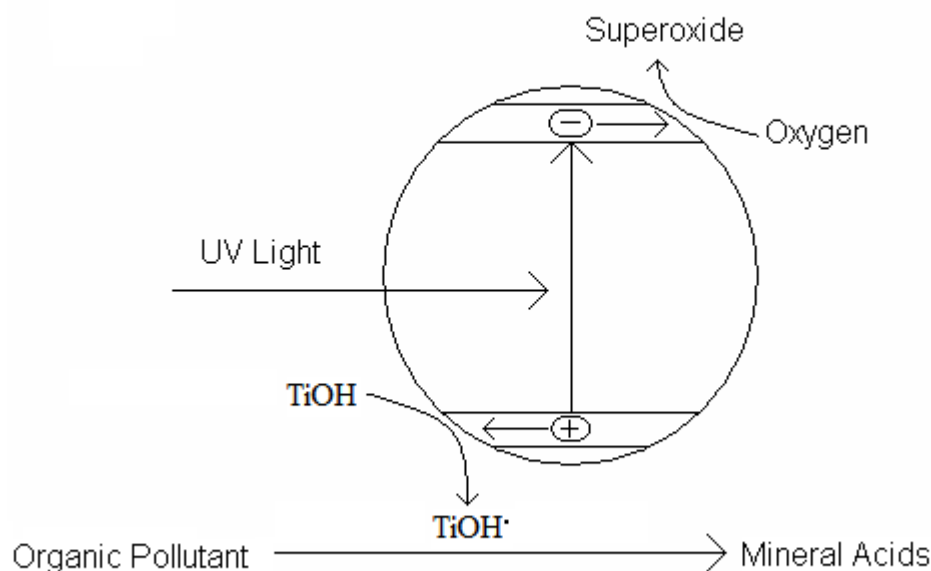


Figure 1.4.: The use of TiO₂ in SPC to destroy an organic pollutant. Note that the '+' sign represents a photogenerated hole, whilst the '-' sign symbolises a photogenerated electron

Conversely, the photogenerated electron is capable of reducing any adsorbed O₂ (or, indeed, any other adsorbed species) since it has a highly negative redox potential ($E_0(e^-) = -0.52 \text{ V}^{42}$). The reduction of O₂ by the photogenerated e⁻ yields superoxide, O₂⁻, which is itself capable of trapping any photogenerated holes⁴³, generating atomic oxygen radicals, O[·]. These radicals are also powerful oxidants, thus providing a second species for use in organic destruction. In addition, since superoxide is also a highly unstable anionic species, it can rapidly decompose to hydrogen peroxide and, subsequently, water, particularly in the presence of an acid, where there is a source of H⁺ ions³⁴. Hydrogen peroxide is a highly oxidising species ($E_0 = 1.32 \text{ V}^{44}$), which in turn decomposes rapidly, presenting another potential source of highly oxidising hydroxyl radicals.

As was indicated above in equation 1.4., the oxidation of adsorbed surface organic species by SPC yields a combination of CO₂, H₂O and mineral acids. However, the relative proportions of such species are not easy to predict. In some instances, e.g. the

oxidation of stearic acid, no mineral acids are detected over short irradiation times, i.e. all the organic is believed to be converted directly to CO_2 and H_2O ⁴⁵. In other instances, not only do we observe the formation of other oxidation products (i.e. mineral acids), but the actual products observed, and their relative ratios, can differ under varying reaction conditions, e.g. in the degradation of trichloroethylene (TCE), one author has reported that the amount of phosgene produced is affected by the oxygen concentration present during photocatalysis⁴⁶, whilst other research conducted on the same organic substrate suggests that the products formed depend on the relative humidity present⁴⁷. It would appear from the literature that the generation of such mineral acids is enhanced by the presence of a heteroatom (e.g. Cl, S, N) in the contaminant being mineralised. So whilst the general mechanism of photocatalysis of organic substrates is understood, the actual mechanism for an individual substrate can vary markedly with both the reaction conditions and the nature/phase of the photocatalyst.

1.4. SPC in Environmental Remediation and Other Uses – Commercial Opportunities

Whilst section 1.3. dealt with SPC for the destruction of organic substrates, it is important to note that the general theory can be applied to other materials. As was demonstrated initially by Frank and Bard¹²⁻¹³, SPC can also be used in the removal of inorganic ions, namely CN^- and SO_3^{2-} , from solution via the same oxidation mechanism proposed above, generating OCN^- and SO_4^{2-} respectively. In addition, Hoffmann et al²⁶ provide an extensive list in their review article of other inorganic species which have been found to be sensitive to this mechanism, such as the nitrogen oxides (commonly referred to in the literature as NO_x species), ammonia, and halide ions, to name but three. They also claim that photocatalysts, in particular zinc oxide (ZnO), can generate large amounts of H_2O_2 via reductive pathways, which in turn has implications for contaminant destruction technologies via a reduction mechanism.

However, other work by Ferry and Glaze (substituted nitrobenzenes and nitropropanes)⁴⁸, Zhang et al (p-chloronitrobenzene)⁴⁹ and Tan et al (selenate, Se(VI))

ions)⁵⁰, to name but three, has demonstrated the use of SPC in a photoreduction capacity. Such reactions are generally conducted in O₂-free environments (presumably since it would compete for the photogenerated e⁻ produced as described above in figure 1.4.) and in the presence of an e⁻-acceptor, e.g. methanol or isopropanol⁴⁸, which acts as a valence band hole scavenger, thus reducing the likelihood of both h⁺/e⁻ recombination, and oxidation of the pollutant under test by such species. Although the number of papers which cite a photoreduction mechanism is much less than those exhibiting photooxidation, there appears to be no major issues with using such a technique for environmental remediation as yet.

Using a similar mechanism to that described in figure 1.4., SPC can also be used to destroy harmful microorganisms⁴². Whereas previously the photogenerated hole, and the subsequent surface titanium hydroxide radical (plus any potential oxidisers generated from the conversion of superoxide to water) were utilised in the oxidation of an organic species, so it is that in the presence of microorganisms such as bacterium, viruses or even moulds, the cell walls of such materials can be oxidised by such species instead. Such cell damage results in the death of the microorganisms. Fujishima et al⁴² demonstrated that, through the use of SPC, they were able to destroy a strand of *E. coli*, the bacteria responsible for many outbreaks of food poisoning and which can potentially prove fatal, within 4 hours illumination under low irradiance (0.4 mW cm⁻²) in the presence of TiO₂. Over a similar time period, the authors noted that 80 % of the initial bacteria present still remained in a sample that had been left in the dark, highlighting the potency of the SPC effect.

The same authors have also demonstrated the use of SPC in the destruction of tumour cells which ultimately cause cancer⁴². From initial work on the destruction of HeLe cells, the authors then demonstrated through animal testing that SPC could be used to destroy cancerous growths below a certain size; although they have noted that the practicalities of such a system for use in human patients have still to be resolved.

It is due to these potential uses, as described above and in figure 1.1., that SPC has become more potent as a viable commercial product. An excellent review on the

emergence of SPC-based technology can be found elsewhere³⁴, although it is likely that the list it provides will have increased in the intervening 7 year period. There now exists photocatalyst products for air and water purification, deodorisation and sterilisation/disinfection. Such products vary from flat bed reactors (Clearwater Industries, USA) and air coolers with combined SPC technology (Shenzhen Sunzone Electrical Appliances Ltd., China) to self-cleaning glass (Pilkington Glass plc, UK), tiles (TOTO, Japan) and paving stones (Mitsubishi Materials Co., Japan). In the majority of the products listed³⁴, the photocatalyst in question is invariably TiO₂, and the light sources used tend to be near UVA (supplied as part of the unit for air and water purification systems) or utilise the small UVA component emitted by sunlight. In addition, the observation of photoinduced superhydrophilicity, or PSH, has also demonstrated that not only will such exterior coatings (self-cleaning glasses and tiles in particular) be capable of destroying pollutants which adhere to the surface, but when it rains, or when water is applied to the surface, the water will simply flow off like a sheet, taking the mineral acids produced with it and thus negating the need for any external cleaning. Such technologies even led to the review authors concocting the “home of the future”, as demonstrated in figure 1.5., where SPC technology is a part of everyday life, in everything from the living room and pavement, to the car and even the street lights!

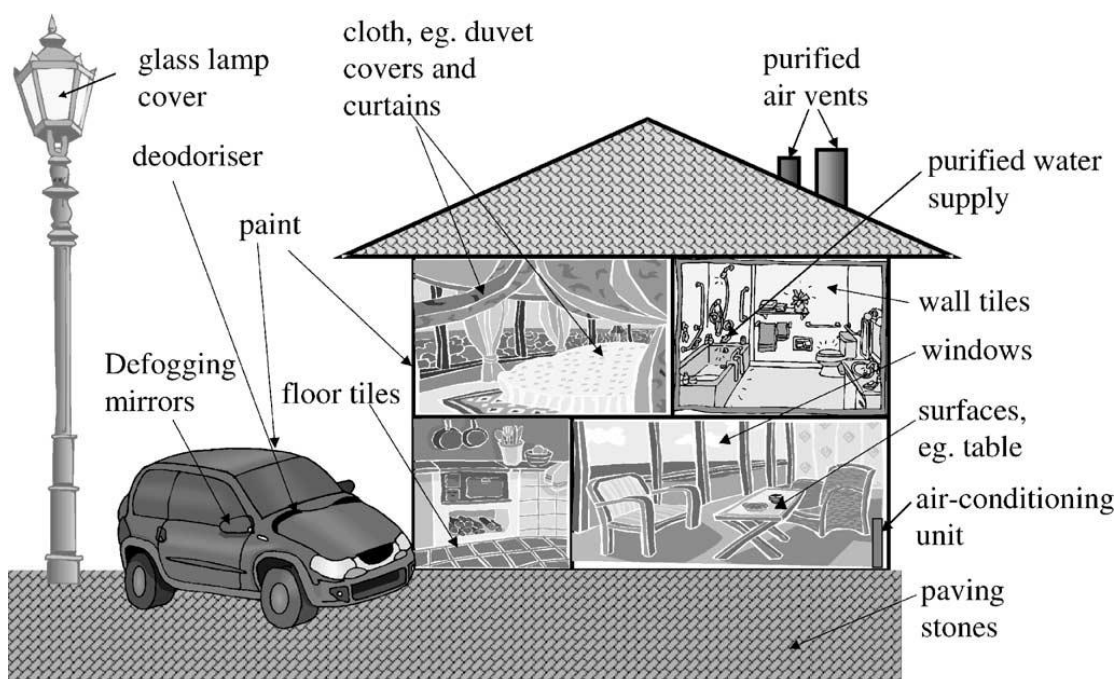


Figure 1.5.: The home of the future, as predicted and kindly reproduced from [34]

1.5. TiO_2 Powders and Films

In the “home of the future” postulated by Mills and Lee, and indeed in many of the products listed in their review³⁴, it is immediately apparent that such technologies cannot rely on the semiconductor in its powder form. Indeed, for technologies such as self-cleaning glasses and tiles, the use of a powder is wholly impractical; instead, a film of the semiconductor, which is usually TiO_2 , is present.

It would be assumed, and indeed has been demonstrated elsewhere, that TiO_2 films could be applied to substrates simply by dip-coating or spin-coating the necessary substrate using an aqueous dispersion of the semiconductor. However, work conducted on films of Degussa P25, the so-called “gold standard” photocatalyst, has demonstrated that whilst it is possible to create films in this manner⁵¹, and that such films can possess a high photocatalytic activity⁷, the films are mechanically unstable, and can be easily wiped off through hard rubbing with a cloth³⁴ or with a pencil. A common technique which has emerged to test the mechanical frailty of films is the so-called Scotch Tape

test⁵², i.e. a strip of the tape is applied to the film and then removed. If the film is properly adhered to the substrate surface, no removal occurs; unfortunately, P25 films are easily removed using this test.

Within the context of this work, TiO₂ films prepared via a Chemical Vapour Deposition (CVD) method and sol-gel processing were used, and the major processes involved are elaborated upon below. It is important to note, however, that the CVD samples used in this work, i.e. Activ™, were commercial, and hence more focus is placed on sol-gel processing since films were produced via this route in-house. TiO₂ films can also be generated using sputtering, physical vapour deposition and solvothermal methods, to name but three, and an excellent review of these and many other techniques, and their corresponding limitations and benefits, can be found elsewhere⁸.

1.5.1. Chemical Vapour Deposition (CVD)^{8,53}

As we shall see later, many of the self-cleaning products on the market (e.g. Pilkington Activ™) rely on CVD to produce the TiO₂ film. Such a technique has the benefit over sol-gel processing that films can easily be reproduced, both in terms of the ratio of their components and thickness. Many variations on the theme exist, e.g. the technique can be performed using electrical rather than thermal energy to initiate the homogeneous reactions (Plasma-assisted or plasma-enhanced CVD), or the use of organometallic precursors gives rise to Metal-organic CVD. Indeed, in the preparation of Activ™, the technique used is referred to as Atmospheric Pressure CVD, or APCVD.

The underlying general mechanism and properties of CVD are loosely demonstrated in figure 1.6. The precursors used to prepare the film on the desired substrate are initially evaporated into the gas phase before being flown into the heated CVD chamber in an inert gas stream (typically N₂ or Ar is used, indicated as (1) in figure 1.6.). Once inside the chamber, the precursor species then react, generating a gas-phase product which will constitute the desired film (2). In addition, other reaction intermediates and by-products can be generated, although these are usually removed from the chamber via an exhaust outlet. The desired gaseous film product then moves toward the substrate surface via

mass transport (3) and is adsorbed on to it, diffusing to suitable sites where growth is encouraged (4). By controlling the volume of the precursor gases flown into the chamber, the thickness of the product film can be tailored to a suitable range, if not an exact value.

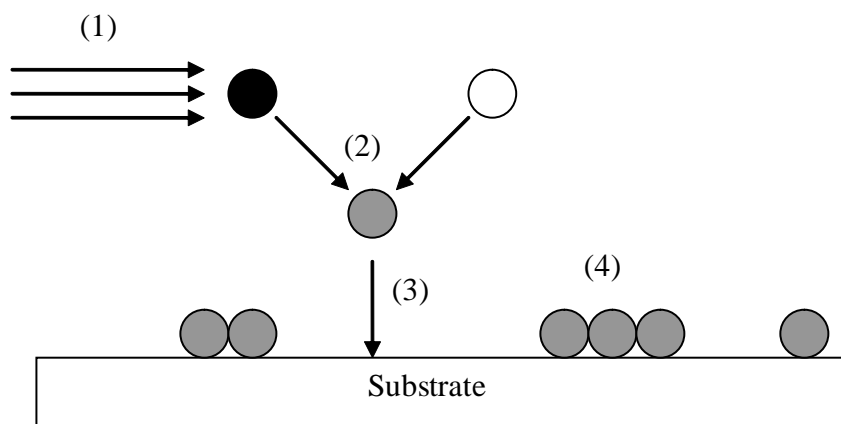


Figure 1.6.: The basic CVD technique

Clearly, for such a technique to be viable, the reactant precursors need to be highly volatile and thermally stable. For films of TiO_2 , TiCl_4 or an organometallic variant of titanium (e.g. titanium tetraisopropoxide⁵⁴) tend to be used as the titanium precursor, the two listed here representing the most popular within the literature according to others⁵⁵. For the O_2 source, either the gas itself⁵⁴ or a low volatility organic such as ethyl acetate⁵⁴ is used. The advantage of using CVD compared to other techniques is that by controlling various factors such as the precursors used, the temperature of the CVD reactor and the growth rate, the TiO_2 film produced can be tailored to be phase-specific⁵⁵, of a desired thickness and utilise relatively cheap precursors.

Such a technique is now being efficiently utilised in the commercialisation of photocatalyst products and in 2001, Pilkington Glass announced the arrival of a self-cleaning glass product, ActivTM, which is produced using an APCVD technique⁵⁶. A 4 mm thick piece of float glass is used as the substrate, with ethyl acetate as the O_2 source and TiCl_4 as the titanium precursor. The anatase TiO_2 film is grown to a thickness of 15 nm, with SEM data reported elsewhere⁴¹ showing the TiO_2 particles in the film to be ca.

30 nm in diameter. In addition, the film is also resistant to the Scotch tape test described previously, implying a high mechanical stability.

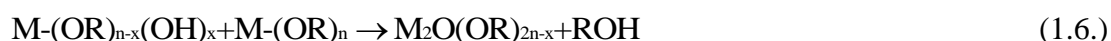
1.5.2. Sol-Gel Synthesis^{8,57}

Based on the literature, sol-gel synthesis would appear to be the most popular method for the production of TiO₂ films. Indeed, the paste films generated in this work in chapter 5 are based upon previous work conducted by Mills et al⁵⁸⁻⁵⁹ (for photocatalysis) and Barbé et al⁶⁰ (for photovoltaic applications) and utilise a sol-gel technique. The sol-gel technique has been brilliantly described, particularly for metal alkoxides, by Jacques Livage and his group, and much of the description which follows here is based on articles which they have published.

Essentially, sol-gel chemistry is based on the use of metal alkoxides in hydrolysis/condensation reactions⁶¹⁻⁶⁵. The hydrolysis reaction sees the reaction of the metal alkoxide with water to form a (substituted) metal hydroxide, typically via an S_N2 nucleophilic substitution mechanism;

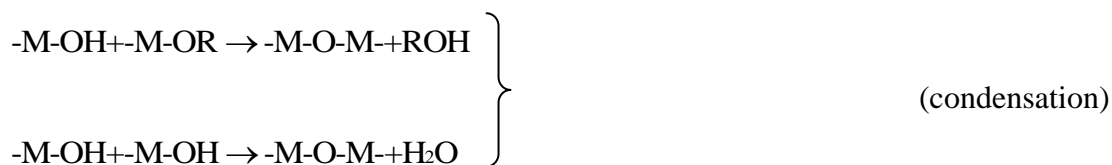


Following this, the (substituted) metal hydroxide can then undergo condensation with other metal alkoxide species or other (partially) hydroxylated alkoxides to give the (partially substituted) metal oxide, i.e.



Elsewhere⁵⁹, such reactions are usually further short-handed, whereby complete elimination of the alkoxide groups on the precursor occurs, to the following form;





The condensed oxide species formed can generate oxopolymers initially and, in an excess of water, the end result is the formation of a hydrous metal oxide. As shall be seen later in chapter 2, within this work the metal alkoxide of choice is titanium tetraisopropoxide ($\text{Ti}(\text{iOPr})_4$). Indeed, this alkoxide precursor appears to be very popular within the literature⁶⁶⁻⁷⁰, as is titanium butoxide ($\text{Ti}(\text{OBu})_4$)⁷¹⁻⁷³. Work by Livage et al⁶¹ and Doeuff et al⁶⁴ has also shown that the use of an acid (e.g. acetic acid, as is used here) in the reaction can lead to the formation of other substituted alkoxide species, i.e. $\text{M}(\text{OR})_{x-n}(\text{Acid})_n$, which are more reactive kinetically to hydrolysis and also increase the gel time, preventing unwanted precipitation of the material from occurring. This acetate group is also a better leaving group than its alkoxide counterpart, thus promoting hydrolysis.

Following their preparation, the TiO_2 sol-gels can either be used to generate a powder, or they can be applied to a desired substrate typically via dip-coating or spin-coating. Such films tend to be fragile and amorphous in nature, hence they are typically calcined/annealed in an oven at a specific temperature prior to use. Based on the thermal stability of the TiO_2 phases, the temperature used in the annealing process is chosen so as to try and control the phase of TiO_2 generated, i.e. at low temperatures (typically ≤ 700 °C), the anatase phase tends to dominate whilst above this temperature, rutile emerges, becoming more dominant as the temperature increases. Obviously this is a broad generalisation, and the actual ratio of product phases will vary depending on the conditions used to generate both the sol-gel and its subsequent film. However, it is worthwhile noting such a thermal phenomenon since, as alluded to previously, the photocatalytic activity is so dependent upon the phase, or the ratio of such phases, present. Heating the film or powder produced from a sol-gel route also serves to

encourage particle growth via sintering and the formation of a polymeric network, as opposed to discrete particles.

The advantages of sol-gel synthesis are many, as described by Wright and Sommerdijk⁵⁷, but include low temperature syntheses (neglecting the drying and subsequent calcination steps), mild reaction conditions with respect to pH, pressure, concentration, etc., the formation of highly porous materials, and control of the hydrolysis/condensation reaction via precursor modification (as described above for acetic acid usage). However, such sol-gels can also suffer from undesirable cracking and flaking when calcined on the substrate surface, although this can be negated through the use of a polymer, as is used in this work (i.e. Carbowax), to form a TiO₂ 'paste'.

1.6. Assessment of Photocatalytic Activity – Standard Tests

As has been alluded to previously, the number of test compounds which have been used to assess the photocatalytic activity of both commercial-, and laboratory-prepared photocatalyst powders and films, and which in some instances have been subjected to further kinetic studies, is immense, encompassing both organic and inorganic species. In addition to this, it is also possible to assess the photocatalytic activity of photocatalyst films using the water contact angle, owing to the photoinduced superhydrophilicity (PSH) effect. However, whilst such a feat is staggering, and emphasises the power and scope of SPC for environmental remediation, there is both a desire and a need for researchers to adopt a standardisation approach, so that this wealth of information can be efficiently compared between groups, allowing identification of the most potent photocatalysts for certain applications (i.e. one photocatalyst may be identified as the best for the removal of dyes from industrial wastewater, whilst another may be more efficient for generating a film capable of the greatest PSH effect on glass). Owing to the crystal phase, surface morphology, semiconductor pre-treatment, reaction conditions, etc., it is possible to observe very different rates of reactions for the removal of a certain species⁶.

Within the literature, there have been many suggestions of possible ways for researchers to correlate/standardise their data, and thus bring it into context within the widening photocatalysis community. Whilst many compounds appear regularly in the literature, e.g. 4-chlorophenol^{6,74}, stearic acid^{7,75}, trichloroethylene⁷⁶⁻⁷⁷ or NO_x⁷⁸⁻⁷⁹ to name but four, under specified reaction conditions, others have proposed that values such as the formal quantum efficiency (FQE) or the quantum yield (QY) are used. Such factors are calculated as described below⁶ in equations 1.8. and 1.9.

$$\text{FQE} = (\text{Rate of reaction of sample})/(\text{Incident irradiance}) \quad (1.8.)$$

$$\text{QY} = (\text{Rate of reaction of sample})/(\text{Rate of absorption of light}) \quad (1.9.)$$

By using one of the calculations detailed above, as opposed to assessing the rate of SPC compared to a standard test, the amount of work required to be undertaken for a comparison to be drawn is reduced. However, such parameters can often be difficult to determine, e.g. to determine QY, there is a need to know how much incident irradiation is absorbed by the photocatalyst and, similarly, how many of these photons correlate to a reaction. Such complications are obviously undesirable, hence a standard test, despite imparting more work, would appear to provide the more attractive option.

In Japan, where photocatalysis continues to be a major area of both research and commercial focus, a dedicated committee exists for developing a set of standard tests for researchers to adhere and compare their findings to. Based on their work, the International Organisation for Standardisation (ISO) now list several standards/projects which describe methods for assessing the photocatalytic activity, including, but not exclusively, the removal of NO_x gases and the measurement of the water contact angle⁸⁰, although more would also appear to be in the process of development. Such proposals do not appear unreasonable, with many researchers already assessing photocatalytic activity with such tests. Even more recently, a European group through the COST Action program has emerged⁸¹, one of whose aims is to develop a set of standard tests for SPC. This group appears to be taking its lead from the initial work in

Japan and the ISO publications, with a view to correlating and liaising with the previous findings, ultimately leading to implementation worldwide.

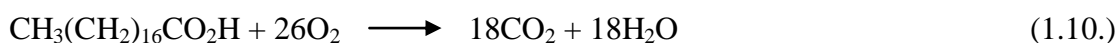
As was noted above, many compounds (or techniques) appear more frequently within the literature than others as ways of assessing SPC. Two such compounds are stearic acid (SA) and methylene blue (MB), and their testing is discussed in a little more detail below.

1.6.1. The Stearic Acid (SA) Test

Stearic acid, a long chain carboxylic acid ($\text{CH}_3(\text{CH}_2)_{16}\text{CO}_2\text{H}$), has been widely used and investigated by both this research group^{7,41,58-59,75,82} and others^{24,45,83-84} as a common technique for assessing photocatalytic activity. The major appeal of SA is five-fold⁸², namely;

1. Stearic acid, when coated as a film, resembles the type of atmospheric pollution which adheres itself to both indoor and outdoor surfaces;
2. It is reasonably stable when irradiated under ultra-bandgap light (ca. 365 nm) when no photocatalyst is present, suggesting little or no photo-decomposition occurs;
3. It can be easily laid down using a suitable solution of the acid dissolved in an organic solvent, e.g. chloroform, by spin- or dip-coating;
4. The kinetics appear to be zero order in nature, hence an appreciable level of stearic acid can be laid down, thus making the reaction easier to follow, and;
5. There are three main ways in which the rate of SPC can be monitored, all *vide infra*, namely gas chromatography (via the evolution of CO_2)⁴⁵, ellipsometry⁸⁵ and infra-red spectroscopy^{7,24,45,58}, the latter of which appears to be the most popular within the literature

The overall oxidation reaction, sensitised by TiO_2 and ultra-bandgap light, is given in equation 1.10.;



i.e. no mineral acids are believed to be formed in the process, with complete (stoichiometric) conversion to CO_2 and H_2O having been noted in work conducted elsewhere⁷⁵. The process involves the total transfer of 104 electrons; hence the quantum yield is typically less than 0.01, making the reaction rapid only in the presence of thick, highly active TiO_2 films. For a film such as that found on ActivTM, the kinetics are relatively slow, with work conducted by this group⁴¹ estimating the rate of photodegradation to be ca. 20 times slower than that observed using a film of Degussa P25 coated on to barrier glass.

Interestingly, whilst the oxidation reaction as written above is generally accepted as the mechanism of SPC, other work has suggested that the oxidation of the organic does indeed yield mineral acids⁴⁵, which can cause the reaction to slow or halt with prolonged irradiation. In addition, although it is now generally accepted that the reaction is zero order, work by both Mills et al⁵⁸ and Minabe et al⁴⁵ has noted that, particularly at high stearic acid concentrations, the reaction can slow after some time due to the accumulation of a small amount of material which is resistant to SPC and/or blocks the incident UV light from reaching the photocatalyst surface. This is obviously undesirable, but its emergence can be controlled by limiting the concentration of stearic acid present on the surface.

1.6.2. The Methylene Blue (MB) Test

The methylene blue (MB) test appears to be just as, if not more popular than the stearic acid test for assessing photocatalytic activity⁸⁶⁻⁹⁵, probably due to the fact that it can be used in conjunction with both powders and films, whilst stearic acid is only suitable for the latter. Indeed, a standard test method utilising MB as the ‘pollutant’ for measuring photocatalytic activity is currently under development according to the ISO website⁹⁶. Typically, an aqueous solution of the dye is placed in contact with the photocatalyst under test and the oxidative reaction occurs as described by equation 1.11⁸²;



As opposed to stearic acid, where the general consensus seems to suggest that the oxidation reaction yields no mineral acids, the presence of both an N and S heteroatom in the structure of MB means acidic products are also formed alongside the predicted CO_2 and H_2O . In addition, since MB is a highly coloured dye (molar absorptivity = $10^5 \text{ dm}^3 \text{ mol}^{-1} \text{ cm}^{-1}$ at 660 nm, the λ_{max} of the dye⁸²), and none of the oxidation products from the reaction are noted for their colour, it follows that not only can the reaction be followed via spectrophotometry, it is visually accessible. By typically monitoring the variation in the absorbance at λ_{max} with time, a first order kinetic dependence has been noted⁸⁸, hence the data can be easily manipulated in order to find the initial rate of reaction or the first-order rate constant, k_1 .

Despite all this, however, the methylene blue test does suffer from one major complication. Since it is a dye, MB can be reduced in the presence of highly energetic electrons, such as those photogenerated by irradiation of TiO_2 with ultra-bandgap light ($E_0(\text{e}^-) = -0.52 \text{ V}$). The product of such a reduction reaction is leuco-MB (LMB), which, like the products of oxidation noted above, is also colourless, i.e.;



On first glance, therefore, it would appear to be impossible to ascertain whether the removal of MB in a photocatalyst system is due to photodegradation or reduction of the dye. However, work conducted elsewhere^{89,97} has suggested that the latter photoreduction mechanism is only viable in the presence of a suitable sacrificial electron donor (SED), e.g. methanol, which acts as a scavenger for the photogenerated holes, much as is observed in other work published on the photoreduction of species noted earlier in section 1.4. In addition, to further promote the photoreduction reaction, the solution should also be free of oxygen, since it is a well known e^- scavenger, as utilised in the photooxidation mechanism. Work by Mills and Wang has also sought to alleviate fears that photoreduction occurs, even in the absence of such SEDs or

anaerobic conditions, by demonstrating that, in neutral or slightly alkaline solutions, no recovery of MB colour is observed following irradiation. However, in acidic (pH 2) solutions, following bleaching of the dye and subsequent exposure to O₂ in a radiation-free environment, ca. 66 % of the original MB colour was recovered, implying that the photoreduction reaction, though not exclusive, predominates under such conditions. This level of sensitivity of MB to the presence of SEDs, atmospheric environment and pH means that whilst such a test is still inherently useful to assess the photocatalytic activity, it requires researchers to be very detailed in their conditions used, such that comparisons can be drawn with new systems/photocatalysts.

1.6.3. Standard Tests in the Field

Whilst the focus of the discussion above has been on the stearic acid and methylene blue tests, because they frequently occur in the literature and are used in this work, it is necessary to take a step back and examine all the standard tests suggested within the literature, and analyse them from an industrial and commercial viewpoint. Whilst all such tests may be suitable for use in the laboratories, where there is ready access to equipment, manpower, chemicals and data analysis sources, testing in the field is very different. With so many photocatalyst products now being made available to the general public, there is a strong desire for a standard test which can be utilised to demonstrate the SPC activity of a customer's purchase. Whilst stearic acid and methylene blue are excellent within the laboratory, taking them into the field is not an attractive option. Firstly, there is a need for a portable analysis rig (e.g. IR spectroscope for stearic acid or a UV-Vis spectrophotometer for methylene blue), and hence a trained technician to conduct the analysis. In addition, more so for MB than stearic acid, the process is wholly impractical since a solution of the dye would have to be held in contact with the photocatalyst layer under test. For stearic acid, although it is possible to apply a layer of material to the substrate under test using, for example, a brush, work in the literature typically utilises monolayer(s) coverage of stearic acid. Such a scenario is highly unlikely to be achieved through application with a paintbrush! Finally, as was alluded to above, work by Mills et al⁴¹ has demonstrated that the stearic acid test, whilst fairly rapid (ca. 20 hours) for a 90 nm thick photocatalyst film made from Degussa P25,

is not as rapid for a product such as Activ™, where the photocatalyst layer is ca. 15 nm. Typically, photocatalyst products which have realised a commercial potential employ a photocatalyst layer in the nanometre-scale range, thus stearic acid testing would be slow, requiring a repeat visit from the salesman. Similar timescales would also be anticipated for the MB test with such commercial products.

For most of the species, both organic and inorganic, whether solid, liquid or gaseous, the scenario is much the same; the analysis of SPC using such materials is complicated, requiring sophisticated equipment and a trained expert. Most importantly, however, is an understanding of the customer and their reaction to photocatalysis. Many consumers will not have studied any science since their time in high school, let alone have a degree, and whilst it may be possible to develop a small cell for MB or a way of applying stearic acid to monolayer(s) coverage say, the underlying chemistry of such techniques, as detailed above, is not accessible to the general public. However, there are some benefits to be gained from the standardisation work conducted by many in the literature. Whether it be MB or another dye of choice, the idea of a colour change system is excellent. Whilst the underlying chemical process and the kinetics may be difficult to comprehend for many consumers, their ability to ‘see’ the SPC action via the change in colour of the dye is a powerful tool for any salesman to have. Whilst a solution of a dye is impractical, a solid film of the dye may be more appealing, since, as was suggested for stearic acid, this could be applied with a brush.

Some researchers have tried to apply the dye directly to the photocatalyst with little success, whereas others have found it more useful to incorporate the dye in a polymer film solution initially, and then dry a film of this solution on to the photocatalyst surface. Work by Julson and Ollis⁹⁸ examined the possibility of using a dye when applied to the surface of a photocatalyst (Degussa P25) as a means of assessing the photocatalytic activity, and their work also provides a brief review of the majority of the literature previously published on the topic. Their work was then extended by Chin and Ollis⁹⁹ who examined the oxidative bleaching of dye films on the surface of Activ™. In both instances, whilst a dye layer can be applied and is bleached with a very visual colour change, the times taken for such changes are ca. 240 minutes (4 hours) with

Degussa P25-coated particles and ca. 1700 minutes (ca. 28 hours) with Activ™. Although these findings represent a step in the right direction, the kinetics are still relatively slow. What is needed is a visual test, preferably utilising the change in colour of a dye, which is rapid and can relay to a customer just how ‘active’ their new photocatalyst product is.

1.7. Indicator Inks

In 2005, Mills et al¹⁰⁰ published their findings into the development of a novel, UV dosimeter which works via a photoreduction mechanism. A dye, namely methylene blue, was incorporated in a polymer film (hydroxyethyl cellulose) along with a mild reducing agent (triethanolamine, TEOA) and titania nanoparticles. Upon irradiation of a film of the solution, a photogenerated e^-/h^+ pair is produced as usual. The h^+ is then scavenged by the TEOA, producing an oxidised version of the reducing agent (referred to within the article as $TEOA_{ox}$). The electron, meanwhile, is used in the photoreduction of the dye, generating leuco-MB using the process described previously in equation 1.12. As a result, irradiation of such a film causes the film to change colour from blue to colourless according to the mechanism shown in figure 1.7.

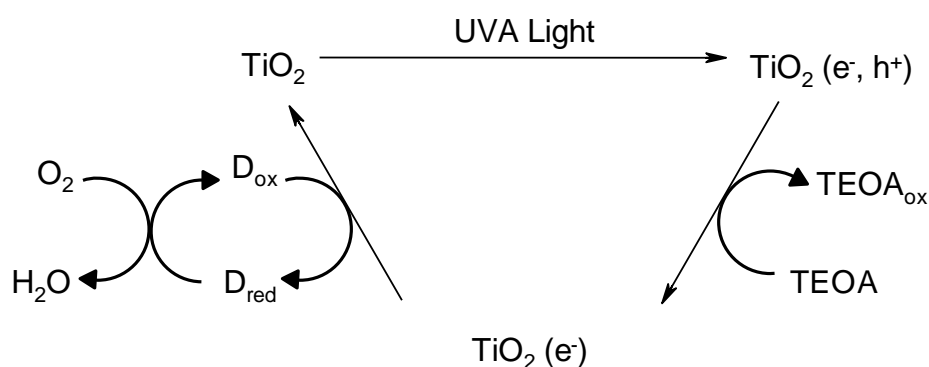


Figure 1.7.: The mechanism used in the novel UV dosimeter developed by Mills et al, where D_{ox} and D_{red} represent the oxidised and reduced forms of the dye, respectively

Owing to the reversible nature of MB dye reduction, upon removal of the UV irradiation source the MB would be regenerated due to leuco-MB oxidation by

atmospheric oxygen, although the authors duly noted that such a process could be restricted by applying an O₂-impermeable barrier to the film, e.g. Sellotape™. One of the main attractions of such a film was the time taken for complete MB reduction to occur, namely 10 minutes using 3.5 mW cm⁻² UVA light, which is less than the output from the sun on a typical summer's day¹⁰¹.

In the same year, Mills et al¹⁰² also applied this novel photoreduction mechanism to an ink film applied to the surface of a photocatalyst, namely Activ™, as a means of measuring the photocatalytic activity. Whereas for their UV dosimeter the mild reducing agent, or SED, used was TEOA and the dye used was MB, in this latter work glycerol and resazurin (Rz) were used, respectively. By switching to Rz, re-oxidation of the dye by atmospheric O₂ was thought to be eliminated since its reduction is electrochemically irreversible – instead of involving the transfer of both protons and electrons, reduction of Rz proceeds by the removal of a dative N to O bond as shown in figure 1.8.

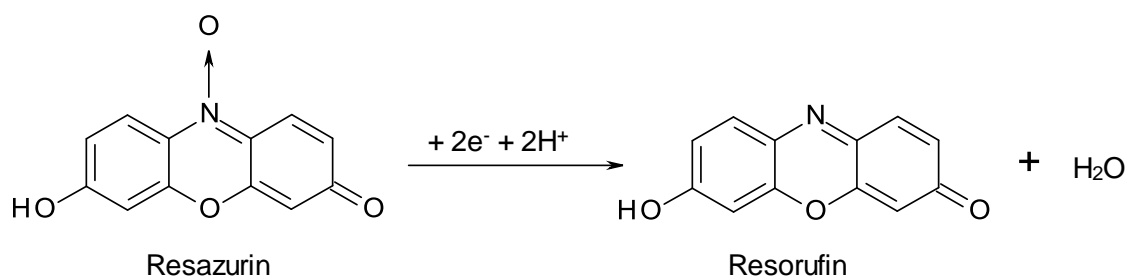


Figure 1.8.: The structures of resazurin (Rz) and its reduced product, resorufin (Rf)

By applying the Rz ink film to the surface of Activ™, which is representative of the type and activity of the SPC products which have flooded the market in recent years, the authors demonstrated that, under a modest UV light intensity (12.4 mW cm⁻² UVA), the dye was effectively reduced in ca. 6.5 minutes. Whilst the ink was spin-coated on to the photocatalyst surface in this work, further work by the same author has since demonstrated that the ink can be encompassed in a felt-tipped pen¹⁰³. Such a pen is suitable for use in the field by sales representatives since it can be easily carried from

location to location, and is stable for a period of 3 months. More importantly, the ink film is aesthetically appealing to potential customers since the reduction of the dye from Rz to its reduced product, resorufin (Rf) yields a colour change from blue to pink. Although the underlying chemistry, namely the removal of the dative N to O bond, is difficult to explain, the colour change is restricted to occurring only on SPC active materials. Hence, by simply applying the ink to a non-SPC surface, it is possible to demonstrate to potential customers the difference between self-cleaning and standard glasses, tiles and even paints.

Whilst such a colour change system is obviously appealing, however, the Rz system does suffer from one major flaw; namely that the reduced product, Rf, is pink. Whilst the occurrence of the colour change is restricted to the ink's application to SPC-active products, it would be more aesthetically pleasing to potential customers if the reduced product was colourless, since there is a general, admittedly scientifically inaccurate train of thought that the generation of a bleached product is representative of a complete cleaning action. As a consequence, a dye which reduces to a colourless product would be preferred. Three such dyes of the many which fit this criterion are resorufin (Rf), methylene blue (MB) and 2,6-dichloroindophenol (DCIP), the structures of which are shown in figure 1.9.

All three dyes are reduced via a typical proton/electron transfer mechanism. Interestingly, the reduction of Rf suggests that should a film of Rz be applied to the surface of Activ™ and irradiated for a prolonged period, the ink will change colour from blue to pink initially, and then from pink to colourless as the latter Rf reduction reaction occurs. Such a consecutive set of reactions further emphasises the difficulty of explanation that would be required if the Rz ink was used in the field.

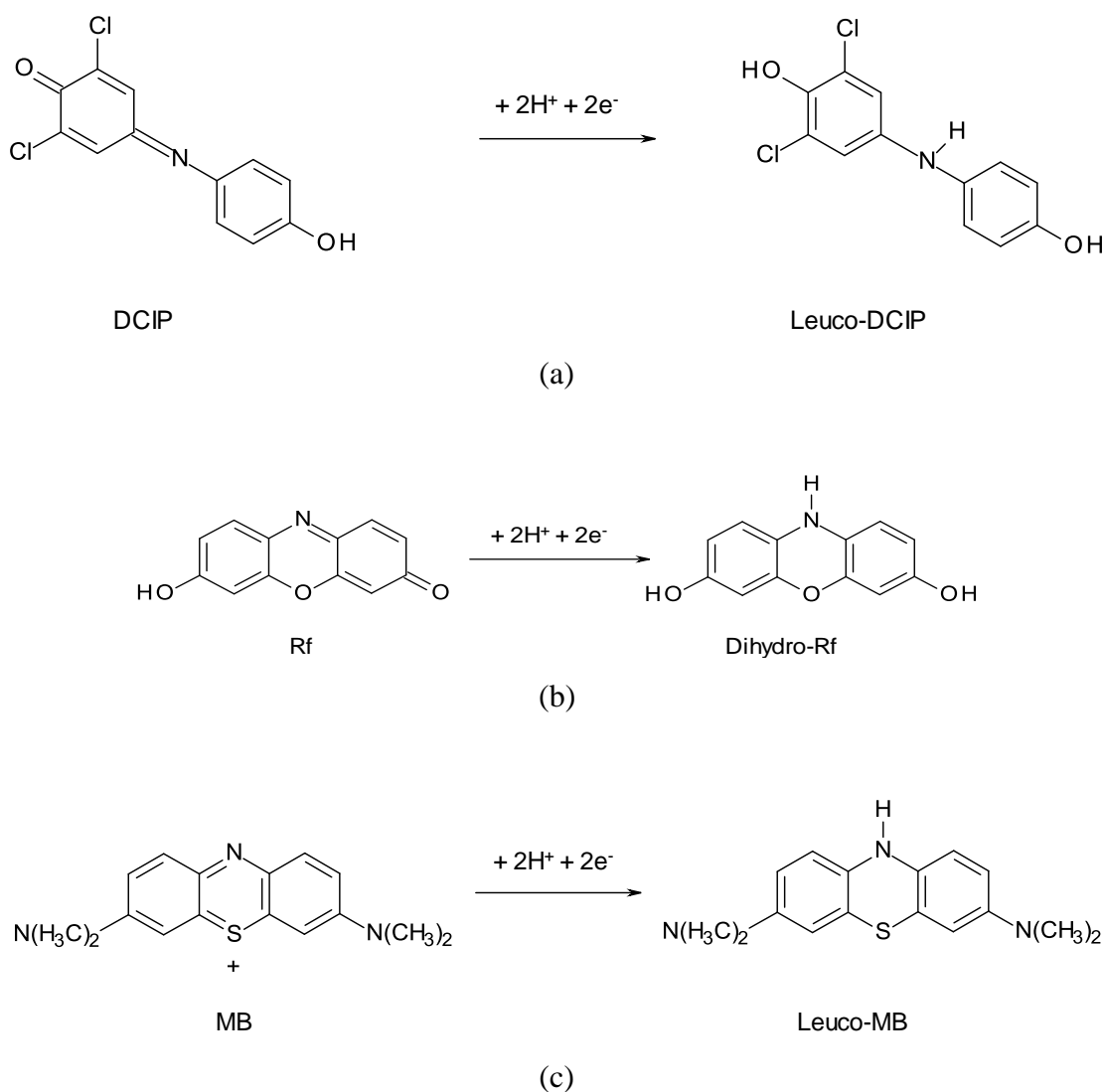


Figure 1.9.: The structures of; (a) 2,6-dichloroindophenol (DCIP), (b) resorufin (Rf) and, (c) methylene blue (MB), and their reduced products

1.8. Project Aims

The main aim of this project is to develop an indicator ink test which is not only suitable for use in the field, but which can also be correlated to other tests already widely accepted within the scientific community. Initially, an ink based on the dye 2,6-dichloroindophenol (DCIP) is assessed for its possible usage as an indicator for photocatalytic activity. Such an ink would be preferred to the Rz indicator ink

developed by Mills et al¹⁰² from a commercial viewpoint since the reduced product of DCIP, leuco-DCIP, is colourless. The ink is characterised to assess the effect of SED, polymer and light intensity on its performance, as well as altering the levels of each component present in order to ascertain both the ideal formulation for maximum performance and the kinetics of dye photoreduction.

The DCIP ink is then assessed against novel indicator inks based on Rf and MB, and the Rz indicator ink of Mills et al¹⁰². The performance of the inks under anaerobic conditions is assessed initially, before conditions more representative of that which would be encountered in the field are applied, with any anomalies and intriguing observations highlighted and discussed.

Finally, the DCIP ink will then be used as one 'standard test' for the assessment of the photocatalytic activity of sol-gel paste films produced in-house. By annealing such films at various temperatures, the phase and surface properties of the films are found to vary, and hence these are discussed and compared to similar work in the literature. The photocatalytic activity of the films is then assessed using the ink described above, and the MB and stearic acid tests discussed previously. The variation in photocatalytic activity with annealing temperature is discussed for each test, and any correlations between tests will be highlighted. Ultimately a correlation between the ink test and these other, more generally accepted methods of assessing photocatalytic activity is sought in order to emphasise the importance of the ink test to the wider scientific community.

As an aside, the performance of the MB ink will then be revisited. Recent work by Mills et al¹⁰⁴ has demonstrated that through acidification of the ink, the rate of the undesirable re-oxidation of leuco-MB by atmospheric O₂ can be slowed, and this will be examined in more detail here. The performance of other dyes from the thiazine, phenazine and oxazine families when incorporated in this new formulation will also be compared and contrasted to what is observed using 'standard' ink conditions, with a view to proposing a new indicator ink for assessing photocatalytic activity.

1.9. References

- (1) A. Fujishima; K. Honda *Bulletin of the Chemical Society of Japan* **1971**, *44*, 1148.
- (2) A. Fujishima; K. Honda *Nature* **1972**, *238*, 37.
- (3) <http://www.google.co.uk/search?q=semiconductor+photocatalysis&ie=utf-8&oe=utf-8&aq=t&rls=org.mozilla:en-GB:official&client=firefox-a>, 30/09/2009
- (4) http://www.sciencedirect.com/science?_ob=ArticleListURL&_method=1ist&_ArticleListID=1029750421&_sort=r&_view=c&_acct=C000046979&_version=1&_urlVersion=0&_userid=875629&md5=f8ada59c9b219a5d55c45fce7e9ab567 30/09/2009
- (5) <http://pubs.acs.org/action/doSearch?action=search&searchText=semiconductor+photocatalysis&qSearchArea=searchText> 30/09/2009
- (6) A. Mills; S. L. Hunte *Journal of Photochemistry and Photobiology A: Chemistry* **1997**, *108*, 1.
- (7) A. Mills; N. Elliott; I. P. Parkin; S. A. O'Neill; R. J. Clark *Journal of Photochemistry and Photobiology A: Chemistry* **2002**, *151*, 171.
- (8) O. Carp; C. L. Huisman; A. Reller *Progress in Solid State Chemistry* **2004**, *32*, 33.
- (9) P. W. Atkins *Physical Chemistry*; Oxford University Press, 1990.
- (10) H. Benson *University Physics*; John Wiley and Sons, Inc., 1995.
- (11) A. Fujishima; K. Honda *Journal of the Chemical Society of Japan* **1971**, 74.
- (12) S. N. Frank; A. J. Bard *Journal of the American Chemical Society* **1977**, *99*, 303.
- (13) S. N. Frank; A. J. Bard *The Journal of Physical Chemistry* **1977**, *81*, 1484.
- (14) A. L. Pruden; D. F. Ollis *Journal of Catalysis* **1983**, *82*, 404.
- (15) C.-Y. Hsiao; C.-L. Lee; D. F. Ollis *Journal of Catalysis* **1983**, *82*, 418.
- (16) X. Deng; Y. Yue; Z. Gao *Applied Catalysis B: Environmental* **2002**, *39*, 135.
- (17) S. Yamazaki; S. Tanaka; H. Tsukamoto *Journal of Photochemistry and Photobiology A: Chemistry* **1999**, *121*, 55.

-
- (18) V. Augugliaro; S. Coluccia; V. Loddo; L. Marchese; G. Martra; L. Palmisano; M. Schiavello *Applied Catalysis B: Environmental* **1999**, *20*, 15.
- (19) A. V. Vorontsov; V. P. Dubovitskaya *Journal of Catalysis* **2004**, *221*, 102.
- (20) J. Chen; D. F. Ollis; W. H. Rulkens; H. Bruning *Water Research* **1999**, *33*, 669.
- (21) M. Muneer; J. Theurich; D. Bahnemann *Journal of Photochemistry and Photobiology A: Chemistry* **2001**, *143*, 213.
- (22) S. Parra; S. E. Stanca; I. Guasaquillo; K. R.Thampi *Applied Catalysis B: Environmental* **2004**, *51*, 107.
- (23) V. A. Sakkas; I. M. Arabatzis; I. K. Konstantinou; A. D. Dimou; T. A. Albanis; P. Falaras *Applied Catalysis B: Environmental* **2004**, *49*, 195.
- (24) R. Fretwell; P. Douglas *Journal of Photochemistry and Photobiology A: Chemistry* **2001**, *143*, 229.
- (25) B. Kraeutler; A. J. Bard *Journal of the American Chemical Society* **1978**, *100*, 5985.
- (26) M. R. Hoffmann; S. T. Martin; W. Choi; D. W. Bahnemann *Chemical Reviews* **1995**, *95*, 69.
- (27) A. J. Maira; K. L. Yeung; C. Y. Lee; P. L. Yue; C. K. Chan *Journal of Catalysis* **2000**, *192*, 185.
- (28) <http://ec.europa.eu/environment/waste/titanium.htm> 22/09/2009
- (29) http://en.wikipedia.org/wiki/Titanium_dioxide 22/09/2009
- (30) <http://www.icis.com/v2/chemicals/9076547/titanium-dioxide/process.html>
01/10/2009
- (31) <http://como.cheng.cam.ac.uk/preprints/c4e-Preprint-42.pdf> 01/10/2009
- (32) R. M. Christie *Colour Chemistry*; The Royal Society of Chemistry, 2001.
- (33) <http://monographs.iarc.fr/ENG/Meetings/93-titaniumdioxide.pdf> 30/09/2009
- (34) A. Mills; S.-K. Lee *Journal of Photochemistry and Photobiology A: Chemistry* **2002**, *152*, 233.
- (35) D. Chatterjee; S. Dasgupta *Journal of Photochemistry and Photobiology C: Photochemistry Reviews* **2005**, *6*, 186.
- (36) F. A. Cotton; G. Wilkinson; C. A. Murillo; M. Bochmann *Advanced Inorganic Chemistry*; John Wiley and Sons Inc., 1999.

-
- (37) D. Reyes-Coronado; G. Rodriguez-Gattorno; M. E. Espinosa-Pesqueira; C. Cab; R. d. Coss; G. Oskam *Nanotechnology* **2008**, *19*, 1.
- (38) J. Yu; J. C. Yu; M. K.-P. Leung; W. Ho; B. Cheng; X. Zhao; J. Zhao *Journal of Catalysis* **2003**, *217*, 69.
- (39) K. V. Baiju; S. Shukla; K. S. Sandhya; J. James; K. G. K. Warriar *J. Phys. Chem. C* **2007**, *111*, 7612.
- (40) <http://hyperphysics.phy-astr.gsu.edu/hbase/solids/fermi.html> 04/12/2011
- (41) A. Mills; A. Lepre; N. Elliott; S. Bhopal; I. P. Parkin; S. A. O'Neill *Journal of Photochemistry and Photobiology A: Chemistry* **2003**, *160*, 213.
- (42) A. Fujishima; T. N. Rao; D. A. Tryk *Journal of Photochemistry and Photobiology C: Photochemistry Reviews* **2000**, *1*, 1.
- (43) K. Hashimoto; H. Irie; A. Fujishima *Japanese Journal of Applied Physics* **2005**, *44*, 8269.
- (44) P. G. Furtmuller; J. Arnhold; W. Jantschko; M. Zederbauer; C. Jakopitsch; C. Obinger *Journal of Inorganic Biochemistry* **2005**, *99*, 1220.
- (45) T. Minabe; D. A. Tryk; P. Sawunyama; Y. Kikuchi; K. Hashimoto; A. Fujishima *Journal of Photochemistry and Photobiology A: Chemistry* **2000**, *137*, 53.
- (46) H.-H. Ou; S.-L. Lo *Journal of Hazardous Materials* **2007**, *146*, 302.
- (47) W. A. Jacoby; M. R. Nimios; D. M. Blake; R. D. Noble; C. A. Koval *Environ. Sci. Technol.* **1994**, *28*, 1661.
- (48) J. L. Ferry; W. H. Glaze *Langmuir* **1998**, *14*, 3551.
- (49) T. Zhang; L. You; Y. Zhang *Dyes and Pigments* **2006**, *68*, 95.
- (50) T. T. Y. Tan; D. Beydoun; R. Amal *Journal of Molecular Catalysis A: Chemical* **2003**, *202*, 73.
- (51) J. Yang; D. S. Warren; K. C. Gordon; A. J. McQuillan *Journal of Applied Physics* **2007**, *101*, 023714.
- (52) Y. Paz; Z. Luo; L. Rabenberg; A. Heller *Journal of Materials Research* **1995**, *10*, 2842.
- (53) A. C. Jones; M. L. Hitchman *Chemical Vapour Deposition*, 2008.
- (54) P. Evans; S. Mantke; A. Mills; A. Robinson; D. W. Sheel *Journal of Photochemistry and Photobiology A: Chemistry* **2007**, *188*, 387.

-
- (55) Z. Ding; X. Hu; P. L. Yue; G. Q. Lu; P. F. Greenfield *Catalysis Today* **2001**, 68, 173.
- (56) K. D. Sanderson; J. A. Knowles Self-Cleaning Glazing Sheet, WO 03/050056
- (57) J. D. Wright; N. A. J. M. Sommerdijk *Sol-Gel Materials Chemistry and Applications*; OPA, 2001.
- (58) A. Mills; G. Hill; M. Crow; S. Hodgen *Journal of Applied Electrochemistry* **2005**, 35, 641.
- (59) A. Mills; N. Elliott; G. Hill; D. Fallis; J. R. Durrant; R. L. Willis *Photochem. Photobiol. Sci.* **2003**, 2, 591.
- (60) C. J. Barbé; F. Arendse; P. Comte; M. Jirousek; F. Lenzmann; V. Shklover; M. Grätzel *Journal of the American Ceramic Society* **1997**, 80, 3157.
- (61) J. Livage; C. Sanchez *Journal of Non-Crystalline Solids* **1992**, 145, 11.
- (62) C. Sanchez; J. Livage; M. Henry; F. Babonneau *Journal of Non-Crystalline Solids* **1988**, 100, 65.
- (63) M. Nabavi; S. Doeuff; C. Sanchez; J. Livage *Journal of Non-Crystalline Solids* **1990**, 121, 31.
- (64) S. Doeuff; M. Henry; C. Sanchez; J. Livage *Journal of Non-Crystalline Solids* **1987**, 89, 206.
- (65) F. Babonneau; C. Sanchez; J. Livage *Journal of Non-Crystalline Solids* **1988**, 106, 170.
- (66) F. G. Delgado; K. V. Gómez; C. M. Morales *Microelectronics Journal* **2008**, 39, 1333.
- (67) J. Marugán; P. Christensen; T. Egerton; H. Purnama *Applied Catalysis B: Environmental* **2009**, 89, 273.
- (68) C. G. Silva; J. L. Faria *Journal of Molecular Catalysis A: Chemical* **2009**, 305, 147.
- (69) D. J. Kim; S. H. Hahn; S. H. Oh; E. J. Kim *Materials Letters* **2002**, 57, 355.
- (70) Y. Chen; D. D. Dionysiou *Journal of Molecular Catalysis A: Chemical* **2006**, 244, 73.
- (71) T. Wen; J. Gao; J. Shen; Z. Zhou *Journal of Materials Science* **2001**, 36, 5923.
- (72) J. Yu; X. Zhao; Q. Zhao *Thin Solid Films* **2000**, 379, 7.
- (73) J. Zhu; J. Zhang; F. Chen; K. Iino; M. Anpo *Topics in Catalysis* **2005**, 35, 261.

-
- (74) A. Mills; J. Wang *Journal of Photochemistry and Photobiology A: Chemistry* **1998**, *118*, 53.
- (75) A. Mills; J. Wang *Journal of Photochemistry and Photobiology A: Chemistry* **2006**, *182*, 181.
- (76) J.-S. Kim; K. Itoh; M. Murabayashi *Chemosphere* **1998**, *36*, 483.
- (77) K. Demeestere; A. D. Visscher; J. Dewulf; M. V. Leeuwen; H. V. Langenhove *Applied Catalysis B: Environmental* **2004**, *54*, 261.
- (78) F. Nakajima; I. Hamada *Catalysis Today* **1996**, *29*, 109.
- (79) G. Ok; Y. Hanai; T. Katou *Chemosphere* **1993**, *26*, 2167.
- (80) http://www.iso.org/iso/iso_catalogue/catalogue_tc/catalogue_tc_browse.htm?commid=54756 15/10/2009
- (81) <http://www.cost540.com/content/cost2.html> 15/10/2009
- (82) A. Mills; M. McFarlane *Catalysis Today* **2007**, *129*, 22.
- (83) P. Sawunyama; L. Jiang; A. Fujishima; K. Hashimoto *J. Phys. Chem. B* **1997**, *101*, 11000.
- (84) L. Peruchon; E. Puzenat; A. Girard-Egrot; L. Blum; J. M. Herrmann; C. Guillard *Journal of Photochemistry and Photobiology A: Chemistry* **2008**, *197*, 170.
- (85) J. T. Remillard; J. R. McBride; K. E. Nietering; A. R. Drews; X. Zhang *J. Phys. Chem. B* **2000**, *104*, 4440.
- (86) S. Lakshmi; R. Renganathan; S. Fujita *Journal of Photochemistry and Photobiology A: Chemistry* **1995**, *88*, 163.
- (87) C. H. Kwon; H. Shin; J. H. Kim; W. S. Choi; K. H. Yoon *Materials Chemistry and Physics* **2004**, *86*, 78.
- (88) R. W. Matthews *J. Chem. Soc. Faraday Trans. 1* **1989**, *85*, 1291.
- (89) A. Mills; J. Wang *Journal of Photochemistry and Photobiology A: Chemistry* **1999**, *127*, 123.
- (90) M. Wark; J. Tschirch; O. Bartels; D. Bahnemann; J. Rathousky *Microporous and Mesoporous Materials* **2005**, *84*, 247.
- (91) T. Zhang; T. Oyama; A. Aoshima; H. Hidaka; J. Zhao; N. Serpone *Journal of Photochemistry and Photobiology A: Chemistry* **2001**, *140*, 163.

-
- (92) N. Xu; Z. Shi; Y. Fan; J. Dong; J. Shi; M. Z.-C. Hu *Ind. Eng. Chem. Res.* **1999**, *38*, 373.
- (93) M. Inagaki; Y. Nakazawa; M. Hirano; Y. Kobayashi; M. Toyoda *International Journal of Inorganic Materials* **2001**, *3*, 809.
- (94) G. Sivalingam; K. Nagaveni; M. S. Hegde; G. Madras *Applied Catalysis B: Environmental* **2003**, *45*, 23.
- (95) K. Baba; R. Hatada *Surface and Coatings Technology* **2001**, *136*, 241.
- (96)
- [http://www.iso.org/iso/iso_catalogue/catalogue_tc/catalogue_detail.htm?
csnumber=46019](http://www.iso.org/iso/iso_catalogue/catalogue_tc/catalogue_detail.htm?csnumber=46019) 12/01/2010
- (97) H. Yoneyama; Y. Toyoguchi; H. Tamura *J. Phys. Chem.* **1972**, *76*, 3460.
- (98) A. J. Julson; D. F. Ollis *Applied Catalysis B: Environmental* **2006**, *65*, 315.
- (99) P. Chin; D. F. Ollis *Catalysis Today* **2007**, *123*, 177.
- (100) A. Mills; S.-K. Lee; M. Sheridan *The Analyst* **2005**, *130*, 1046.
- (101) A. Mills; M. McFarlane; S. Schneider *Anal. Bioanal. Chem.* **2006**, *386*, 299.
- (102) A. Mills; J. Wang; S.-K. Lee; M. Simonsen *Chem. Commun.* **2005**, 2721.
- (103) A. Mills; J. Wang; M. McGrady *J. Phys. Chem. B* **2006**, *110*, 18324.
- (104) A. Mills; J. Hepburn; M. McFarlane *ACS Applied Materials and Interfaces* **2009**, *1*, 1163.

2 Experimental

All reagents used in this work were Analar grade, purchased as indicated and, unless stated otherwise, used as received. In all experiments, deionised and doubly distilled water was used to prepare any aqueous solutions and the water-based photocatalyst indicator inks. All gas cylinders used in the modification of the atmospheric conditions were purchased from BOC gases and used as received. All dyes studied were used as received, with no further purification.

2.1. Indicator Inks

2.1.1. Preparation of the Photocatalyst Indicator Inks

The photocatalyst indicator inks described in this work comprise three major components, namely:

- An aqueous polymer solution;
- A sacrificial electron donor (herein referred to as an SED), and;
- A dye

Various combinations of these components can be found, amongst other compounds, in fountain pen and fibre-tip pen inks¹. In such inks, water is by far the most dominant component present (97.5 and 71.8 %, respectively). Both formulations also have non-ionic surfactants and a water soluble dye to generate the desired ink colour. However, of the two formulations only the fibre-tip pen ink is observed to contain polymer, in this instance polyvinylpyrrolidone¹. In addition, although glycerol is not present in the fibre-tip pen formulation cited, 1,2-propylene glycol is added, presumably acting as a moisturiser and helping to stabilise the ink in both the pen and the nib¹. It has to be kept in mind that glycerol is only added to the indicator ink formulation described here to act as a hole scavenger (i.e. the SED) - the fact that it may help stabilise the ink when incorporated into a felt-tipped pen by acting as a moisturiser, like the structurally similar 1,2-propylene glycol, is merely a beneficial coincidence.

Hydroxyethyl cellulose (supplied by Fluka, viscosity 145 mPa s 1% in H₂O (20°C), herein referred to as HEC) was the preferred polymer for the preparation of the photocatalyst indicator inks, since it is both water soluble, and has been shown previously to be excellent in the preparation of inks for other purposes in-house, namely UV dosimetry² and an O₂ indicator³. It should be noted that reasonably similar kinetic results for ink photoreduction were achieved when polyvinyl alcohol (supplied by Aldrich, 98-99 % hydrolysed, typical molecular weight 146000-180000, herein referred to as PVA) was used as the polymer (see chapter 3). HEC was the preferred polymer simply because it is easier and faster to produce an aqueous solution of it in comparison to PVA. 1.5 g of the polymer was placed in a suitably sized powder round and made up to 100 g with water, thus generating a 1.5 % w/w aqueous polymer solution. For the HEC solution, vigorous stirring at room temperature for ca. 4 hours was necessary in order to fully dissolve and dissipate the polymer. For PVA, it was necessary to heat the solution in an oven at 90 °C overnight in order to fully dissolve the polymer, hence the initial preference for HEC. Once cool, the PVA solution requires stirring for 30 minutes before use to ensure homogeneity.

To prepare the ink, 3 g of the 1.5 % w/w polymer solution was placed in a suitably sized sample vial and to it was added the SED. For the bulk of this work, the SED used was glycerol (supplied by Aldrich, A. C. S. reagent, 99.5+ %). However, other compounds, the majority of which were polyols, were also assessed as potential SEDs in the characterisation of the photocatalyst indicator ink based on 2,6-dichloroindophenol (chapter 3). For the standard ink formulation, 0.3 g of glycerol (or other SED) was added to the polymer solution and the resulting mixture was gently stirred at room temperature for at least 5 minutes to ensure homogeneity.

The final component of the photocatalyst indicator ink formulation to be added was the dye. For the bulk of the work conducted on Activ™ self-cleaning glass (i.e. chapters 3 and 4), 2,6-dichloroindophenol (DCIP, supplied by Alfa Aesar, sodium salt hydrate, 98 % dry weight) was used, although other dyes examined for their suitability in the standard Activ™ indicator ink formulation were resazurin (Rz, dye content 95 %), methylene blue (MB), and resorufin (Rf, sodium salt), all three of which were supplied

by Aldrich. For DCIP, MB and Rf, 5 mg of dye was added to the formulation, resulting in an ink which, when cast as a dry film using the standard protocol described below, gave similar peak absorbance values at their λ_{\max} ; for Rz, 4 mg of the dye was added to the indicator ink formulation to produce a similar peak absorbance to those of the other inks used in this work.

For the Activ™ indicator inks based on MB, Rz and DCIP, the components were added in the order as they are described above, i.e. polymer/SED/dye. For the Rf indicator ink, however, it was found to be necessary to add the dye to the polymer solution prior to the SED. Addition of Rf after the SED had been added to the ink formulation resulted in an ink which was red/brown in colour as opposed to the deep pink anticipated, with the dye also appearing slightly insoluble.

Since the DCIP indicator ink described above was found to only be suitable in the measurement of the photocatalytic activity of thin, low activity TiO₂ films, such as that found on Activ™ (15 nm) or on the paste films annealed at high temperature in chapter 5, an indicator ink based on Patent Blue VF (PB, sodium salt, supplied by Fluka) was developed for the assessment of the thicker, more active paste films described in chapter 5. This ink had a similar composition to that detailed above for the Activ™ indicator inks, with 5 mg of the dye added to the polymer/SED mixture. For the paste films annealed at higher temperatures (≥ 800 °C), the resulting drop in activity permitted the use of the DCIP indicator ink described above.

For the work conducted on the comparison between the dye families in an acidic photocatalyst indicator ink formulation, as described in chapter 6, i.e. the thiazine/oxazine/phenazine study involving MB, Thionine (Th, supplied by Aldrich), Toluidine Blue (TB, supplied by Aldrich), Brilliant Cresyl Blue (BCB, supplied by Fluka) and Safranin O (SO, supplied by BDH), the standard ink was prepared in a similar manner to that outlined above; for all dyes, 5 mg was added to the polymer/SED formulation. However, when preparing the acidic inks, a slight adjustment was made in order to alter the pH of the formulation. Rather than preparing an aqueous solution of the polymer, the HEC polymer was dissolved to a concentration of 1.5 % w/w in 10⁻² M

hydrochloric acid. The inks were then prepared as described above for the standard Activ™ indicator inks.

In all instances, following addition of the final component, the resulting ink solution was gently stirred for 5 minutes before being placed in an ultrasound bath and sonicated in water for 5 minutes. This process is thought to ensure complete dissolution of the dye in the polymer/SED mixture. The ink was then subjected to a further 30 minutes gentle stirring, after which point it was ready for use.

2.1.2. Pre-treatment of Activ™ Prior to Activity Measurements Using the Indicator Inks

The production of Activ™ self-cleaning glass (supplied by Pilkington Glass) has been discussed previously in section 1.5.1. In short, a thin (ca. 15 nm) photocatalytically active layer of anatase TiO₂ is deposited on the surface of soda-lime glass using an atmospheric pressure CVD technique⁴, producing a self-cleaning glass which appears slightly yellow (or smoky) to the eye. In order to minimise any fluctuations in the sample activity between tests, it was necessary to develop a protocol to generate a relatively reproducible sample surface between experiments.

A chamber was prepared for the pre-treatment method, which was effectively a box with a slot cut into the top and two small holes at the back, as shown in figure 2.1. The slot at the top was cut so as to be the size of a hand-held lamp. Two, 4 W UVC bulbs were mounted in the hand-held lamp to be used as the irradiation source for the cleaning procedure. Into one of the smaller holes at the back was fed a line of tubing from a Dresher bottle full of doubly distilled and deionised water, which air from a bench tap or a cylinder was flown through; the other small hole acted as an outlet. The Activ™ samples were initially wiped with a lens tissue soaked in ethanol before they were placed in the bottom of the chamber and irradiated under the UVC lamp for 50 minutes in the wet air stream.

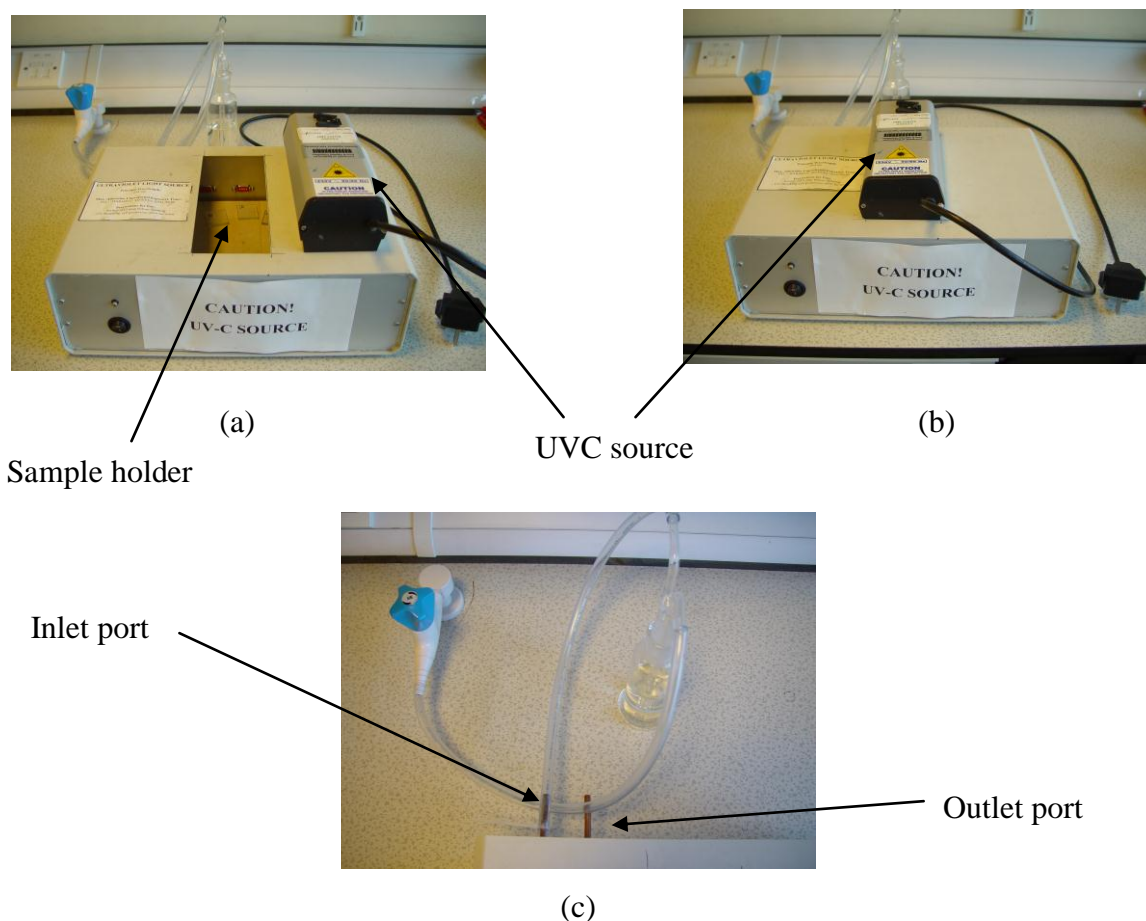


Figure 2.1.: The arrangement used to ‘clean’ the samples of Activ™. An enclosed box is used into which a slit is cut allowing a hand-held UVC lamp to be held in place in order to irradiate the samples (figures (a) and (b)). Over a period of 50 minutes, a stream of wet air is flown into the sample chamber from an inlet port to the rear (figure (c)) which acts in tandem with the UVC to ‘scour’ the sample surface, thus ensuring reproducibility

After 50 minutes had elapsed, the air stream to the box was closed off and the samples were irradiated under the UVC lamp for a further 10 minutes, after which time they were removed and were ready to use. This cleaning method builds from a previous technique used in this laboratory where wet ozone, as opposed to wet air, was flown into the chamber⁵. The rationalisation for using ozone was that, in conjunction with the UVC source, a ‘scrubbing’ action would occur on the substrate surface, which would not only remove any grease and/or organics from the substrate, but would also render

the surface hydrophilic, making it ideal for coating with a water-based ink. However, tests conducted in-house (data not shown) indicated that there was no significant difference observed for the rate of reduction of a DCIP ink on Activ™ regardless of whether the flowing stream of gas constituted ozone or air. A stream of wet air was chosen owing simply to the safety issues associated with ozone.

2.1.3. Preparation of a Photocatalyst Indicator Ink Film

To prepare a film of the ink on the desired substrate, two methods could be employed. The main technique used during this work was spin-coating, for which an Electronic Micro Systems Model 4000-1 spin coater was used. Typically the substrates used were either Activ™ glass, which had been cut to specification (ca. 25 mm x 25 mm), a Hydrotec tile, again cut to personal specification (ca. 25 mm x 25 mm), or a quartz disc on to which a TiO₂ paste film had been annealed (25 mm diameter; see section 2.2.2. for more details on the preparation of the TiO₂ paste films on quartz). Approximately 1 mL of the ink was smeared over the substrate surface using a Pasteur pipette before spinning the substrate at the desired speed. For the bulk of this work, and therefore unless stated otherwise, the substrate was spin-coated at 500 rpm for 15 s. The ink film was then dried on the substrate surface by placing in an oven at 70 °C for 10 minutes. It should be noted, however, that allowing a spun-coated Activ™ sample to dry in ambient air (ca. 60 % humidity and 20 °C) in a darkened cupboard for 1 hour resulted in similar kinetic behaviour for the photocatalytic reduction of the dye as to what is observed when the ink is dried on the substrate surface in an oven (data not shown). After this oven-drying period, the sample was allowed to cool briefly in ambient air before proceeding with the irradiation of the ink. Ink films produced in this way are referred to as ‘dry’, despite feeling slightly tacky to the touch.

Alternatively, the ink could be applied on to the substrate surface using a refillable, felt-tipped pen. Such refillable pens can be purchased from most art stores (for the bulk of this work, a Copic marker or metal-bodied felt-tip pen was used) and resemble that shown in figure 2.2. In order to enhance the ink colour delivered from such pens, it was necessary to increase the dye loading level in the ink three-fold (i.e. to 15 mg per

formulation for DCIP, MB and Rf, and to 12 mg per formulation for Rz). Depending on the pen used, ca. 6-10 mL of the ink could be loaded into the pens from a Pasteur pipette before saturation point was achieved. The pens were then given ca. 30 minutes in order for the ink to diffuse through from the bulk to the nib before use. As was alluded to earlier in section 2.1.1, the inks prepared in this work bear some resemblance to those used in fibre-tip pens¹, and hence are suitable for such a purpose.



Figure 2.2.: A typical sample of the standard DCIP ink and a Copic felt-tipped marker

2.1.4. Assessment of the Photocatalytic Activity Using an Indicator Ink

The photoreduction reaction of any of the aforementioned inks was monitored in most instances using UV-Visible spectroscopy. Depending on the atmospheric conditions under which the reduction reaction was to be monitored, the spun-coated substrate was placed in a specially designed spectrometer sample cell holder, shown in figure 2.3. The cell holder could be used directly to assess the reduction reaction under ambient atmospheric conditions; however, it could also be modified in order for the reduction reaction to be monitored under other atmospheric conditions, namely anaerobic or oxygen-saturated atmospheres, as supplied from a gas cylinder. For such experiments, the sample was mounted in a reverse position to that described above, the chamber to

which the sample was exposed to being sealed off with a coverslip, since these absorb a negligible amount of any incident UVA light, hence subjecting the ink film to the desired atmospheric conditions. It should also be noted that such work was only possible when Activ™ was the substrate under test owing to the cell holder design.

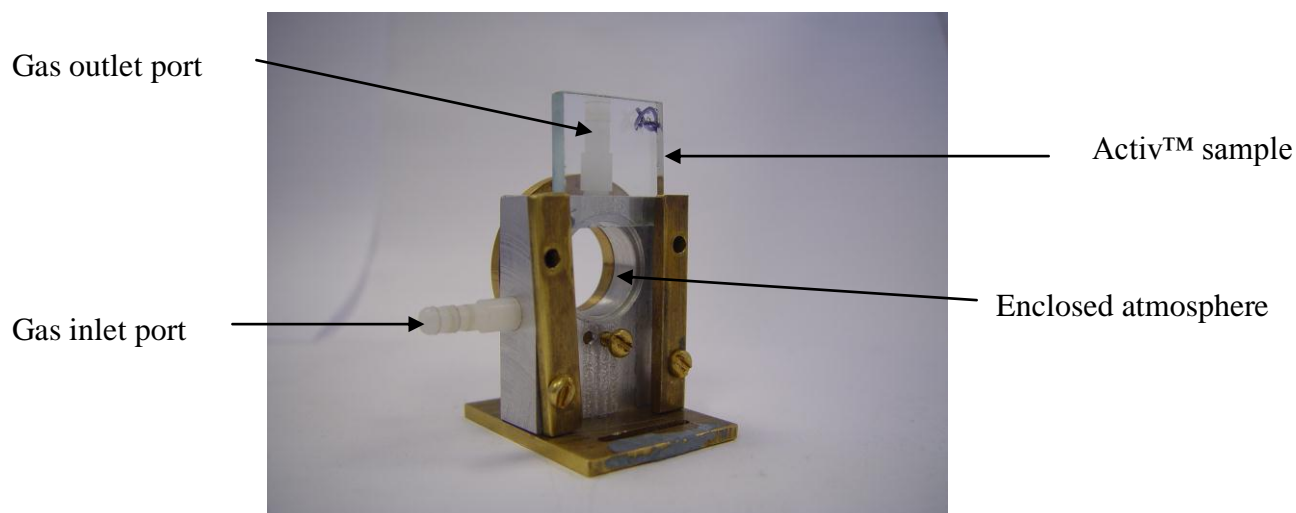


Figure 2.3.: The sample cell holder used to irradiate indicator ink films on Activ™ self-cleaning glass under various atmospheric conditions

Under these various atmospheric conditions, the relative humidity that the sample was subjected to, when held under a cylinder atmosphere, was ca. 10 % as measured using a Hanna Instruments HI 8564 thermo hygrometer. In order to alter the relative humidity, the gas stream could be flowed through a Drescher bottle full of water prior to the cell holder, creating an atmosphere with a relative humidity of ca. 100 %.

For all experiments conducted under ambient atmospheric conditions, the spun-coated sample could be used once cooled having been dried either in the oven or in a cupboard; for experiments conducted under other atmospheric conditions (i.e. O₂ concentration and/or humidity), once the sample had been removed from the oven and allowed to cool briefly, it was transferred to the specially-designed cell holder shown in figure 2.3. and held under the desired conditions for 10 minutes prior to irradiation. In doing so, most, if not all of the ambient atmosphere enclosed in the cell chamber would be flushed out.

The flow of gas into the cell was maintained throughout the irradiation at ca. 500 mL min⁻¹.

All UV-Visible spectroscopy was conducted using a Cary 50 Bio Varian spectrophotometer. Absorbance measurements were typically recorded over the wavelength range 300 – 800 nm at a scan rate of 4800 nm min⁻¹. Compatible PC software distributed with the spectrometer was used to record and manipulate the obtained data.

Unless stated otherwise, samples were irradiated using a 2 x 4W UVA Black Light Blue (BLB), hand-held lamp, as shown in figure 2.4. The irradiance of all lamps used in this work was measured using a Multi-Sense™ MS-100 Optical Radiometer and reported in mW cm⁻². For comparison⁶, the typical UVA output from the sun on a summer's day is ca. 4.49 mW cm⁻².

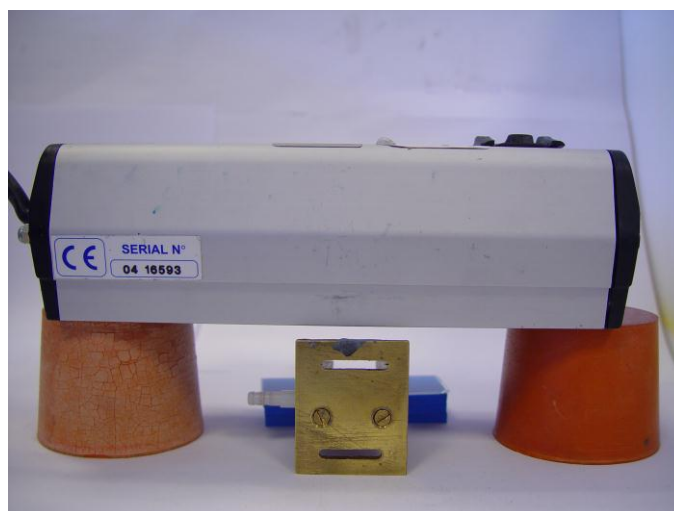


Figure 2.4.: The typical positioning of the Activ™ sample under the UVA source in the specially designed cell holder. By adjusting the distance between the sample under test and the lamp, the irradiance could be altered

The irradiance provided by the lamp could be altered simply by adjusting the distance between the lamp and the sample. It is important to note that in all instances, the lamp

was switched on a minimum of 30 minutes prior to commencing the experiment. The irradiated sample was removed from under the lamp at designated time intervals (usually in the region of 10 s – 10 minutes depending on the observed/anticipated rate of photoreduction) in order to measure the UV-Visible absorbance spectrum.

The photocatalytic activity of Activ™, or any other thin film semiconductor, can be quoted via the indicator ink test using one of two methods. In the first method, the initial rate of reduction (referred to throughout as r_i for all tests) of the dye under test could be determined, giving a measure of how rapidly the absorbance at the peak wavelength changes initially with irradiation time. This factor was calculated as follows. Figure 2.5. shows the standard absorbance spectrum obtained for the DCIP ink on Activ™ and its subsequent change in spectral shape with increased UV irradiation. The inset diagram shows how the absorbance at the wavelength of maximum absorbance (herein referred to as λ_{\max}) varies with time. Using the inset diagram in figure 2.5., the initial rate of reduction of the encompassed dye is calculated based upon the time taken for this initial absorbance at λ_{\max} to drop by 20 %. In practice, an exact decrease in the peak absorbance of 20 % was rarely achieved, hence results acquired both prior to and directly after this calculated value were used and an average r_i determined from them.

In some instances, the rate of reduction was too rapid to allow accurate measurement of the initial rate to be possible. Hence, the second method which could be used was to report the rate of photoreduction in terms of the $t_{50\%}$, i.e. the time taken for the initial absorbance to decrease by 50 % from its original value. The first step in calculating the $t_{50\%}$ for any process involves ascertaining whether the kinetics are zero or first order. It is now generally accepted following other work conducted in this laboratory⁷, and from results presented later in chapters 3 and 4, that the photoreduction of the dyes MB, DCIP and Rz in indicator inks on Activ™ follows a zero-order mechanism, i.e. the rate of reduction is independent of the amount of dye present. It is therefore assumed that all dyes, when encompassed in this indicator ink formulation, will adhere to such kinetic behaviour, and hence this theory is applied here.

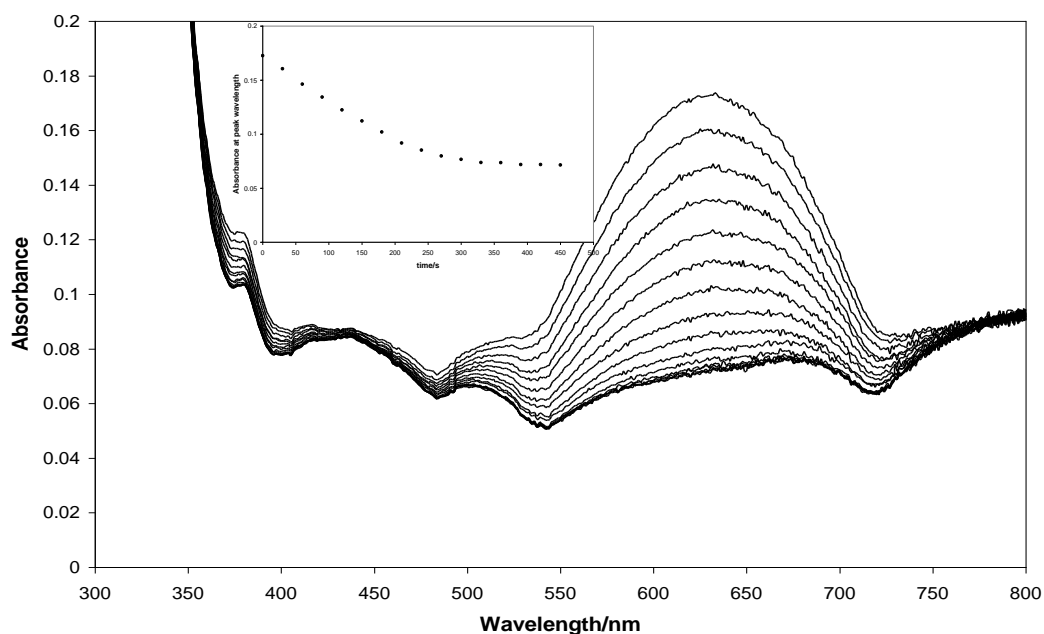


Figure 2.5.: The typical change in the absorbance spectrum of the DCIP indicator ink with irradiation time, and (inset) the change in the absorbance at λ_{\max} with time

The zero order rate equation is expressed in equation 2.1.⁸;

$$r = -\frac{dD}{dt} = k \quad (2.1.)$$

where r denotes the rate of reaction, t is the time, k is the zero order rate constant and D is a species associated with the reaction, i.e. the dye in our indicator ink formulations. By rearrangement and integration of this differential equation, we obtain equation 2.2.;

$$[D]_t - [D]_0 = -kt \quad (2.2.)$$

where $[D]_t$ and $[D]_0$ denote the concentrations of species D at a given time t and $t = 0$ s, respectively. To calculate the t_{50} %, we let $[D]_t = [D]_0/2$, such that the integrated zero order rate equation now reads;

$$\frac{[D]_0}{2} - [D]_0 = -kt_{50\%} \quad (2.3.)$$

This equation can be rearranged to give an expression for $t_{50\%}$;

$$t_{50\%} = \frac{[D]_0}{2k} \quad (2.4.)$$

In most instances in the results and discussions chapters which follow, both the rate of reduction, r_i , and the appropriate $t_{50\%}$ value are reported for the process.

For the application of the indicator inks to paste films annealed at higher temperatures, as described in chapter 5, and indeed to samples of Hydrotect tile, it is not possible to use UV-Visible spectroscopy to monitor the reduction reaction for the ink. Instead, diffuse reflectance spectroscopy is used. As the name suggests, rather than measuring the amount of light absorbed by a sample, diffuse reflectance spectroscopy measures the amount of light reflected by a sample at various wavelengths over the UV-visible wavelength range. In this work, a lambda 35 UV-Visible spectrometer was fitted with a Labsphere RSA-PE-20 Reflectance Spectroscopy Accessory. A reference disc supplied with the instrument was used to calibrate it and a red cardboard test card was scanned prior to testing in order to confirm that the accessory had been fitted properly. The wavelength range scanned was similar to that used in UV-visible spectroscopy. Figure 2.6. shows the diffuse reflectance accessory used.

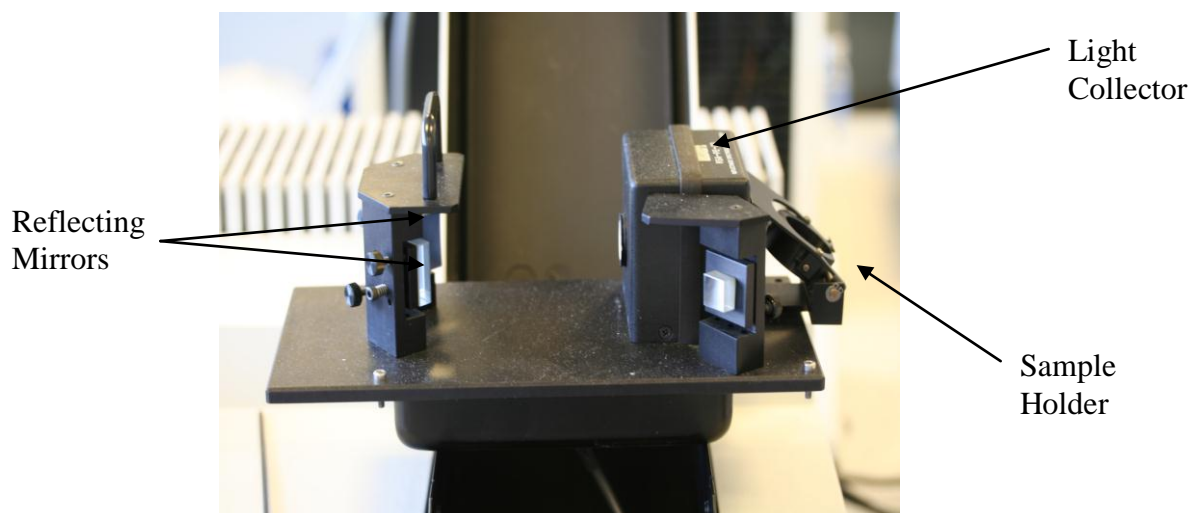


Figure 2.6.: The diffuse reflectance accessory used in this work with the major components highlighted

2.2. The Production of Paste Films and the Measurement of Their Photocatalytic Activities

2.2.1. Synthesis of a TiO_2 Paste for the Preparation of Photocatalyst Films of Varying Activity

The TiO_2 paste used in this work was prepared via a sol-gel technique according to a similar method first outlined by Barbé et al⁹, who were interested in preparing such a formulation for use in their research into dye-sensitised solar cells. The modified paste preparation method described below has previously been used by others in this group to prepare thick (estimated 4 μm) TiO_2 paste films on both quartz and glass¹⁰⁻¹¹.

The TiO_2 paste preparation can be broken down into three main steps, namely:

- Hydrolysis of the titanium precursor and synthesis of TiO_2 via a sol-gel process/peptisation;
- Particle size growth at high temperature and pressure via Ostwald ripening, and;
- Reduction of the sol-gel solution to form the paste

For this work, the titanium precursor used was titanium (IV) isopropoxide (supplied by Aldrich, 97 %). Initially, 4.65 g of glacial acetic acid (supplied by Aldrich, 99 – 100 %) was placed in a round-bottomed flask. Then, using a syringe, 20 mL of the titanium tetraisopropoxide precursor was added to the acid. Due to the high sensitivity of this precursor to moisture, it was necessary to attach a needle to the end of the syringe and then add the precursor with the tip of the needle below the surface of the acid. Almost immediately, the round-bottomed flask became warm to the touch due to the highly exothermic nature of the reaction.

This ‘pre-reaction’ of the precursor with acetic acid is based on research conducted by Doeuff et al¹². Their work looked at the hydrolysis of titanium n-butoxide by acetic acid and how varying the ratio present, and the amount of water present, affected the properties of the TiO₂ produced. Of greatest importance for the work here was their observation that whenever acetic acid is added to the alkoxide prior to hydrolysis, no precipitation occurs, thus preventing colloid formation and facilitating the production of the TiO₂ sol-gel.

By using acetic acid, the authors¹² observed that the acetate anion was able to replace some of the n-butoxide groups bonded to the titanium, presumably since addition of the acid protonates these groups and thus increases their lability, making them susceptible to nucleophilic substitution. In doing so, mixed-ligand titanium species were formed, provided the molar ratio of acetic acid to titanium was < 2.

Following this pre-reaction of the titanium tetraisopropoxide, in a separate 250 mL conical flask, 120 mL of doubly distilled and deionised water and 1.08 g of concentrated nitric acid were added together and rapidly stirred. To this solution was then added the modified titanium precursor solution described above. Upon addition of the modified precursor¹³, the alkoxide/acetate groups bound to titanium will be hydrolysed by the water to produce titanium hydroxide, presumably via a S_N2 nucleophilic attack mechanism¹³, the nitric acid present acting as the catalyst for the process. Since some of the isopropoxide groups are believed to be substituted by acetate groups prior to hydrolysis, the subsequent condensation reaction described

below generates anisotropic polymeric TiO_2 , thus further eliminating any possible precipitation¹⁰ and hence colloid formation.

The generated titanium hydroxide units can then undergo one of two possible condensation steps. They can either react directly with the (acetate-modified) titanium precursor units, or they can react with other titanium hydroxide units generated in situ via the hydrolysis reaction. In both instances, a $-\text{Ti-O-Ti}-$ linkage will be generated. It seems rational to assume that, initially, any titanium hydroxide functionalities formed by hydrolysis condense predominantly with the (modified) titanium precursor present. However, as the hydrolysis reaction continues, the concentration of this (modified) titanium precursor will decrease, and hence the concentration of titanium hydroxide increases. As a result, the balance would be expected to shift, such that condensation of two titanium hydroxide units would become the predominant process for formation of the $-\text{Ti-O-Ti}-$ linkage towards the end of the reaction.

The conical flask was then immediately placed in an oil bath on a hotplate stirrer equipped with a Fuzzy Logic temperature controller and stirred rapidly at 80 °C for 8 hours. During this time, the solution was observed to gel after only a few minutes, before reverting back to a liquid after 1-2 hours. This heating process promotes peptisation, whereby any agglomerates are destroyed and the resulting particles are re-dispersed throughout the solution⁹⁻¹⁰.

After this 8 hour period, the solution was typically left to cool overnight, producing a translucent blue/white solution sol. This solution was passed through a 0.45 μm syringe filter in order to remove any remaining larger aggregates which have not undergone peptisation¹⁰. It was then necessary to analyse the solids (i.e. TiO_2) content of the solution. This was done by placing a known mass of the solution in a sample bottle and evaporating down to the solids by heating at 450 °C in a Nabertherm Program Controller S27 furnace for 1 hour. Once allowed to cool, the remaining solids could be weighed and a yield determined. Typically, the solids content of the solution at this point was in the region of 5 – 7 %. Work conducted previously by this group estimates

the colloidal TiO_2 particles present at this stage to have a diameter of ca. 5 nm, as measured via transmission electron microscopy¹⁰.

After the determination of the TiO_2 solids content, 80 mL of the filtered sol was transferred from the conical flask to a 125 mL Teflon™ liner (supplied by Parr instruments). The lid of the Teflon™ liner was sealed with Teflon™ tape before the liner and its contents were placed in an acid digestion bomb (supplied by Parr instruments), the major components of which are shown in figure 2.7. Once sealed, the acid digestion bomb was placed in an oven at 220 °C for 12 hours. The high temperature of the oven and the high pressure created by the acid digestion bomb combine to increase the solubility of the colloid, which in turn encourages the growth of TiO_2 crystals¹⁰.



Figure 2.7.: The major components of the acid digestion bomb

This crystallisation of the TiO_2 occurs by a process known as Ostwald ripening¹⁴, which is a spontaneous process whereby larger crystals are formed in preference to smaller ones, owing to the former being energetically (i.e. thermodynamically) favourable and the latter being more readily soluble despite their kinetic favourability. Molecules on the surface of any material are more unstable than those in the material bulk since they are not subjected to as many of the intermolecular and lattice forces which aid in

keeping a solid together. However, those molecules on the surface of a large crystal will be more energetically stable than those on the surface of a smaller crystal, due to the greater volume to surface area ratio. As a result, as our TiO₂ system attempts to lower its energy in the acid digestion bomb, molecules on the surface of smaller crystals tend to diffuse back into solution, whereby they can then become incorporated into developing, larger crystals. The size of the resulting large TiO₂ crystals generated by this process, as a result, are found to be relatively uniform, since the growth is controlled by the energy associated with each crystal¹⁰.

After heating for 12 hours, the acid digestion bomb is typically left to cool in the oven overnight. The next day it was found that the TiO₂ solution had separated into two distinct layers. To the bottom of the Teflon™ pot, the larger TiO₂ particles could be found agglomerated into a solid, whilst above this layer there was found to be a milk-white, opaque solution. In order to re-disperse the accumulated large particles in the underlying solid back into solution, it was necessary to sonicate using a Lucas Dawe Ultrasonics Soniprobe. The sonication probe was immersed deep in the Teflon pot, and the solution was sonicated for ca. 3 minutes at full power, or until all the solid agglomerated TiO₂ particles present were observed to have re-dispersed.

Once again, at this point the solids content of the solution was measured using the same method as described previously. Typically, a TiO₂ content of 5 – 7 wt% was once again observed. TEM analysis conducted previously by this group¹⁰ has shown that the TiO₂ particles at this stage in the synthesis are typically 10 – 15 nm in diameter, validating the theory that Ostwald ripening, whilst primarily acting to increase the particle size, also generates a narrow particle size distribution.

The final step in the preparation of the paste was to concentrate the TiO₂ content of the solution via reduction. After sonication, the solution was transferred from the Teflon™ pot to a round bottomed flask, and then subsequently connected to a Bibby RE200 rotary evaporator. The rotary evaporator was held under vacuum and the water bath set to ca. 40 °C. As the TiO₂ was concentrated, usually over a period of ca. 1 hour, the solution was observed to change in viscosity, presumably since the large colloidal

particles formed via Ostwald ripening are brought together as the liquid is removed. Eventually, a material resembling sandwich mayonnaise in both viscosity and appearance was generated. The solids content was once again measured in order to ensure that the TiO_2 had been concentrated sufficiently. If the solids were found to be in the region of 10 – 12 wt%, the reduction reaction was deemed complete. If the value obtained was lower than this, further rotary evaporation was required. On the contrary, a paste with higher solids content required dilution with doubly distilled and deionised water.

The paste recovered was weighed by transferring the contents of the round-bottomed flask to a powder round; typically, 10 – 20 g was generated per synthesis according to the production outlined above. Based on the results from the determination of the solids content, it was possible to equate the mass of paste recovered to an actual mass of TiO_2 present. Using this TiO_2 mass, to the paste was then added 50 wt% of carbowax (20 M, supplied by Supelco, also referred to as polyethylene glycol) which had first been ground into fine particles using a mortar and pestle. The resulting mixture was stirred until the carbowax had fully dispersed in the paste, a process which typically occurs overnight.

The longevity of the paste was indefinite provided that it was sealed in a powder round with some Parafilm™ and stored in a refrigerator. Prior to casting films, the paste was stirred on a hotplate stirrer at room temperature for 15 – 20 minutes, since prolonged storage caused some separation of the paste to occur, with two layers visible in the sample vial.

2.2.2. Preparation of a TiO_2 Paste Film

Films of the paste were laid down on an appropriate substrate (which is quartz for the bulk of this work, but can also be glass) using a doctor-blade method, as shown figuratively in figure 2.8. Prior to casting a film, the substrate (20 or 25 mm quartz disc) was firstly wiped with a lens tissue soaked in ethanol in order to remove any residual organics or grease from its surface. It has also been observed that wiping with

ethanol aids in the prevention of film cracking as the paste film cools in the furnace after annealing (detailed below).

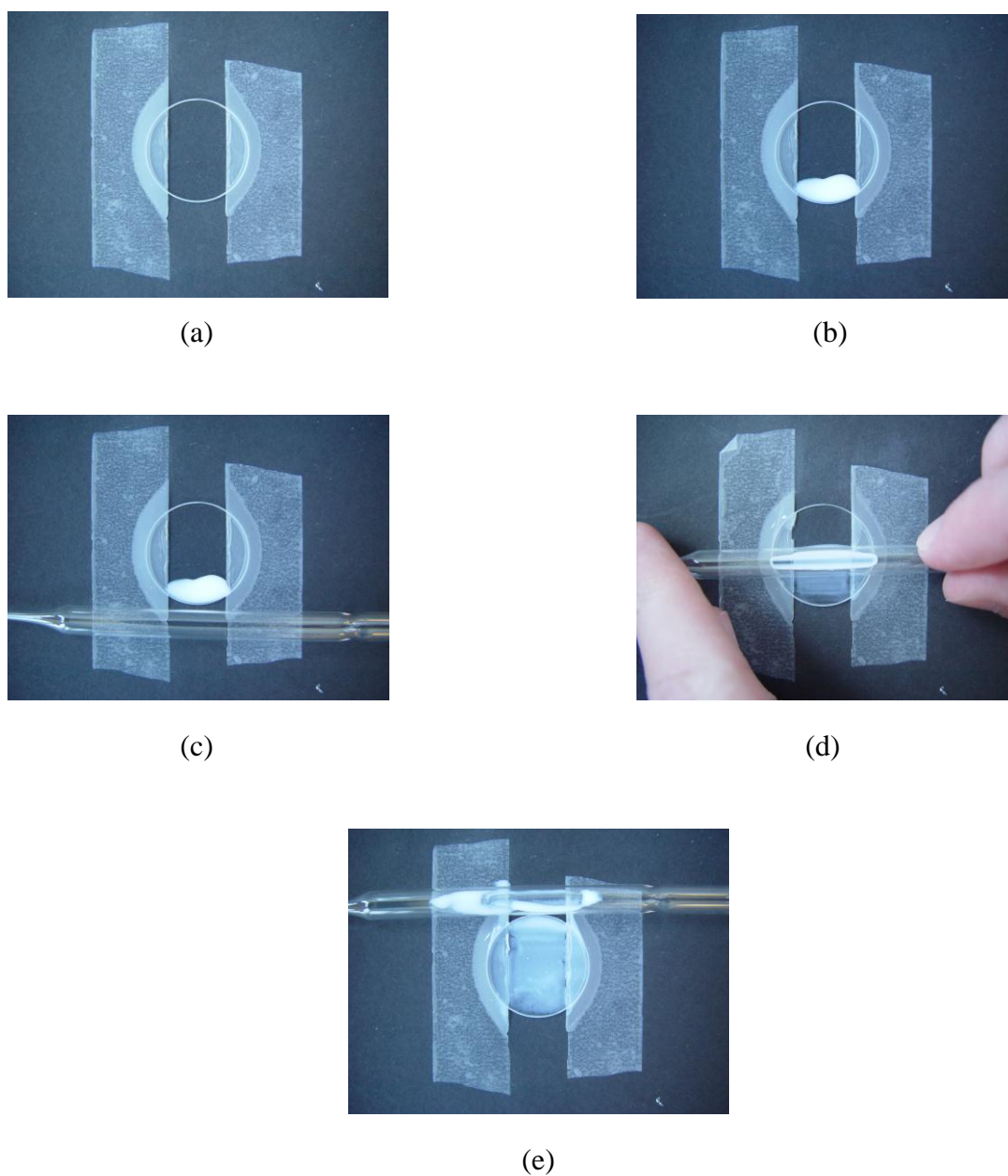


Figure 2.8.: The generation of a TiO_2 film from paste. Initially a quartz disc is taped down with a layer of Scotch Magic Tape™ (a) and a spatula-tip of paste is applied (b). The paste is then doctor-bladed across the sample surface using the edge of a Pasteur pipette (c)-(e), creating the paste film, the opacity of which decreases as it dries due to a reduction in the film thickness

Once wiped, the substrate was taped down to a suitable support using Scotch Magic Tape™. The tape was laid down so as to create a substrate ‘track’ ca. 15 mm wide, on to which the film is cast. Using the tip of a spatula, a small sample of the TiO₂ paste was deposited at one end of the substrate and gently smeared to cover the width of the visible substrate between the tape tracks. The paste was then drawn down the substrate strip using the edge of a Pasteur pipette and left to dry. During the drying process, the opacity of the film was observed to decrease until the film was translucent and slightly blue to the naked eye. Previous work by Mills et al¹¹ has monitored the change in absorbance of the film during this drying period and demonstrates that the film evaporates from an initial thickness of ca. 60 μm when cast, to ca. 4 μm when dry, which is believed to be the cause of the reduction in the observed opacity.

Once all of the TiO₂ paste had dried on the substrate surface, the tape tracks were removed and the sample was transferred to a furnace in order to anneal (or calcine) the film. The furnace, a Nabertherm Program Controller S27 furnace as used previously in the determination of the solids content of the paste, could be set to any temperature ≤1100 °C. The standard temperature for annealing a paste film was 450 °C, based on previous work conducted within this laboratory, where it was demonstrated that such films were anatase in nature¹⁰ and exhibited a high photocatalytic activity towards stearic acid removal¹⁰⁻¹¹. Typically 5 samples of the film were prepared at each temperature.

All paste films were subjected to a ramping increase in temperature of ca. 30 °C min⁻¹ and were then held at the appropriate annealing temperature for 30 minutes, before being allowed to cool naturally (usually overnight) within the furnace. Removing the films from a furnace which has only begun to cool naturally, or rapidly cooling the furnace by exposing its interior to the laboratory temperature was observed to increase the probability of film cracking, particularly for low temperature (i.e. 450-600 °C) films on quartz. Using glass appears to provide the film with a greater mechanical stability, but limits the temperature range over which paste films can be annealed since it has a lower melting point compared to quartz.

2.2.3. Characterisation of the Annealed Paste Films

The TiO₂ films produced using the doctor-blade method were characterised by UV-Visible Spectroscopy, Diffuse Reflectance Spectroscopy, Scanning Electron Microscopy (SEM), Atomic Force Microscopy (AFM) and X-ray diffraction (XRD). Both SEM and AFM allow surface ‘maps’ of the films to be produced, whilst the purpose of XRD in this work was to analyse the anatase:rutile ratio within the film and, using various equations, allow the determination of the crystallite size present. Whilst unable to provide a qualitative description of the film in terms of its particle size and phase components, UV-Visible spectroscopy gives a measure of the degree of light scattering from a sample, and thus allowed rapid comparison between samples annealed at the same temperature, highlighting any inconsistencies. As the annealing temperature increases, the opacity of the films also increases, particularly above 800 °C, and with this comes a marked change in the UV-Visible absorbance spectrum. This increase in opacity is thought to be due to an increase in the particle size of the TiO₂ film, which is confirmed through SEM and AFM analysis (see sections 5.1.3. and 5.1.4.).

UV-Visible spectroscopic analysis was again conducted using a Cary 50 Bio Varian spectrophotometer, set to scan at 600 nm/min over the wavelength range 200 – 800 nm. The sample was placed in a specially designed cell holder, similar to that used previously in the assessment of the indicator inks, and scanned in the dark in order to minimise any interference from laboratory light sources. For diffuse reflectance spectroscopy, similar equipment to that outlined previously in section 2.1.4. for monitoring dye reduction in the indicator inks on tiles was used here.

2.2.3.1. Scanning Electron Microscopy (SEM)¹⁵⁻¹⁶

Scanning electron microscopy (SEM) involves the use of a high energy beam of electrons incident on the surface of a sample in order to measure its topography. Typically tungsten, or another material which has a high melting point and a low vapour pressure, is used as a filament cathode in the electron gun. By heating the filament, a discharge beam of electrons is produced thermionically from the cathodic material. This electron beam varies in energy depending on the source, though is typically in the

range of several hundred to thousands of eV, and it can be focussed using a series of lenses and apertures to a desired spot diameter in the nanometre range. The beam is then passed through a set of charged plates, the potential between which can be altered, thus causing the beam to scan over the surface of the substrate under test in a ‘raster’ fashion. Such a process is remarkably similar to what is observed in a cathode ray tube present in most, admittedly older television sets.

When this incident beam of electrons is focussed on to the substrate surface, the electrons are absorbed by the atoms within the material to a surface depth representative of their incident energy, and of the substrate’s density and atomic number. Energy transfer from the beam occurs upon impact, resulting in the reflection of high energy electrons (i.e. back scattering) via elastic scattering, the emission of secondary electrons via inelastic scattering, or indeed the emission of a photon of light. Although all processes are viable, most mainstream SEM are equipped with a detector for only one of these processes, with secondary electron detection being the most common.

SEM analysis was conducted at the University of Glasgow under the supervision of Dr Laurence Tetley. Prior to recording data, the films were pre-coated with gold using a sputter coater in order to improve their electrical conductivity, and hence make them visible via SEM. A JEOL 6400 SEM was used to record the images operating at 6 kV with an ADDA3 digital image acquisition system (supplied by Olympus-Soft Imaging Solutions, Munster, GmbH). Images were recorded at low resolution (scale bar 5 μm) and, where possible, at a higher resolution (scale bar 1 μm) using a small portion of the paste film cleaved from the bulk, 25 mm quartz sample. It was also possible to use the system described above to view the edge of such fragments, allowing estimation of the film thickness to be made, simply by mounting the sample on the stage at a desirable angle. Measurements were obtained using iTEM image analysis software (supplied by Olympus-Soft Imaging Solutions, Munster, GmbH). For samples annealed at temperatures below 800 °C, it was found to be impossible to obtain clear SEM images at high magnification, believed to be due to charging effects, hence only low

magnification images were obtained for such samples. Figure 2.9. shows the high magnification SEM image of a paste film annealed at 1000 °C.

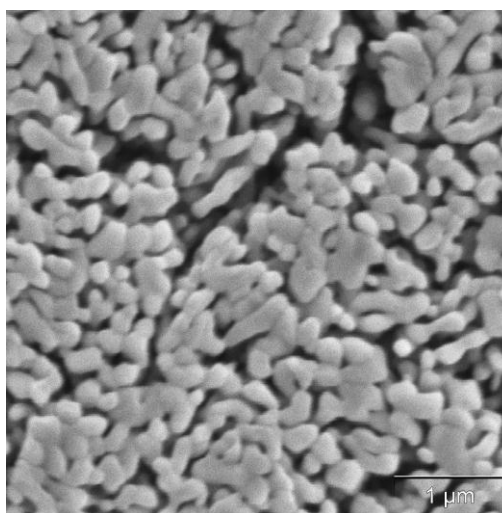


Figure 2.9.: The high magnification SEM image of a paste film annealed at 1000 °C

2.2.3.2 Atomic Force Microscopy (AFM)¹⁷⁻¹⁹

Atomic force microscopy (AFM) is an alternative surface analysis technique to SEM since it allows the imaging of surfaces which are non-conductive. It typically requires no pre-treatment so that, in effect, the sample is not destroyed by the technique and can be recovered at the end of the analysis; in SEM, non-conductive samples, such as the paste films generated here, must be rendered conductive via the application of a sputter layer (usually gold), which is difficult to remove. In AFM, the surface of the sample is scanned by a very small tip (nm range) attached to the underside of a stiff cantilever. Depending on the mode of operation of the AFM, the tip does not necessarily come into contact with the substrate; instead, the van der Waals forces which exist between the tip and the surface atoms of the substrate under test can cause the tip to be deflected, either due to attraction or repulsion. By focussing a laser on the reverse side of the cantilever from the tip, and through application of Hooke's law, the changes in the deflection due to such interactions between the tip and the surface atoms can be represented by changes in the direction of the reflected beam, which is captured using a photodiode.

The photodiode co-ordinates this output with the sample position to create an image of the substrate surface. Usually the cantilever is fixed whilst the sample is mounted on a stage and moved below it in a raster scan, building an image of the surface in a similar way to that described previously for SEM.

As was alluded to above, it is not necessary for the cantilever to actually come into contact with the surface in order to produce an image of it. Lateral force microscopy (LFM) makes use of the frictional forces between a surface and the cantilever tip, with the twist of the cantilever and the subsequent deflection of the laser producing an image of the surface. Conversely, noncontact AFM involves oscillating the cantilever at high frequency and pushing it so close to the surface that the attractive van der Waals forces are triggered, although contact between the surface and the tip is forbidden. The tapping mode AFM used in this work is similar to noncontact AFM, with the exception that the cantilever is oscillated closer to the sample surface, such that it does make contact with the surface. In general, tapping mode AFM is the preferred method since it gives improved lateral resolution on soft surfaces and eliminates drag.

AFM images were recorded under the guidance of Dr Pik Leung Tang at ambient atmospheric conditions using a Digital Instruments Nanoscope Multimode SPM with a JV-type scanner and a Nanoscope III controller. Tapping mode, silicon pyramidal cantilevers (Olympus) were used with a tip curvature of < 10 nm and a normal force constant of 42 N/m. Scans were carried out on the paste films over sample areas varying from $40\ \mu\text{m} \times 40\ \mu\text{m}$ to $150\ \text{nm} \times 150\ \text{nm}$ at a scan rate of 0.5-1.0 Hz and with a scan resolution of 512 lines per image. No image processing was conducted on any of the data presented here. Using the built-in instrument software, the particle size of the TiO_2 present in the film could be estimated from the AFM data provided. Figure 2.10. shows the output generated from an $1100\ ^\circ\text{C}$ paste film at both low and high magnification.

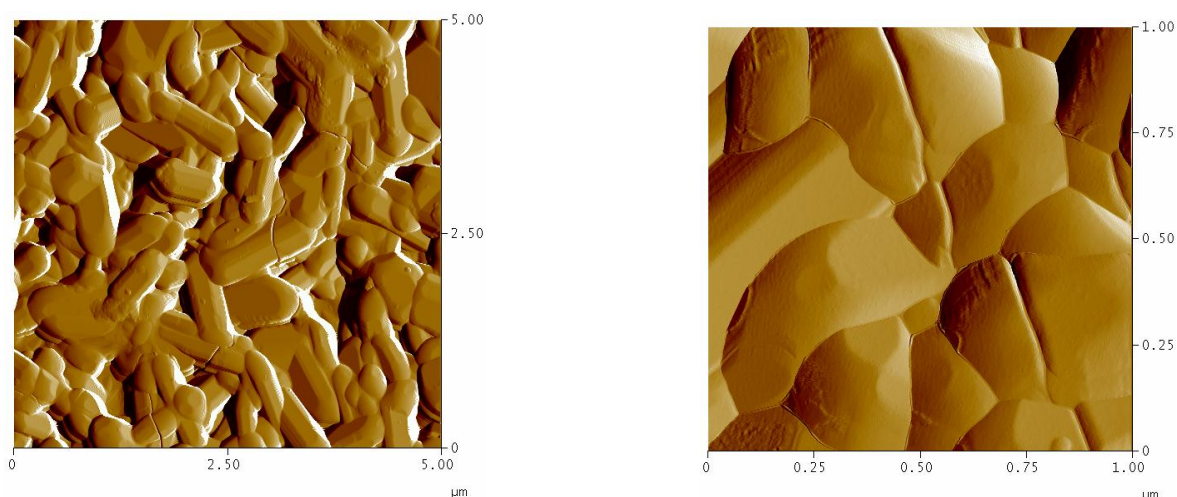


Figure 2.10.: The AFM images obtained for a paste film annealed at 1100 °C at low magnification (left) and higher magnification (right)

2.2.3.3. X-ray diffraction (XRD)^{8,17,20-21}

X-ray diffraction (XRD) was utilised in this work as a means of determining the relative anatase:rutile ratio of the annealed paste films and, through application of the Scherrer equation, the crystallite size of the TiO₂ present in the film.

X-rays are a form of electromagnetic radiation; hence they possess a wavelength in the region of 10^{-8} - 10^{-11} m. Within a well-structured crystal, the atoms/molecules are arranged in ordered, 3-dimensional distributions, forming a series of parallel planes, the distance between which is referred to as the interplanar spacing, d . This is a constant for each individual crystal system. In addition, this interplanar spacing is of the same order of magnitude as the wavelength of x-rays. When the x-rays are incident on the ordered planes present, it follows that diffraction can occur, since such planes can effectively act as a mirror, with the angle of reflection of the x-rays similar to that of the incident angle from the instrument.

If we consider two x-ray waves incident on a crystal, where the waves are reflected by different lattice planes within that crystal, we have the situation depicted in figure 2.11. When these two waves leave the X-ray source, they are either in phase (i.e. the peaks

and troughs of the individual rays match exactly) or they are out of phase. However, upon reflection from the aforementioned lattice planes within the crystal, it is more likely that the reflected beams will be out of phase. These reflected waves will destructively interfere, reducing the reflected beam intensity. However, under certain conditions, the reflected waves will emerge from the crystal in phase. This is termed constructive interference, and the intensity of the reflected beam will be greater than that of the incident beam.

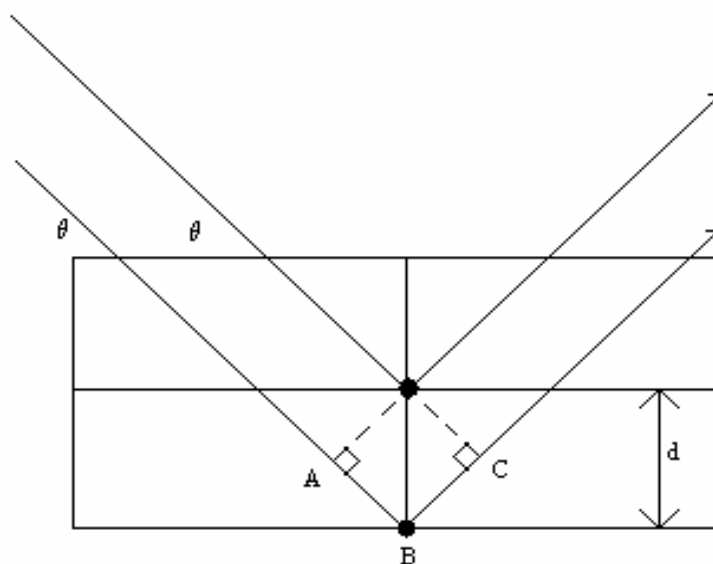


Figure 2.11.: The path of two separate x-ray beams of incident angle θ reflected by alternate lattice planes within a crystal, the distance between which is given by the interplanar spacing d . Note the difference in the path length between the two reflected waves is defined by $AB + BC$

It was found that for this constructive interference to occur, the path length difference (i.e. $AB + BC$ in figure 2.11.) must equate to some integral number of wavelengths, $n\lambda$. However, this path length difference is also observed to equate to $2d \sin \theta$, where θ is the incident angle and d is the interplanar spacing described above. Such a relationship is described accurately using the Bragg law given in equation 2.5., i.e.;

$$n\lambda = 2d \sin \theta \quad (2.5.)$$

The technique described above is more correctly defined as single crystal X-ray diffraction. However, not all substances can be used to grow high quality crystals, and hence an alternative method needs to be used to determine the structure of such compounds, e.g. the paste films used in this work. If these compounds can exist in powdered form, powder X-ray diffraction is one such technique. Here, all the crystallites present within the sample are randomly orientated; however, some will be orientated in such a way that they satisfy the Bragg condition stated above, i.e. they reflect incident x-rays constructively, providing a peak in the reflected x-ray intensity. By altering the angle of incidence over a defined range, the intensity of the reflected beam is altered according to the composition of the crystallite(s) present in the sample. As a result, an XRD spectrum can be generated for such samples.

For this work, since the three major phases of TiO₂ (namely anatase, rutile and brookite) exhibit peaks in a powder XRD at different incident angles, by scanning across a range of incident angles it is possible to determine the phase composition of the TiO₂ samples annealed at different temperatures. The XRD patterns recorded in-house for anatase and rutile are given in figure 2.12. The crystal planes associated with each reflection are also highlighted, as determined in work by Reyes-Coronado et al²² and from the standard XRD cards for both anatase (JCPDS 21-1272)²³ and rutile (JCPDS 21-1276)²⁴.

In addition to allowing an accurate determination of the phase composition of a TiO₂ sample, XRD data can also be used to provide a measure of the particle size (or radius), r , using the Scherrer equation²⁵, given in equation 2.6.;

$$r = K\lambda/\beta\cos\theta \quad (2.6.)$$

where λ is the wavelength of the incident x-rays, θ is the angle of incidence, β is the full width half maximum (FWHM) for the peak obtained in the XRD spectrum and K is the shape factor. The shape factor varies depending on the shape of the crystallite under test, but is usually quoted as being 0.9; hence this value is used here.

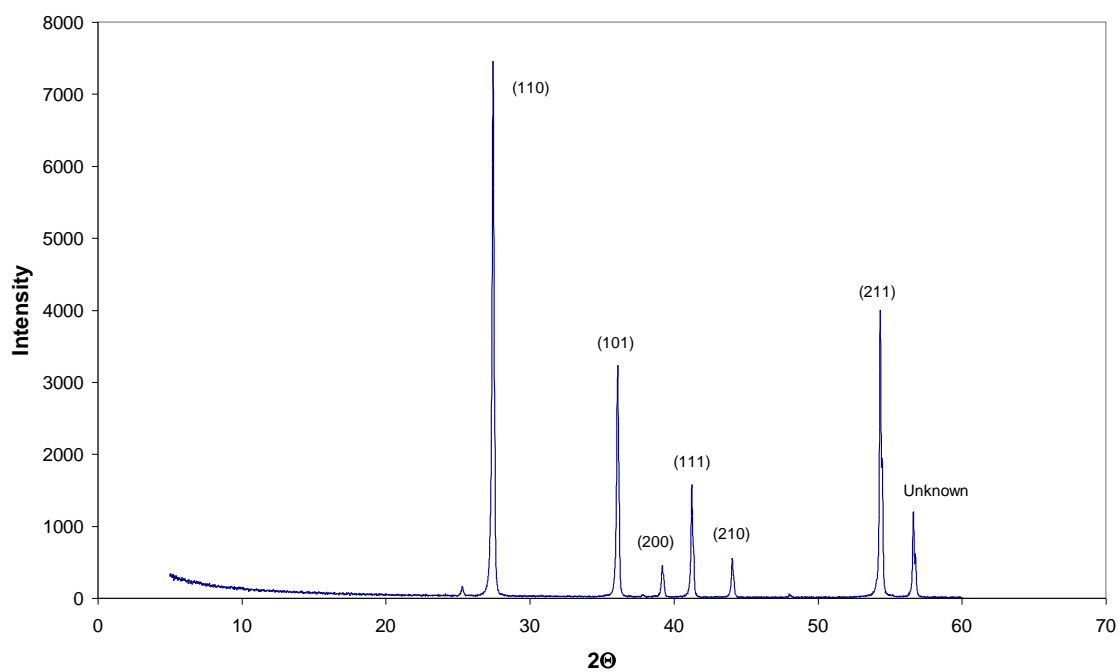
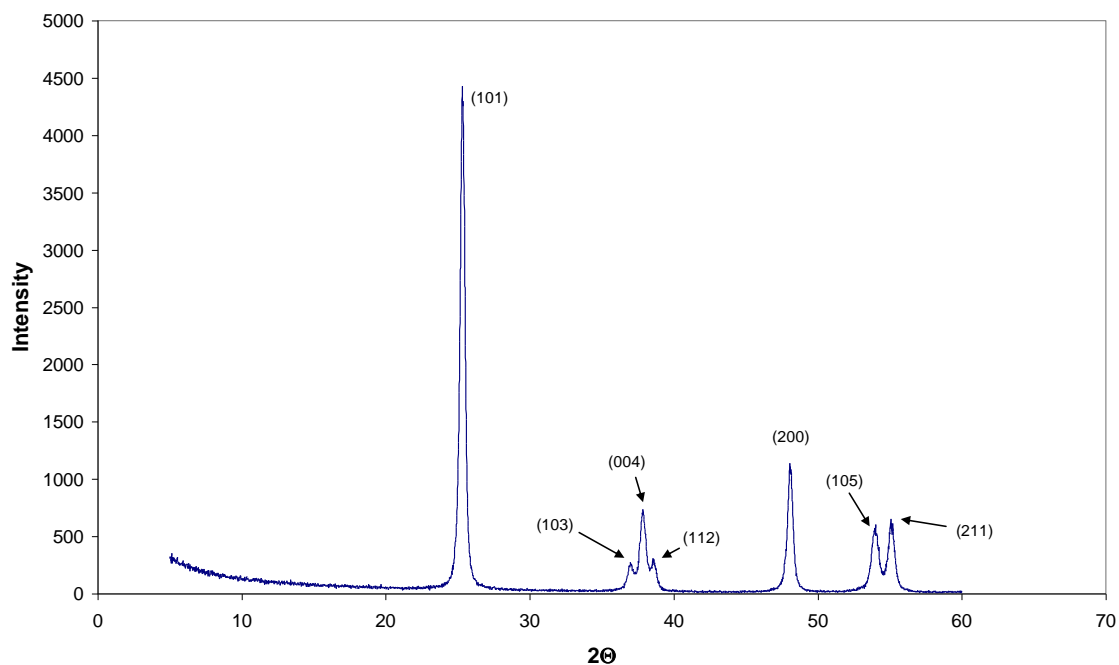


Figure 2.12.: The as-measured XRD spectra of pure anatase (top) and pure rutile, with the crystal plane reflections as indicated

Powder XRD patterns for the titania films produced in this work were recorded under the guidance of Dr Pik Leung Tang using a Siemens D500 powder diffractometer with a Kristalloflex 710 generator, the tube head of which was mounted at 30° to the vertical and operated at 40 kV and 20 mA. Copper was used as the target material, producing x-rays with a wavelength, λ , of 1.5406 \AA (Cu K- α). The output emitted from the sample following x-ray bombardment was detected using a scintillation counter. Samples were scanned over the 2θ range from 5 to 60° using a step scan mode of 0.04 degrees step size and 2 s count time per step. Intensity readings were recorded as a function of 2θ . Figure 2.13. shows the typical XRD output for a paste film annealed at 825°C , with the peaks due to anatase and rutile highlighted. The broad peak at low incident angles is due to reflection from the underlying quartz substrate.

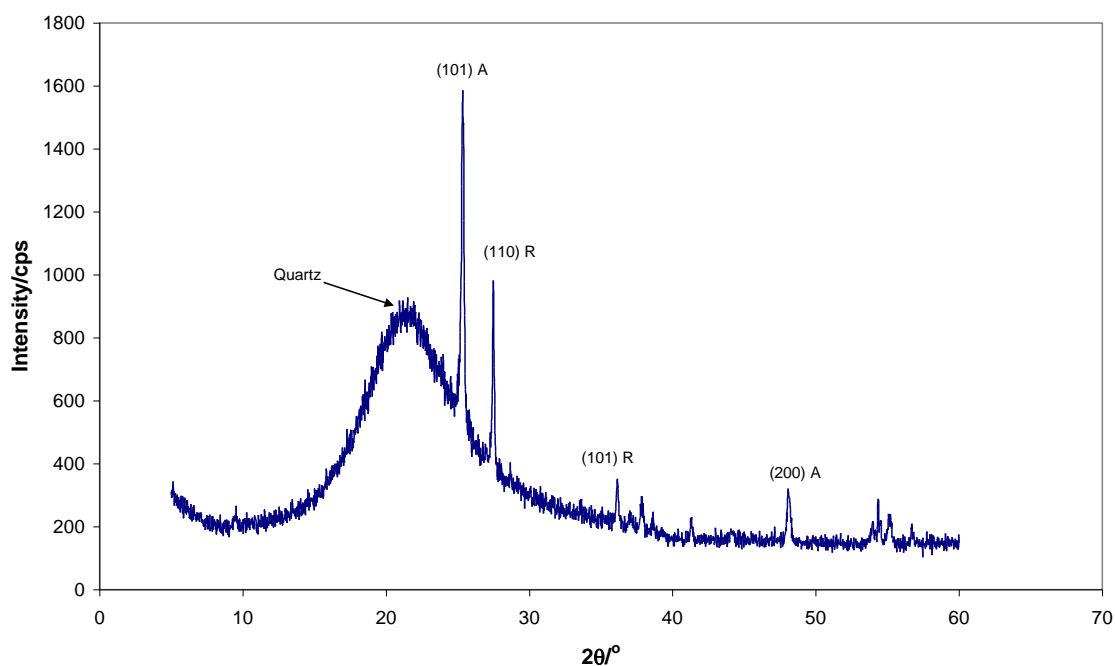


Figure 2.13.: The XRD spectrum of an 825°C paste film annealed on quartz, with the major peaks highlighted. Note that A denotes anatase, whilst R denotes a peak due to rutile

2.2.4. The Stearic Acid Test

One of the most common methods used to assess the photocatalytic activity of both laboratory-prepared and commercial titania films in the literature is to monitor the photooxidation of stearic acid. Indeed, this technique has been used previously within our laboratory to assess the photocatalytic activity of paste films prepared in a similar vain as to those detailed in this work¹¹ since stearic acid, when dried as a film on any surface, resembles the type of organic pollutants from the atmosphere which adheres to windows and exterior surfaces.

Stearic acid (supplied by Aldrich, 99+ %) was dissolved in chloroform (supplied by VWR) to a concentration of 30 g/L. Using a Pasteur pipette, 3 drops of this solution (equivalent to a volume of ca. 0.3 mL) were deposited on the substrate under test and subsequently spun at 500 rpm for 10 s. The spun-coated sample was then transferred to an oven at 100 °C for 30 s in order to remove any residual chloroform. Since stearic acid has a melting point of 69.6 °C, after drying in the oven it forms a waxy film on the substrate surface. After being left to cool briefly, the sample was ready for testing.

All stearic acid photooxidation experiments were monitored using Fourier Transform Infrared Spectroscopy (or FT-IR). Although both gas chromatography²⁶ and ellipsometry²⁷ have been shown in the literature to be useful for monitoring the removal of the organic film, FT-IR was chosen here since it is well established both within this laboratory and in the literature^{10-11,28-30} (or at least more so than that of gas chromatography and ellipsometry). It is also more straightforward to analyse, since the use of gas chromatography requires knowledge of conversion factors and the fabrication of suitable gas cells, and ellipsometry usually requires some form of modelling to be conducted in order to interpret the results. A complete infrared spectrum of the film (i.e. across a wavenumber range of 6000 – 450 cm⁻¹) was recorded at select time intervals during irradiation according to the observed or anticipated rate of photooxidation. Within this wavenumber range, stearic acid produces peaks at 2957.5, 2922.8 and 2853.4 cm⁻¹. The first of these corresponds to the asymmetric, in-plane C-H stretch of the CH₃ group, whilst the others correspond to the asymmetric and symmetric

C-H stretching of the CH₂ group respectively³¹. Using the built-in instrument software, it was possible to manipulate the data in order to determine the integrated area over the wavenumber range 3500 – 2500 cm⁻¹, which encompasses the aforementioned peaks. Usually, depending on the nature of the film, the initial integrated area was in the range of 8 – 15 Absorbance Units cm⁻¹ (herein shortened to A. cm⁻¹).

The stearic acid-coated sample was irradiated using a 6 x 8 W semi-circular UVA source, the centre of which was mounted 13 cm above the sample surface to provide an incident irradiance of ca. 2.4 mW cm⁻² for all films. It is important to note that the light source was switched on at least 30 minutes before commencing the experiment in order for the UVA output from the lamp to achieve maximum intensity. The TiO₂-coated quartz disc was held rigid in a specially-designed cell holder during irradiations which had been specifically designed for use in the FT-IR. A Perkin Elmer Spectrum One FT-IR Spectrometer was used for all infrared measurements. Figure 2.14. shows the peaks obtained for a stearic acid film over the range 3500-2500 cm⁻¹ coated on a paste film annealed at 450 °C, and the subsequent change in the peak shape with increasing UV irradiation.

Typically 3 – 5 stearic acid runs were performed on each annealed sample in order to assess the reproducibility of the film. Although most tests were run until all the stearic acid was removed from the sample surface (i.e. until the integrated area under the peaks was 0 A. cm⁻¹), it was still necessary between runs to treat the sample in order to remove any residual organic contaminants from the surface and to maintain surface reproducibility. The easiest way in which to achieve this cleaning of the surface was found to be a ‘burn-off’ of the organic film, which is achieved by heating the paste film at 350 °C for 1 hour in a furnace between runs. The temperature was chosen specifically to be lower than the minimum annealing temperature for the paste films (i.e. 450 °C) such that no further particle growth and/or phase changes would occur, whilst still being high enough to clean the sample surface. After this 1 hour heating period, samples could be removed from the furnace directly and allowed to cool in ambient atmospheric conditions before use.

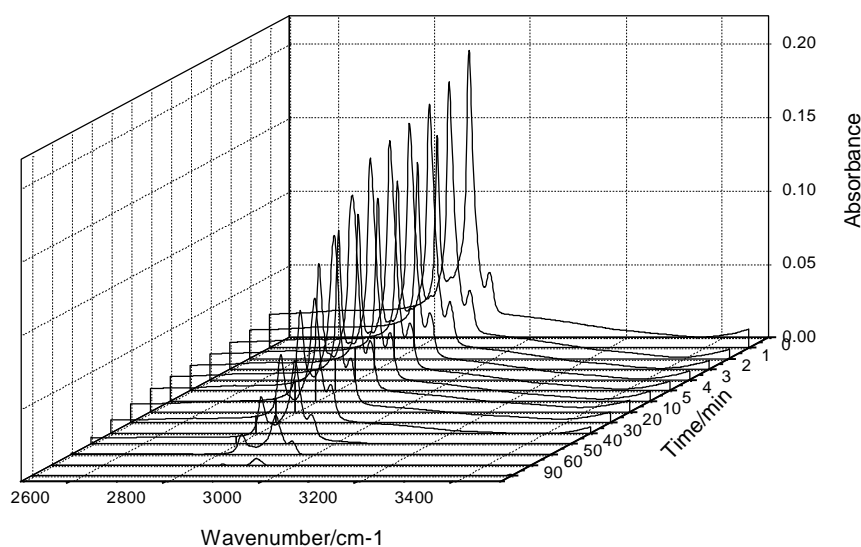


Figure 2.14.: The peaks observed due to stearic acid when the film is coated on to a 450 °C paste film, and the subsequent change in the peak shape with irradiation as the stearic acid is photooxidised

The initial rate of stearic acid photooxidation was measured assuming zero order kinetics, since this has been reported previously by others and is generally accepted within the literature, discussed in detail in chapter 5. It was assumed that the initial rate was indicated by the time taken for the initial integrated area of the aforementioned peaks to drop by 20 %. In practice, a measurement was rarely taken at a time interval corresponding to exactly 20 %, hence the initial rate was calculated using an average of the two measurements recorded prior to, and after this 20 % limit. In addition, the zero order $t_{50\%}$ could also be calculated using a similar method as discussed previously in section 2.1.4. for the photocatalyst indicator inks.

2.2.5. The Methylene Blue Test

Whilst the stearic acid test has emerged as one of the forerunning techniques to analyse the photocatalytic activity of TiO₂ films, the methylene blue test is as increasingly popular a test of the photocatalytic activity towards the removal of contaminants in

solution for both powders and films³²⁻³⁷. In this work, the paste titania film under test was placed in a specially-designed cell whereby the paste film was in contact with a methylene blue solution through a hole that had been cut into a plastic cuvette. The methylene blue stock solution (1×10^{-3} M) was prepared by dissolving 0.3739 g of methylene blue in 1 L of doubly distilled and deionised water, from which it was then possible to produce a 1×10^{-5} M solution. This latter solution is known to have a peak absorbance at 665 nm of ca. 1 when measured by UV-Visible spectroscopy owing to the molar absorptivity of the dye equating to ca. $10^5 \text{ dm}^3 \text{ mol}^{-1} \text{ cm}^{-1}$ at this wavelength³⁵. However, as a precaution, a fresh methylene blue solution was prepared from the stock every day and its spectrum recorded in order to minimise experimental error and detrimental photofading of the dye.

Approximately 10 mL of the 1×10^{-5} M methylene blue solution was added to the cuvette of the specially designed cell and the solution was vigorously stirred for 10 minutes in the absence of UVA light in order to allow any absorption of the dye from solution on to the paste film surface. Although it is probable that not all of the dye which is to absorb to the paste film surface will do so in this 10 minute period, it is believed that the majority of the available absorption sites on the film will become occupied during this time period, thus minimising any further absorption during photocatalysis and allowing a more accurate determination of the initial rate of photomineralisation. Previous work conducted by Xu et al suggests that 10 minutes is required for the dye to saturate all the available absorption sites when placed in contact with a solution of TiO_2 powder³⁷. After this 10 minute period, the spectrum of the solution was recorded before irradiation commenced, and in all instances was similar to that shown in figure 2.15. Similar to the stearic acid test, the illumination source was a 6 x 8 W semi-circular UVA lamp, mounted at an angle of 45° relative to the sample cell. The irradiance was measured as ca. 0.3 mW cm^{-2} from behind the paste film with the dye solution in place. As with the stearic acid test, it is important to note that the UVA source was switched on a minimum of 30 minutes before irradiations took place.

The sample was irradiated under stirring for time periods varying from 5 – 30 minutes depending on the anticipated or observed rate of mineralization. The specially designed

sample cell allowed the reaction to be followed using a Cary 50 Bio Varian UV-Visible spectrometer, since the solution changes colour from blue to colourless with the photomineralisation of the dye. The UV-Visible absorbance spectrum was recorded over the range 300 – 800 nm, with the spectrometer scanning at 4800 nm min^{-1} , between irradiations. The specially designed cell holder was crafted in such a way that it could be mounted in the spectrometer perpendicular to both the direction of irradiation and the paste film itself, thus enabling the spectrometer beam to pass through the solution without having to pass through the film. This is preferred since the paste film, particularly when annealed at high temperatures, has a strong absorbance spectra over the wavelength range used and hence would impact the observed MB spectrum with time. Such a setup also alleviated the need to remove aliquots of the dye at designated intervals.

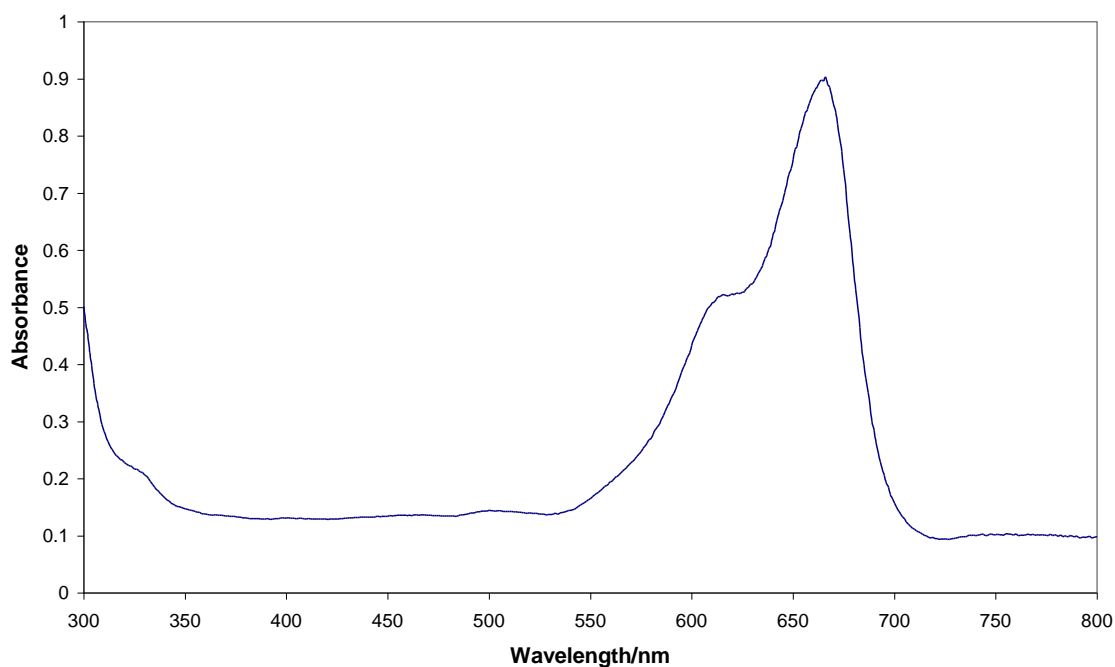


Figure 2.15.: The absorbance spectrum of a $1 \times 10^{-5} \text{ M}$ MB solution after being placed in contact with an $800 \text{ }^\circ\text{C}$ paste film for 15 minutes. Absorption of the dye by the underlying paste film has decreased the dye's peak absorbance by ca. 0.1 absorbance units

After each test, the sample was cleaned in a similar way as to the stearic acid tests detailed previously, whereby any residual MB solution which had absorbed to the paste film was ‘burned off’ by heating the sample at 350 °C for 1 hour. Typically, 3 – 5 methylene blue tests were run per sample. As with the stearic acid test, the initial rate of methylene blue photomineralisation was determined by measuring the time taken for the initial, peak absorbance at 665 nm to drop by 20 %. This was achieved by calculating the average rate from the readings prior to, and beyond this 20 % barrier. Alternatively, the $t_{50\%}$ could be reported, since it has been previously documented within the literature that the photomineralisation reaction is first order³⁴.

The treatment of first order kinetics is different to that described previously for zero order kinetics, which alters the calculation of the $t_{50\%}$. As the MB reaction proceeds, the peak absorbance will decrease as the dye is photomineralised; however, it does not decrease to 0 due to absorbance by the cell and the remaining LMB solution. Hence, it is necessary to calculate the total change in absorbance, ΔAbs , at λ_{max} for the photomineralisation reaction using equation 2.7.;

$$\Delta\text{Abs} = \text{Abs}_t - \text{Abs}_\infty \quad (2.7.)$$

where Abs_t is the absorbance at λ_{max} after any given time t , and Abs_∞ is the absorbance at λ_{max} when all of the dye has been photomineralised.

The first order rate equation can be represented as shown in equation 2.8.⁸;

$$r = \frac{-dD}{dt} = k[D] \quad (2.8.)$$

where again r is the rate of reaction, $[D]$ represents the concentration of a species, D , and dD/dt is the rate of change of the concentration of D with time. In this instance, however, k is the first order rate constant for the reaction. Since concentration is directly related to absorbance using the Beer-Lambert law⁸, i.e.,

$$A = \varepsilon cl \quad (2.9.)$$

it follows that we can use ΔAbs in the first order rate equation directly. Through rearrangement and integration of equation 2.8., we obtain equation 2.10.;

$$\ln[D]_t = -kt + \ln[D]_0 \quad (2.10.)$$

This equation is similar to that for any straight line (i.e. $y = mx + c$), and so it follows that a plot of $\ln [D]_t$ vs. time should yield a straight line of gradient $-k$ and intercept $\ln [D]_0$. For discerning the kinetics of photomineralisation here, a plot of $\ln (\Delta\text{Abs})$ vs. time should yield a straight line of gradient $-k$ if the reaction is first order.

If we wish to find $t_{50\%}$, this will correspond to the time at which the concentration of D is 50 % of its original value, i.e.;

$$\ln \frac{[D]_0}{2} = -kt + \ln[D]_0 \quad (2.11.)$$

Rearranging equation 2.11. gives equation 2.12.;

$$kt_{50\%} = \ln[D]_0 - \ln \frac{[D]_0}{2} \quad (2.12.)$$

And using the rule for subtracting natural logarithms, we obtain the following;

$$kt_{50\%} = \ln 2 \quad (2.13.)$$

This can be suitably rearranged to give equation 2.14.;

$$t_{50\%} = \ln 2 / k \quad (2.14.)$$

Hence from a plot of $\ln \Delta\text{Abs}$ vs. time, it is possible to extract the first order rate constant, k , and hence calculate the $t_{50\%}$ for the process.

2.3. References

- (1) K. Hunger *Industrial Dyes*; Wiley-VCH, 2003.
- (2) A. Mills; S.-K. Lee; M. Sheridan *The Analyst* **2005**, *130*, 1046.
- (3) S.-K. Lee; A. Mills; A. Lepre *Chem. Commun.* **2004**, 1912.
- (4) A. Mills; A. Lepre; N. Elliott; S. Bhopal; I. P. Parkin; S. A. O'Neill *Journal of Photochemistry and Photobiology A: Chemistry* **2003**, *160*, 213.
- (5) A. Mills; M. Crow *International Journal of Photoenergy* **2008**, *2008*, 1.
- (6) A. Mills; M. McFarlane; S. Schneider *Anal. Bioanal. Chem.* **2006**, *386*, 299.
- (7) A. Cusick *The Kinetics of Dye Photocatalysis* University of Strathclyde, Glasgow 2009.
- (8) P. W. Atkins *Physical Chemistry*; Oxford University Press, 1990.
- (9) C. J. Barbé; F. Arendse; P. Comte; M. Jirousek; F. Lenzmann; V. Shklover; M. Grätzel *Journal of the American Ceramic Society* **1997**, *80*, 3157.
- (10) A. Mills; N. Elliott; G. Hill; D. Fallis; J. R. Durrant; R. L. Willis *Photochem. Photobiol. Sci.* **2003**, *2*, 591.
- (11) A. Mills; G. Hill; M. Crow; S. Hodgen *Journal of Applied Electrochemistry* **2005**, *35*, 641.
- (12) S. Doeuff; M. Henry; C. Sanchez; J. Livage *Journal of Non-Crystalline Solids* **1987**, *89*, 206.
- (13) J. Livage; C. Sanchez *Journal of Non-Crystalline Solids* **1992**, *145*, 11.
- (14) <http://xray.bmc.uu.se/terese/crystallization/tutorials/tutorial6.html> 20/10/2009
- (15) <http://mse.iastate.edu/microscopy/college.html> 20/10/2009
- (16) J. Goldstein; D. Newbury; D. Joy; C. Lyman; P. Echlin; E. Lifshin; L. Sawyer; J. Michael *Scanning Electron Microscopy and X-Ray Microanalysis*; Springer, 2003.
- (17) D. D. Ebbing; S. D. Gammon *General Chemistry*; Houghton Mifflin Company, 1999.
- (18) <http://www.nanoscience.com/education/AFM.html> 28/10/2009

-
- (19) C. R. Blanchard *The Chemical Educator* **1996**, *1*, 1.
- (20) <http://www.panalytical.com/index.cfm?pid=135> 28/10/2009
- (21) M. A. S. McGrady An Investigation of the Electrochemical Formation of Native Oxide and Sulphide Layers on Cd_xHg_{1-x}Te University of Strathclyde, Glasgow 2005.
- (22) D. Reyes-Coronado; G. Rodriguez-Gattorno; M. E. Espinosa-Pesqueira; C. Cab; R. d. Coss; G. Oskam *Nanotechnology* **2008**, *19*, 1.
- (23) JCPDS Powder Diffraction File, Card No. 21-1272 Swarthmore, PA
- (24) JCPDS Powder Diffraction File, Card No. 21-1276 Swarthmore, PA
- (25) C. Hammond *The Basics of Crstallography and Diffraction*; Oxford University Press, 2003.
- (26) T. Minabe; D. A. Tryk; P. Sawunyama; Y. Kikuchi; K. Hashimoto; A. Fujishima *Journal of Photochemistry and Photobiology A: Chemistry* **2000**, *137*, 53.
- (27) J. T. Remillard; J. R. McBride; K. E. Nietering; A. R. Drews; X. Zhang *J. Phys. Chem. B* **2000**, *104*, 4440.
- (28) A. Mills; J. Wang *Journal of Photochemistry and Photobiology A: Chemistry* **2006**, *182*, 181.
- (29) R. Fretwell; P. Douglas *Journal of Photochemistry and Photobiology A: Chemistry* **2001**, *143*, 229.
- (30) A. Mills; N. Elliott; I. P. Parkin; S. A. O'Neill; R. J. Clark *Journal of Photochemistry and Photobiology A: Chemistry* **2002**, *151*, 171.
- (31) P. Sawunyama; L. Jiang; A. Fujishima; K. Hashimoto *J. Phys. Chem. B* **1997**, *101*, 11000.
- (32) S. Lakshmi; R. Renganathan; S. Fujita *Journal of Photochemistry and Photobiology A: Chemistry* **1995**, *88*, 163.
- (33) C. H. Kwon; H. Shin; J. H. Kim; W. S. Choi; K. H. Yoon *Materials Chemistry and Physics* **2004**, *86*, 78.
- (34) R. W. Matthews *J. Chem. Soc. Faraday Trans. 1* **1989**, *85*, 1291.
- (35) A. Mills; J. Wang *Journal of Photochemistry and Photobiology A: Chemistry* **1999**, *127*, 123.
- (36) T. Zhang; T. Oyama; A. Aoshima; H. Hidaka; J. Zhao; N. Serpone *Journal of Photochemistry and Photobiology A: Chemistry* **2001**, *140*, 163.

- (37) N. Xu; Z. Shi; Y. Fan; J. Dong; J. Shi; M. Z.-C. Hu *Ind. Eng. Chem. Res.* **1999**, *38*, 373.

3 Results and Discussion: Characterisation of a Photocatalyst Indicator Ink Based on the Redox Dye 2,6-dichloroindophenol

As was alluded to previously in chapter 1, there are many methods available to researchers for measuring the photocatalytic activity of both laboratory-prepared and commercial products. The diverse nature of the photocatalytic reaction, coupled with the observation of photoinduced superhydrophilicity, has allowed researchers to use both organic and inorganic compounds, biological microorganisms and even changes in the water contact angle to measure the activity of photocatalyst films and powders. However, as commercial photocatalyst products have begun to evolve, it is readily apparent that, particularly for films, most compounds are highly impractical for use in the field. All usually require a trained technician and bulky analytical equipment to conduct the test; most importantly, however, the chemistry behind such reactions can be complex and thus inaccessible to the average customer. In addition, since most commercial products encompass a thin (i.e. nm) layer of photocatalyst, such tests would also be rather slow. What is needed is a rapid method of assessing the photocatalytic activity of thin films which requires no expensive equipment and which is visually accessible to the customer.

The resazurin (Rz) indicator ink developed by Mills et al¹⁻² for the determination of the photocatalytic activity of thin films represents a major step forward from a commercial viewpoint. The photocatalytic reduction reaction is confirmed by the colour change as Rz (blue) is reduced to resorufin (Rf, pink). The ink can be conveniently stored in a felt-tipped pen, hence there is no need for a trained technician to conduct the test, and is visual, thus eliminating the need for analytical equipment. In addition, under UVA sunlight conditions, the reduction of Rz on Activ™ is complete in ca. 5 minutes, which is fairly rapid, compared to the anticipated rate of photomineralisation reactions on such a substrate. However, whilst the ink is certainly appealing, it does suffer from one major drawback. It would be more aesthetically appealing for the ink to reduce to a colourless product, since customers would equate (wrongly) the photoreduction to a

complete cleaning action by the photocatalyst. As was noted above, R_z reduces to a pink product, R_f.

One such dye which is known to reduce to a colourless product is 2,6-dichloroindophenol (DCIP). Theoretically, it should be possible to switch the R_z dye directly with DCIP and thus generate an ink which satisfies all the criteria required for use in the field. This chapter details the characterisation of such a DCIP photocatalyst indicator ink and examines how deviations from the standard formulation described in the experimental can either hinder, or improve the ink's performance relative to both this prototype and the R_z indicator ink. The kinetics of dye photoreduction will also be considered. Recent work conducted by Cusick³ has suggested that the indicator inks based on R_z, MB and DCIP all exhibit zero order kinetics. In this chapter, since the effect of dye concentration on the rate of photoreduction is examined for the DCIP ink, it should be possible to confirm such findings.

3.1. Spectral Properties of the Substrate

As detailed in previous chapters, Activ™ self-cleaning glass comprises 4 mm float glass with a ca. 15 nm TiO₂ layer on the surface, which has been deposited using a CVD technique⁴. Figure 3.1. shows the UV-Visible absorbance spectra of the photocatalyst in the wavelength region 300 – 400 nm, along with the spectra of ordinary 4 mm float glass (referred to herein as plain glass) and quartz. Whilst quartz is observed to absorb a minimal amount of radiation over this wavelength range, it can be seen that the absorbance of both Activ™ and plain glass increases at wavelengths below ca. 360 nm. This observed increase in absorbance is slightly greater for Activ™ in comparison to the plain glass, and is attributed to the presence of the titania photocatalyst layer on the surface. As will be demonstrated later when we come to discuss the in-house prepared paste films in chapter 5, and as would be expected based on Beer's law, the increase in absorbance in this wavelength region due to the photocatalyst layer is directly proportional to its thickness. As a result, the increase in absorbance noted here for Activ™ compared to plain glass is not exceptionally large owing to the small thickness of the TiO₂ layer (ca. 15 nm) present, as indicated from the inset diagram in figure 3.1.

Work by Mills et al⁵ has shown that, owing to the photocatalyst layer thickness, the absorbance of Activ™ at 365 nm is ca. 0.07, which is similar to that predicted by calculation for a 15 nm thick film of titania.

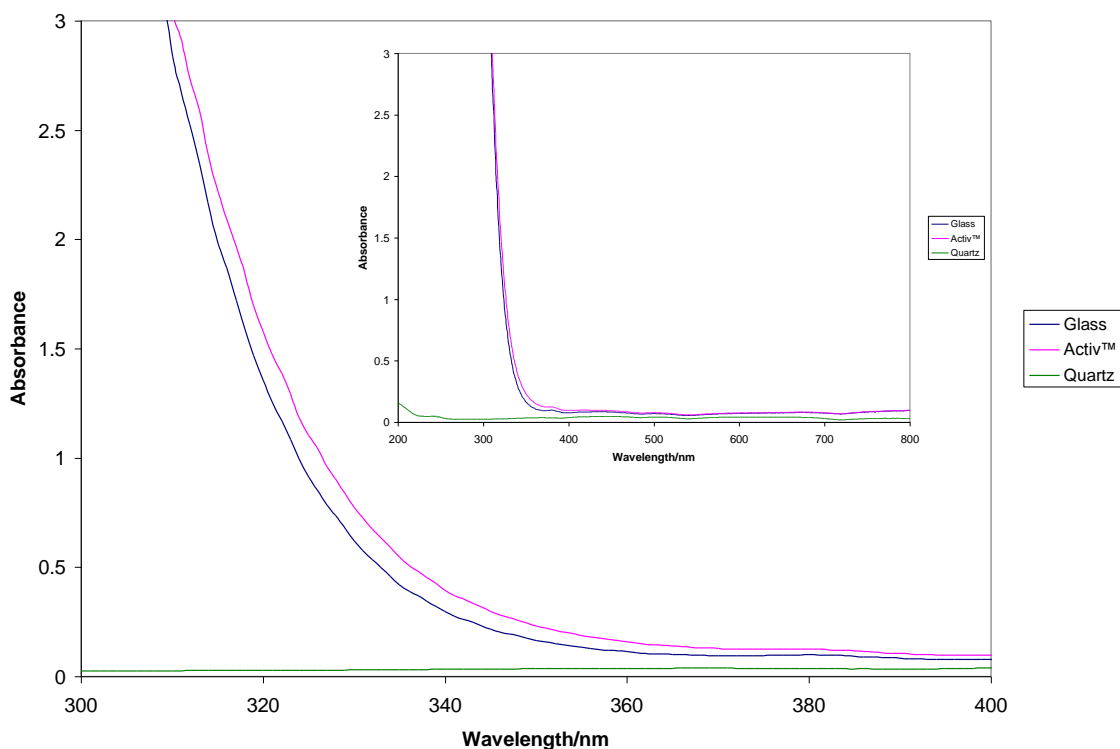


Figure 3.1.: The UV-Visible absorbance spectra of plain glass (blue trace), Activ™ (pink trace) and quartz (green trace) over the wavelength range 300 – 400 nm. The inset diagram shows the UV-Visible absorbance spectra of all three materials over the wavelength range 200 – 800 nm

3.2. The Standard DCIP ink – Reduction and Recovery in Ambient Atmospheric Conditions

DCIP is a blue dye and a water soluble variant of the classic indophenol blue. The dye can be used as a redox indicator, but is more commonly known for its use in determining the vitamin C (ascorbic acid) content of solutions, and as a monitor of the light reactions which occur in photosynthesis. Such uses are due to the fact that it can be so easily reduced⁶⁻⁸. This ability of the dye to accept electrons easily has also been

exploited in other biological systems for assessing enzyme activity⁹⁻¹⁰. Interestingly, the redox nature of the dye has also seen it used to produce a thin film oxygen sensor, implying an undesirable affinity for O₂¹¹. Such findings may have implications here for the dye's use in the indicator ink formulation in the field. The structure of the dye, and its reduction reaction to leuco-DCIP, is given in figure 3.2.

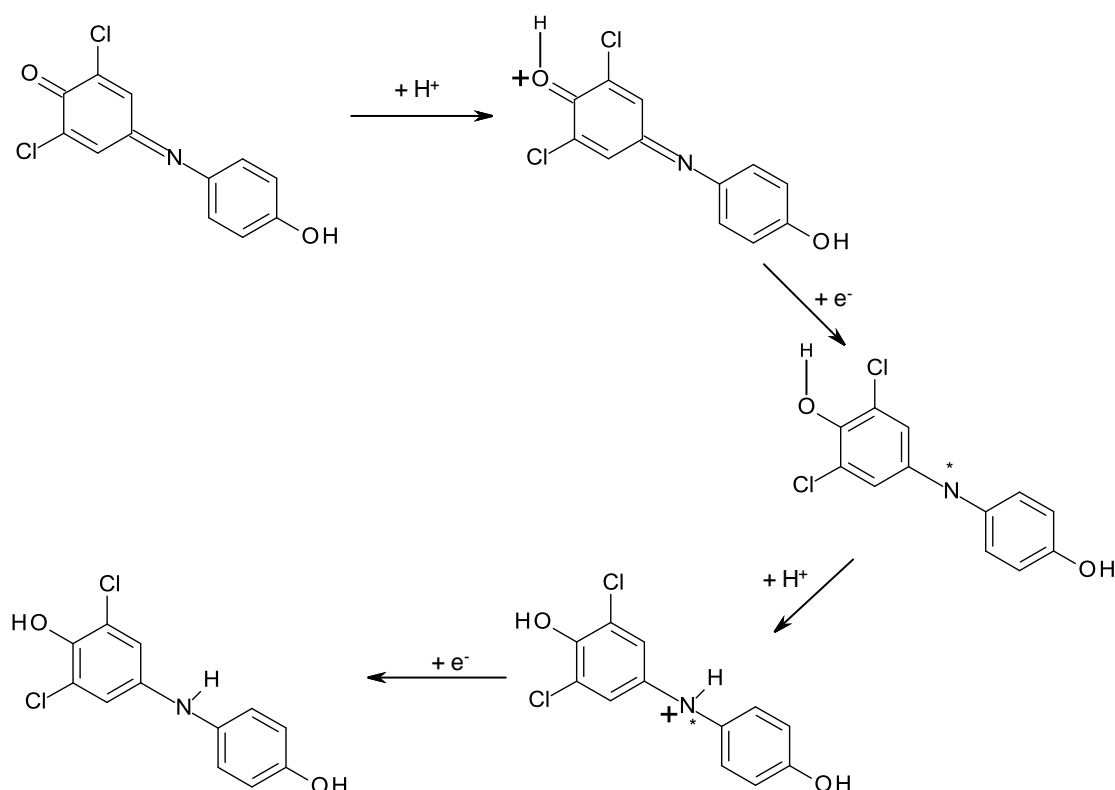


Figure 3.2.: The structure of DCIP and its reduction mechanism in the indicator ink formulation

The performance of the standard DCIP indicator ink, prepared as described in chapter 2, was initially assessed under ambient atmospheric conditions in order to ascertain its reduction and recovery performance. Although it is possible that by conducting such tests in these conditions that O₂ may interfere, causing undesirable re-oxidation of leuco-DCIP, it is necessary since the ink will ultimately be used in such conditions. Figure 3.3. shows the UV-Visible absorbance spectrum for the standard DCIP ink when spun-coated on Activ™, and the subsequent change in the dye's spectral shape with UV irradiation under ambient atmospheric conditions.

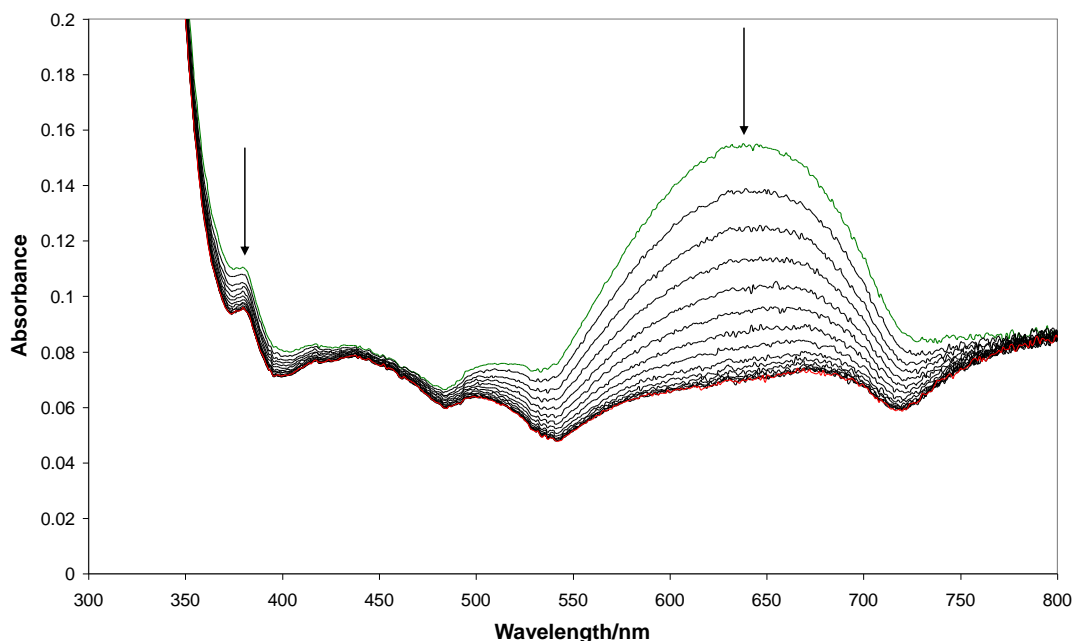


Figure 3.3.: The change in the UV-Visible absorbance spectrum of the standard DCIP ink on Activ™ with increasing UV irradiation time under ambient atmospheric conditions. The green trace shows the initial spectrum obtained for the ink film, whilst the red trace shows the spectrum obtained after 7.5 minutes of UVA irradiation. Spectra were recorded at 30 s intervals

Profilometry work has suggested that the ink films generated in this work as standard are ca. 900 nm thick. The peak absorbance for the dye is observed to occur at ca. 629 nm, although this peak is observed to be extremely broad, encompassing ca. 200 nm. This implies that despite the relatively low level of dye present (5 mg per ink formulation), multimeric dye species have been formed. In aqueous solution (ca. 10^{-4} M), the peak absorbance is observed to occur at 600 nm for the dye, hence the presence of the other ink components would appear to have caused a slight red-shift of the λ_{\max} . However, even in solution, the half peak base width (HPBW) is observed to be ca. 130 nm; for the indicator ink described here, the HPBW is ca. 150 nm. Given that the concentration of the dye in the indicator ink is ca. 0.064 M, it should therefore come as no surprise that dimer and multimer formation has occurred.

Figure 3.4. shows how the peak absorbance at λ_{\max} (629 nm) varies with increasing irradiation time based on the data presented in figure 3.3. The peak absorbance for the ink film prior to irradiation is observed to be ca. 0.16 Absorbance Units, which is relatively low, thus providing plenty of scope for increasing the dye level in the formulation. With increasing irradiation, the peak absorbance decreases to a baseline figure relative to the underlying photocatalyst substrate. From figure 3.4., the initial rate of reduction is calculated to be 4.871×10^{-4} AbsU s^{-1} . Assuming zero order kinetics, the calculated $t_{50\%}$ is 126 s. A complete discussion on the kinetics of dye photoreduction follows later.

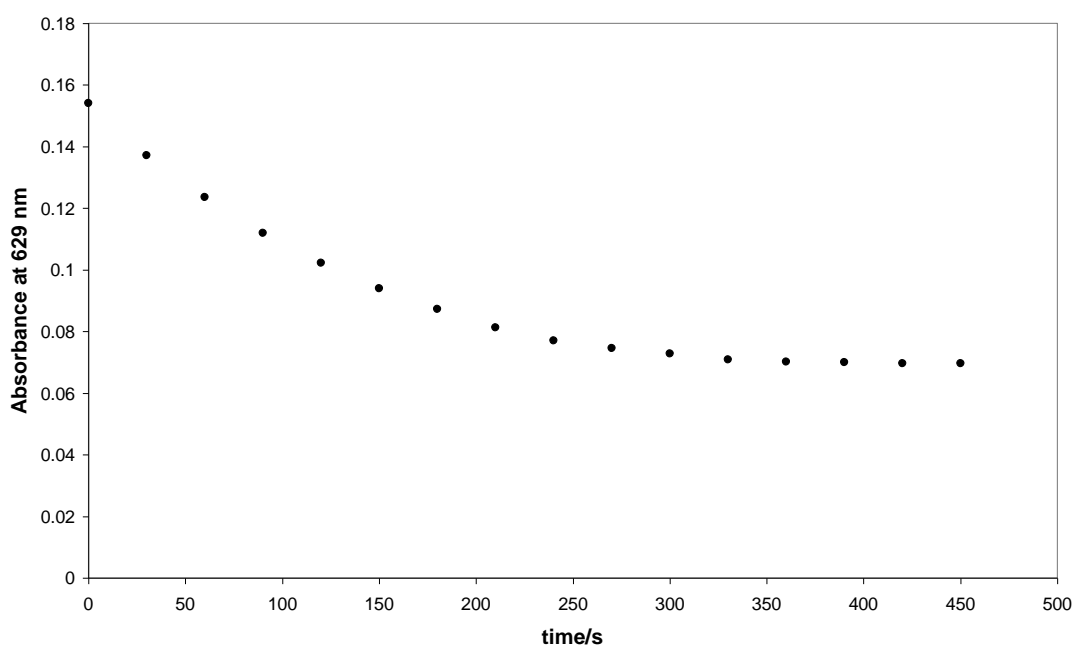


Figure 3.4.: The variation in the absorbance at λ_{\max} for the DCIP ink with UV irradiation time, based on the data presented in figure 3.3.

The mechanism of reduction for such an ink formulation is thought to be the same for all the dyes described in this work and is as postulated by Mills et al for the Rz ink¹⁻². Essentially, after the photogeneration of the electron-hole pair when TiO_2 is irradiated with ultra-bandgap light, the hole reacts irreversibly with the SED (i.e. glycerol), which is subsequently oxidised to SED_{ox} . It is postulated that this oxidation may lead to the

formation of a α -hydroxylalkyl radical, which due to its postulated instability and free electron will also possess the ability to reduce the dye, in addition to the photogenerated electrons produced by irradiation of the semiconductor.

The existence of such a radical species has been noted elsewhere, with previous work by Hilgendorff et al¹² having shown that hole (or one electron) oxidation of other short chain alcohols (namely methanol, ethanol and 2-propanol) can result in the formation of α -hydroxylalkyl radicals capable of reducing carbon tetrachloride. Other work by Mandelbaum et al¹³ has also shown that such radical species are able to initiate the injection of an electron into the conduction band from the valence band of a semiconductor material, thus providing more electrons from the photocatalyst that could theoretically be available for dye reduction.

Both these scenarios of dye reduction (i.e. via a postulated radical species or via the photogenerated electrons) generate two, individual theories, which are believed to work in tandem in the dye photoreduction process. If it were merely the postulated α -hydroxylalkyl radicals which were responsible for the reduction process, they would be required to diffuse through the ink film to locate the dispersed dye molecules. In contrast, if the reduction depended solely upon the photogenerated electrons, then diffusion of the dye molecules through the film to the photocatalyst surface would be necessary. It is believed using the theory of Mills et al² that both the dye molecules and the photogenerated α -hydroxylalkyl radicals diffuse throughout the ink film as the semiconductor is irradiated, the reduction of the dye being caused either by the photogenerated electrons or the radicals, depending upon which is encountered first by the diffusing dye molecules.

Figure 3.5. shows how the absorbance at λ_{\max} varies with irradiation time for a DCIP ink cast on plain glass, i.e. in the absence of a layer of photocatalyst. Over the 1 hour irradiation time period, no significant change in the absorbance at λ_{\max} is observed, suggesting little or no photoreduction has actually occurred. Indeed, it is likely that the decrease in the absorbance due to DCIP noted in figure 3.5. is merely due to

photofading and/or evaporation of the ink from the surface of the glass, since the UVA source emits heat and is relatively close to the sample surface. Obviously in the absence of any photocatalyst layer, no electron-hole pairs are produced upon irradiation, and hence no photoreduction is theoretically possible, whether it is by photogenerated electrons, or α -hydroxylalkyl radicals produced in situ. What figure 3.5. also demonstrates is that if the ink should be applied to plain glass in the field, and compared to glass coated with a photocatalytic layer, a comparison can be drawn, thus demonstrating the self-cleaning effect to non-scientific consumers.

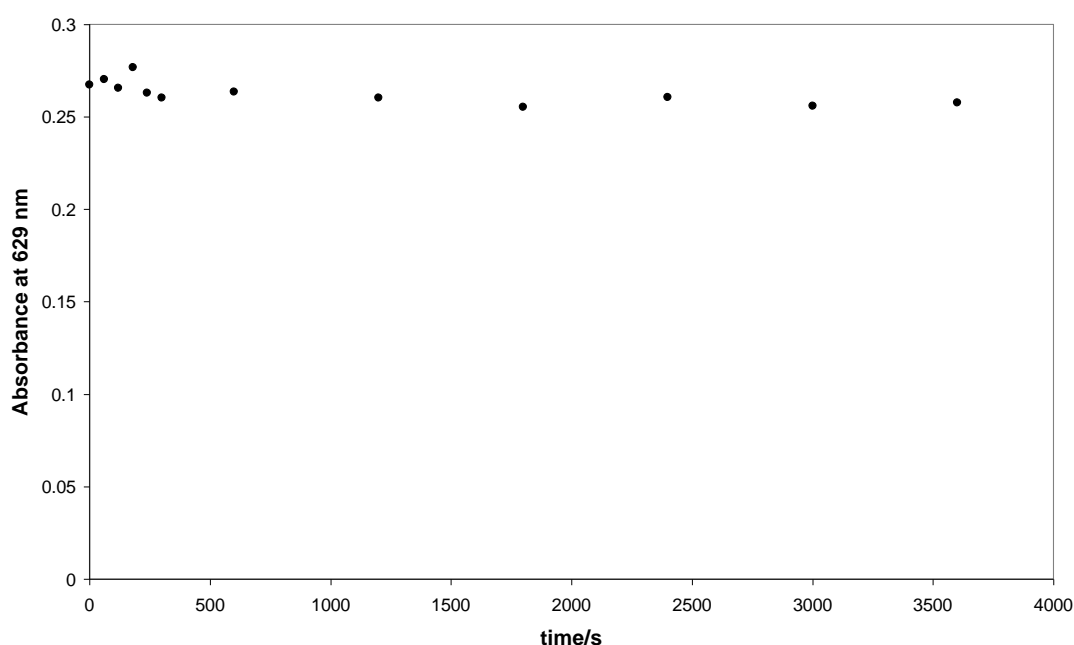


Figure 3.5.: The variation in the absorbance at λ_{\max} with irradiation time for a DCIP ink cast on plain glass

Following reduction of the dye, it is obviously necessary that the reduced form, leuco-DCIP, is stable and does not react with atmospheric O_2 . Figure 3.6. shows how the absorbance at 629 nm due to DCIP varies upon reduction of the dye on ActivTM (as was observed in figures 3.3. and 3.4.), followed by recovery, both under ambient atmospheric conditions. The recovery was monitored over a 40 hour time period and in

the dark in order to observe the theoretical maximum which should occur assuming that the leuco- form of the dye is O₂-sensitive.

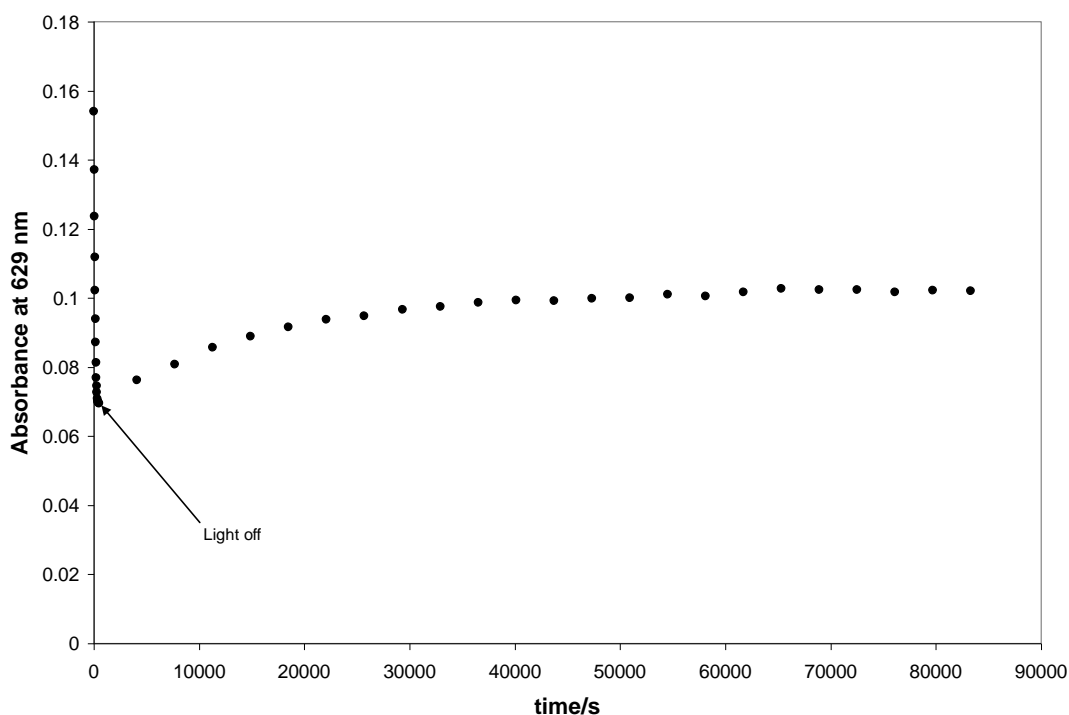


Figure 3.6.: The reduction, and subsequent recovery, of a DCIP ink on Activ™ under ambient atmospheric conditions. The recovery was monitored over a period of ca. 40 hours in the dark with spectra being recorded at 1 hour intervals and the absorbance at 629 nm extracted from it

Over the course of 23 hours, the ink recovers ca. 38 % of its original blue colour due to re-oxidation. However, what is important to note here is the conditions under which the recovery was allowed to occur. During the 40 hour recovery period of the experiment, the sample was sealed in the spectrometer chamber such that little or no ambient light was incident on its surface. Such darkened conditions are not terribly realistic for the ink's use in the field. Indeed, a reasonable period of darkness in the field could be taken to be 12 hours; over this time period, the ink recovers ca. 35 % of its original blue colour according to the data presented in figure 3.6.

Beyond this 23 hour time period, the absorbance at λ_{\max} due to DCIP is then observed to begin to decrease slightly. This was unanticipated since the ambient atmospheric conditions should remain constant, although obviously both the temperature and relative humidity will vary slightly throughout the experimental time period. As such we had believed that the ink would continue to recover so long as no irradiation of the sample occurred. However, it is immediately obvious from figure 3.6. that after the fairly rapid increase in absorbance at λ_{\max} over the first 10 hours of the dark recovery period, the recovery rate begins to slow and subsequently plateau. It is believed that this slight decrease beyond 23 hours is an effect from the low stability of the DCIP ink, which will be discussed later.

For reference, the maximum rate of recovery in the dark, which is observed over the first 4 hours, is found to be $1.35 \times 10^{-6} \text{ AbsU s}^{-1}$, which is ca. 100 times slower than the rate of reduction calculated from figure 3.4. above. It would seem reasonable to assume, therefore, that re-oxidation of the leuco- form of the dye does not interfere considerably with DCIP reduction due to the photocatalytic action.

The DCIP ink, as described above, has a lifetime of ca. 1 month under ambient atmospheric conditions and ca. 3 months when stored in the fridge. Beyond these times, the ink is observed to change colour from blue to red, suggesting that the dye has been modified in some way. Indeed, such a change is also observed if the dye is placed in deionised water and left sealed for a similar time period, implying that water is responsible for the induced colour change. Interestingly, it is known that DCIP is red in acidic solutions whilst being blue in alkali¹⁴, which would suggest that whatever is responsible for the observed colour change is related to the solution pH. This apparent instability in water has been noted by others previously¹⁵⁻¹⁶, although no thorough explanation is given. It is also suggested that in acidic solutions, precipitation of the dye occurs, which is observed in the indicator ink described above to accompany the colour change. Following discussions within this group, it is postulated that hydrolysis of the Cl groups may occur in solution, which would remove the majority of the ionic character from the dye and thus render it insoluble in water.

3.3. The Effect of the Polymer on the Performance of the DCIP Ink – Assessment of Polyvinyl Alcohol (PVA)

For all the indicator inks, the standard polymer used in the formulation is hydroxyethyl cellulose (HEC). It was chosen here since previous work has shown it to be suitable for the preparation of the original photocatalyst indicator ink based on Rz^{1-2} , and also for the preparation of other O_2 indicator¹⁷ and UV indicator¹⁸ inks in this laboratory. In order to assess whether the polymer plays a significant role in the reduction/recovery of the ink, the effect of changing to polyvinyl alcohol (PVA) was assessed for the DCIP ink. The shorthand structures of both PVA and HEC are given below in figure 3.7. The structures of the two polymers are markedly different and as such, we would anticipate that the polymers will have differing physical properties. One such physical property is that of O_2 permeability. Ethyl cellulose (EC), which possesses a similar structure to HEC, has an O_2 permeability of $11 \times 10^{-13} \text{ cm}^2 \text{ s}^{-1} \text{ Pa}^{-1}$. Conversely, PVA has an O_2 permeability of $0.00665 \times 10^{-13} \text{ cm}^2 \text{ s}^{-1} \text{ Pa}^{-1}$, ca. 10000 times smaller than that of EC¹⁹. As a result, we would anticipate that with PVA as the polymer, the rate of recovery of the DCIP ink will be slowed since the O_2 diffusion through the polymer film to the leuco- form of the dye will be slower.

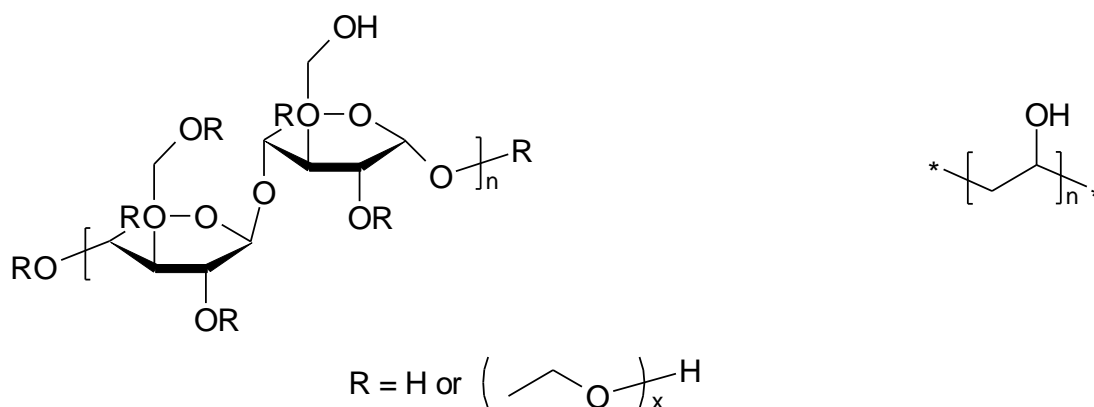


Figure 3.7.: The shorthand structures of both HEC (left) and PVA

A DCIP ink using PVA as the polymer was successfully prepared and cast as a film on the surface of Activ™. Figure 3.8. shows the changes in spectral shape which occur

when such an ink film is then irradiated using UVA light. As was anticipated, the peak shape is not altered significantly compared to when HEC is used as the polymer, a ca. 200 nm broad peak in the spectrum suggesting that multimer formation of DCIP is again occurring.

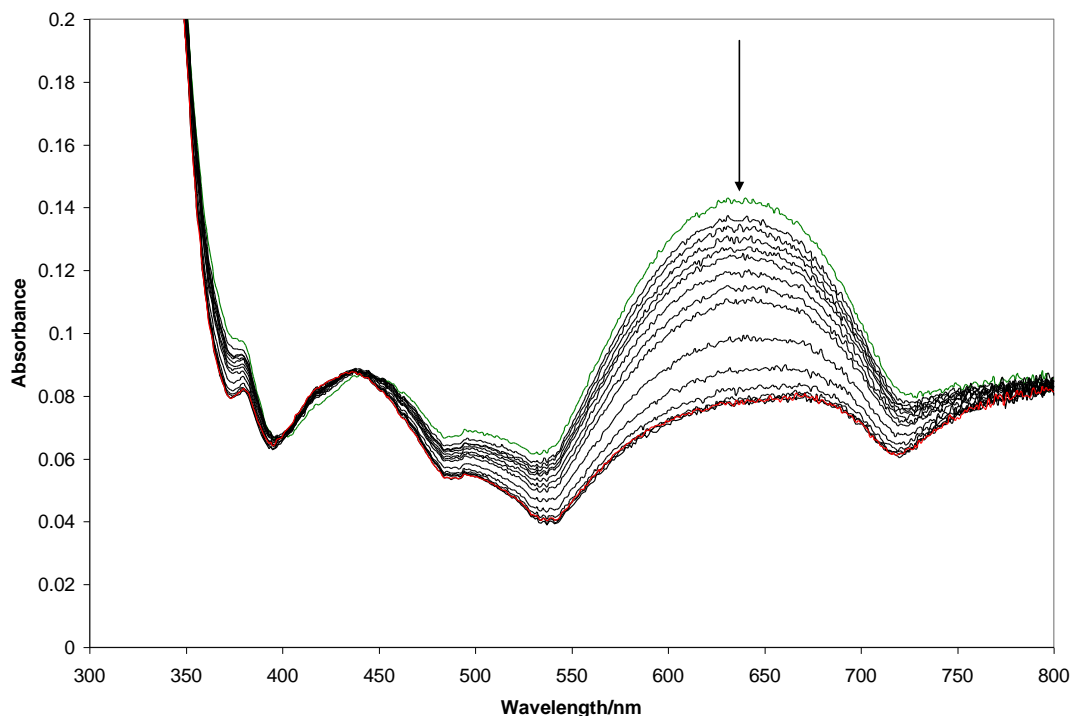


Figure 3.8.: The change in spectral shape obtained as a DCIP indicator ink with PVA as the polymer is irradiated on the surface of Activ™. The green trace shows the initial ink spectrum, whilst the red trace shows that obtained after 9 minutes of UVA irradiation. Spectra were recorded at 20 s intervals for 2 minutes, then at 1 minute intervals up to 9 minutes

However, the peak absorbance ($\lambda_{\max} = 629 \text{ nm}$) is repeatedly observed to be ca. 0.14 absorbance units, which is slightly less than what is typically observed with HEC as the polymer (ca. 0.16-0.2 absorbance units). The offshoot of this is that the blue colour observed for the spun-coated ink film is slightly less intense. This is not so much of an issue for the testing of the photocatalytic activity of laboratory-prepared samples since spectrophotometry would be used to monitor the colour change with increasing irradiation time. However, for an ink used to measure the photocatalytic activity of

samples in the field, the intensity of the blue colour is important. Although the dye loading level in such pens is typically tripled, it implies that the difference in the intensity of the blue colour would be further reduced compared to that of a HEC-based ink.

Figure 3.9. shows how the absorbance at λ_{\max} varies with irradiation time for the PVA-based DCIP ink. The initial rate of reduction for the indicator ink is calculated from this plot to be $2.76 \times 10^{-4} \text{ AbsU s}^{-1}$. This initial rate of reduction is ca. 2 times slower than what was observed previously with HEC as the polymer in figure 3.4. Based on this finding alone, HEC would appear to be the more attractive polymer for the ink formulation.

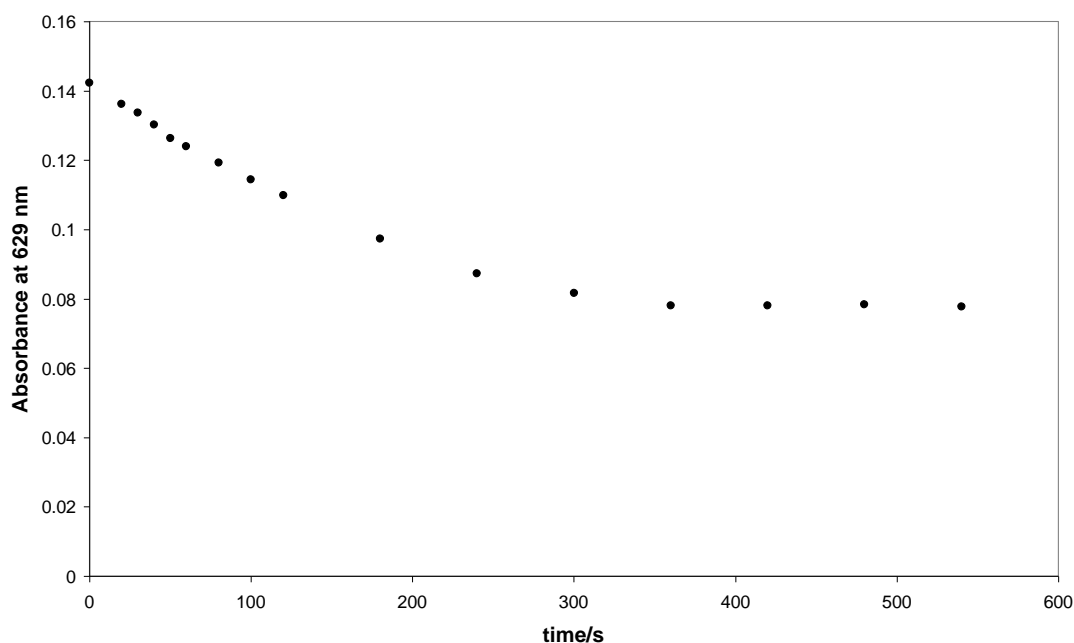


Figure 3.9.: The variation in the absorbance at λ_{\max} with irradiation time for the PVA-based, DCIP ink, extracted from figure 3.8.

Although the PVA-based ink is slower to respond, where it was hoped it would excel was in slowing the recovery of the ink following reduction. Since the ink recovery is believed to be facilitated by atmospheric O_2 , and PVA has a lower O_2 permeability than

ethyl cellulose, a structural analogue of HEC, it was believed that the use of PVA in the ink formulation would slow the rate of the recovery reaction, hence prolonging the colourless, reduced product. Figure 3.10. shows the recovery profile observed for the PVA-based ink over a 1 hour time period. From figure 3.10., the rate of recovery of a PVA-based DCIP ink is calculated to be $2.79 \times 10^{-6} \text{ AbsU s}^{-1}$. Previously, we reported that the rate of recovery of the HEC-based ink was $1.35 \times 10^{-6} \text{ AbsU s}^{-1}$ over a 4 hour time period – from the results given in figure 3.6., the rate of recovery over 1 hour is calculated to be $2.55 \times 10^{-6} \text{ AbsU s}^{-1}$. This value is similar to what we observe with PVA as the polymer.

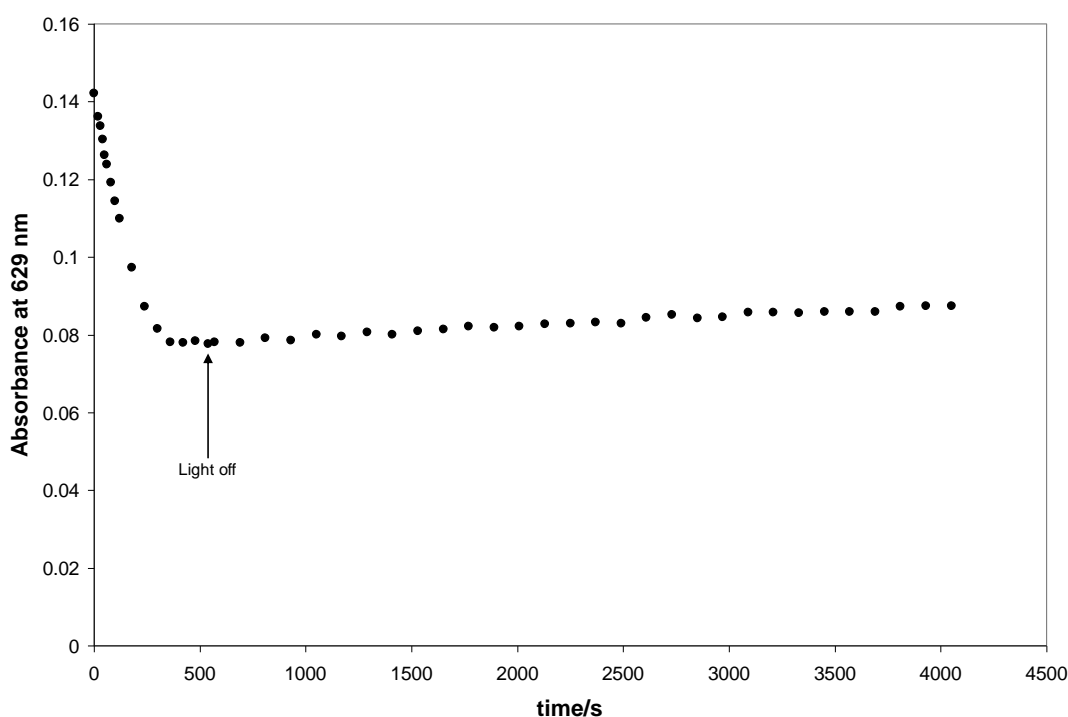


Figure 3.10.: The variation in the absorbance at λ_{max} for the PVA-based ink due to reduction and the subsequent recovery observed over 1 hour

Since the rate of recovery is unaffected by changing the polymer, and there is no increase in the intensity of the ink colour when cast as a film on Activ™ or the rate of reduction, a shift to PVA as the polymer does not provide any significant advantages over HEC. There is also noted to be no improvement in the longevity of the ink when

PVA is used, with precipitation of the dye and a colour change from blue to red still noted over similar timescales to that for the HEC-based ink. Therefore it would seem unwise to change from HEC as the standard polymer for the ink formulation.

3.4. The Effect of the Glycerol Level and the use of Other Polyols

Glycerol (or 1,2,3-propantriol) is a short chain polyol and, as previously stated in section 1.7., is used in the ink formulation as a sacrificial electron donor (SED). It reacts with the photogenerated holes produced by the irradiation of the photocatalyst with UV light (see figure 1.7.). Such holes are powerful oxidants (redox potential = $+2.53 \text{ V}^{20}$) and will facilitate oxidation of the glycerol, with the products most likely to be glyceraldehyde and reactive intermediates, such as the α -hydroxylalkyl radicals postulated previously.

In addition to reacting with the photogenerated holes, glycerol also helps to adhere the ink to the surface of Activ™. This is supported by findings on an indicator ink prepared with no SED present, whereby the ink is observed to undergo some degree of reticulation/beading during spin-coating. When such an ink is successfully cast and then irradiated with UVA light over a 1 hour time period, the change in spectral shape observed is as depicted in figure 3.11. The increase in the initial absorbance at λ_{max} for such an ink compared to what we have observed previously is believed to be due to a lesser dilution of the dye in the absence of glycerol - it has to be remembered that the standard formulation contains 0.3 g of the SED. In addition, the λ_{max} is also observed to have red-shifted slightly, lying now at 638 nm, which is attributed to a solvatochromic effect.

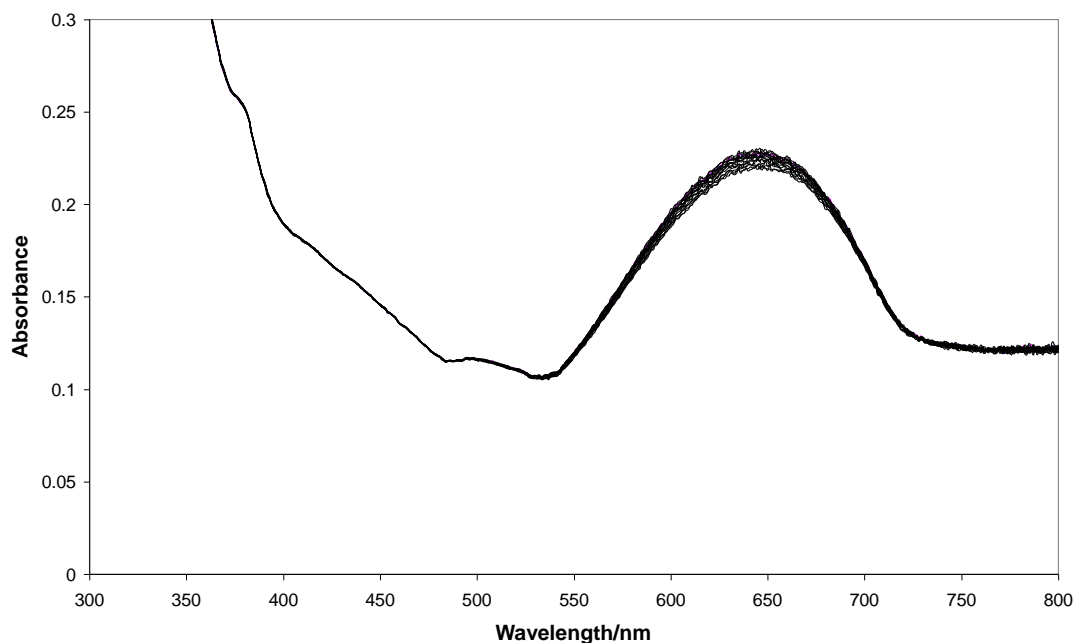


Figure 3.11.: The variation in the spectral shape obtained for a DCIP ink with nil glycerol when irradiated on the surface of Activ™. Spectra were recorded at 30 s intervals for 1 minute, at 1 minute intervals up to 5 minutes, then at 5 minute intervals up to 1 hour

Over the course of the 1 hour irradiation time period, no significant change in the spectral shape is observed, i.e. the absorbance at λ_{max} does not drop significantly, implying that no reduction of the dye has occurred. This is confirmed in figure 3.12., which depicts the change in the absorbance at λ_{max} with time for this ink.

This inability for the ink to reduce was anticipated since by removing the SED from the formulation, there is nothing present in the ink film which can react with the photogenerated holes produced. As a result, electron-hole recombination is likely to become the dominant process, reducing the number of electrons available to reduce the DCIP molecules. It was also postulated previously that any α -hydroxylalkyl radicals, formed on the oxidation pathway from glycerol to glyceraldehyde, assist in the reduction process. Since there is no glycerol present here, no such radicals can be generated. Indeed, the slight reduction in the peak absorbance over the 1 hour time period is not anticipated to be indicative of any photocatalysis. Photofading of the dye

is a possibility, as is evaporation of the ink film owing to the close proximity of the lamp, which generates a significant amount of heat.

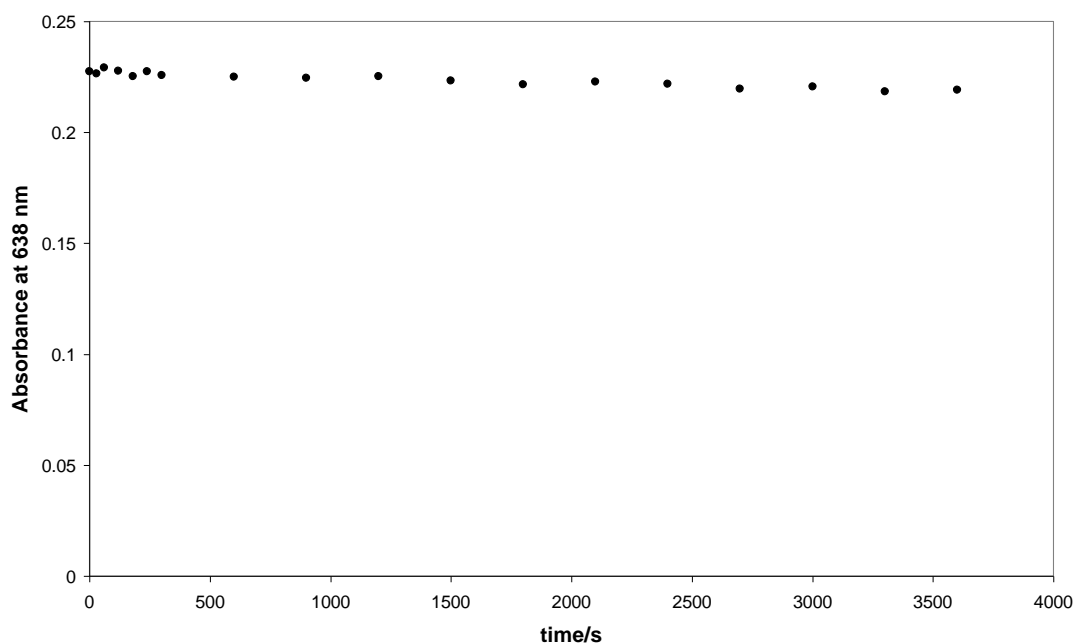


Figure 3.12.: The variation in the absorbance at λ_{\max} (638 nm) with time for a DCIP ink with no SED present

The glycerol level was then varied over the range 0 - 0.9 g in the standard indicator ink formulation in order to determine a critical SED level. Initially, based on a similar study conducted by Mills et al for the Rz ink², the glycerol level was varied in 0.1 g increments and the initial rate of reduction measured. Figure 3.13. shows the results obtained. Within the plot, the average initial rate of reduction between 0.1 and 0.9 g glycerol loading level ($= 5.15 \times 10^{-4} \text{ AbsU s}^{-1}$) is also indicated. The data is seen to vary around this average as the glycerol level is altered, but there is no definitive correlation between the initial rate of reduction observed and the amount of glycerol in the ink.

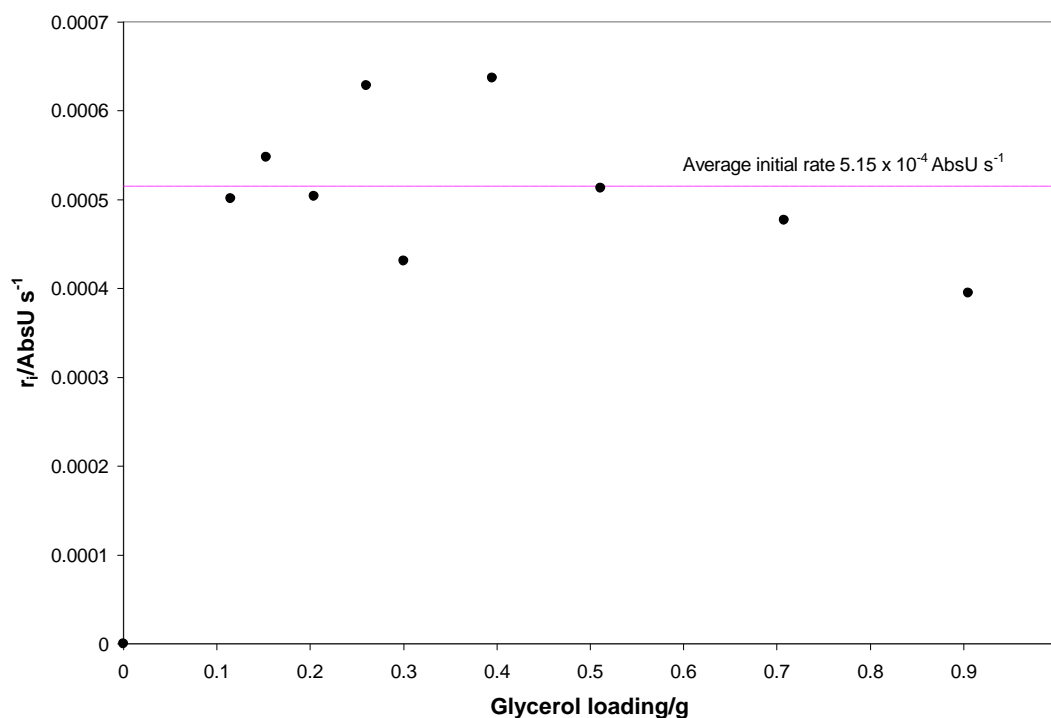


Figure 3.13.: The variation in the initial rate of reduction, r_i , with glycerol loading

Despite the findings in figure 3.13., however, we know that glycerol level is important, since we have previously demonstrated in figures 3.11. and 3.12. that, in its absence, no reduction occurs. Even with 0.1 g of glycerol in the formulation, the initial rate of reduction is ca. $5 \times 10^{-4} \text{ AbsU s}^{-1}$. Previously, Mills et al observed that for the Rz ink, there was a gradual increase in the rate of reduction as the glycerol level was varied from 0.15 to 0.3 g². It would appear from figure 3.13. that, for the DCIP indicator ink, there is a greater sensitivity to the level of glycerol present.

The results observed could also be a function of the large concentration of glycerol present, and thus easily described through Langmuir-Hinshelwood kinetic theory. It has previously been postulated by others that the kinetics of photomineralisation of organic substrates follows such a model²¹, so it would seem logical that the oxidation of the SED in the overall photoreduction mechanism is influenced similarly. The general equation is given in equation 3.1. below;

$$R_i = \frac{-d[S]_i}{dt} = \frac{k(S)K(S)[S]_i}{(1 + K(S)[S]_i)} \quad (3.1.)$$

where R_i is the rate of reaction, $[S]_i$ is the initial substrate concentration, $k(S)$ is a proportionality constant which gives a measure of the reactivity between the photoactivated TiO_2 surface and the substrate, and $K(S)$ is the Langmuir absorption constant between the surface and the substrate, S . At high substrate concentrations, i.e. as $[S]_i \rightarrow \infty$, equation 3.1. collapses to $[S]_i/[S]_i$, i.e. 1, implying zero order kinetics. Hence the results observed in figure 3.13. should come as no surprise. According to Carp et al²², substrate concentrations above 5×10^{-3} M result in a maximum reaction rate, and hence zero order kinetics. Given that at the levels described above, the pphr of glycerol varies from 222 to 2000 pphr, it would appear reasonable to assume that the concentration is above this threshold.

The glycerol level was then varied over the range 0 to 0.1 g in order to observe how such small volumes of the polyol affect the measured reduction rate. The results of this study are presented in figure 3.14. Based on the initial rate data, we observe a sharp increase in reduction rate as the SED level is increased from 1 mg to 30 mg per formulation. Beyond this, the graph is then observed to plateau, with an average rate corresponding to that observed previously in figure 3.13. The implication of such findings is that it may be possible to reduce the glycerol content of our standard ink ten-fold without any detrimental effect to the rate of reduction.

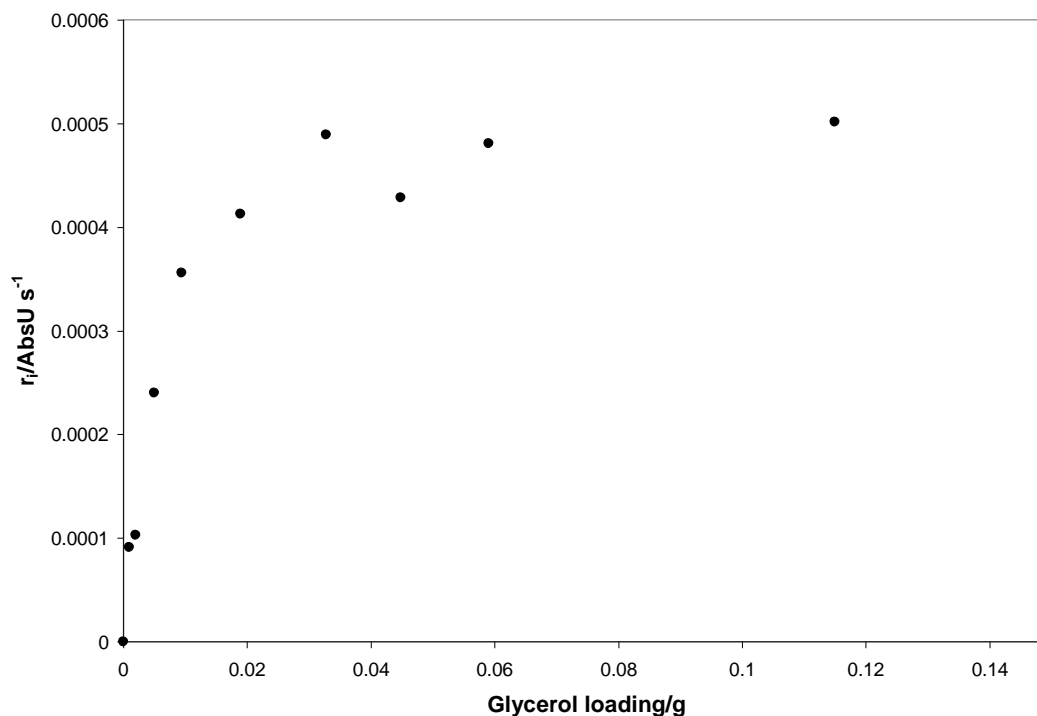


Figure 3.14.: The variation in the initial rate of reduction of the DCIP indicator ink with glycerol content over the glycerol loading range of 0 to ca. 0.1 g

This behaviour is markedly different from that observed by Mills et al for the Rz ink² and emphasises the sensitivity of the DCIP ink reduction rate to the SED level present. It also proves just how potent an SED the polyol is, since even 1 mg per formulation is enough to facilitate dye reduction. Mills et al suggested that the behaviour of the Rz indicator ink formulations with changing glycerol level depended upon the plasticizing effect glycerol had on the HEC polymer solution². This postulation was based on previous work conducted by Van Keuren et al, who demonstrated that the value of the diffusion coefficient for the dye rhodamine B altered by a factor of 10^4 in a PVA/glycerol film as the glycerol level was varied between 10 and 40 wt%²³. Since the glycerol level is varied markedly here, it is assumed that the rate of reduction is somewhat dependent upon the diffusion rate of glycerol towards the photocatalyst surface, where it can then be oxidised by the photogenerated holes to produce the postulated α -hydroxylalkyl radical. In the work by Van Keuren et al, they found that the maximum diffusion rate for the dye in a PVA/glycerol film was achieved when the

glycerol content was 40 % of the solution by weight. They postulated that such a diffusion rate was similar to what would be observed with neat glycerol, based on the ratio of its viscosity to that of water and the diffusion coefficient for the dye in water. For the DCIP ink presented here, the plot is observed to level off at glycerol levels above ca. 30 mg per formulation, which corresponds to a solution constituting 38 % glycerol by weight. It is therefore postulated that the reason for the levelling off of the initial rate above such levels here is due to the values of the diffusion coefficients for both the dye and the postulated α -hydroxylalkyl radicals approaching that which would be observed in neat glycerol.

The observed trend in initial rate can also be explained using the Langmuir-Hinshelwood expression given earlier in equation 3.1. At high glycerol levels, i.e. above 30 mg (67 pphr), we can infer that the concentration is above the critical concentration, and hence we observe zero order kinetics. However, as the concentration decreases (i.e. as $[S]_i$ decreases), we move away from the limiting scenario described previously and enter a non-linear dependence, as evidenced in figure 3.14. At low concentrations, i.e. as $[S]_i \rightarrow 0$, however, the expression simplifies to that shown in equation 3.2.;

$$R_i = k(s)K(S)[S]_i \quad (3.2.)$$

i.e. the rate of reaction is first order with respect to glycerol. This explains the existence of a linear dependence in the initial part of the graph.

In addition to this observed effect on the initial rate with glycerol level, there was also observed to be some variation in the λ_{\max} for the dye as the glycerol content is varied. A plot of this is shown in figure 3.15. The results here mirror the findings by Mills et al for the Rz indicator ink². In both instances, the peak wavelength is observed to be blue-shifted as the glycerol level is increased, which is thought to be due to a slight solvatochromic effect. Evidently, the liquid environment in which the dye finds itself will alter significantly with the glycerol level, especially since an increase from 0 to 30

mg glycerol in the formulation sees the glycerol content of the indicator ink vary from 0 to 38 % as noted above.

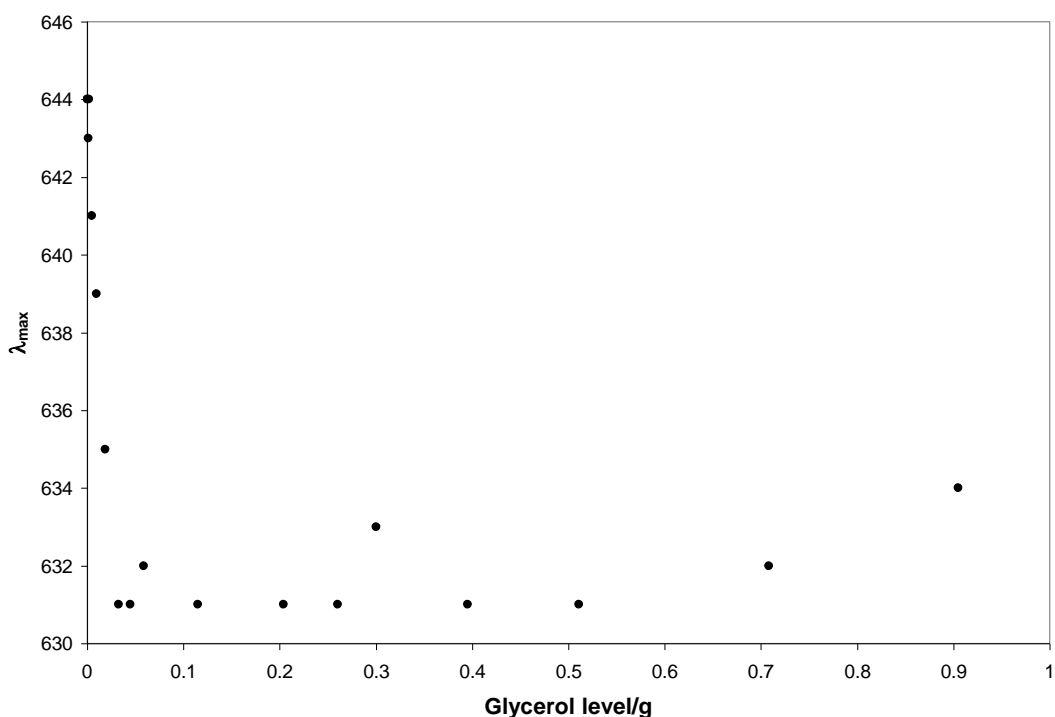


Figure 3.15.: The variation of λ_{\max} with glycerol level

In addition to glycerol, a range of other compounds, some of which are polyols, which have been shown by others to be suitable SEDs were assessed in the indicator ink formulation. A summary of those tested is presented in table 3.1. A quick scan of all the SEDs listed shows that whilst several facilitate reduction of the dye in the indicator ink formulation, many are immediately unsuitable. For some compounds, e.g. EDTA and DL-threitol, it is not possible to make an ink using 300 mg of the SED owing to poor solubility and/or changes in the ink colour. In other instances, e.g. with myo-inositol as the SED, the ink can be cast as a film on the surface of Activ™ but no reduction is then observed to occur, suggesting that such polyols are poor SED agents.

Of the six SEDs which do facilitate dye reduction, none of them produce an initial rate greater than that observed with glycerol. Indeed for triethanolamine (TEOA), which has the fastest calculated rate of reduction after glycerol (2.88×10^{-4} AbsU s⁻¹), it is ca. 2 times slower than that detailed previously for the standard ink. Of all the materials tested as suitable SEDs which do produce an ink capable of facilitating DCIP reduction on Activ™, only TEOA, xylitol and D-sorbitol produce inks which do not present any obvious, detrimental or complicating features; however, the inks produced with such SEDs are slower to reduce in comparison.

3.5. The Effect of Light Intensity on the Performance of the DCIP Ink

In all the work outlined thus far, the UVA irradiance used to facilitate reduction of the ink film on Activ™ has been 4.8 mW cm⁻². Such irradiance is similar to the UVA output from the sun on a summer day (ca. 4.49 mW cm⁻²)²⁴, and hence is indicative of the rate of reduction which would be observed should such an ink be used in the field. As was stated previously in chapter 2, the irradiance of the lamp can be altered simply by increasing or decreasing the distance between the lamp and the sample. Hence, figure 3.16. shows the variation in the rate of reduction for the standard DCIP ink with increasing UV irradiance over the range 0.44 to 7.41 mW cm⁻².

As the light intensity is increased, a linear increase in the initial rate of reduction is observed. Such a linear dependence is attributed to the relatively low irradiance used, the poor absorbing qualities of the UVA light by the photocatalyst layer on Activ™, and the likelihood that, at such low irradiance levels, the reduction of the dye in the ink film will be controlled by the reaction at the ink/photocatalyst interface by the photogenerated h⁺/e⁻ pairs, as opposed to their recombination. At higher irradiance levels, recombination of such h⁺/e⁻ pairs would be anticipated to be the controlling factor. Such results mirror the findings of Mills et al for the Rz indicator ink, attributed to similar factors².

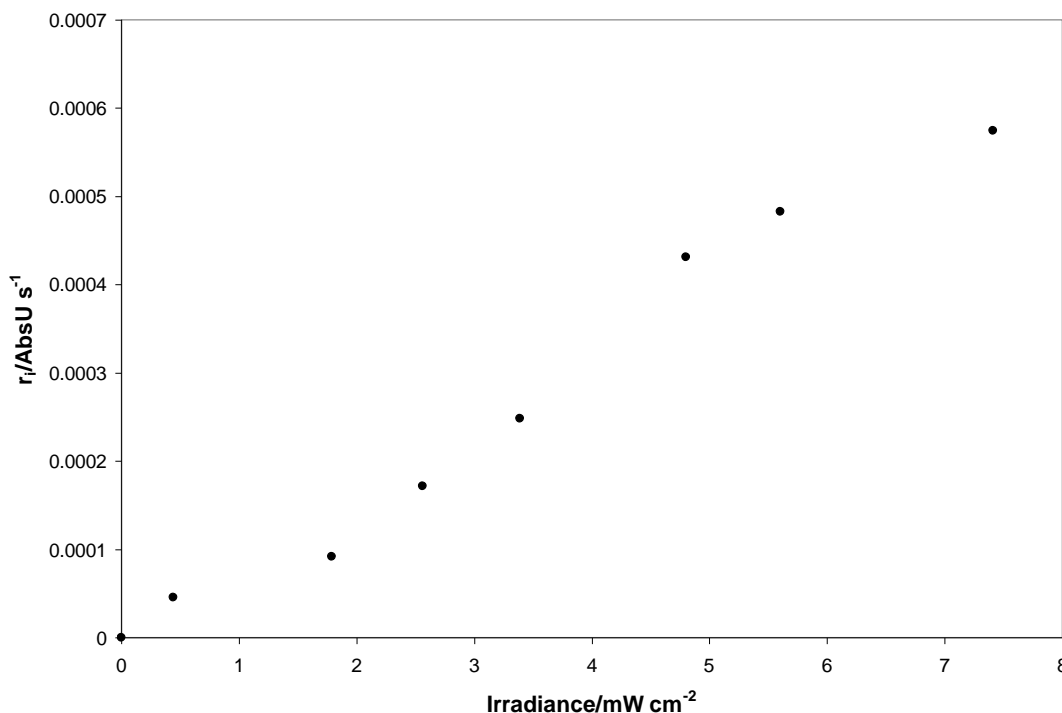


Figure 3.16.: The variation of the initial rate of reduction, r_i , of the DCIP ink on Activ™ with increasing UV irradiance

Over the course of the reduction reaction for the standard DCIP ink, the change in absorbance at λ_{\max} is ca. 0.085 Absorbance units. We also know² that 1 mW cm⁻² irradiance from the UVA source (where the maximum intensity occurs at 365 nm) is equivalent to 1.1×10^{17} photons per cm² per minute. Using these, the quantum efficiency for DCIP reduction can be estimated as follows. The concentration of the dye in the ink film can be determined using equation 3.3.:

$$c = \frac{pphr_{dye}/MW_{dye}}{\left[\frac{(pphr_{poly}/\rho_{poly}) + (pphr_{SED}/\rho_{SED})}{1000} \right]} \quad (3.3.)$$

where $pphr_{dye}$, $pphr_{poly}$ and $pphr_{SED}$ are the parts per hundred resin of the dye, polymer and SED comprising the ink, respectively, MW_{dye} is the dye's molecular weight, and ρ_{poly} and ρ_{SED} are the densities of the polymer and the SED, respectively. For DCIP, the

concentration is found to be 0.065 M. Since the thickness of the ink film, d , is known to be 900 nm from profilometry, the number of moles of dye per cm^2 , x , can be determined using equation 3.4.:

$$x = \frac{c}{1000} d \quad (3.4)$$

From figure 3.16., the gradient of the plot of r_i vs. irradiance can be calculated to be $8.31 \times 10^{-5} \text{ AbsU s}^{-1} \text{ mW}^{-1} \text{ cm}^2$. Hence, it can be inferred that at 1 mW cm^{-2} UVI, the initial rate of reduction, r_i , is $8.31 \times 10^{-5} \text{ AbsU s}^{-1}$. Similarly, the change in absorbance at λ_{max} with time, ΔAbs , for a standard DCIP ink film on Activ™ is ca. 0.085 AbsU. Using these values, the rate of reaction, R_i , can be expressed in the number of moles of dye converted per cm^2 via equation 3.5.:

$$R_i = \frac{r_i}{\Delta\text{Abs}} x \quad (3.5)$$

Again for DCIP reduction, this is calculated to be $5.69 \times 10^{-12} \text{ moles cm}^{-2} \text{ s}^{-1}$. Using Avogadro's number, this can be converted to $3.43 \times 10^{12} \text{ molecules cm}^{-2} \text{ s}^{-1}$. Since the reduction reactions were conducted using a BLB lamp, which is known to emit 1.83×10^{15} photons per second UVA light, the quantum efficiency for the process can be calculated to be 0.0018 molecules per photon. Spectral studies conducted elsewhere have also demonstrated that the photocatalyst layer on Activ™ has an absorbance of ca. 0.065 AbsU at 365 nm^5 . Hence, the quantum yield for the process can be estimated to be 2.5 %. Both the value of the quantum efficiency and the quantum yield are greater than those calculated for the Rz ink by Mills et al², which is highly unexpected since the Rz ink has a faster rate of reduction in comparison, but would appear to be attributable to a slightly greater film thickness (900 nm vs. 590 nm for Rz) and a lesser ΔAbs over the course of the reduction reaction (0.085 AbsU vs. 0.1 AbsU for Rz).

3.6. The Effect of Dye Loading Level on the Performance of the DCIP Ink

The next variable to be examined in the standard DCIP indicator ink formulation was the dye loading level. Previously, 5 mg of DCIP per ink formulation was chosen as standard in order to produce an ink which, when cast on Activ™, would give a similar absorbance to that of the original Rz ink examined previously by Mills et al². The DCIP level was varied over the range 1 to 10 mg (equivalent to 2.2-22 pphr) and the inks produced assessed for their rates of reduction on Activ™. The results are plotted in figure 3.17.

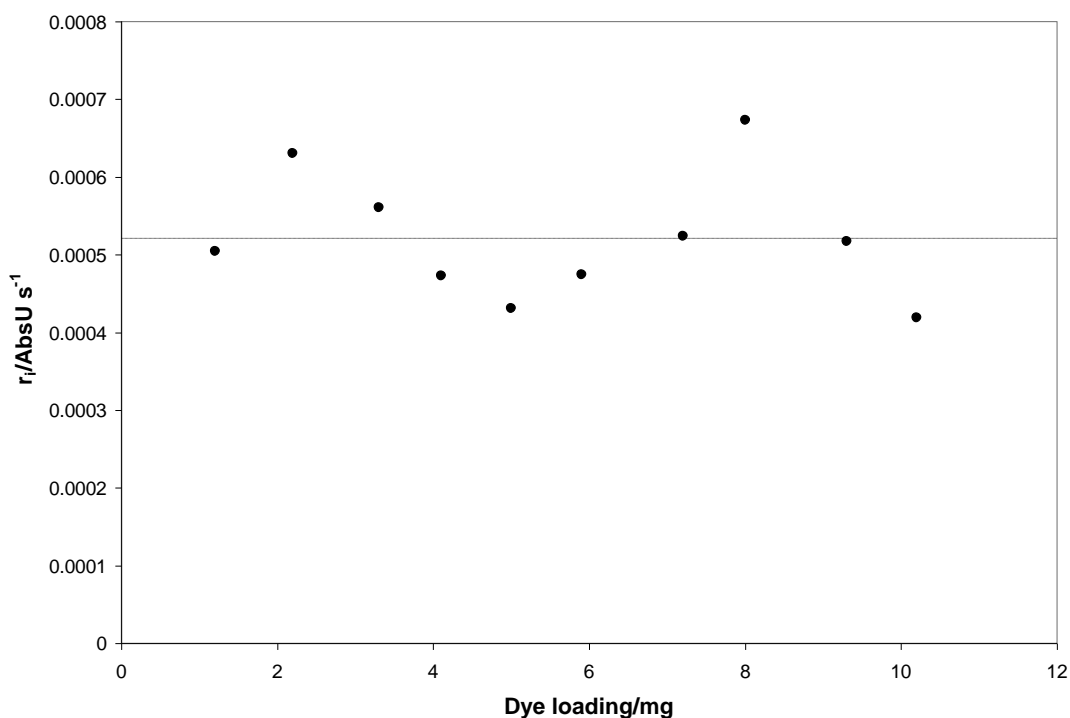


Figure 3.17.: The variation in the initial rate of DCIP reduction on Activ™ with increasing dye level

As was observed previously with varying glycerol level, there is no significant trend to the variation in the rate of reduction obtained with dye loading. The dashed line in figure 3.17. indicates the average r_i of 5.21×10^{-4} AbsU s⁻¹. Again, if we assume a

Langmuir-Hinshelwood kinetic treatment of the data, it can be inferred that the concentration of the dye in such formulations is significant so as to collapse the expression into that for $[S]_i \rightarrow \infty$, i.e. the initial rate is zero order and independent of the dye level.

This result is in stark contrast to the behaviour of the Rz photocatalyst indicator ink reported previously by Mills et al over a similar dye loading range², where the initial rate of reduction was observed to decrease by a factor of 4 as the dye level was increased from 1 to 8 mg. This was attributed by the authors to an increasing level of less reactive Rz dimers with increasing dye loading, supported by spectral changes showing a shoulder peak emerging at 570 nm as the dye loading was increased up to 40 mg per formulation. In contrast, the shape of the peak in the absorption spectrum of the DCIP ink does not change significantly as a function of dye loading, as is indicated in figure 3.18. for inks containing 2 and 10 mg of dye, respectively. This finding implies that dimer (and/or multimer) formation occurs at very low DCIP levels, and that such species do not inhibit the rate of reaction. Indeed, the broad peak due to DCIP (ca. 200 nm in wavelength) confirms that such species are present even at 2 mg per formulation.

The implication from figure 3.17. is that the initial rate of DCIP reduction is independent of the amount of dye present. Such an observation is not unusual in semiconductor photochemistry and implies that either all the reactive sites associated with dye reduction are occupied by molecules of DCIP, or that the rate-determining step does not involve the reduction of DCIP. However, such results cannot be used directly to indicate the kinetics of the reduction reaction. Hence, the data obtained across the dye loading level was treated assuming zero order kinetics, and the $t_{50\%}$ calculated using equation 3.6., i.e.;

$$t_{50\%} = [D]_0/2k \quad (3.6.)$$

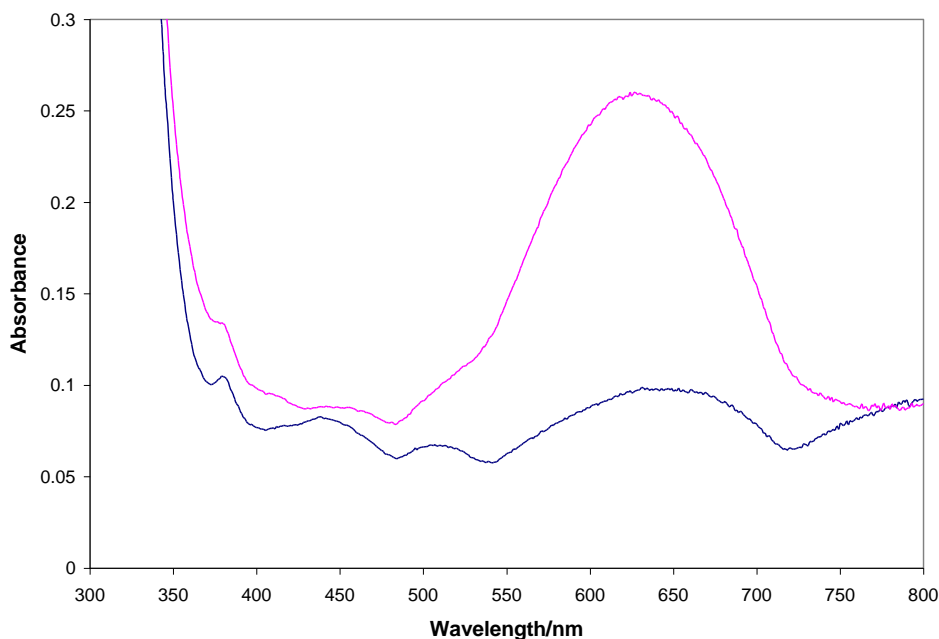


Figure 3.18.: A comparison between the initial ink film traces obtained at 2 mg (blue trace) and 10 mg (pink trace) dye loading levels

The variation in the zero order $t_{50\%}$ with dye level is plotted in figure 3.19. As the dye loading level is increased in the indicator ink formulation, so we observe the zero order $t_{50\%}$ to increase almost linearly. Such behaviour for the DCIP, Rz and MB indicator inks has recently been verified by other work conducted within this laboratory³, and is indicative of zero order kinetics, as equation 3.6. shows that $t_{50\%}$ is directly related to the initial dye concentration, $[D]_0$. If the reaction was governed by first order kinetics, the $t_{50\%}$ would be independent of dye level, as indicated by equation 3.7.;

$$t_{50\%} = (\ln 2)/k \quad (3.7.)$$

Although only three inks have been observed to conform to this behaviour, with the number of theoretical inks which can be made much greater than this, it would appear reasonable to assume that all indicator inks will follow a zero order reaction on Activ™.

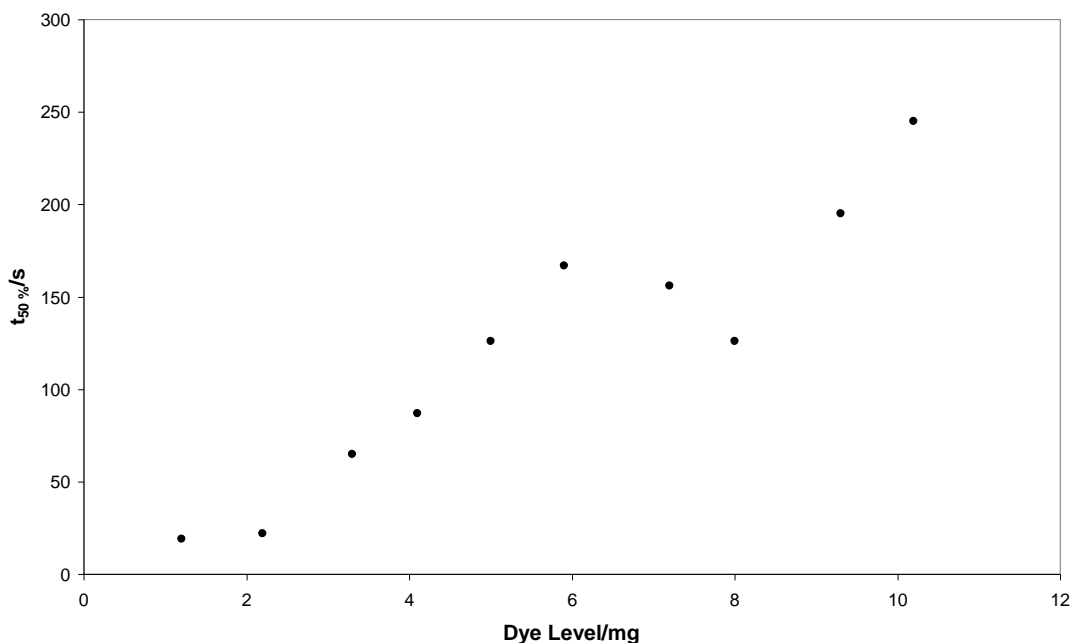


Figure 3.19.: The variation in zero order $t_{50} \%$ for DCIP reduction on Activ™ with increasing dye level

3.7. The Effect of Spin Speed on the Performance of the DCIP Indicator Ink

The final variable assessed for its effect on the rate of reduction of the DCIP indicator ink was that of the spin speed used to coat the film on to the surface of the Activ™ photocatalyst. Obviously as the spin speed is altered, so the thickness of the cast ink film will change, with the standard 500 rpm spin speed yielding a film thickness of ca. 900 nm, as measured by profilometry. As the spin speed is increased, so the film thickness would be expected to decrease accordingly.

Figure 3.20. shows how the initial rate of reduction, r_i , varies with increasing spin speed. Again, as was observed previously for the variation in r_i with both glycerol and dye loading level, no significant trend to the data is observed. The dashed line indicates the average r_i ($= 5.06 \times 10^{-4} \text{ AbsU s}^{-1}$) around which the values obtained at each spin speed vary.

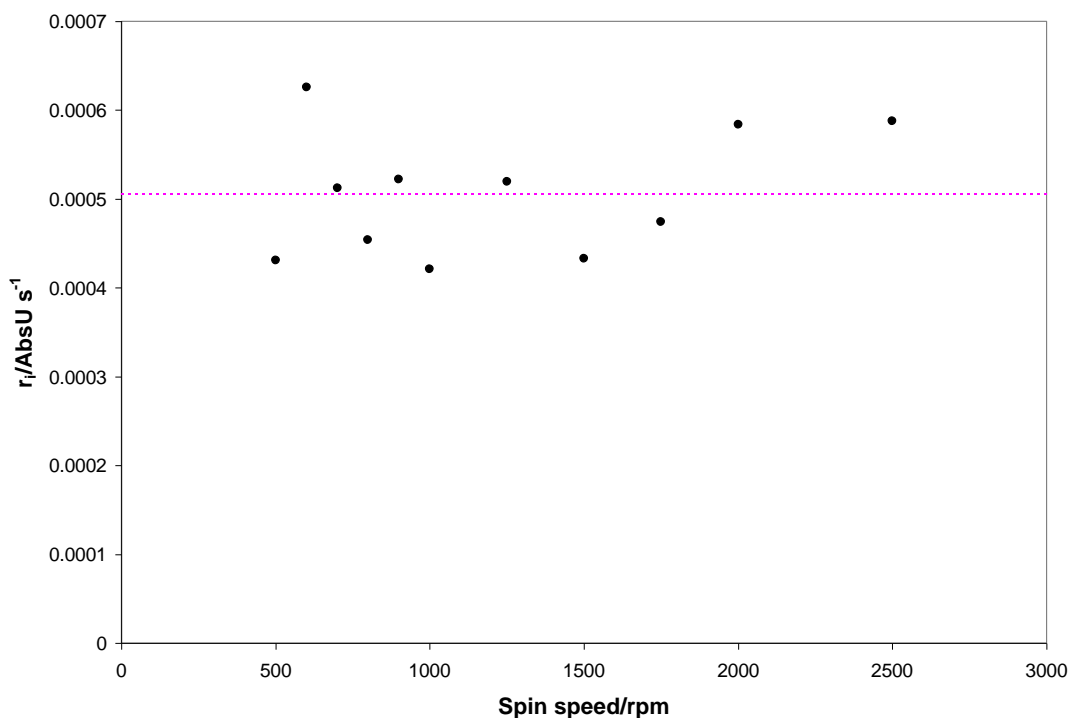


Figure 3.20.: The variation in r_i with spin speed for the DCIP indicator ink

Hence, the spin speed was then plotted against the zero order $t_{50\%}$ for the reaction and the results are shown in figure 3.21. As the spin speed is increased, the zero order $t_{50\%}$ decreases, implying a faster rate of reduction as the film thickness decreases. This is to be expected since at lower film thicknesses, the initial concentration due to DCIP will be less. Since the zero order rate equation shows that $t_{50\%}$ is directly proportional to $[D]_0$, it follows that as $[D]_0$ decreases, so the $t_{50\%}$ must decrease. The curved nature of the plot, however, suggests that the $t_{50\%}$ does not decrease linearly with decreasing film thickness. Instead, at very low film thicknesses, a limiting value of the $t_{50\%}$ is approached (ca. 40 s from figure 3.21.). Presumably at higher dye loading levels, the amount of photocatalyst present becomes the critical factor in deciding the rate of reduction, whereas at lower levels all of the photocatalyst sites will be occupied by dye molecules, giving a higher reduction rate.

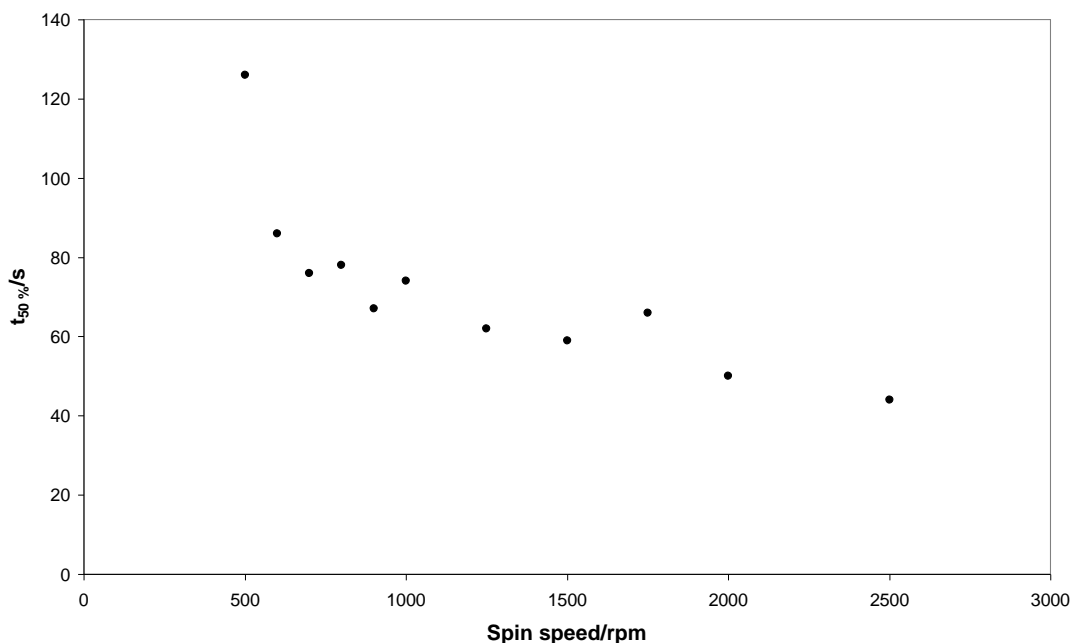


Figure 3.21.: The variation in the zero order $t_{50} \%$ with increasing spin speed for the DCIP indicator ink

3.8. The Stability of the DCIP Indicator Ink

Within the work of Mills et al on the Rz indicator ink², probably their most important finding, from an industrial perspective, is that the indicator ink is stable within a sample vial or felt-tipped pen for > 6 months. For the DCIP ink, unfortunately, the stability is much less, of the order of 1 month at room temperature and ca. 3 months when stored in a fridge, as mentioned previously. After such periods of time, the ink is observed to change colour from blue to red and insoluble species are also noted to be present. As a result, the ink cannot be spun as a film on the surface of ActivTM. Such a change in the colour is also noted if the dye is simply placed in water and left under similar conditions. Samples of a fresh DCIP ink and a similar ink following storage for 1 month at room temperature are shown in figure 3.22.



Figure 3.22.: The DCIP indicator ink (left) and a similar ink after 1 month at room temperature (right)

As would be anticipated, such changes in the colour of the ink impact the spectrum observed for the ink. Indeed, the λ_{\max} of the dye is blue-shifted ca. 85 nm as it changes colour from blue to red following the 1 month storage at room temperature (data not shown). In addition, the pH of the two solutions was also recorded. For the standard DCIP indicator ink, the pH was determined to be 6.83, whereas the degraded sample registered a pH of 5.82, i.e. a factor of 10 times more acidic than it was originally. Such results would suggest that a pH effect is the source of the colour change within the indicator ink. However, this does not answer the question of why such a change is also observed for the dye in solution, as has been noted both here and by others¹⁵⁻¹⁶.

One possible explanation could be that the dye is susceptible to hydrolysis, since this explains the observed change in both solution and the indicator ink. It is postulated that the chlorine groups, which are known to be excellent leaving groups in nucleophilic substitution reactions, can be easily displaced by hydroxyl groups. Such a displacement would affect both the electronic structure of the dye, causing it to change colour, and its solubility in water, which would explain the emergence of the insoluble species.

One way in which this low shelf-life for the DCIP indicator ink can be extended is to change the SED from glycerol to xylitol, one of the potential SED species tested and reported previously in table 3.1. Whilst such a change leads to some retardation in the reduction kinetics, the shelf-life for such an ink increases to ca. 3 months at room temperature. Whilst shelf-life is less of an issue in the laboratory, where the necessary chemicals are on hand, in industry it is a much more important factor since the ink will be encompassed in felt-tipped pens to be used to demonstrate photocatalytic activity to potential customers in the field. A balance therefore has to be struck within the minds of potential users of the pen as to whether the ink's shelf-life or a slightly faster rate of reduction of the ink is more important. For comparison, the time taken for complete reduction of the standard DCIP ink under summer sun conditions (i.e. UVA irradiance ca. 4.8 mW cm^{-2}) is 7.5 minutes, whilst with xylitol as the SED, the time taken for complete reduction of the ink to occur increases to 9.5 minutes. What is more important – a 2 minute increase in the total reduction time, or a pen that has the potential to last 2 months longer?

3.9. The DCIP Indicator Ink in a Felt-Tipped Pen – A Rapid Method for Assessing the Photocatalytic Activity in the Field

Despite the issue with the glycerol-based DCIP ink's stability, it is still possible to incorporate such an ink into a felt-tipped pen. Such a pen is suitable for use primarily in the field, the ink being easily applied by simply writing on to the photocatalyst surface. The user can then simply watch for the colour change occurring using UVA from the sun, indicating that their product is photocatalytically active. Not only do the use of a pen and the subsequent colour change of the DCIP indicator ink make semiconductor photocatalyst technology accessible to non-scientific consumers, but it also provides industry with a means of rapidly determining the activity of commercial products in the field without the need for trained personnel. The pen also eliminates the need for an analytical tool to monitor the reaction i.e. it is self-indicating. Figure 3.23. shows the type of pen used in this laboratory (a Copic felt-tipped pen) along with a sample of the ink, whilst figure 3.24. shows how the ink could be used to write on Activ™ and a self-

cleaning tile (Hydrotect, supplied by Deutsche-Steinburg), and the subsequent effect of irradiating these samples with UVA light.



Figure 3.23.: The type of felt-tipped pen commonly used with a sample of the DCIP ink

It can be seen that the blue writing on both the self-cleaning glass and tile samples turns colourless after irradiation. The longer irradiation time necessary to complete the reduction on Activ™, as indicated by the legend in figure 3.24. (note that the UVI is ca. 7 mW cm^{-2} in this instance) is thought to be due to the ink thickness on the sample surface being greater than that when spun-coated at 500 rpm, i.e. greater than ca. 900 nm. The dye concentration is also 3 times greater than that in the standard formulation in order to emphasise the colour change, and hence this will impact the kinetics. In addition to this, we also observe that the time taken for reduction of the dye to occur on the photocatalyst tile is ca. 12 times greater than that observed on Activ™ glass. If we make the crude assumption that the thickness of the ink film applied to both substrates is the same, and ignoring the effect of porosity, one can infer that the photocatalytic activity of the tile is thus ca. 12 times less. Such a test emphasises the usefulness of the felt-tipped pen, as companies could possibly use them to demonstrate to potential

customers the relative activity of their product in comparison to others available on the market.



(a)

(b)



(c)

Figure 3.24.: The photoreduction of the DCIP ink when applied to Activ™ self-cleaning glass and Hydrotect tile using an indicator pen. At 0 minutes (a), the ink is observed to produce a striking blue colour on both the tile and glass surface. After 5 minutes irradiation (b) at a UVI of ca. 7 mW cm^{-2} , the ink is observed to have changed colour on the surface of Activ™, though is still visible on Hydrotect. Further irradiation up to 1 hour eventually leads to dye photoreduction on the tile surface (c)

3.10. Conclusions

An ink based on the dye 2,6-dichloroindophenol (DCIP) has been successfully prepared and can be used to rapidly assess the photocatalytic activity of thin photocatalyst films. On Pilkington Activ™, a commercial self-cleaning glass, the ink can be cast by either spin-coating or via a felt-tipped pen, and reduces completely under a UVA output equivalent to sunlight conditions in ca. 7.5 minutes. Despite this slightly slower rate of reduction compared to the Rz indicator ink, the DCIP ink is more desirable for industry since the dye reduces to a colourless product. The maximum recovery obtained in unrealistic conditions (i.e. sustained darkness) is ca. 38 %, with ca. 35 % recovery noted over a 12 hour time period.

The DCIP indicator ink is found to be extremely sensitive to the amount of glycerol present, with a similar initial rate of reduction achieved using 30 mg glycerol to that for the standard ink, where the glycerol level is 10 times greater. Below 30 mg, the initial rate of reduction decreases rapidly, appearing to conform to Langmuir-Hinshelwood kinetics, with no reduction possible in the absence of the SED. It is postulated that oxidation of the SED by photogenerated holes leads to the formation of glyceraldehyde and reactive α -hydroxylalkyl radicals, the latter assisting in the photoreduction of the dye. Other materials, mainly polyols, were also assessed for their suitability as SEDs and whilst some proved ineffective, those which facilitated dye reduction were all observed to do so at a slower rate compared to glycerol. Similarly, changing to PVA as the polymer for the ink was observed to make no positive impact on either the reduction or recovery characteristics of the ink.

As would be anticipated, increasing the UVA irradiance causes the initial rate of reduction to increase, driven by the reaction at the ink/photocatalyst interface by the h^+/e^- pairs owing to the low irradiance used. In addition, by varying the UVA irradiance both the quantum yield and the quantum efficiency for the reduction process could be estimated to be 2.5 % and 0.0018 molecules per photon respectively. Both of these values are greater than that observed by Mills et al for the Rz indicator ink², which is

unexpected since the latter reduces faster on Activ™ under similar atmospheric conditions.

At first glance, the reduction of the ink would appear to be independent of dye level, with no significant trend in the initial rate of reduction noted as the dye level is increased. However, when the zero order $t_{50\%}$ values are plotted against increasing dye level, a linear trend is observed, implying a zero order kinetic dependence. This observation is in agreement with recent work conducted by others in this group on three separate indicator inks³. So whilst the ink can be made more blue, hence giving a more striking film when coated on to the surface of the semiconductor, the kinetics will be retarded as a consequence, which has implications in the manufacture of the proposed indicator pen.

The major drawback to the DCIP ink is its lack of stability. Over the course of 1 month at room temperature (or ca. 3 months in a fridge), the ink is observed to change colour from blue to red, accompanied by the development of some insoluble species. In addition, such an effect is also observed if the dye is simply left in water for similar periods of time. It is believed that the dye undergoes hydrolysis, the Cl groups being relatively labile and hence easily displaced by hydroxyl groups via a nucleophilic substitution reaction. This affects the electronic structure of the dye, and hence its colour and solubility. One way in which the shelf life can be prolonged is to use xylitol, a 5-carbon polyol as the SED, but such a change causes the kinetics of reduction to slow by a factor of ca. 2.

3.11. References

- (1) A. Mills; J. Wang; S.-K. Lee; M. Simonsen *Chem. Commun.* **2005**, 2721.
- (2) A. Mills; J. Wang; M. McGrady *J. Phys. Chem. B* **2006**, *110*, 18324.
- (3) A. Cusick The Kinetics of Dye Photocatalysis Univeristy of Strathclyde, Glasgow 2009.
- (4) K. D. Sanderson; J. A. Knowles Self-Cleaning Glazing Sheet, WO 03/050056

-
- (5) A. Mills; A. Lepre; N. Elliott; S. Bhopal; I. P. Parkin; S. A. O'Neill *Journal of Photochemistry and Photobiology A: Chemistry* **2003**, *160*, 213.
 - (6) M. Siu; V. A. Yaylayan; J. M. R. Bélanger; J. R. J. Paré *Tetrahedron Letters* **2005**, *46*, 5543.
 - (7) E. Kishida; Y. Nishimoto; S. Kojo *Anal. Chem.* **1992**, *64*, 1505.
 - (8) J. P. Markwell; C. D. Miles; R. T. Boggs; J. P. Thornber *FEBS Letters* **1979**, *99*, 11.
 - (9) Y. Yang; J.-X. Xu; H.-M. Zhou *The International Journal of Biochemistry and Cell Biology* **1998**, *30*, 1147.
 - (10) C. Trampitsch; A. Slavica; W. Riethorst; B. Nidetzky *Journal of Molecular Catalysis B: Enzymatic* **2005**, *32*, 271.
 - (11) K. Eaton *Sensors and Actuators B* **2002**, *85*, 42.
 - (12) M. Hilgendorff; D. W. Bahnemann *Environmental Aspects of Electrochemistry and Photoelectrochemistry*; Pennington: N. J., 1993.
 - (13) P. A. Mandelbaum; A. E. Regazzoni; M. A. Blesa; S. A. Bilmes *J. Phys. Chem. B* **1999**, *103*, 5505.
 - (14) R. W. Horobin, *Conn's Biological Stains*; Ch23. Polymethine dyes - 1. Cyanines, oxonols, benzimidazoles, indolenines and azamethines, R. W. Horobin, J. A. Kiernan, BIOS Scientific Publishers Ltd, 2002
 - (15) W. Lojander *Chem Abstr.* **1941**, 35.
 - (16) E. Bishop *Indicators*; Pergamon Press, 1972.
 - (17) S.-K. Lee; A. Mills; A. Lepre *Chem. Commun.* **2004**, 1912.
 - (18) A. Mills; S.-K. Lee; M. Sheridan *The Analyst* **2005**, *130*, 1046.
 - (19) S. Pauly, *CRC Handbook of Chemistry and Physics; Permeability and Diffusion Data*, CRC Press, 2004
 - (20) A. Fujishima; T. N. Rao; D. A. Tryk *Journal of Photochemistry and Photobiology C: Photochemistry Reviews* **2000**, *1*, 1.
 - (21) A. Mills; S. L. Hunte *Journal of Photochemistry and Photobiology A: Chemistry* **1997**, *108*, 1.
 - (22) O. Carp; C. L. Huisman; A. Reller *Progress in Solid State Chemistry* **2004**, *32*, 33.
 - (23) E. V. Keuren; W. Schrof *Macromolecules* **2003**, *36*, 5002.

(24) A. Mills; M. McFarlane; S. Schneider *Anal. Bioanal. Chem.* **2006**, 386, 299.

4 Evaluation of New Photocatalyst Indicator Inks

In the previous chapter, a new indicator ink based on the redox dye 2,6-dichloroindophenol was developed for assessing the photocatalytic activity of thin, self-cleaning films, such as those found on many commercial glasses and tiles. The ink was characterised and comparisons were drawn, where possible, with the Rz ink of Mills et al¹⁻². Whilst direct comparisons of the rate of reduction are difficult to ascertain owing to slight variations in the reaction conditions, the DCIP ink is more suitable for use in the field owing to its colourless, reduced product (leuco-DCIP). Conversely, however, the Rz ink is known to be stable for longer. As a result, the choice of ink would appear to be very much down to the researcher. What is needed is an insight into the performance of the inks under similar conditions such that their attributes, in particular the kinetics of reduction and recovery, can be fairly compared.

In addition to these two inks, it is also possible to produce inks based on the redox dyes methylene blue (MB) and resorufin (Rf). Both dyes have the immediate advantage over Rz that they reduce to colourless products, namely leuco-MB and dihydro-Rf respectively. However, neither dye has been characterised in the indicator ink formulation, hence their performance is unknown. This chapter details the findings of a study whereby the four dyes were examined for their suitability in the photocatalyst indicator ink formulation. Pilkington Activ™ was chosen as the test substrate, although similar results would be anticipated using e.g. BioClean™ glass, a Saint-Gobain product. The inks will be compared based on their ease of reduction and their recovery characteristics, with a view to ultimately determining the most suitable for use by product manufacturers in the field.

4.1. Properties of the Redox Dyes for Photocatalyst Inks Used to Assess the Photocatalytic Activity of Activ™ Self-Cleaning Glass

Table 4.1. shows the structures of the dyes assessed for their suitability in the indicator ink formulation for the measurement of the photocatalytic activity of Activ™ self-cleaning glass, namely MB, Rf, Rz and DCIP.

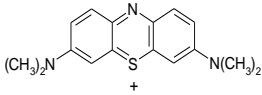
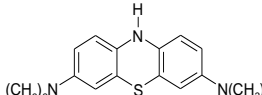
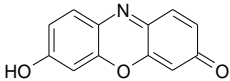
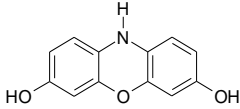
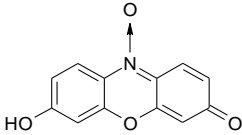
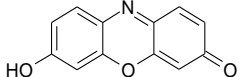
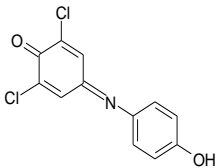
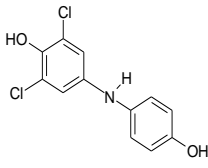
Dye	Oxidised indicator dye (D_{ox})	Reduced indicator dye (D_{red})	$E^\circ(D_{ox}/D_{red})/V$ at pH 7 vs. SHE ³	$\lambda_{max}(D_{ox})/nm$ (solvent) ⁴
MB			+0.011	661 (H ₂ O)
Rf			-0.051	573 (CH ₃ OH)
Rz			N/A	598 (H ₂ O)
DCIP			+0.228	605 (H ₂ O + 2ml 1 N NaOH)

Table 4.1.: The 4 dyes assessed for their suitability in the indicator ink formulation for measuring the photocatalytic activity of Activ™ self-cleaning glass. The oxidised and reduced forms of the dye are shown along with the redox potential of the couple and the wavelength of maximum absorbance (λ_{max}) of the oxidised form of the dye

MB belongs to the thiazine family of dyes, whilst Rf and Rz are oxazines. DCIP, on the other hand, does not specifically fall into any dye family, although the many related compounds to it are traditionally referred to as indophenols dyes and classified loosely as azamethines.

The electrochemical reduction of the oxidised forms of the redox dyes MB, DCIP and Rf, is reversible, and the values of the redox potentials in table 4.1. indicate that DCIP, with its positive redox potential of + 0.228 V, should be the easiest, and hence the most rapid of the dyes to be reduced on thermodynamic grounds, since for the photogenerated electrons in TiO₂, $E_0(e^-) = - 0.52 \text{ V}^5$. Correspondingly, leuco-DCIP (i.e. the reduced form of DCIP) should be the most difficult of the leuco forms of the dyes to be re-oxidised by oxygen, since $E_0(\text{O}_2/\text{H}_2\text{O}) = 1.23 \text{ V}$. For all dyes, the reduction reaction should be spontaneous in the presence of the photocatalyst, since the redox potential of the photogenerated electrons is much more negative than that for any of the redox couples.

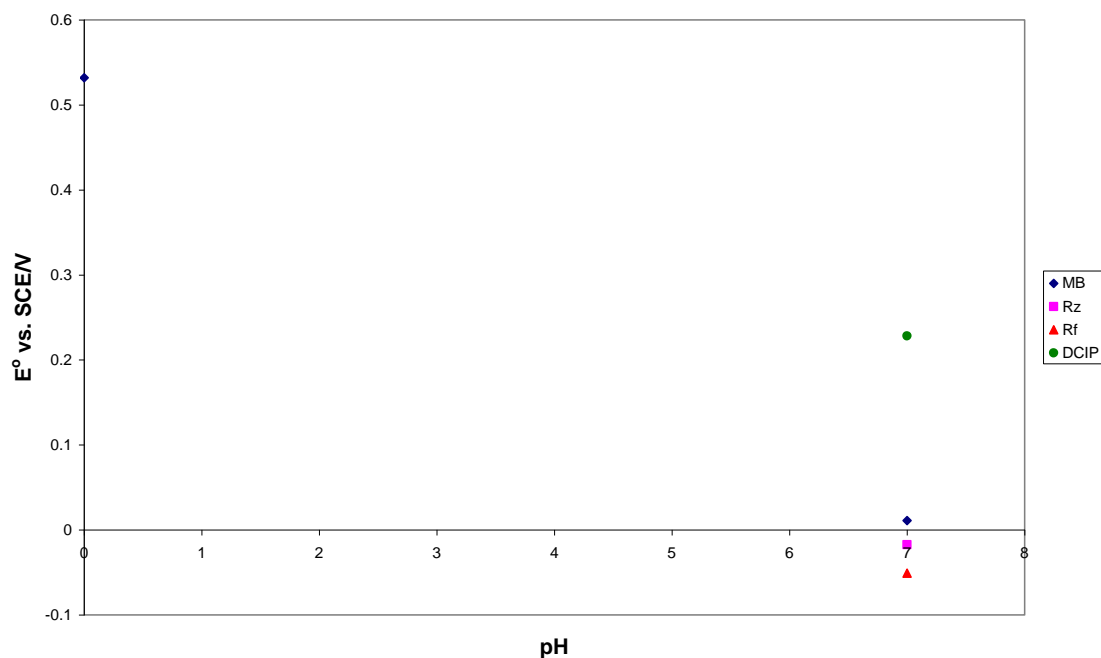
In contrast, Rz reduction is electrochemically irreversible, thus no formal redox potential can be quoted for the dye. However, the results of work carried out elsewhere³ suggests that the dye reduces at a potential somewhere between that of MB and indigo tetrasulfonate, i.e. between + 0.011 and – 0.046 V vs. the standard hydrogen electrode (SHE) at pH 7.

In table 4.1., the values of the wavelength of maximum absorbance in the visible region (λ_{max}) for the oxidised form of each dye in a typical solvent are also quoted⁴. However, as will be seen later, the λ_{max} of each dye in the indicator ink formulation, when cast as a film on the Activ™ photocatalyst, is shifted compared to those values quoted above. This is attributed to two things. First and foremost, the dye is in a different solvent medium when incorporated into the indicator ink formulation compared to what is quoted in table 4.1. Secondly, due to the high concentration of the dyes in the indicator ink formulations, multimer formation is believed to be facilitated. As a result, broader

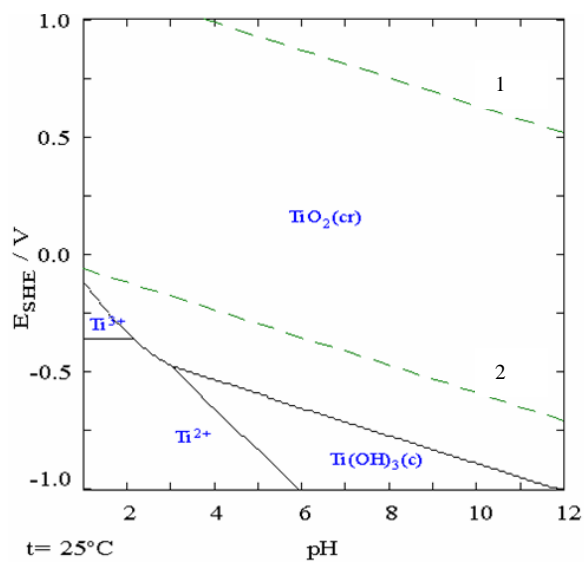
peaks are anticipated in the film spectra due to the formation of dimers, trimers, etc, which can, and in this instance does, lead to a shift in the observed λ_{\max} .

Table 4.1. also gives the structures of the final reduced forms of the dye, and it can be seen that, in most cases, the reduction of the dye involves a two electron transfer step accompanied by the addition of one or two protons. There is an exception, however. For Rz, reduction involves the removal of a dative N to O bond, and the subsequent loss of the O atom from the molecule. It is believed that the reduced forms quoted above for each dye are the ultimate products from their photoreduction when incorporated in the indicator ink formulation. With the exception of Rz, the reduced product for each dye given in table 4.1. above is colourless, and as a result the ink should appear colourless when the reduction reaction is complete on the photocatalyst surface. From table 4.1., it can be seen that the reduced product of Rz, however, is the dye Rf, which is pink. Hence, the complete photoreduction of Rz when incorporated into an indicator ink is a two-stage process, the first of which involves a colour change from blue (Rz) to pink (Rf), followed by pink to colourless (DihydroRf). This is even more undesirable from a commercial viewpoint since a double colour change would presumably be more difficult to explain to potential customers.

Figure 4.1. shows the redox potential of the dyes plotted as a function of pH. The importance of the MB redox potential being quoted at pH 0 will become apparent later in chapter 6. For comparison, the Pourbaix diagram for titanium is also shown⁶. It can be seen that all of the dye redox potentials lie in the region corresponding to TiO_2 in the titanium Pourbaix diagram, and all well below the O_2 reduction line, further emphasising the preference of the dyes to be photoreduced ahead of O_2 by the photogenerated electrons.



(a)



(b)

Figure 4.1.: A plot showing the variation in the dye redox potential for the dyes studied here (a) and the Pourbaix diagram for titanium (b, kindly reproduced from [6]). On the titanium Pourbaix diagram, dashed line 1 corresponds to the variation in the redox potential for the reduction of O_2 to water, whilst dashed line 2 corresponds to the variation in the redox potential for the reduction of protons to give H_2

4.2. Indicator Inks Under Anaerobic Conditions – A Comparison of the Rate of Dye Photoreduction

The reduction of the indicator inks was assessed initially under an atmosphere of N₂, since the presence of atmospheric O₂ could possibly lead to the undesirable re-oxidation of the reduced forms of the dyes under test. As noted earlier, since Rz is irreversibly reduced, it would be anticipated that photoreduction of this dye is the least likely to be affected by the presence of oxygen. In addition, although reduction of the DCIP ink has been shown previously in chapter 3 to be unaffected by the presence of oxygen, it is tested here in order to allow a complete comparison to be drawn.

4.2.1. Methylene Blue (MB)

The first of the four dyes studied for their suitability in an indicator ink formulation was methylene blue (MB). MB is a thiazine dye which has previously found use in many medical fields, including, but not exclusively⁷⁻⁸;

- As an anti-malaria drug;
- To treat cyanide poisoning, and;
- As a veterinary antiseptic

From a chemistry standpoint, the dye is an excellent stain, useful for, but not exclusively limited to, staining bone marrow and most general bacteria⁹, and for determining whether yeast is still active, since the enzyme activity causes the dye to change colour from blue to colourless¹⁰. The dye is also frequently used in the classic ‘Blue Bottle’ undergraduate experiment¹¹, where it is placed in contact with glucose and a suitable alkali. The alkali deprotonates the sugar, which in turn facilitates the reduction of the dye to leuco-MB. By shaking the mixture, oxygen from the headspace above the solution dissolves into it, thus regenerating the blue colour of MB through re-oxidation of the leuco- form. This transformation is only temporary, with the reduced form of the dye slowly being regenerated as the deprotonated glucose reduces the MB. The dye essentially acts as a redox indicator in the system, and can thus be applied to

other reactions for the same purpose, including polymerisation of the dye for use in a redox electrode¹². Industrially, the dye is typically used in the manufacture of pigments and to colour leather, paper and wood⁹. Figure 4.2. shows the structure of MB and its reduction mechanism.

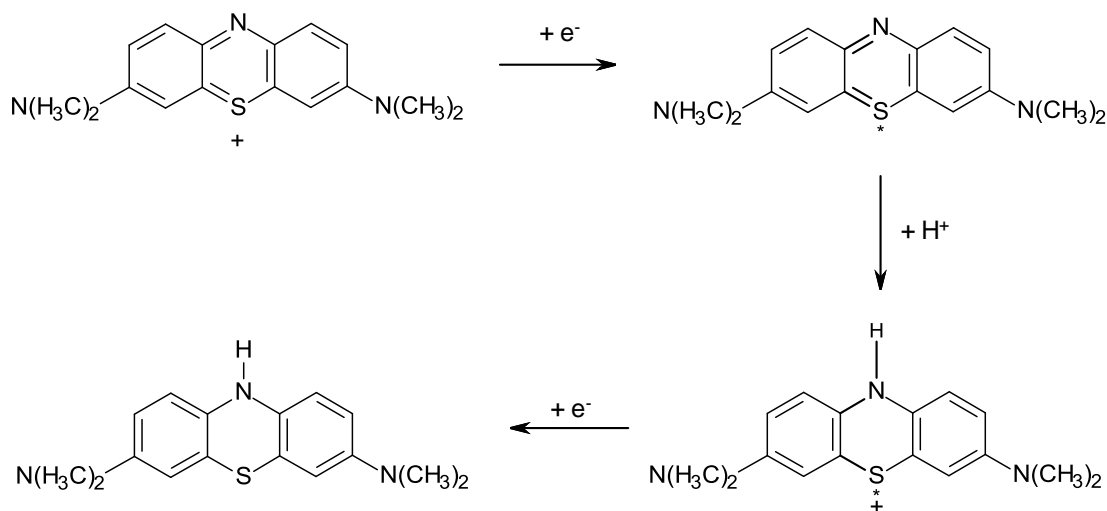


Figure 4.2.: The structure of MB and its subsequent reduction reaction

Figure 4.3. shows the UV-visible absorbance spectra of MB (ca. 1×10^{-5} M) in aqueous solution and the corresponding dye spectra when cast as an ink film on Activ™. In solution, the peak absorbance (λ_{\max}) of MB occurs at 665 nm, which is slightly different to the value quoted in table 4.1., with a shoulder peak at ca. 615 nm. For the dried ink on the surface of Activ™, 2 peaks are observed in the absorbance spectrum at ca. 608 and 663 nm. It will be seen later that as the dye is photoreduced in the ink due to the action of the photocatalyst, so the colour of the ink changes from blue to colourless, and thus the peaks observed in the UV-Vis absorbance spectrum disappear with irradiation time; therefore, either peak is suitable for use to monitor the photoreduction of the dye. The peak at 608 nm is chosen simply because it's absorbance in the spun ink is greater.

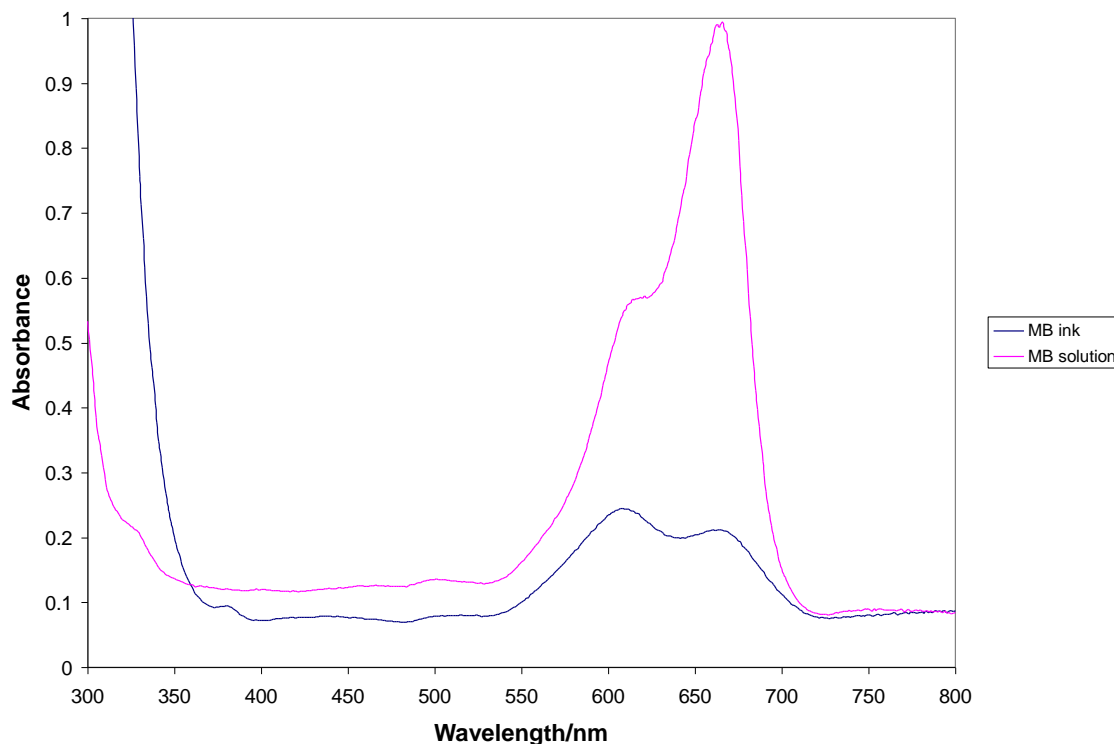


Figure 4.3.: The UV-Visible absorbance spectra of MB (1×10^{-5} M) in aqueous solution (pink trace) and when placed in the indicator ink formulation and cast as a film on the surface of Activ™ (blue trace)

Figure 4.4. shows the change in the absorbance spectra observed for a spun MB ink which occurs when it is irradiated under anaerobic conditions on the surface of Activ™. With UV irradiance (UVI) of ca. 1.3 mW cm^{-2} , the dye is observed to reduce completely to leuco-MB in 1 hour. Further irradiation causes no further colour, or indeed spectral changes to occur, with slow mineralization (or photooxidation) of the other ink components, namely the polymer (HEC) and the SED (glycerol) likely to be facilitated. This has previously been suggested by Mills et al for the standard Rz ink². Owing to the thickness of the photocatalyst film (ca. 15 nm), this slow mineralization process is not believed to compete with the reduction reaction over the timescales noted here, with Mills et al postulating that a time period of ca. 50 hours is necessary².

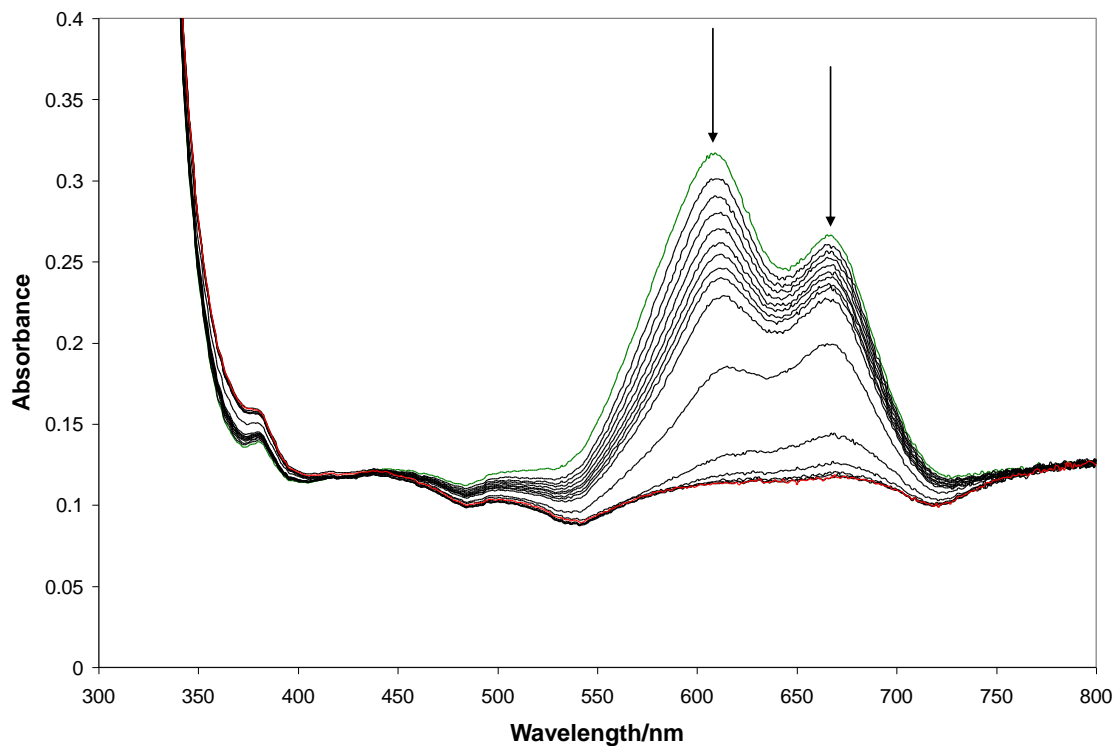


Figure 4.4.: The change in the UV-Visible absorbance spectrum of a MB ink with irradiation under N_2 . The green trace indicates the initial ink spectra, whereas the red trace shows the ink spectra after 1 hour of UVA irradiation. Spectra were recorded at 30 s intervals for 5 minutes and then at 10 minute intervals from 10 minutes up to 70 minutes

As with the DCIP ink characterised in chapter 3, the initial rate of photoreduction of the MB ink can be determined by plotting the variation in the absorbance at λ_{\max} with time, as shown in figure 4.5. From this, r_i is calculated to be $3.458 \times 10^{-4} \text{ AbsU s}^{-1}$.

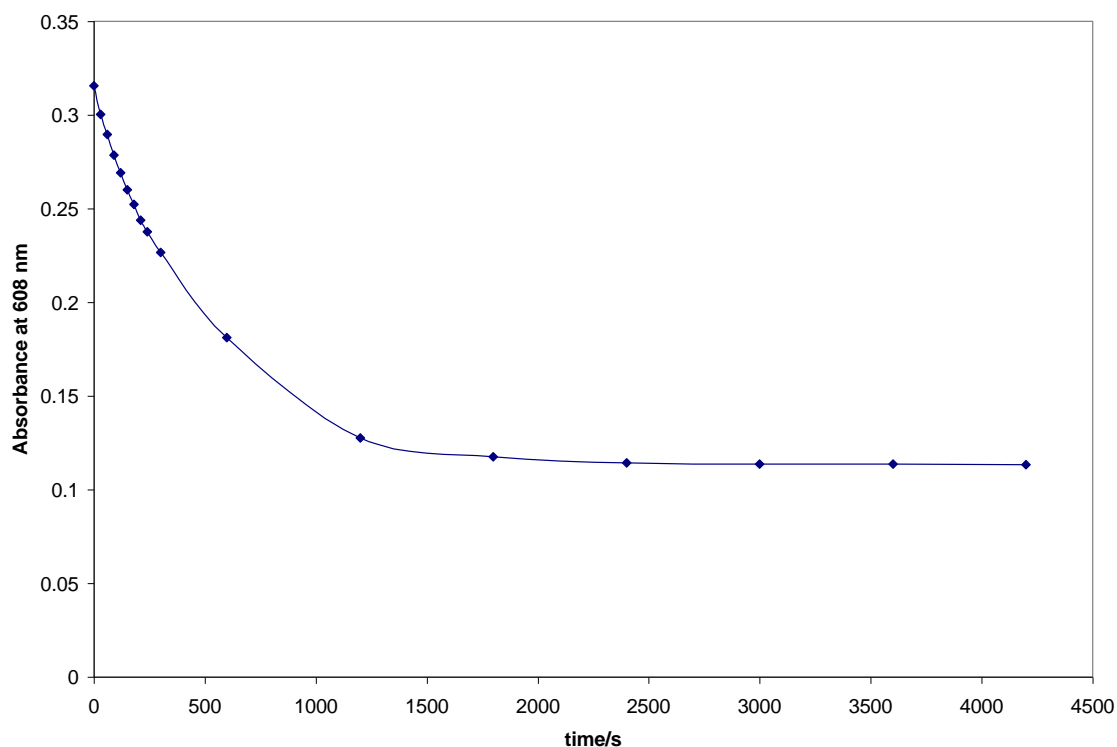


Figure 4.5.: The change in absorbance at λ_{\max} (608 nm) with irradiation time for a MB ink on Activ™

4.2.2. Resorufin (Rf)

Resorufin (Rf), as mentioned previously, is the reduced form of the dye resazurin (Rz), but is itself a useful dye. It can be used as a redox indicator, much like methylene blue, changing from pink to colourless as it is reduced to dihydro-Rf¹³. The dye itself is not commonly used in biology and medicine, although esters, ethers and N-acetyl derivatives of the dye appear to be prominent in such fields. However, Rf is fluorescent¹⁴, and since it can be formed by the enzyme catalysed oxidation of amplex red, i.e. 7-ethoxy resorufin, the latter can be used to determine the level of H₂O₂ present based on the intensity of fluorescence of the Rf produced¹⁵. Others have utilised the fluorescence of the dye as a method for determining the amount of dissolved O₂ present in a solution based on the oxidation of the reduced form of the dye, dihydro-Rf¹⁶. Figure 4.6. shows the structure of resorufin and its reduction mechanism.

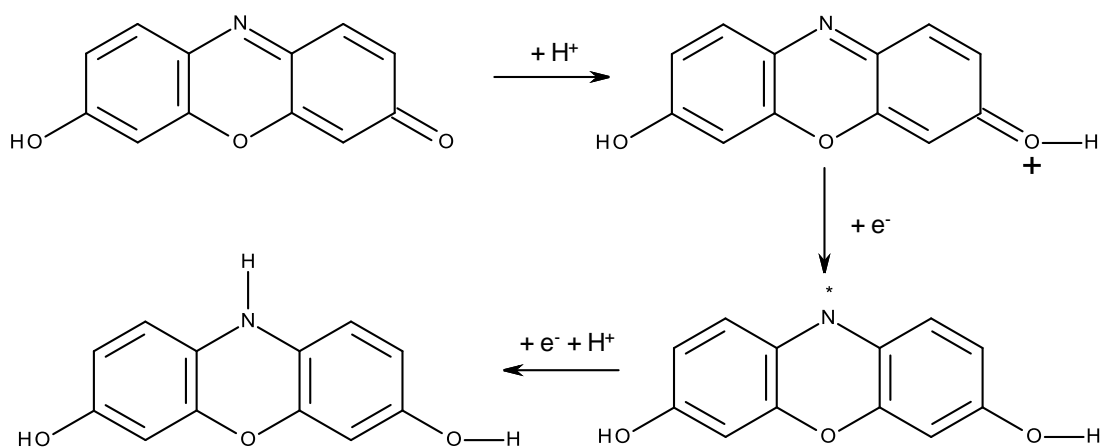


Figure 4.6.: The structure of resorufin and its subsequent reduction reaction

From table 4.1., it can be seen that its λ_{\max} is the lowest of all the dyes studied (573 nm in CH_3OH)⁴, and as a result an indicator ink based on Rf is pink in colour. Figure 4.7. shows the UV-Visible absorbance spectra for both an Rf film on the surface of ActivTM, and for a 10^{-5} M aqueous solution of the dye.

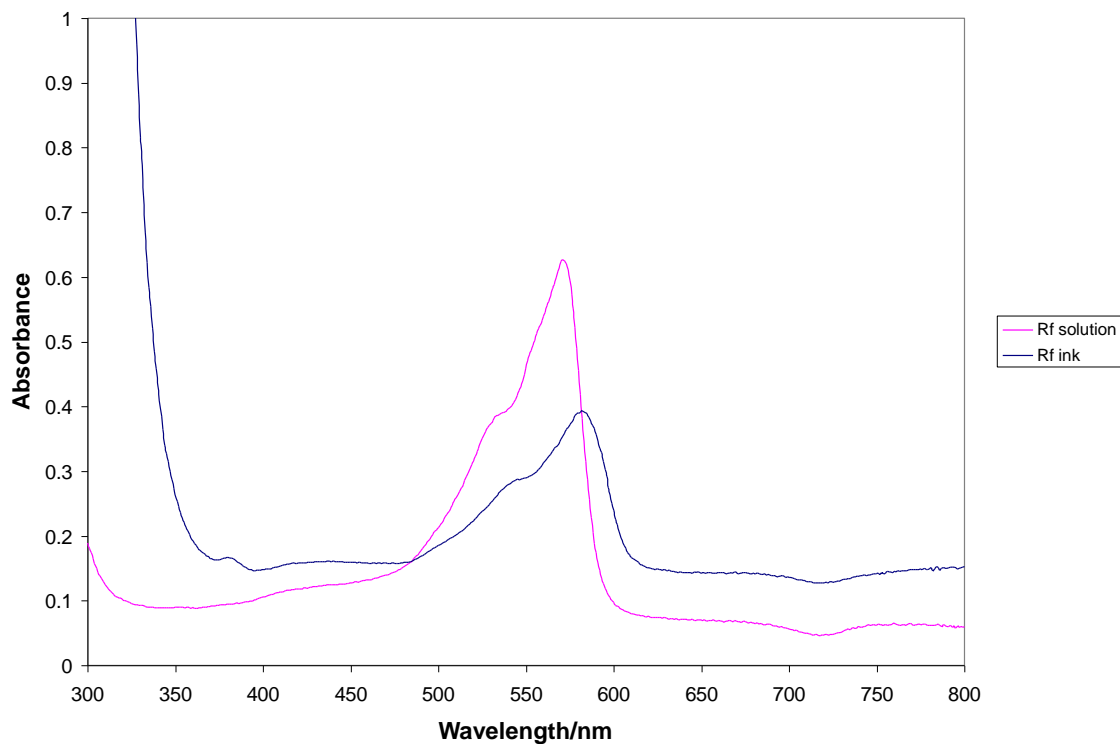


Figure 4.7.: A comparison of the UV-Visible absorption spectra for Rf as a 10^{-5} M aqueous solution (pink trace) and when cast as an ink film on the surface of Activ™

As with MB outlined above, a significant difference is observed in terms of the peak height and the wavelength of the peak absorbance for the dye in both solution and the ink formulation. However, both dye spectra in figure 4.7. are seen to exhibit a distinct peak (580 nm in the ink, 570 nm in solution), with a shoulder peak further downfield. It is this distinct peak for the ink which is used to determine r_i for dye reduction. Figure 4.8. shows the change in the UV-Visible absorption spectrum for Rf as the ink is irradiated with time, and subsequently reduced to dihydro-Rf, on the surface of Activ™.

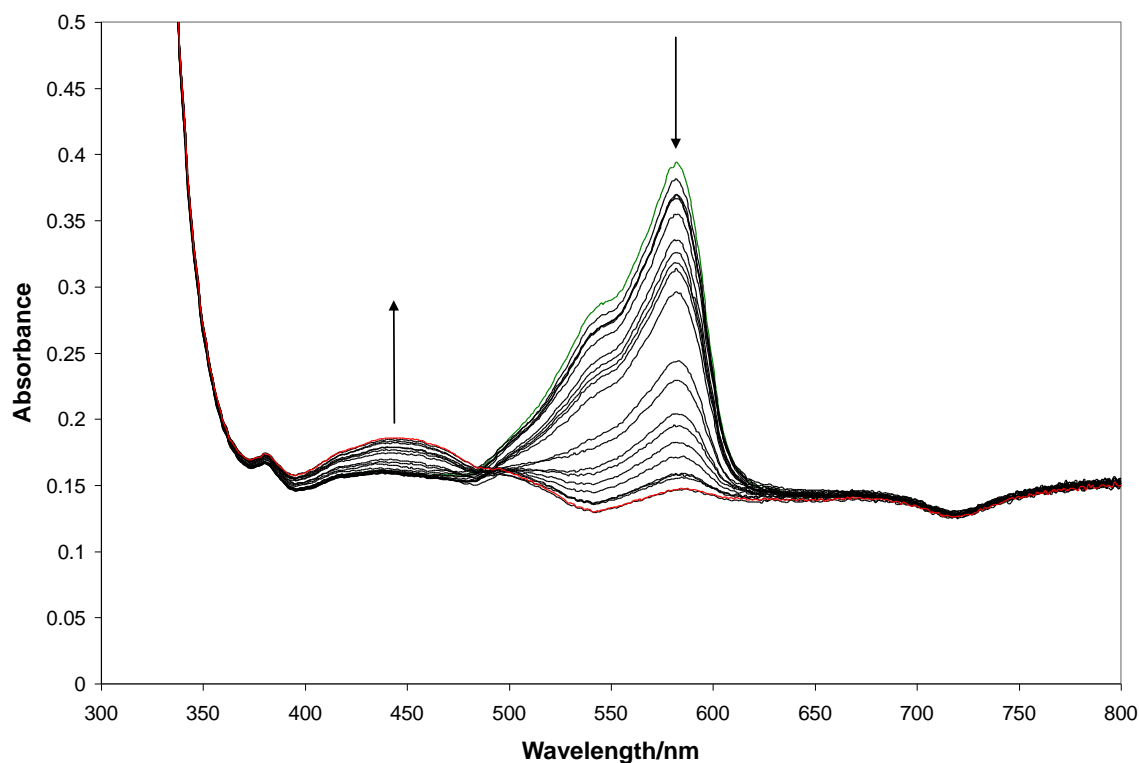


Figure 4.8.: The change in the UV-Visible absorbance spectrum of an Rf ink with irradiation under N_2 . The green trace indicates the initial ink spectra, whereas the red trace shows the ink spectra after 2 hours of UVA irradiation. Spectra were recorded at 30 s intervals for 2 minutes, at 1 minute intervals up to 7 minutes, at 10 minutes, and then every 10 minutes up to 2 hours

As with MB, the peak absorbance decreases with increasing UVA irradiation time, providing us with a convenient method for monitoring the progress of the reaction. Indeed, the reduction of the dye can also be seen visibly, since the film changes colour from pink to colourless as the reaction proceeds. Interestingly, whilst both the main and shoulder peaks due to Rf decrease with increasing irradiation time, a broad peak emerges with a maximum at ca. 450 nm, which is attributed to the photoreduction product, dihydro-Rf. It should be noted that after complete irradiation, the film appears colourless despite the presence of this broad peak, further affirming the notion that the final dye product is indeed dihydro-Rf.

Figure 4.9. shows the variation in the absorbance at λ_{\max} due to Rf with UVA irradiation time, and from this it can be seen that the reduction reaction occurs over a period of 110 minutes, which is longer than that observed previously for MB (ca. 70 minutes) under similar conditions. The obvious implication is that the rate of reduction of Rf is slower in comparison to MB, and this is verified by the initial rate of reduction, which is calculated to be $1.923 \times 10^{-4} \text{ AbsU s}^{-1}$. For comparison, this calculated r_i is almost 2 times slower than that observed for MB.

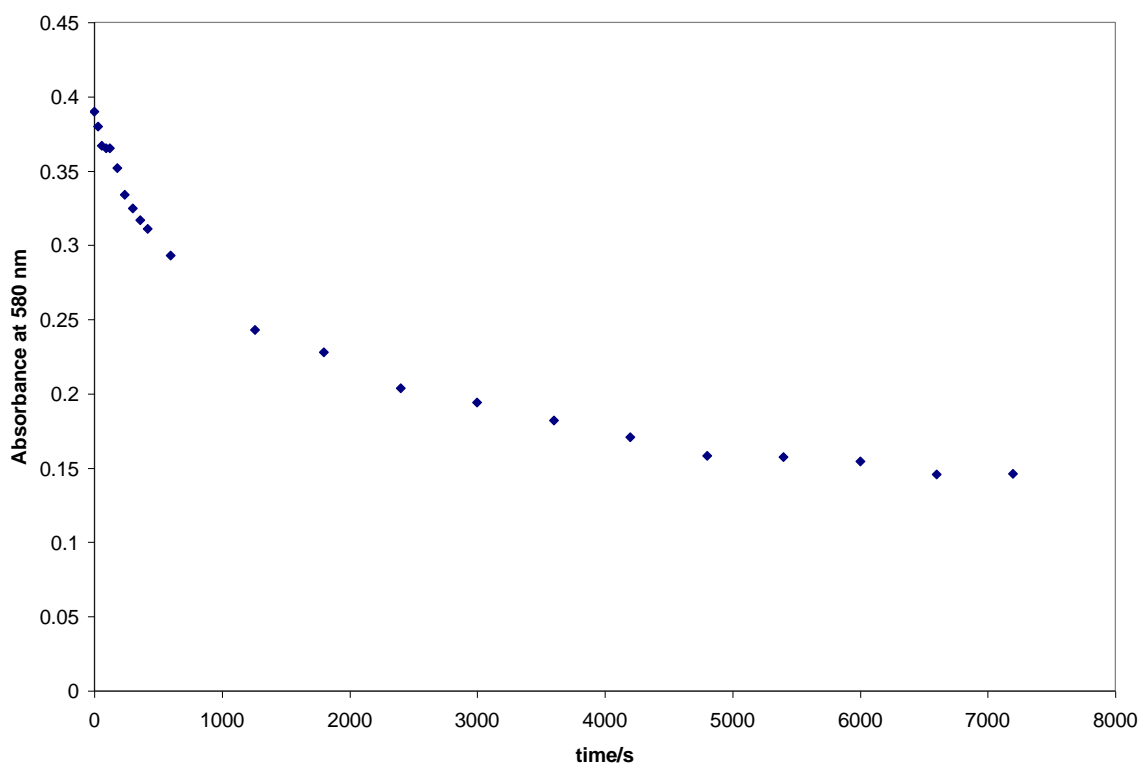


Figure 4.9.: The change in the absorbance at 580 nm due to Rf with UVA irradiation time

4.2.3. Resazurin (Rz)

As was alluded to above, Rz is similar in structure to Rf, the only difference being the presence of a dative N to O bond. As with Rf, the dye can also be used as a redox indicator, and whilst Rf is not suitable for use as a stain, Rz was widely used originally for the detection of bacterial reduction in milk¹³. Since it reduces to fluorescent Rf,

whilst being non-fluorescent itself, the reduction reaction can be followed by the change in fluorescence intensity. This has been utilized by Guilbault and Kramer in the determination of the activity of many dehydrogenases, including the nicotinamide adenine dinucleotide system¹⁷. Compared to the other dyes studied here, its reduction mechanism is also much more simplistic, with the removal of the dative bond yielding resorufin. A comparison between the solution spectrum (10^{-5} M) and the ink film spectrum, on ActivTM, of resazurin (Rz) is depicted in figure 4.10.

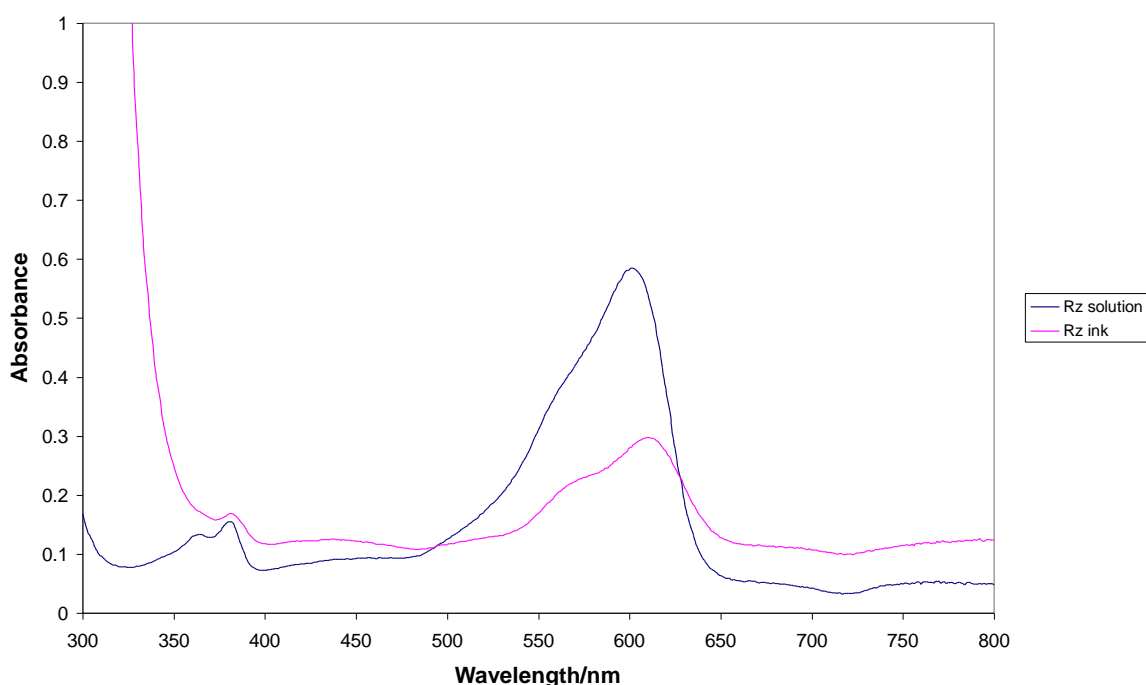


Figure 4.10.: The UV-Visible absorbance spectra of Rz in solution (blue trace) and when cast as an ink film on the surface of ActivTM

Similar to Rf, a red-shift and a reduction in the peak absorbance in the spectrum of the dye is observed in the ink compared to the aqueous solution. The shoulder observed in both the spectra correlates with the Rf peaks observed previously in figure 4.7., which is of no great surprise since Rf is the reduction product of Rz. Structurally the two dyes differ only in the presence of the dative nitrogen to oxygen bond in Rz, which is

removed during the photoreduction process, and thus it would be anticipated that there may be some Rf impurity in the dye as purchased (ca. 85 % purity from Aldrich).

When the dye is reduced on the surface of Activ™ due to the action of the photocatalyst, the initial colour change observed is from blue to pink as Rz is reduced to Rf initially. With prolonged irradiation, the reduction reaction would proceed further as the produced Rf is converted to dihydro-Rf, and from the results given in figures 4.8. and 4.9. above, we know that this latter process occurs over a period of ca. 2 hours. The photoreduction of Rz in the ink formulation has previously been studied extensively within this laboratory¹⁻², since it is the original technology in this area. However, the characterisation work described in the latter of these references deals only with the ink's performance under ambient atmospheric conditions. It would be anticipated that the ink's response under anaerobic conditions would differ since O₂ can potentially interfere with the photoreduction process through reaction with the photogenerated electrons, and is an excellent oxidant and can thus react with the leuco- form of the dye. The latter of these two processes, however, should not be so much of a problem since Rz reduction is electrochemically irreversible³.

Figure 4.11. shows how the spectral shape of the Rz ink changes when irradiated on Activ™ under anaerobic conditions. As anticipated, the peak due to Rz at 610 nm decreases with increasing irradiation time. However, unlike what we have observed previously with MB and Rf, as the Rz peak decreases with irradiation, we see a new peak emerge at 580 nm. This latter peak is due to Rf, and obtains its maximum absorbance at λ_{\max} after 10 minutes of irradiation. Beyond this time, the Rf peak then begins to decrease with further irradiation, alongside the Rz peak, as the dye is reduced to dihydro-Rf. It should be noted that the photoreduction reaction was ceased once the Rz peak had fully disappeared, hence the remnants of the Rf peak still visible in the final trace in figure 4.11.

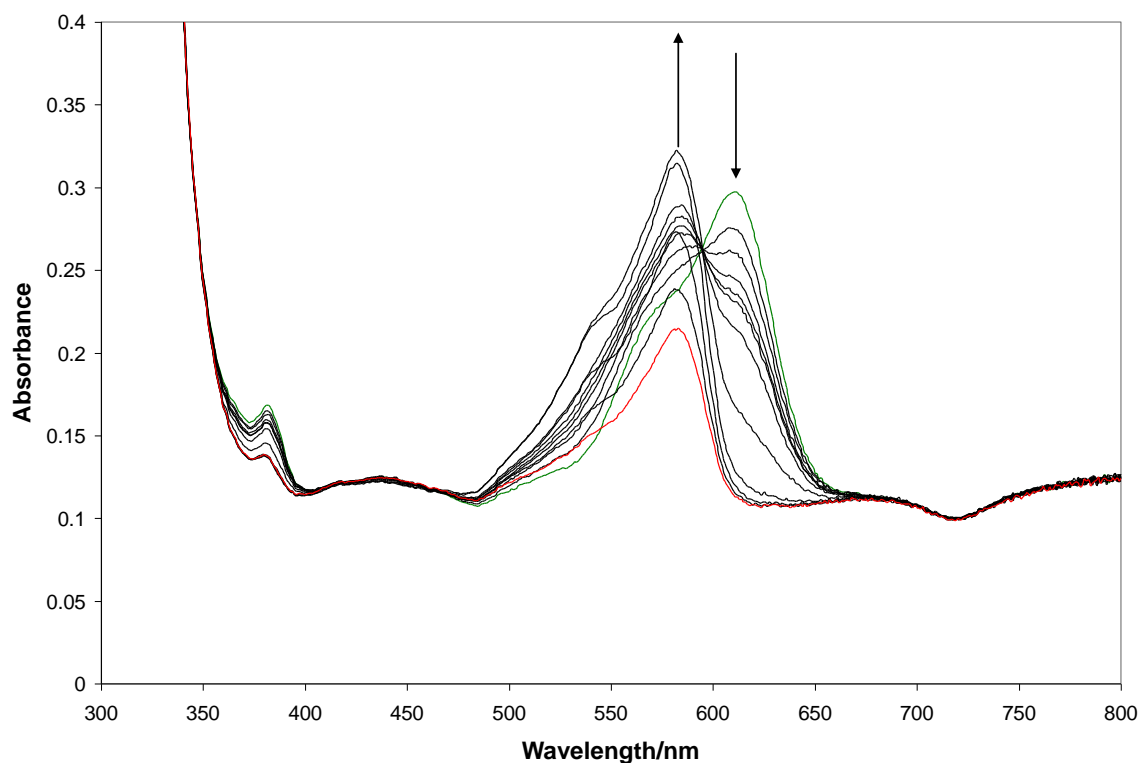


Figure 4.11.: The spectral changes which occur as an RZ ink is irradiated on the surface of Activ™. The green trace shows the initial spectrum of the ink, whereas the red trace shows the spectrum obtained after 50 minutes of UV irradiation. Spectra were recorded at 60 s intervals for 5 minutes, at 10 minutes, and at 10 minute intervals up to 50 minutes

Figure 4.12. shows how the peak absorbance due to both RZ and Rf varies with increasing irradiation time, based on the data presented above in figure 4.11. What is immediately evident is that when the Rf peak starts to decrease from its peak absorbance, it does so at an initial rate much slower than that due to RZ. Similarly, by the time the Rf produced by the reduction of RZ starts to decrease in absorbance (and, hence, concentration), the reduction of RZ is ca. 70 % complete, further suggesting that Rf reduction does not compete at an appreciable rate to that of RZ.

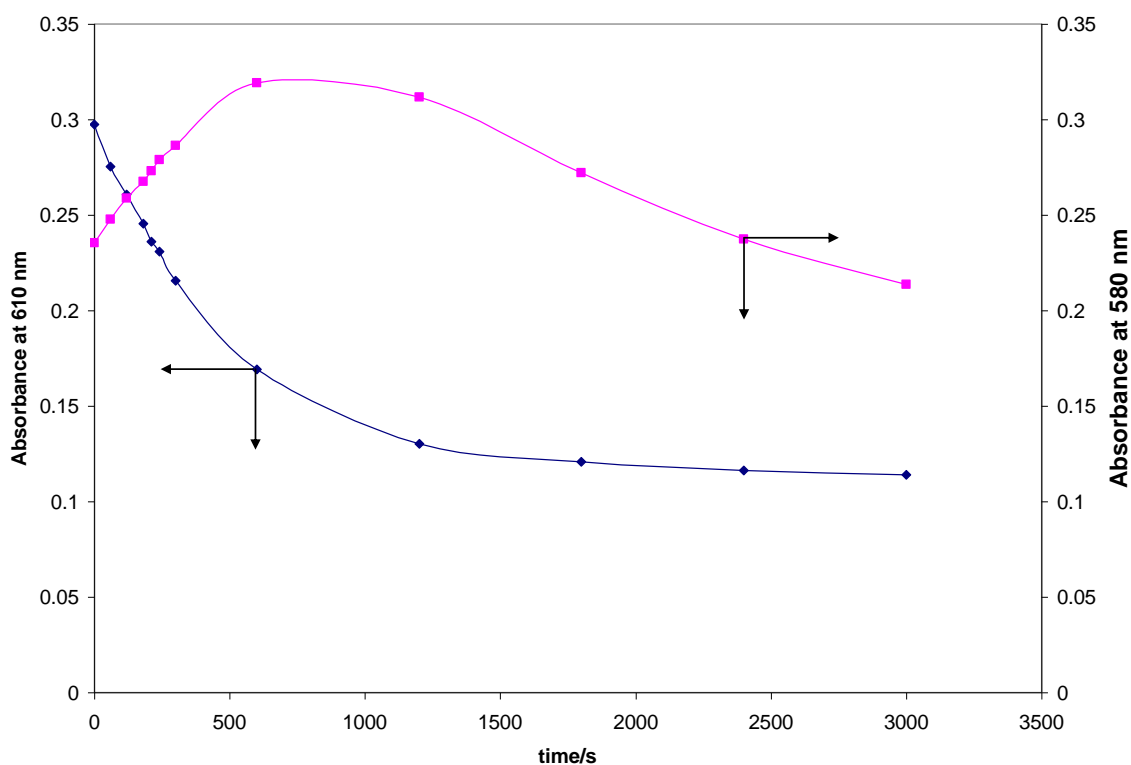


Figure 4.12.: The variation in the peak absorbance due to both R_z and R_f with UV irradiation time. The blue trace shows how the R_z peak at 610 nm varies with irradiation time, whereas the pink trace shows that for R_f at 580 nm

Towards the end of the complete reduction of R_z, it is believed that the R_f present will compete with the reduction of R_z for the available photogenerated electrons. However, the dominant reduction mechanism over the first 10 minutes is surely that of R_z to R_f, confirmed by the ever increasing absorbance at λ_{\max} for the latter of these two dyes. Further to this, from figure 4.12. the initial rate for the R_z reduction reaction is calculated to be $2.841 \times 10^{-4} \text{ AbsU s}^{-1}$. This r_i is greater than that for R_f reduction reported in section 4.2.2., but slower than what was determined for MB under the same conditions.

4.2.4. 2,6-dichloroindophenol (DCIP)

The last of the dyes to be tested was DCIP. Its structure and reduction mechanism was shown previously in chapter 3. A comparison of the solution (10^{-5} M) and cast ink spectra, as shown below in figure 4.13., demonstrates that of all the dyes screened here, DCIP is the only one which has a greater peak absorbance in the ink compared to in aqueous solution at the 10^{-5} M concentration. In addition, compared to the other dyes screened for their suitability, the DCIP ink exhibits the smallest peak absorbance when cast as an ink film on Activ™ at the pre-described dye level of 5 mg per formulation.

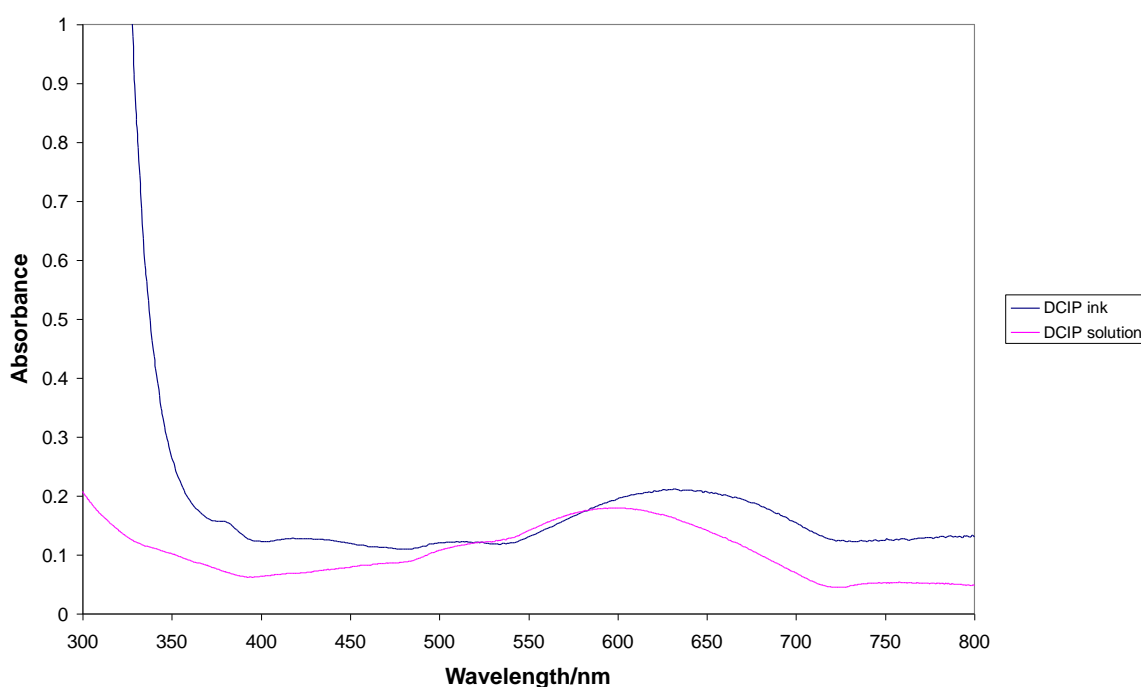


Figure 4.13.: A comparison between the solution (10^{-5} M, pink trace) and cast ink spectra on Activ™ of DCIP

The change in the spectral shape of the cast DCIP ink on Activ™ with UV irradiation time under N_2 is shown in figure 4.14, whilst the change in the absorbance at 629 nm, the λ_{\max} for DCIP in the ink, with increasing irradiation time is shown in figure 4.15. From this, we see that the dye is reduced due to the action of the photocatalyst over a period of 80 minutes under these anaerobic conditions.

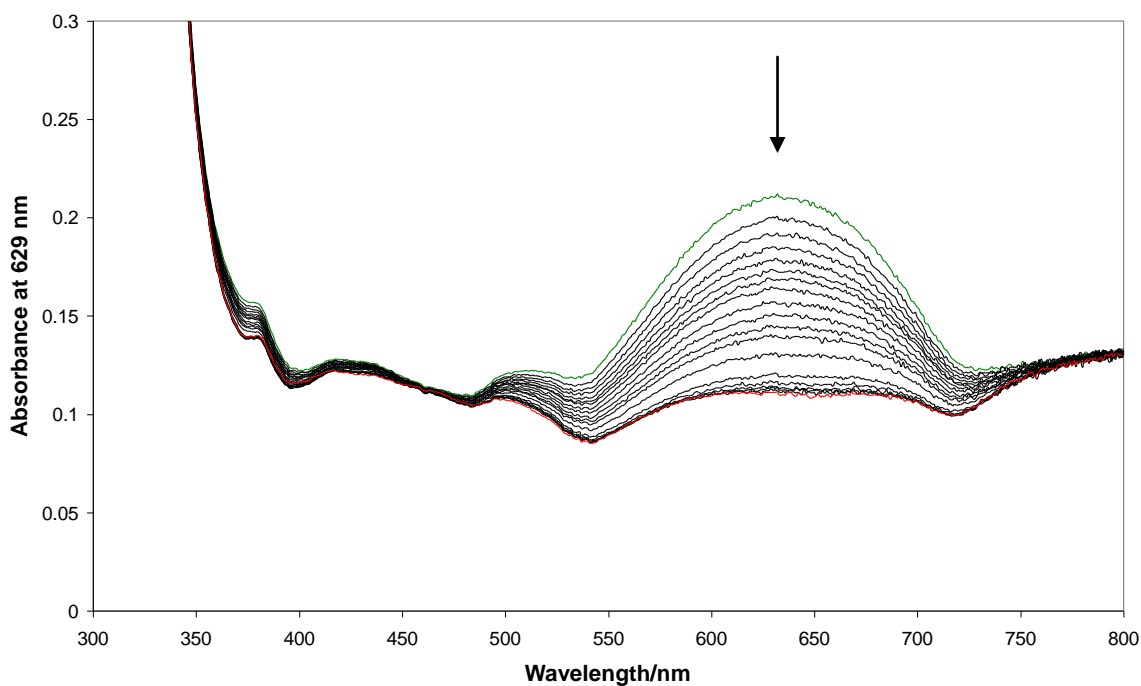


Figure 4.14.: The change in spectral shape for a DCIP ink cast on Activ™ with increasing irradiation time. The green trace shows the initial ink spectrum, whilst the red trace shows that obtained after 80 minutes of UVA irradiation. Spectra were recorded at 1 minute intervals for 7 minutes, at 2 minute intervals up to 15 minutes, at 20 minutes and finally at 10 minute intervals up to 80 minutes

Similar to the data generated previously for MB, Rf and Rz, the r_i for the reduction of DCIP can be determined from figure 4.15. to be $1.097 \times 10^{-4} \text{ AbsU s}^{-1}$. This initial rate is the slowest of all the inks assessed here.

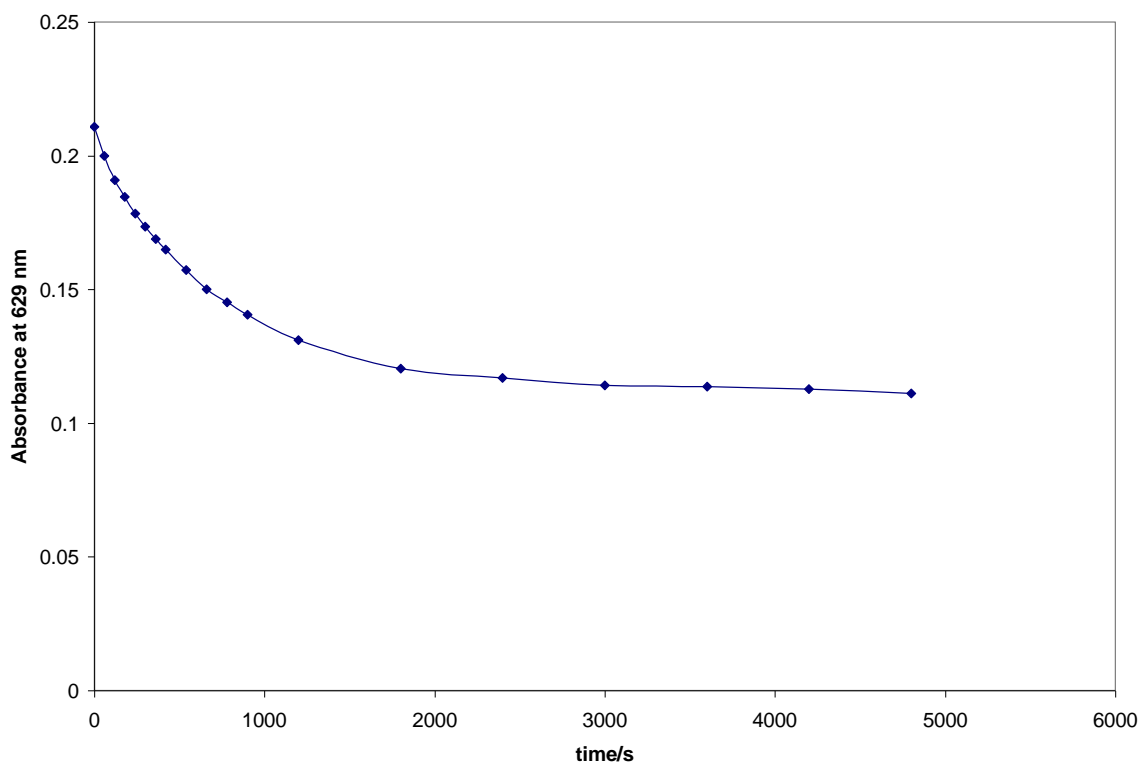


Figure 4.15.: The variation in the absorbance at 629 nm with UVA irradiation time for the DCIP ink when irradiated on Activ™

4.2.5. Comparison of Initial Results Under Anaerobic Conditions – The Elimination of the Rf-based Indicator Ink

Table 4.2. compares the results detailed above for all 4 dyes assessed for their suitability in the indicator ink formulation. Depending on whether the r_i or the zero order $t_{50\%}$ value is taken as the measure of the ink performance, a slightly different ‘pecking order’ is revealed. However, whilst the r_i is an important factor to determine, the $t_{50\%}$ appears the more suitable for use in this context since it gives some indication of the time taken for the colour changes to occur. Since such inks are being examined with a view to using them in the field, reporting the $t_{50\%}$ appears to give a more accurate description of the ink’s performance, and is more suited for explaining to potential customers, in comparison to r_i .

Dye	$r_i/\text{AbsU s}^{-1}$	$t_{50\%}/\text{min}$
MB	3.458×10^{-4}	5.7
Rf	1.923×10^{-4}	10.8
Rz	2.841×10^{-4}	5.6
DCIP	1.097×10^{-4}	7.6

Table 4.2.: The four different dyes studied for their suitability in the indicator ink formulation and their corresponding r_i and $t_{50\%}$ values as determined above

Using the $t_{50\%}$ data, it can be seen that the order of the dyes, from fastest to slowest, is $Rz \approx MB > DCIP > Rf$. Despite Rf having a slightly greater r_i compared to DCIP, based on the calculated $t_{50\%}$ values, it can be seen that the time taken for the absorbance of the dye, and hence the intensity of its colour, to decrease by half is longer. In addition, as was stated previously, for Rf to completely reduce on the surface of Activ™ requires almost 2 hours of UVA irradiation, whereas the other dyes undergo complete reduction in ca. 1 hour. Such a slow reduction compared to the other dyes is not entirely unexpected, since Rf has the most negative redox potential of the dyes, indicating that the thermodynamic driving force for its reduction by photogenerated, conduction band electrons, e^- , on the photocatalyst surface would be less than that for the other dyes under test.

Since the ink is to be used in the field, its performance under ambient atmospheric conditions is obviously more relevant than the conditions which have been used here thus far. Figure 4.16. shows the variation in the absorbance at 580 nm with time for an ink based on Rf as it is irradiated under such conditions. Whereas the work under anaerobic conditions was performed at a UVI of ca. 1.3 mW cm^{-2} , the UVI used here is greater at ca. 4.8 mW cm^{-2} , as was the standard UVI in chapter 3.

From figure 4.16., the calculated $t_{50\%}$ is 710 s, or ca. 12 minutes, under such conditions. Based on results generated later, under such conditions the Rf ink can still be seen to underachieve in comparison to both Rz and DCIP. Based on these results, and on the calculated $t_{50\%}$ values given in table 4.2., the Rf ink is not considered suitable for the

rapid measurement of the photocatalytic activity of thin films. However, such an ink may be suitable for use where either;

1. The film is of a similar activity c/f Activ™, but thicker than 12 nm, or;
2. The film thickness is similar c/f Activ™, but the photocatalytic activity of the sample is greater

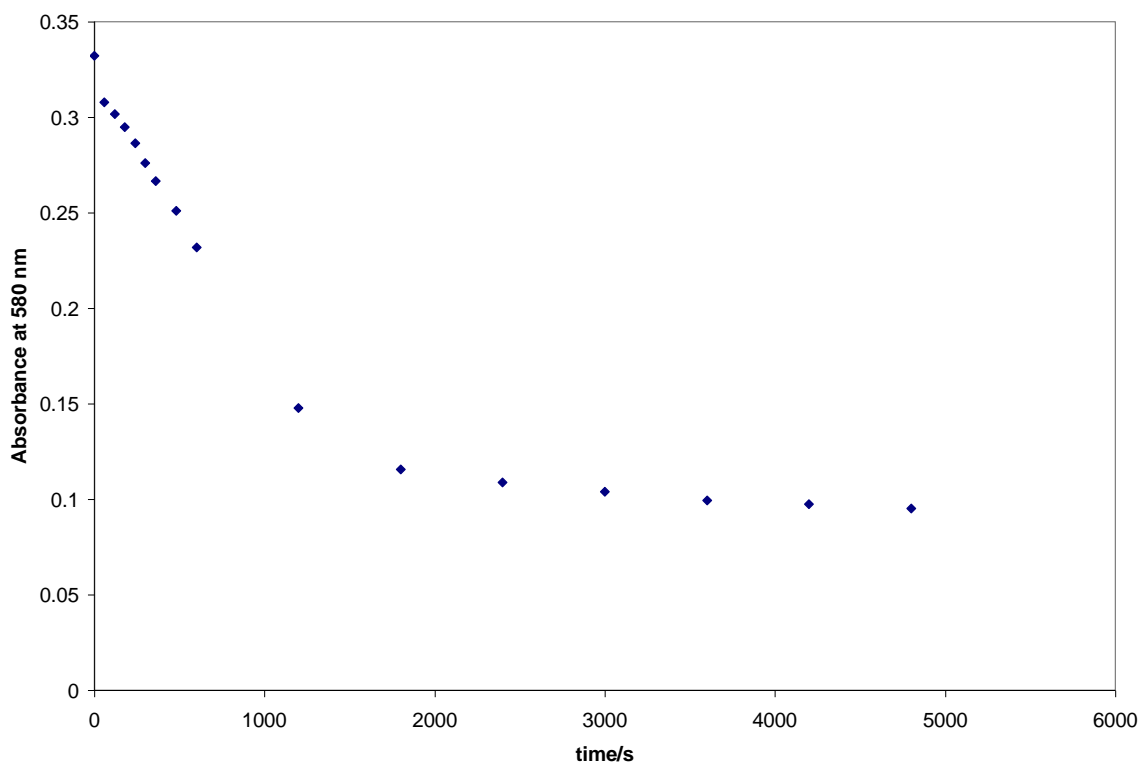


Figure 4.16.: The variation in the absorbance at 580 nm with UV irradiation time as an Rf-based ink is reduced on the surface of Activ™ under ambient atmospheric conditions

4.2.6. The Indicator Inks Under Ambient Atmospheric Conditions – The Elimination of the MB-based Indicator Ink

The above work allowed the efficacy of the dye photoreduction step by the photogenerated electrons to be studied without the complicating feature of interference by oxygen. However, in any practical system for use in the field as well as the

laboratory, a photocatalyst indicator ink must work effectively under aerobic conditions, i.e. the photoreduction kinetics should be independent of ambient levels of oxygen, thus implying that direct reaction of the photogenerated electrons with O_2 , should be non-existent or negligible. Based on the results above, the most attractive inks appear to be those based on either RZ or MB since they have comparably rapid $t_{50\%}$ and r_1 values. However, what must be remembered is that the performance of the inks detailed thus far has been under anaerobic conditions and a low UVI (ca. 1.3 mW cm^{-2}). Whilst the relative humidity experienced differs around the world, the ratio of $O_2:N_2$ is consistent, and hence the inks must be suitable for use in the presence of O_2 . It would also be anticipated that, provided no detrimental effect is observed in the presence of O_2 , the inks could feasibly reduce faster in the field owing to the higher UVA output from the sun compared to what is used here (ca. 4.49 mW cm^{-2} on a summer day¹⁸).

Figure 4.17. shows how the peak absorbance due to RZ varies with irradiation time under N_2 , as was demonstrated previously in figure 4.9. However, figure 4.17. also shows how the peak absorbance then changes after the UV light source is removed and air is introduced into the system for 1 hour. There is observed to be no change in the RZ peak absorbance due to reaction with O_2 from the air as it is introduced into the system. This is to be expected since it has been previously noted that RZ reduction is an electrochemically irreversible process³. For completeness, the behaviour of the peak due to Rf as it is produced over the course of the reduction reaction, and its subsequent re-oxidation by atmospheric O_2 , is also shown in figure 4.17.

It can be seen that when the UVA source is removed and O_2 is introduced into the system, the peak absorbance due to Rf immediately increases, suggesting some O_2 -sensitivity. Again, this is not entirely unexpected since the Rf/dihydro-Rf redox couple has previously been noted to have the most negative redox potential ($-0.051 \text{ V vs. SHE at pH } 7^3$) of all four dyes screened here. This would imply that the reduced product, dihydro-Rf, is the most likely of all the reduced products to be re-oxidised.

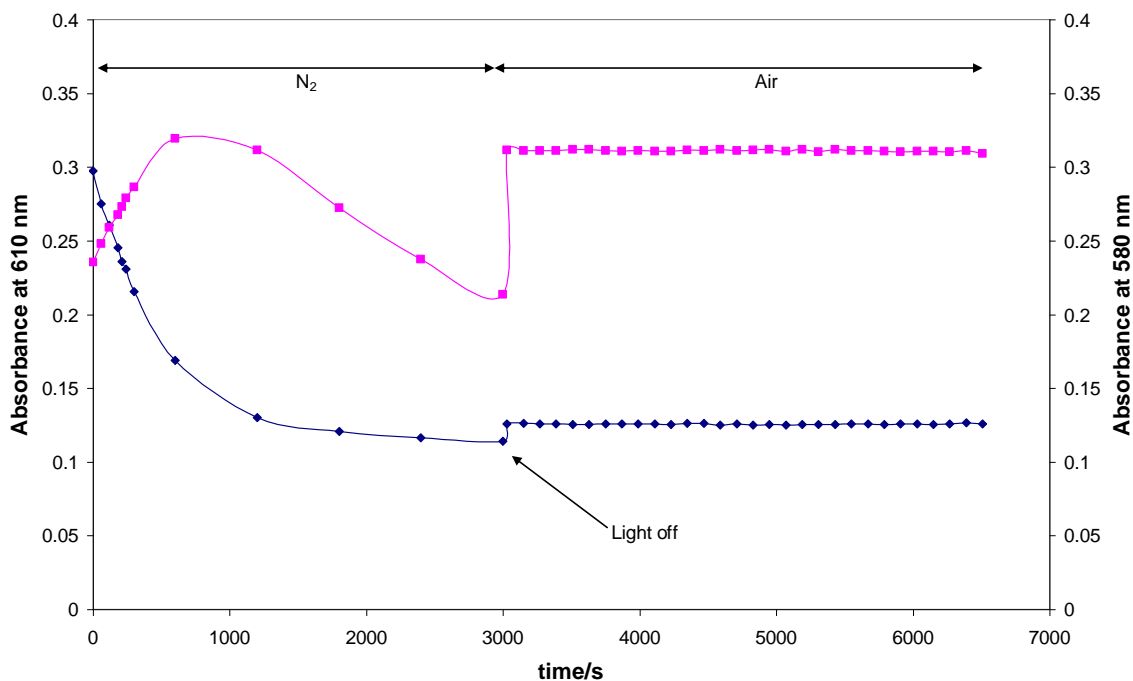


Figure 4.17.: The change in the peak absorbance due to Rz (blue trace, 610 nm) and Rf (pink trace, 580 nm) as an Rz ink is irradiated on the surface of Activ™ under anaerobic conditions before being subjected to ambient atmospheric conditions (nil UVA) once the reduction reaction is complete. When monitoring the performance of the ink post-reduction, spectra were recorded every 2 minutes for 1 hour, from which the peak absorbance is extracted

Similarly, figures 4.18. and 4.19. show how the inks based upon DCIP and MB behave when the reduced dyes are subjected to ambient atmospheric conditions following reduction under anaerobic conditions, respectively. Based on both the redox data presented previously in table 4.1., and the results from the Rz experiment presented in figure 4.17., it would be anticipated that both MB and DCIP would be unaffected by the introduction of O₂ into the system, since their redox potentials are more positive than both Rf and the postulated value of Rz³.

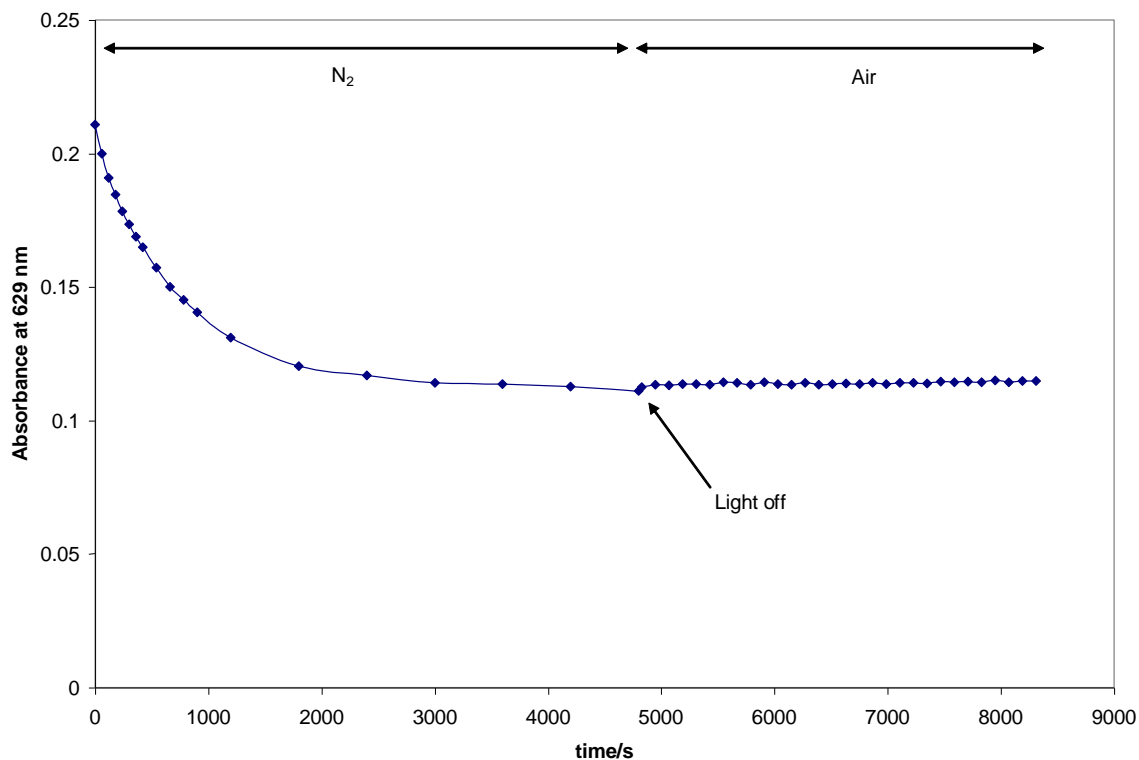


Figure 4.18.: The reduction, and subsequent recovery, of a DCIP ink on Activ™. As for R_z above, recovery spectra were recorded at 2 minute intervals for 1 hour

However, whilst this theory appears to be validated for DCIP, it can be seen that when leuco-MB is subjected to ambient atmospheric conditions post reduction, the peak absorbance due to MB increases rapidly, indicating re-oxidation of the leuco- form of the dye. As a result, the blue colour of the original ink returns. Indeed, the majority of the recovery reaction appears to be complete within ca. 6 minutes, with the dye absorbance recovering to a maximum of ca. 87 % of its original value over the course of 1 hour.

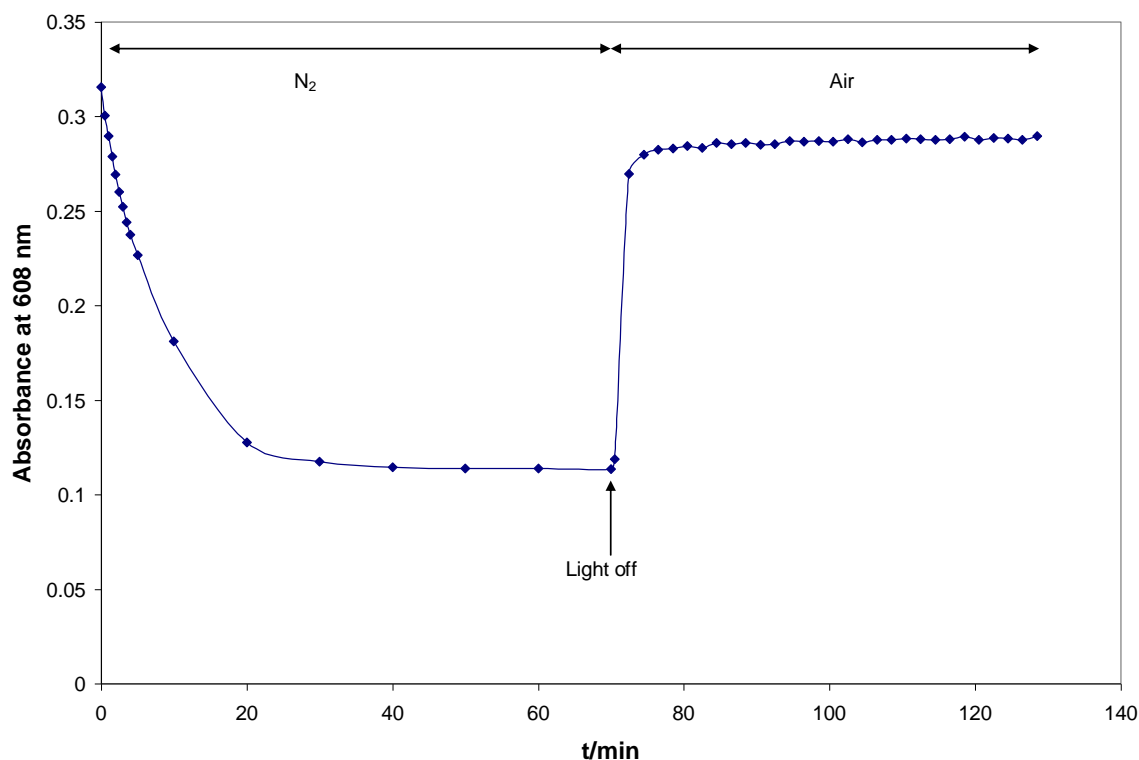


Figure 4.19.: The reduction, and subsequent recovery, of a MB ink on Activ™. As previously, recovery spectra were recorded at 2 minute intervals for 1 hour

This apparent reversal in convention is thought to be due to the differing mechanism of reduction between MB and Rz. From the structures given in table 4.1. for the oxidised and reduced forms of the dyes, it can be deduced that MB follows a traditional two electron reduction process. For Rz, however, the reduction mechanism involves the cleavage of a dative N to O bond. As a result, when leuco-MB is subjected to an O₂-containing atmosphere, oxidation can occur. However, atmospheric O₂, though relatively oxidising, would appear to be unable to facilitate the re-addition of the dative N to O bond observed in the structure of Rz. This would explain the apparent irreversibility of the Rz reduction process.

Obviously, this observed O₂-sensitivity of leuco-MB casts a major doubt on the ink's usage as a rapid method for assessing the photocatalytic activity, since such a formulation would be marketed primarily for use in the field. Indeed, this apparent O₂-

sensitivity for the dye is illustrated further by the results of an experiment in which a MB ink was irradiated under ambient atmospheric conditions on Activ™. Figure 4.20. shows the change in the spectral shape of the MB ink observed with increasing irradiation time. Even after 1 hour of UVA irradiation, it can be seen that the peak absorbance due to MB is relatively high, which suggests one of two possibilities, namely;

1. Photoreduction is not occurring in the system, or;
2. After 1 hour of UVA irradiation, the rate of the formed leuco-MB re-oxidation is similar to that for MB reduction, resulting in the system achieving a steady state

If photoreduction was not occurring in this MB ink system, the other possible mechanism would be photomineralisation of the ink. However, since the photocatalyst layer on Activ™ is a mere 15 nm thick, photomineralisation is highly unlikely to occur at an appreciable rate, as was demonstrated by Mills et al for the Rz ink². In addition, the inset diagram in figure 4.20. shows how the peak absorbance at 608 nm due to MB changes with irradiation time. After a slight drop in the peak absorbance within the first 10 minutes of irradiation, we then observe a relatively constant absorbance value.

If photomineralisation were occurring, it would be anticipated that the peak absorbance would decrease steadily over the irradiation period. It is this plateau in the peak absorbance which supports the hypothesis that, in air, the rate of reduction of MB occurs at a similar rate to that of re-oxidation of leuco-MB. As a result of this, after 1 hour irradiation the ink still appears blue on the surface of Activ™, thus making it unsuitable for use in a photocatalyst indicator ink in the field. However, for rapid analysis of thin films under anaerobic conditions, the MB ink represents an excellent test method ahead of the other inks described here.

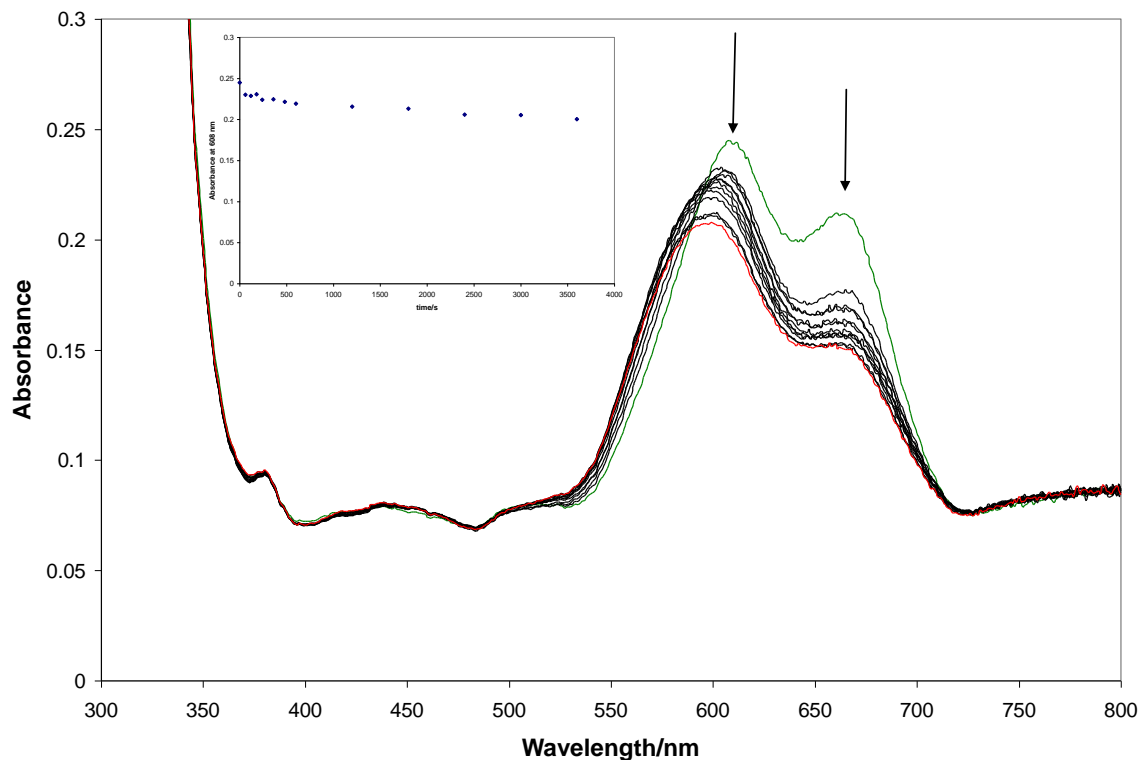


Figure 4.20.: The change in spectral shape for a MB ink as it is irradiated under ambient atmospheric conditions. The green trace shows the initial spectrum of the ink, whilst the red trace shows the ink spectrum 1 hour later. Spectra were recorded at 1 minute intervals for 4 minutes, at 2 minute intervals up to 10 minutes, and finally at 10 minute intervals up to 1 hour. The inset diagram shows the change in the peak absorbance due to MB over this 1 hour irradiation period

4.3. Photocatalyst Inks Under Aerobic Conditions – Rz and DCIP

With the elimination of both the MB and Rf inks as outlined above, only two inks are observed to be suitable for use in the field – namely, the Rz and DCIP inks. From table 4.2. above, we see that the Rz ink outperforms the DCIP ink, and as such would appear the more suitable for use under anaerobic conditions. However, although faster, the Rz ink suffers from a major drawback – the reduced product of Rz, Rf, can also be reduced. As a result, after the initial colour change from blue to pink as Rz is reduced to Rf, the

ink then changes colour from pink to colourless as Rf is reduced to dihydro-Rf. However, as demonstrated above, this latter reduction occurs at a much slower rate. Whilst this double reduction makes no difference to the analysis of photocatalytic activity in the laboratory, since the reduction reaction would be followed spectrophotometrically, the fact that there is two colour changes involved in the complete reduction of the dye could lead to potential confusion when explaining to the general public how the ink works. Preferably, a dye which reduces in one step, with a clear colour change to a colourless product, is desired; this condition is satisfied by the DCIP ink, despite its slightly slower rate of photoreduction compared to the original Rz ink under anaerobic conditions.

Figure 4.21. shows how the Rz and DCIP inks perform relative to each other under ambient atmospheric conditions by plotting the calculated relative ΔAbs at λ_{max} vs. irradiation time for both inks. Immediately, we observe that for both inks, the total reduction time and, as a consequence, the $t_{50\%}$ values are much faster than that observed previously under anaerobic conditions. However, what has to be remembered is that the UV irradiance here is more than 3 times greater compared to that used for the anaerobic tests and, so far, we have yet to consider how humidity affects the reduction of the inks – under ambient atmospheric conditions, the relative humidity is ca. 60 %, whereas under anaerobic conditions it is ca. 10 %.

Despite these changes to the reaction conditions, we still observe that the rate of reduction of the Rz ink is faster than that for the DCIP ink, which still makes it the more attractive option from a kinetic viewpoint. Indeed, the calculated $t_{50\%}$ for the Rz ink based on the results demonstrated in figure 4.21. is ca. 1 minute, whilst that for the DCIP ink is 2 minutes. When their $t_{50\%}$ values were compared previously under anaerobic conditions, the Rz ink was 1.36 times faster than the DCIP ink, whereas under ambient atmospheric conditions it is now 2 times faster, which would appear to suggest that either the influence of atmospheric O_2 or relative humidity, or indeed a combination of both, has resulted in a slight increase in the Rz reduction rate relative to that for DCIP.

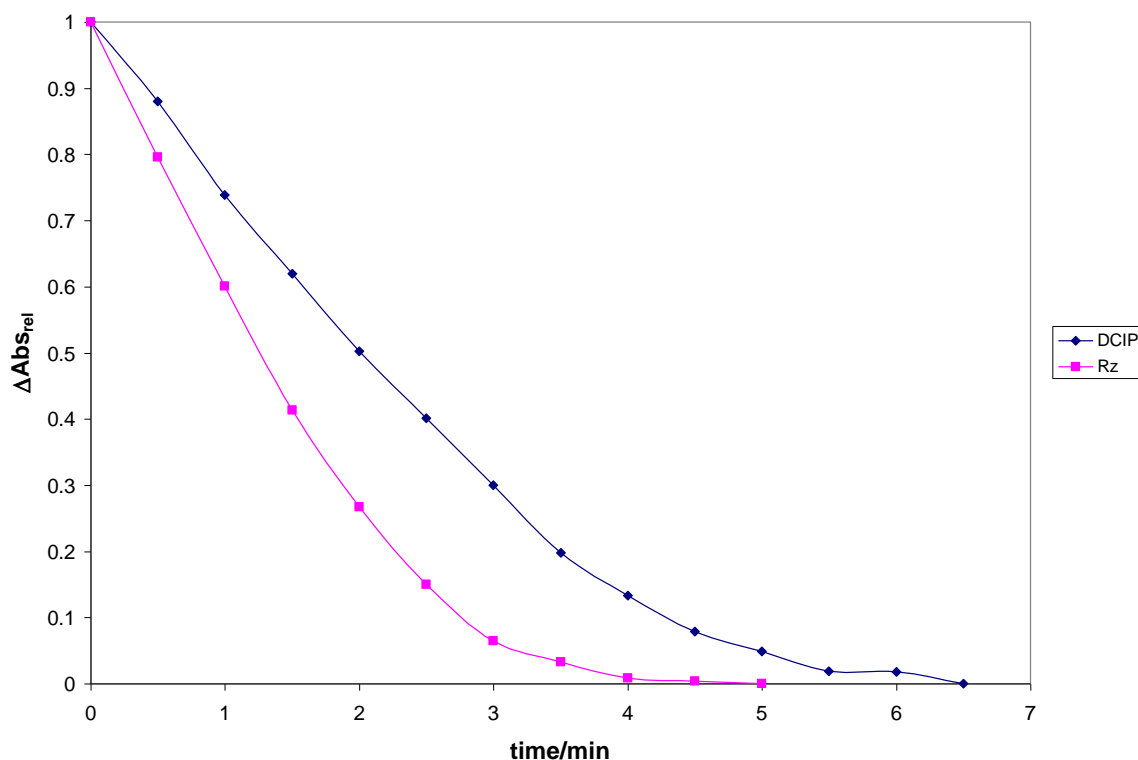


Figure 4.21.: The change in the relative $\Delta\text{Abs}_{\text{rel}}$ at λ_{max} with UV irradiation time for the DCIP (blue trace) and Rz (pink trace) inks under ambient atmospheric conditions

In order to test this hypothesis further, the rate of reduction of the two inks was assessed under varying O_2 concentrations supplied from a cylinder. Since the atmosphere to which the ink was subjected to was delivered to the gas cell directly from the cylinder, all three O_2 concentrations could be assumed to be at ca. 10 % relative humidity. Figure 4.22. shows the reduction profiles obtained for the DCIP ink under varying oxygen concentrations.

As the O_2 concentration is varied from 0 to 100 %, we see no great variation in the Absorbance vs. time profiles for the DCIP indicator ink. The only noticeable difference between the traces is that the final absorbance obtained for the dye following complete photoreduction, i.e. Abs_{∞} , is slightly greater when the reduction reaction is conducted under O_2 compared to both N_2 and air. It was demonstrated previously in figure 4.18. that a reduced DCIP ink, when exposed to ambient atmospheric conditions following

reduction under N_2 , does not significantly recover over a 1 hour period. This suggests that the concentration of O_2 in air is not enough to facilitate dye re-oxidation. However, the O_2 concentration will obviously be much greater when pure O_2 is present, especially since the reduction reaction is also being assessed under such conditions. Hence, a steady state between leuco-DCIP re-oxidation and DCIP reduction could theoretically be established under such conditions, or is at least more likely to be observed here than under the conditions used in figure 4.18. Such an effect may be the root cause of the slight increase in $Ab_{s_{\infty}}$ observed in figure 4.22.

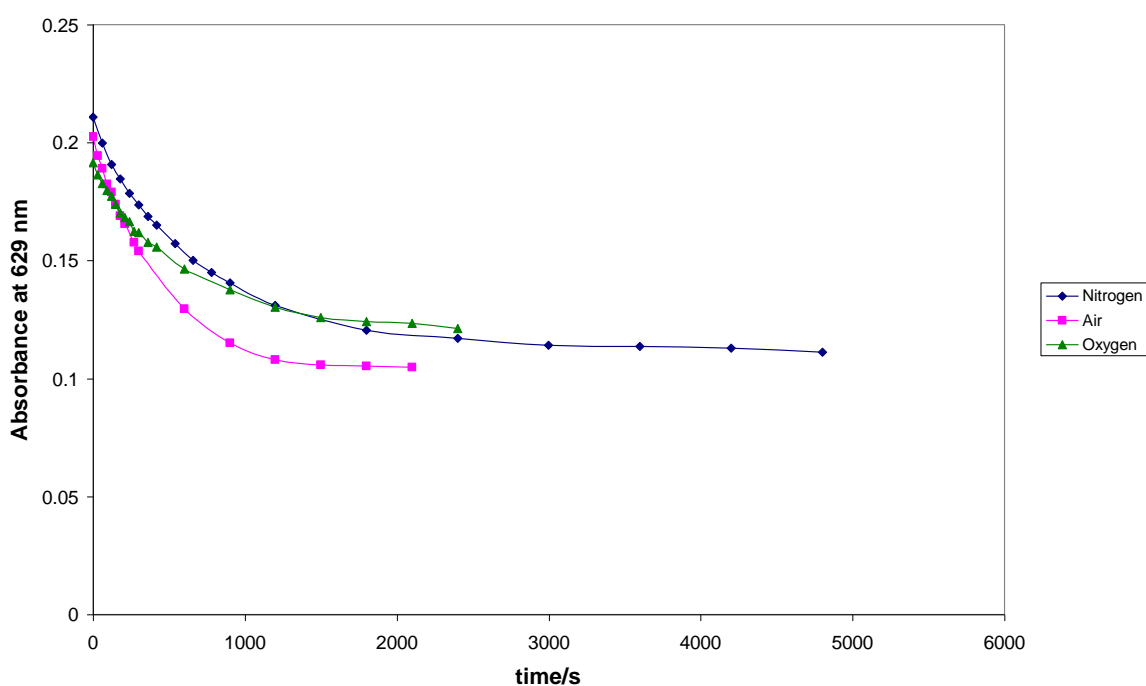


Figure 4.22.: The variation in the reduction profiles for DCIP under various atmospheres

Similarly, figure 4.23. shows the reduction profiles obtained for the Rz ink under similar conditions. Interestingly, we now observe that as the O_2 concentration is increased, the rate of reduction of Rz slows appreciably. This is somewhat unexpected, since it was demonstrated in figure 4.17. that there was no appreciable increase in the peak absorbance due to Rz when a reduced Rz ink (i.e. a Rf ink) is subjected to ambient atmospheric conditions. In addition, we also know that Rz reduction is

electrochemically irreversible, which would again have lead us to expect that the O_2 concentration should not affect the observed rate of reduction.

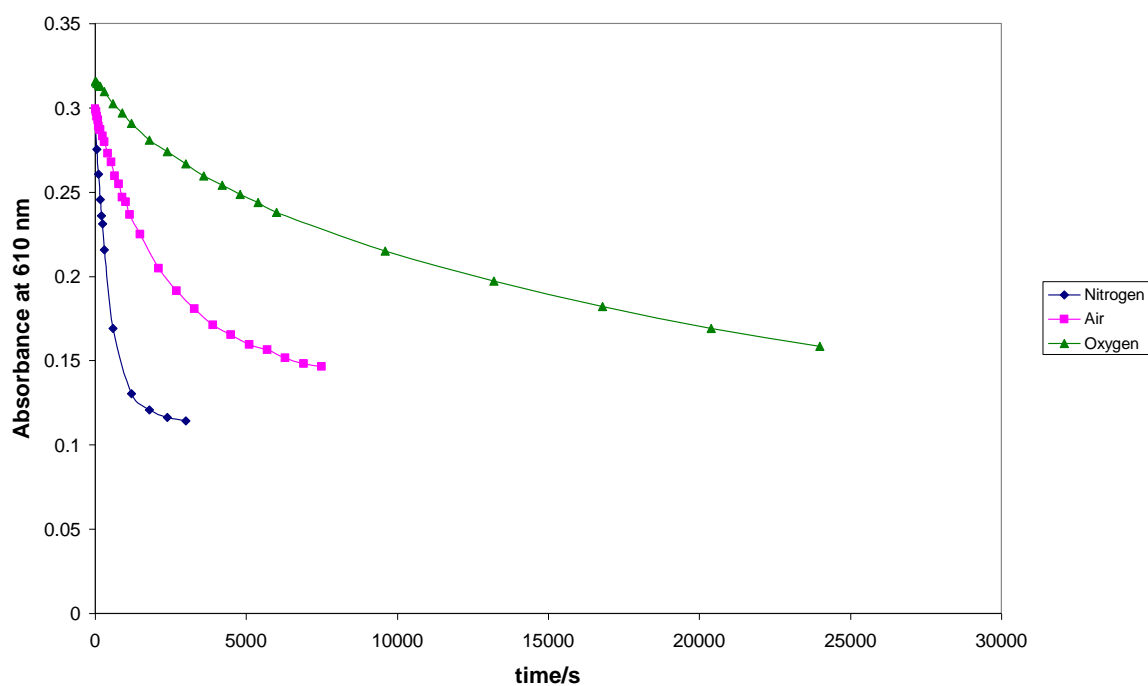


Figure 4.23.: The variation in the reduction profiles for Rz under various atmospheres

The true magnitude of the variation in the Rz reduction rate with O_2 concentration is highlighted further in figure 4.24., which plots the change in the calculated $t_{50\%}$ with $\%O_2$ for both the DCIP and Rz indicator inks, based on the results presented in figures 4.22. and 4.23. As anticipated from figure 4.22., the $t_{50\%}$ for DCIP is relatively constant with respect to the oxygen concentration in the gas cell. However, what is of greater interest is the observation that the $t_{50\%}$ for the Rz ink appears to increase linearly with increasing $\%O_2$. We know from table 4.1. that, of the 4 dyes screened for their suitability in the indicator ink formulation, DCIP has the highest (i.e. the most positive) redox potential³. As a result, we would expect the reduced form of the dye, leuco-DCIP, to be the slowest to re-oxidise in comparison to the reduced forms of the other dyes presented. This in turn would suggest that as the O_2 concentration in the gas cell is increased, the increase in the $t_{50\%}$ for DCIP would be less pronounced in comparison

with Rz. From figures 4.22. and 4.23., this point would seem valid. However, we also know that Rz reduction is electrochemically irreversible, despite its redox potential being estimated to be more negative than that for DCIP³. Assuming this electrochemical irreversibility, the effect on the $t_{50\%}$ observed in figures 4.23. and 4.24. by increasing the O_2 concentration could not have been predicted.

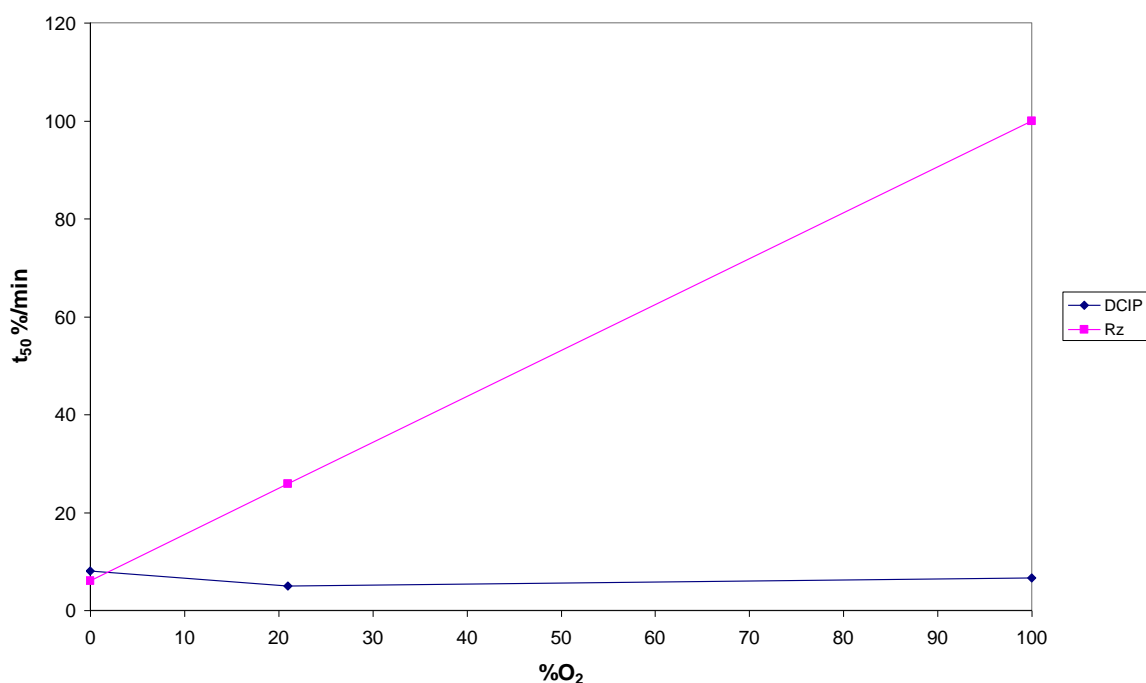


Figure 4.24.: A plot of the variation in the $t_{50\%}$ for DCIP (blue trace) and Rz (pink trace) inks with varying % O_2

The O_2 sensitivity of the Rz ink cannot be described by re-oxidation of Rf, hence other factors must be at work. One possible explanation for this apparent O_2 -sensitivity exhibited by the Rz ink is as follows. As Rz reduces to form Rf, it is possible that there are some short lived intermediates on the reduction pathway, like radicals, e.g. $Rz^{\cdot-}$. One, or indeed many, of these proposed intermediates may be O_2 -sensitive. Hence, by increasing the O_2 concentration, we increase the likelihood that such radicals will be trapped, or react with O_2 before proceeding to form Rf. Such a possibility would lead to

an immediate reduction in the observed $t_{50\%}$ with increasing O_2 concentration in the gas cell.

The results above also pose another interesting question; why does the Rz ink outperform the DCIP ink under ambient atmospheric conditions, but not when subjected to a cylinder air atmosphere in the gas cell? Previously, we have observed the Rz ink to have a lower $t_{50\%}$ than the DCIP ink in figure 4.21. However, in figure 4.24., under an air atmosphere the $t_{50\%}$ for Rz reduction is ca. 5 times greater. As was stated previously, the irradiance exhibited by the UV lamp under ambient atmospheric conditions is greater than that observed under anaerobic conditions, but if this was the sole cause of the increase in the photoreduction time then it would be anticipated that the rate of reduction of both the Rz and DCIP inks would be increased. Whilst the $t_{50\%}$ does indeed increase in both instances on moving to this lower irradiance, it doesn't explain why the change is more pronounced for the Rz ink such that it should now appear to reduce slower than the DCIP ink.

The most obvious explanation would appear to be that the relative humidity influences the rate of reduction of the Rz ink, in addition to the O_2 concentration. Further work into the indicator inks has been conducted in this laboratory¹⁹ and it was observed that as the relative humidity was increased from 10 to 50 %, no significant variation in the $t_{50\%}$ was noted for Rz in air¹⁹. Above 50 % relative humidity, however, the $t_{50\%}$ for Rz photoreduction in air decreased from ca. 6000 to 4000 s. It is important to note that such work was conducted with a different sample of Rz and at a different light intensity to that outlined here. Interestingly, when the experiment was repeated under anaerobic conditions, the $t_{50\%}$ was observed to decrease from ca. 800 to 500 s as the relative humidity was increased from 10 to 50 %. Beyond this, no significant change was observed, implying that the atmosphere to which the sample is subjected to also plays a crucial role in determining the Rz ink's sensitivity to relative humidity. These results indicate that it may not be the best dye to test photocatalytic activity given its apparent sensitivity to both % O_2 and %RH. In contrast, the kinetics of photoreduction of DCIP are unaffected by changes in %RH and % O_2 , and it is photobleached. As a result, the DCIP ink is an attractive alternative to the Rz ink.

4.4. Conclusions

Of the four dyes tested for their suitability in the indicator ink formulation, it has been possible to isolate the DCIP ink as being the most suitable for use in the field as a rapid measure of the photocatalytic activity of thin (i.e. nm) films of titania, such as those found in self-cleaning commercial products. Whilst the MB ink gives the desired colour change (i.e. a colourless product is formed upon reduction) under anaerobic conditions, we have demonstrated that this is not achieved under ambient atmospheric conditions, which is obviously unsuitable for use in the field. In addition, the Rf ink also meets our colour change criteria, but is too slow to be suitably labelled as 'rapid', even under anaerobic conditions, in comparison to the other dyes tested. It is postulated, however, that the dye may be suitable for use for thicker photocatalyst films, particularly under anaerobic conditions, whilst the MB ink outperforms the others under anaerobic conditions.

The leuco- forms of both the DCIP and Rz inks, unlike MB, appear to be O₂-insensitive, with photoreduction of the Rz ink occurring more rapidly under both anaerobic and ambient atmospheric conditions. Initially, it was believed that the only drawback to using the Rz ink in the field was that it underwent a double reduction process, Rz initially being reduced to Rf, followed by Rf reduction, albeit at a much slower rate, to dihydro-Rf. However, we have demonstrated that the Rz ink is O₂-sensitive and postulated that the relative humidity also affects the photoreduction process. Whilst the level of O₂ in the atmosphere is constant, it would be anticipated that self-cleaning glasses and tiles, etc. are installed in areas with very different relative humidities owing to weather conditions. Coupled with this undesirable initial colour change from blue to pink, which would be difficult to explain to non-scientific consumers, the Rz ink is not as attractive for use in the field. This leaves us with the DCIP ink, which would appear to be relatively insensitive to both O₂ and relative humidity.

The O₂ sensitivity of the Rz ink is highly unexpected. It was assumed that DCIP, despite having the most positive redox potential of all the dyes tested, would be more

O₂-sensitive since the reduction of Rz is electrochemically irreversible. It is postulated that a highly reactive intermediate on the Rz to Rf photoreduction pathway, possibly a radical, can be trapped by O₂, thus slowing the photoreduction rate in the presence of high concentrations of the gas. Such a highly reactive species is also thought to be responsible for the observed increase in the photoreduction time of the Rz ink with decreasing relative humidity, although such a species has yet to be confirmed, let alone isolated.

4.5. References

- (1) A. Mills; J. Wang; S.-K. Lee; M. Simonsen *Chem. Commun.* **2005**, 2721.
- (2) A. Mills; J. Wang; M. McGrady *J. Phys. Chem. B* **2006**, *110*, 18324.
- (3) P. G. Tratnyek; T. E. Reilkoff; A. W. Lemon; M. M. Scherer; B. A. Balko; L. M. Feik; B. D. Henegar *The Chemical Educator* **2001**, *6*, 172.
- (4) F. J. Green *The Sigma-Aldrich Handbook of Stains, Dyes and Indicators*; Aldrich Chemical Co., 1990.
- (5) A. Fujishima; T. N. Rao; D. A. Tryk *Journal of Photochemistry and Photobiology C: Photochemistry Reviews* **2000**, *1*, 1.
- (6) <http://en.wikipedia.org/wiki/Titanium> 05/11/2011
- (7) A. Mills; J. Wang *Journal of Photochemistry and Photobiology A: Chemistry* **1999**, *127*, 123.
- (8) J. Burhenne; K.-D. Riedel; J. Rengelshausen; P. Meissner; O. Müller; G. Mikus; W. E. Haefeli; I. Walter-Sack *Journal of Chromatography B* **2008**, *863*, 273.
- (9) R. W. Horobin, *Conn's Biological Stains*; Ch20. Thiazines, R. W. Horobin, J. A. Kiernan, BIOS Scientific Publishers Ltd, 2002
- (10) J. Kucsera; K. Yarita; K. Takeo *Journal of Microbiological Methods* **2000**, *41*, 19.
- (11) A. Mills; K. Lawrie; M. McFarlane *Photochem. Photobiol. Sci.* **2009**, *8*, 421.
- (12) M. Wainwright, *Conn's Biological Stains*; Ch. 7. The use of dyes and fluorochromes as indicators, R. W. Horobin, J. A. Kiernan, BIOS Scientific Publishers Ltd., 2002

- (13) R. Horobin, *Conn's Biological Stains; Ch19. Oxazines and Related Dyes*, R. W. Horobin, J. A. Kiernan, BIOS Scientific Publishers Ltd, 2002
- (14) H. A. Montejano; M. Gervaldo; S. G. Bertolotti *Dyes and Pigments* **2005**, *64*, 117.
- (15) M. Zhou; Z. Diwu; N. Panchuk-Voloshina; R. P. Haugland *Anal. Biochem.* **1997**, *253*, 162.
- (16) H. Golnabi; M. Razani *Sensors and Actuators B* **2007**, *122*, 109.
- (17) G. G. Guilbault; D. N. Kramer *Analytical Chemistry* **1965**, *37*, 1219.
- (18) A. Mills; M. McFarlane; S. Schneider *Anal. Bioanal. Chem.* **2006**, *386*, 299.
- (19) A. Cusick *The Kinetics of Dye Photocatalysis* Univeristy of Strathclyde, Glasgow 2009.

5 Characterisation of Sol-Gel TiO₂ Paste Films and the Measurement of Their Photocatalytic Activities Using Standard and Novel Methods

Whilst the indicator inks discussed previously in chapters 3 and 4 are excellent for the assessment of the photocatalytic activity of thin (ca. 15 nm) semiconductor films in the field, such as that observed on self-cleaning glasses like Activ™, BioClean™, etc, it would be anticipated that as the photocatalytic activity of a film increased, so the inks discussed thus far would be rendered less useful/appropriate, since the kinetics of their photocatalytically-induced colour change would be too rapid to provide an accurate assessment by eye at least. Such inks may still be useful in the laboratory, since the reduction reaction could be followed spectrophotometrically and, if necessary, in the absence of all but the UV light source.

There are many methods in the literature which have been used to assess the photocatalytic activity of samples (usually thick films of titania) in the laboratory. Of these, two of the most common are the stearic acid (SA) and methylene blue (MB) tests, as discussed previously in section 1.6. The SA test involves coating a solution of the organic on to the photocatalyst test substrate and monitoring its photooxidation with irradiation time using infra red spectroscopy, ellipsometry or gas chromatography. Its underlying appeal appears to be centred on the resemblance of the organic film to the dust and grime that can attach itself to surfaces from the atmosphere. In contrast, the MB test involves placing the photocatalyst test substrate (film or powder) in contact with a solution of the dye and monitoring the dye's photodegradation, using UV-Visible spectroscopy, with irradiation. The appeal of such a test is obviously the fact that the destruction of the dye can be monitored visually, as is the case with the indicator inks, owing to the accompanying colour change from blue to colourless with dye degradation.

The aim of this chapter is to assess whether the three tests, namely SA, MB and an indicator ink, can be correlated with each other across a range of photocatalyst samples of different photocatalytic activities. Such samples are prepared in-house from a TiO₂

sol-gel paste prepared as described in chapter 2 and elsewhere¹⁻². Thus the first part of the chapter deals with the characterisation and analysis of the physical properties of the films using a range of techniques such as SEM, AFM and XRD. The activities of each of these samples are then assessed using the above three tests and any correlations between test methods are highlighted accordingly.

5.1. Characterisation of the Sol-Gel Paste Films

5.1.1. Absorbance Spectroscopy

The paste films of varying activity used in this work were prepared using a sol-gel method described previously in section 2.2. In short, titanium (IV) isopropoxide is hydrolysed in the presence of acetic acid at 80 °C for 8 hours. The solution is then filtered, transferred to an acid digestion bomb and placed in an oven at 220 °C for 12 hours, causing the TiO₂ particle size to increase via Ostwald Ripening. Following sonication to remove any agglomerated particles, the solution is then rotary evaporated until the solids content is ca. 10-12 wt%. Carbowax is finally added in order to thicken the solution, forming a paste which can be cast on substrates such as glass and quartz, and appears stable indefinitely when stored in a fridge (ca. 4 °C).

In this work, TiO₂ films were produced by doctor blading the paste on to quartz discs using Scotch Tape™ as tracks, as demonstrated previously in section 2.2. After being allowed to air-dry, the films were then annealed at the desired temperature to create the photocatalyst film. In order to create a set of films of varying photocatalytic activity, the annealing temperature was altered between 450 and 1100 °C. It has previously been demonstrated by Mills et al² for such paste films and by many others including, but not exclusively, Yu et al³, Jung et al⁴ and Baba and Hatada⁵ for both sol-gel and plasma generated TiO₂ films, that by increasing the annealing temperature, the anatase:rutile ratio of the film is altered. Since anatase is formed at lower temperatures and is generally accepted to be of a higher activity than rutile, which is generated at higher temperatures, it follows that in varying the annealing temperature it is possible to vary the overall photocatalytic activity of the film based on the ratio of the two phases

present. The higher photocatalytic activity of anatase is attributed to many factors including⁶, but not exclusively;

- A greater surface area;
- A greater affinity for organic molecules, and;
- A slightly larger bandgap

Figure 5.1. shows the change in the recorded UV-Visible absorbance spectra of the titania paste films as a function of increasing annealing temperature.

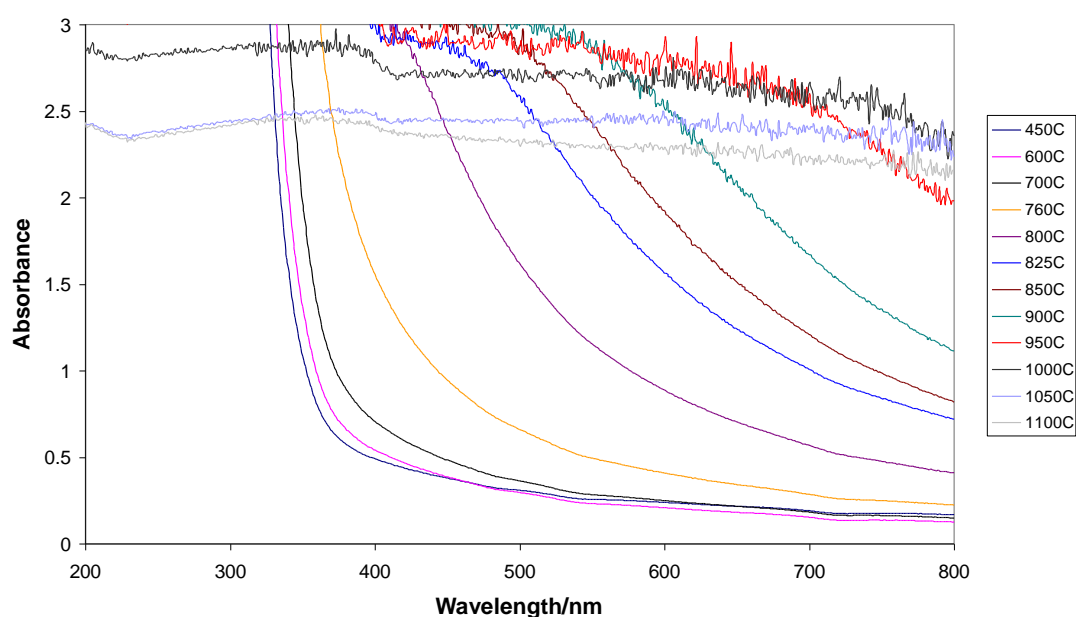


Figure 5.1.: The variation in the UV-Visible absorbance spectra of the paste films with increasing annealing temperature

At low temperatures (450-700 °C), the films are observed to be relatively transparent, with the observed increase in absorbance at low wavelengths (i.e. < 400 nm) due to ultra-band gap absorption of photons by anatase TiO₂, as will be confirmed later from the XRD data. However, as the annealing temperature is increased, the films become more opaque, scattering the incident light and causing the absorbance spectra to

increase rapidly at higher wavelengths. The magnitude of this increase in absorbance at longer wavelengths is such that, by ca. 950 °C, the paste film spectra are completely opaque over the wavelength range 200-800 nm. Similar results for these paste films have been described previously by Mills et al², the increase in the absorbance spectra with annealing temperature attributed to particle growth through sintering, as well as some conversion of anatase to rutile. This change in the absorbance spectra is verified by the photographs of selected paste films given in figure 5.2., where the intensity of the white colour can be seen to increase as the annealing temperature for the film increases.

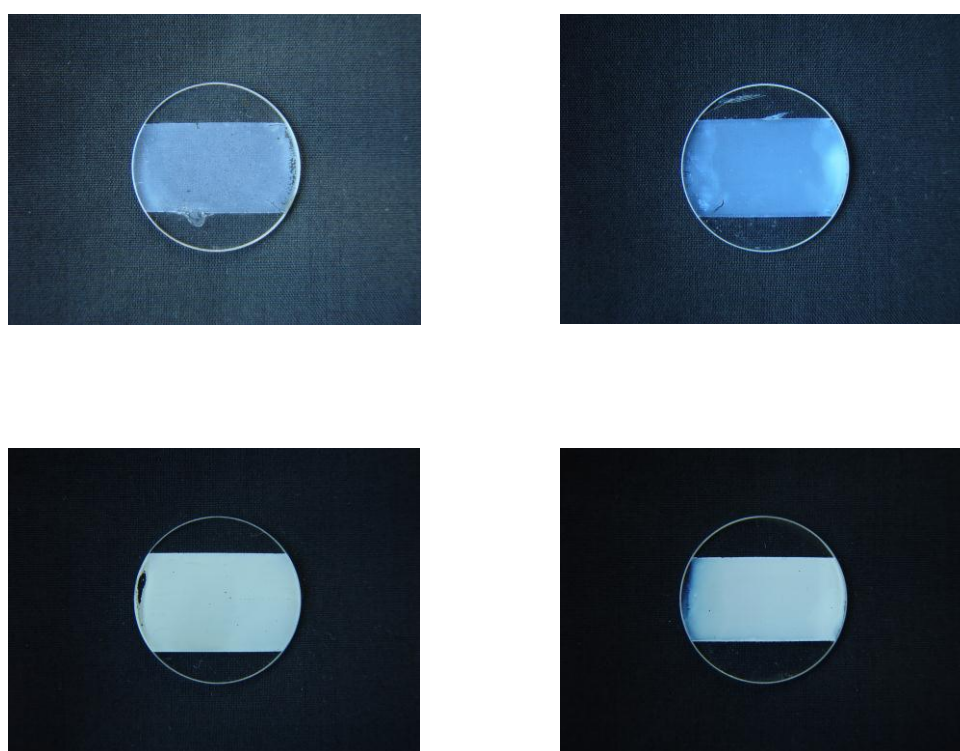


Figure 5.2.: The observed opacity of the paste films annealed on quartz at the following temperatures (clockwise from top left); 450, 760, 900 and 1100 °C

5.1.2. Mechanical Stability of Annealed Paste Films

The mechanical stability of the produced paste films was assessed using 3 simple methods, namely;

- Rubbing with a cloth;
- Sonication in water, and;
- Aqua regia

The stability results obtained for the paste films annealed over the temperature range 450 to 1100 °C are given in table 5.1.

Annealing Temperature/°C	Rubbing with cloth	Sonication	Comments
450	× ×	× ×	Film is 'flaky' on the quartz surface but is more stable on glass
600	× ×	× ×	Film is still flaky and removed by gentle rubbing
700	×	× ×	Requires vigorous rubbing to remove the film
760	×	×	Removed by hard rubbing
800	×	×	“
825	×	×	“
850	×	×	“
900	×	×	Almost completely resistant to rubbing
950	✓	✓	Highly resistant to rubbing
1000	✓ ✓	✓ ✓	“
1050	✓ ✓	✓ ✓	“
1100	✓ ✓	✓ ✓	“

Table 5.1.: The mechanical stability of the paste films annealed at various temperatures. The notations assigned to each technique vary from extremely useful for film removal (××) to unable to remove the film (✓✓)

As the annealing temperature is increased, we observe a parallel increase in the film's stability. At the lowest temperatures used in this work (450 and 600 °C), the film can be removed simply by blowing a gentle stream of gas over the substrate surface, especially if the ramp rate used to produce the film is high (> 30 °C/min). However, even at lower furnace ramp rates (< 10 °C/min), the film still exhibits poor adherence to the quartz substrate, particularly at the edge of the films where the tape tracks were placed. It is believed that as the annealing temperature increases, so the paste film is more susceptible to 'fuse' with the quartz, such that by ca. 950 °C the film is impossible to remove, even with vigorous rubbing or aqua regia. At intermediate temperatures, the film is resistant to rubbing with a cloth. Work by Chen and Dionysiou⁷ demonstrated that for a range of sol-gel films produced using a P25-powder modified sol-gel route, the mechanical stability increases over the temperature range 400-700 °C, with the authors postulating that 500 °C is the critical calcination temperature to ensure good mechanical stability with maximum activity of such films. For the paste films described here, a reasonable degree of stability on quartz is only obtained at temperatures ≥ 700 °C.

5.1.3. Scanning Electron Microscopy (SEM)

Scanning Electron Microscopy (SEM) images of the paste films were recorded under the guidance of Dr Laurence Tetley at the University of Glasgow. Owing to charging, it was only possible to record a select few images at the magnifications specified, and even then mainly on those paste films annealed at higher temperatures (i.e. ≥ 800 °C). Figure 5.3. shows a selection of images recorded at high magnification (scale bar 1 μm). From such images, it is immediately apparent that as the annealing temperature is increased from 450 to 800 °C, there is no obvious change in the surface morphology of the paste films. Such samples seemingly exhibit a similar pore size, distribution and particle size. However, as the annealing temperature is increased from 800 to 900 °C, there appears to be a marked change in all of these properties from the SEM data. The increase in such properties continues as the annealing temperature is increased further up to 1100 °C. The images generated confirm the results from UV-Visible

spectroscopy in section 5.1.1., namely that the particle size increases with increasing annealing temperature.

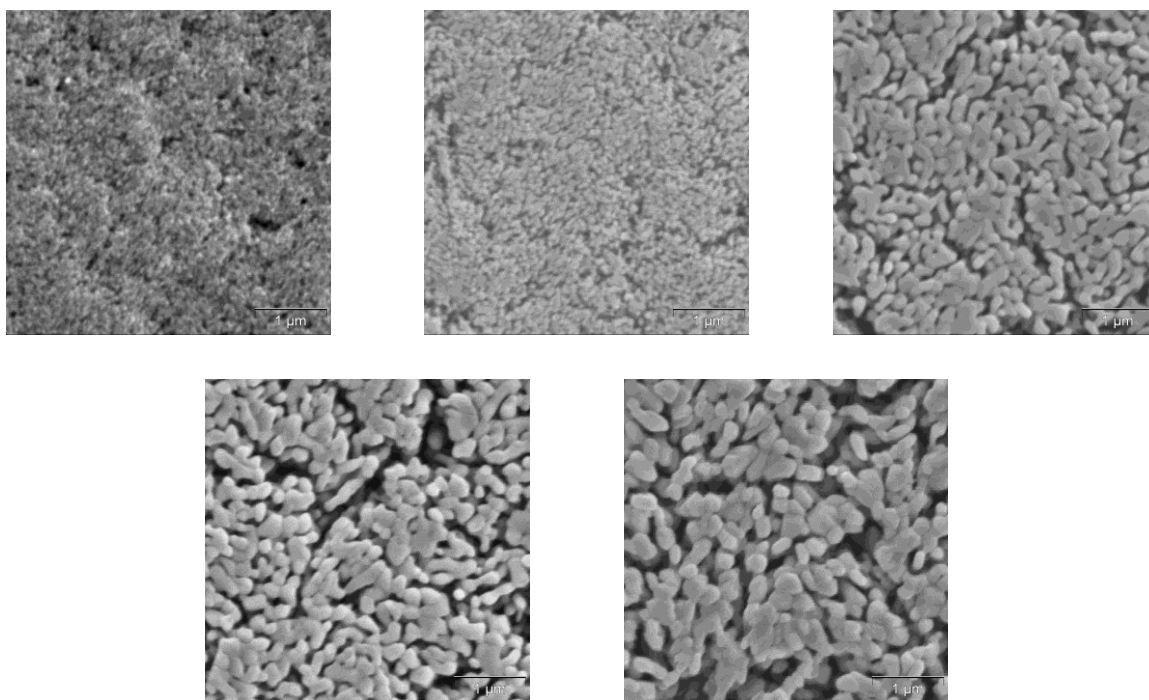


Figure 5.3.: SEM images recorded at higher magnification of paste films annealed at the following temperatures (from left to right); top - 450 °C, 800 °C, 900 °C and bottom – 1000 °C and 1100 °C

5.1.4. Atomic Force Microscopy (AFM)

Although the SEM images in figure 5.3. do go some way to providing us with an understanding of the changes in the titania surface which occur with increasing annealing temperature, owing to charging it was impossible to conduct a more detailed study using this technique. Under the guidance of Dr Pik Leung Tang, therefore, the surface morphology was also studied using Atomic Force Microscopy (AFM). In doing so, it was possible to obtain a more detailed picture of the surface morphology across all samples, i.e. not just those annealed at higher temperatures (≥ 800 °C). Figure 5.4. shows a selection of the images obtained at 5 μm x 5 μm , whilst figure 5.5 shows samples at a sample area of 1 μm x 1 μm .

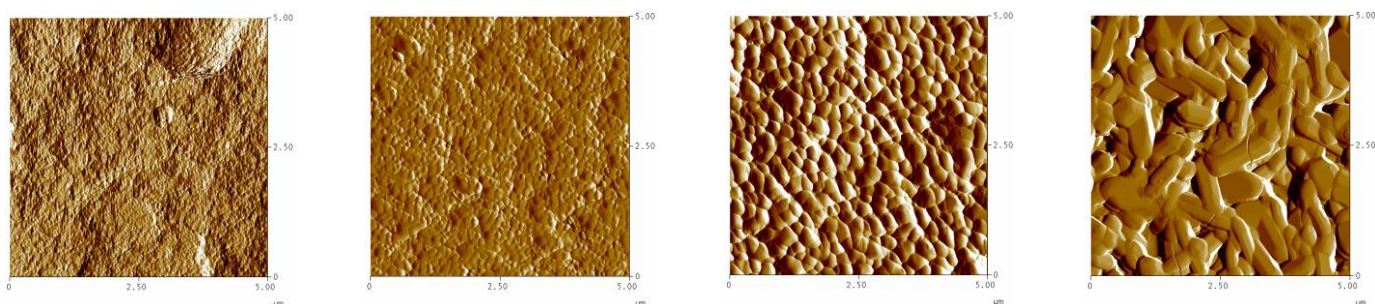


Figure 5.4.: AFM images recorded at low magnification (sample area 25 μm^2) of the paste films annealed at the following temperatures (from left to right): 450, 825, 900 and 1100 °C

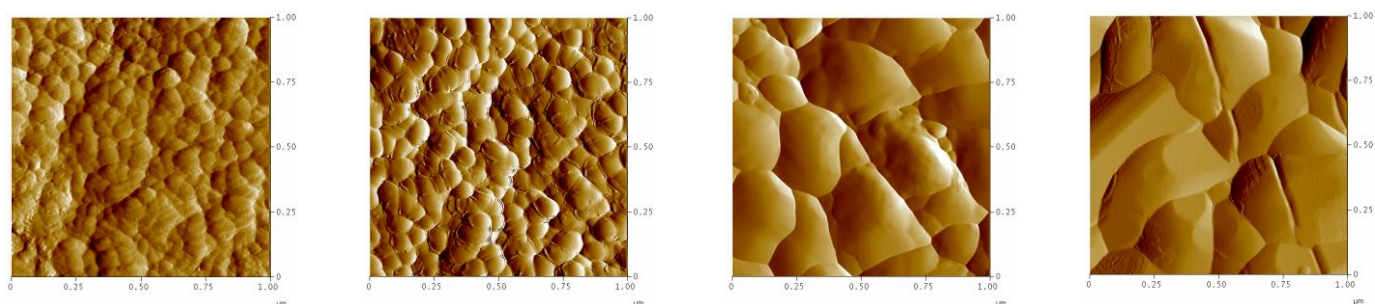


Figure 5.5.: AFM images recorded at higher magnification (sample area 1 μm^2) of the paste films annealed at the following temperatures (from left to right): 450, 760, 900 and 1100 °C

At both magnifications we see a marked increase in the particle size of the paste films as the annealing temperature is increased, corroborating what was derived above from both the SEM images and the UV-Vis data. Whilst a selection of the images are shown here, data was collected over sample areas varying from 1600 to 0.0225 μm^2 , allowing a wealth of data to be obtained to calculate the average particle size at the various annealing temperatures. Figure 5.6. shows the variation in this average particle size with annealing temperature. As anticipated from the results in figures 5.3.-5.5., the average particle size appears constant over the annealing temperature range 450-800 °C, after which a gradual, linear increase occurs. Indeed, in increasing the annealing temperature from ca. 800 °C to 900 °C alone, the average particle size increases ca. 3-

fold, with a ca. 5-fold increase noted over the range 800-1100 °C. Note, however, that such data does not provide us with information as to the phase of such particles.

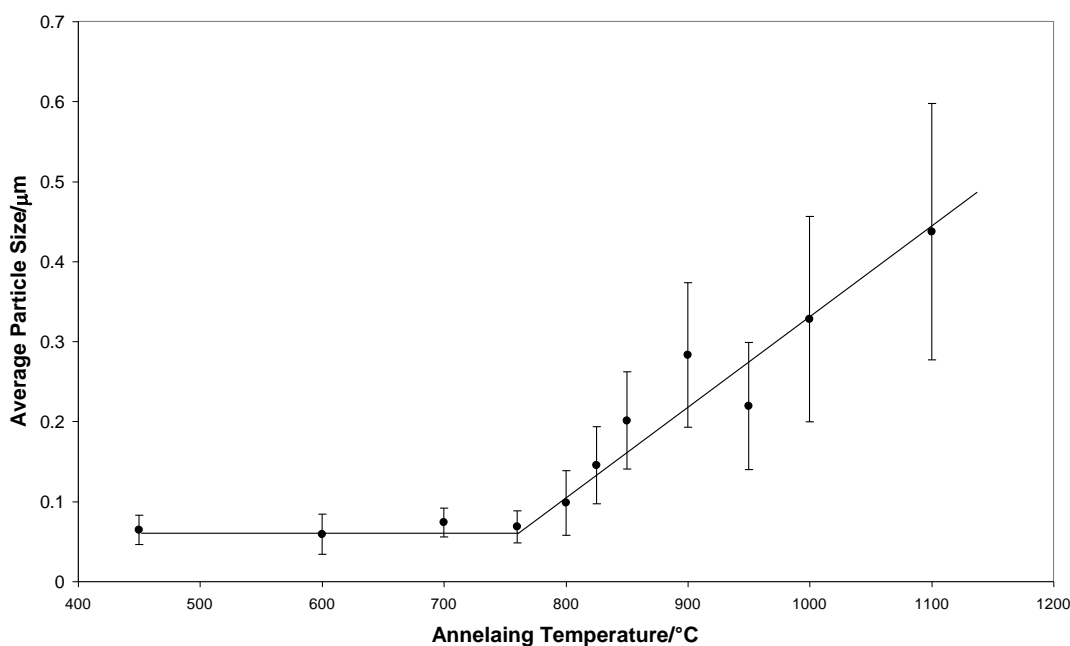


Figure 5.6.: The variation in the average particle size, as calculated from the AFM images, with annealing temperature (30 minutes annealing time) for the paste films. The error bars represent the error in the mean particle size at each temperature

Increasing particle sizes with annealing temperature are commonplace for both TiO₂ films and powders. Since there are many publications which deal with the effect of annealing temperature on the characteristics of TiO₂ powders and films, it would be impossible to encompass all those articles here. However, a survey of some of the literature on the subject appears to confirm the general trend outlined in figure 5.6. Bakardjieva et al⁸ noted that for TiO₂ powders produced from the hydrolysis of TiOSO₄ and annealed over the temperature range 200-1150 °C, the average particle size of anatase remained fairly constant from 200-400 °C before a noticeable increase was observed upon annealing at 600 °C, and then subsequently again at 800 °C. Chen and Dionysiou⁷, on the other hand, reported that for TiO₂ produced from a modified P25 sol-gel technique, annealing at temperatures in the range 400-600 °C produced no

significant change in the crystal size, as is seen here, but by moving to 700 °C, the particle size increased ca. 3-fold. Such an increase was attributed to the conversion of anatase to rutile at this temperature by the authors. Evidently, the methods and substrates used to produce the TiO₂ play a significant role in determining the properties observed at various annealing temperatures.

5.1.5. X-Ray Diffraction (XRD)

In addition to the techniques outlined above, X-Ray diffraction (XRD) images of the paste films were also obtained, under the guidance of Dr Pik Leung Tang. Figure 5.7. shows how the diffraction pattern of the paste films varies as the annealing temperature is increased.

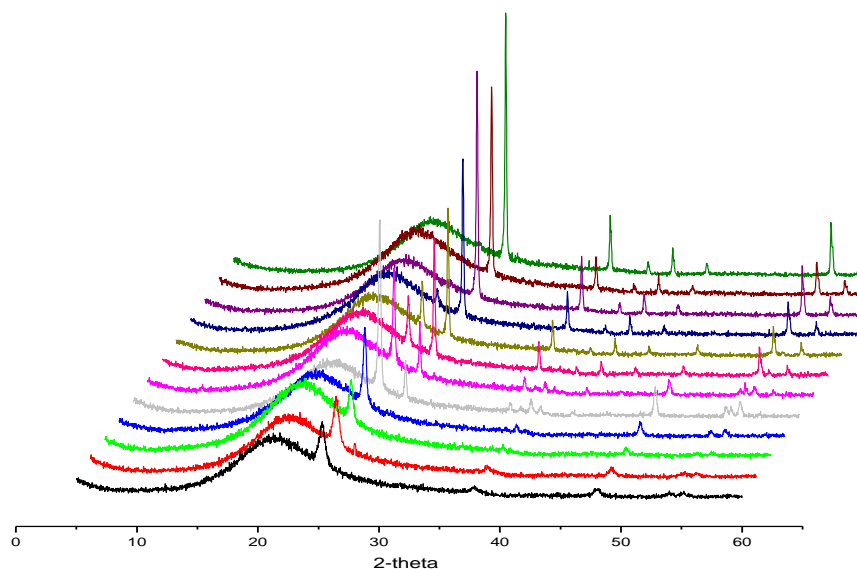


Figure 5.7.: The variation in the XRD pattern obtained for the paste films as the annealing temperature is increased from 450 °C (front, black trace) through to 1100 °C

The broad peak below a 2θ value of ca. 30 ° is due to the underlying quartz substrate, hence its presence across all samples. However, on this amorphous peak we observe a peak at ca. 25.3 ° on the films annealed at 450 – 950 °C. Based on work conducted

elsewhere⁹, and using the standard pattern for anatase (JCPDS 21-1272)¹⁰ this peak is attributed to (101) anatase TiO₂. Since it is the most prominent peak across all low temperature films, it is used as the reference peak for future comparisons and calculations. This peak is observed to increase in height and become sharper as the annealing temperature is increased from 450 to 800 °C, indicating an increase in the crystallinity of the paste films; the lower temperature paste films are thus more amorphous by comparison.

Baiju et al¹¹ observed the crystallinity of their sol-gel films to increase over the much shorter temperature range of 400-600 °C, attributing such an effect to various parameters including greater diffusion kinetics associated with growth at higher temperatures (which reduces the number of crystal defects which develop), the phase transition from amorphous to anatase, an increase in both nanoparticle and nanocrystallite size, and an improvement in the band structure of the film. Puddu et al⁶ even went as far to suggest that the crystallinity was the most important factor in determining the photocatalytic activity towards trichloroethylene conversion using their anatase sol-gel particles, more so than the particle size or the specific surface area. The authors suggested that as noted above by Baiju et al, the more crystalline the sample, the less bulk defects are present, and that such defects tend to be excellent sites for e⁻/h⁺ recombination to occur.

For the paste films annealed at 800 – 1100 °C, a new, more prominent peak is observed at ca. 27.46 °, again superimposed on the amorphous quartz peak, attributed to diffraction from the rutile (110) face. Such a conclusion is based on the work of others⁹ and the standard pattern data for rutile (JCPDS 21-1276), and it is thus used as the reference peak for this TiO₂ phase¹². This emergence of the rutile phase as the annealing temperature is increased is a common feature when TiO₂ is annealed at various temperatures, as reported in the work of others both on sol-gel films and powders. However, the temperature at which the transition from anatase to rutile occurs is seen to vary between studies. Bakardjieva et al⁸ observe the first emergence of rutile at 800 °C, as observed here, for TiO₂ powders produced via hydrolysis of TiOSO₄, whilst Górska et al¹³ observed rutile in TiO₂ powders prepared from a sol-gel at 650 °C.

Indeed, work by Kim et al¹⁴ showed rutile to be present in unsupported xerosel samples annealed at a mere 500 °C produced from a sol-gel method. Evidently, the phase composition of TiO₂ annealed at different temperatures appears to be influenced by a variety of factors, and hence cannot be predicted based on annealing temperature alone. The results generated here for the paste films are in good agreement with prior work by Mills et al² using a similar paste film method, with such work reporting the emergence of the rutile phase at 750 °C.

Based on the peak heights shown in figure 5.7., the anatase dominance is quashed when the annealing temperature reaches 850 °C, with rutile becoming the more dominant phase, before a film which is completely rutile in nature is achieved at 1000 °C. Figure 5.8. shows the percentage of anatase present in the paste films across all samples as the annealing temperature is increased, based on equation 5.1.;

$$X_A = \frac{1}{1+1.26(I_R/I_A)} \quad (5.1.)$$

where X_A is the fraction of anatase and I_R and I_A are the relative intensities of the reflections for the (110) plane of rutile and the (101) plane of anatase, respectively¹⁵.

Using the data in figures 5.7. and 5.8., a crude value for the density of each paste film, ρ_{film} , can be estimated using equation 5.2.;

$$\rho_{\text{film}} = (\% \text{ anatase} \times \rho_{\text{anatase}}) + (\% \text{ rutile} \times \rho_{\text{rutile}}) \quad (5.2.)$$

where % anatase and % rutile are the relative amounts of anatase and rutile present in the paste film, as calculated from equation 5.1., and ρ_{anatase} and ρ_{rutile} are the density of anatase (3.895 g cm⁻³) and rutile (4.274 g cm⁻³) respectively. Using these calculated densities, and the average value of the grain/particle size, d , calculated using the results from AFM previously, it is possible to estimate the specific surface area (SSA) for each film using equation 5.3.;

$$SSA = 6/(\rho_{\text{film}} \times d) \quad (5.3.)$$

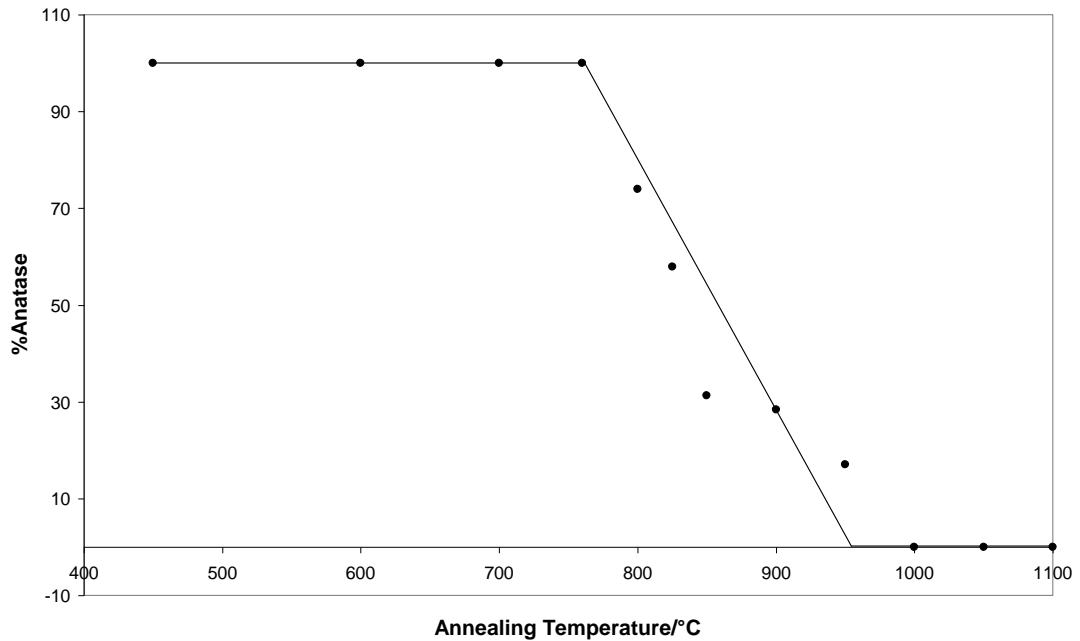


Figure 5.8.: The variation in the amount of anatase TiO₂ present in the paste film with increasing annealing temperature

Figure 5.9 shows how the SSA varies with annealing temperature for the films presented here. In addition, the variation in the average particle/grain size with annealing temperature, as shown previously in figure 5.6., is also shown. Since we had observed previously in figure 5.6. that the average particle size increased with annealing temperature above ca. 760 °C, it comes as no surprise that, having used equation 5.3. to ascertain the SSA of each film, SSA is observed to decrease rapidly over the range 760 to 900 °C. However, despite the calculated increase in particle size above 900 °C, no further significant decrease in the SSA is observed. This is most likely a consequence of the film phase altering from a rutile/anatase blend to purely rutile in nature, which has a slightly larger density than anatase. Indeed, this also explains the decrease in SSA noted above 760 °C being parallel to the emergence of rutile in the film.

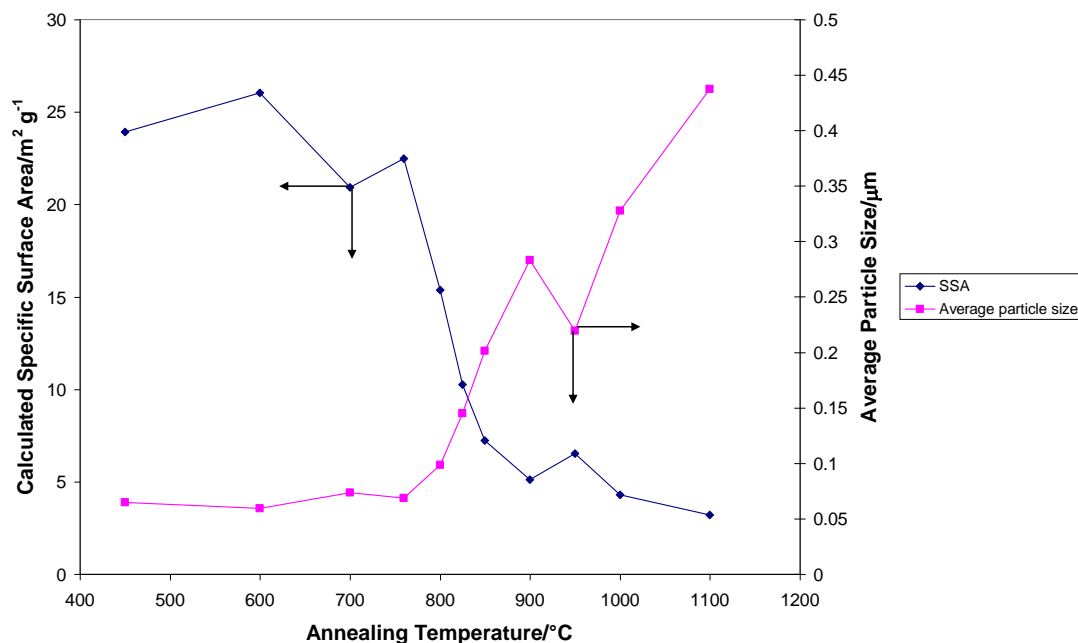


Figure 5.9.: The variation in both the SSA (blue trace) and the average particle size (pink trace) with annealing temperature

These results are further emphasised by figure 5.10., which plots the variation in SSA with % anatase. It would appear that from 700-950 °C, there is a reasonable degree of correlation between %anatase and the SSA. Below 700 °C, the film is 100 % anatase and above 1000 °C it is 100 % rutile. In the three regions of the graph (denoted A, B and C), the increased annealing temperature results in a loss in SSA, as observed in figure 5.9. – but only in region B (i.e. over the range 700-950 °C) is this also associated with a change in phase.

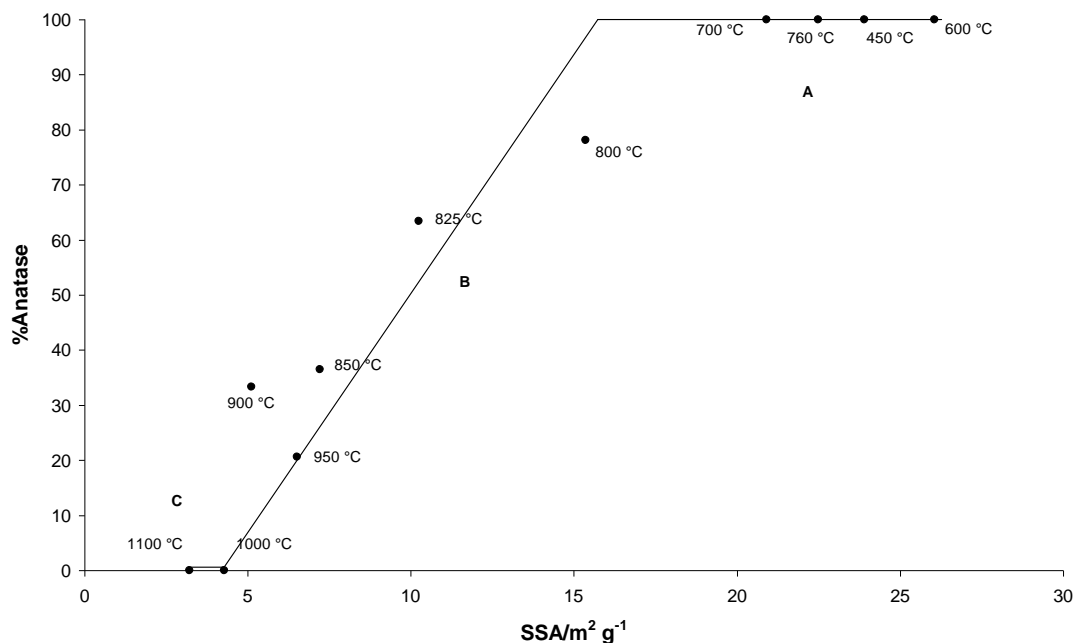


Figure 5.10.: The variation in the SSA with the % anatase present for the paste films

An increase in SSA with decreasing particle size is not entirely unexpected since, once again, similar results are reported in the literature. Bakardjieva et al⁸ noted a decrease in the BET surface area from 279.3 m² g⁻¹ to a mere 3.11 m² g⁻¹ on increasing the annealing temperature (3 hour annealing time) from 200 to 1150 °C for their TiO₂ powders, whilst Chen and Dionysiou⁷ noted a decrease from ca. 80 to 4 m² g⁻¹ for their P25 sol-gel modified films prepared over the much smaller temperature range of 400-700 °C (annealing time 1 hour). The effect has also been observed using commercial TiO₂ powders, namely Degussa P25 and Hombikat TiO₂, on changing the annealing temperature from 600 to 800 °C, the BET surface area decreasing ca. 5-fold across this temperature range¹⁶.

Fernandes-Macahdo and Santana¹⁷ and Górska et al¹³ attributed the loss of SA with increasing temperature to particle agglomeration/crystal growth and sintering, which is believed to be responsible for the changes observed here too. Indeed, we have already demonstrated from the AFM data collected in figure 5.6. that the average particle size increases with annealing temperature. Kim et al¹⁴, Ohno et al¹⁸, Tanaka and

Suganuma¹⁹, Tsai and Cheng²⁰ and Wang et al²¹ all observed similar effects, albeit to varying degrees, of an increasing annealing temperature on the surface area of prepared TiO₂ films and powders.

5.2. Measurement of Photocatalytic Activity of the Paste Films – Correlation of Standard Tests

5.2.1. The Stearic Acid Test

As was stated previously in the introduction, the stearic acid test is commonly used to assess the photocatalytic activity of TiO₂ films²²⁻²⁶. The organic is typically dissolved in a suitable solvent (e.g. chloroform is used here) and applied to the surface of the film usually by either dip coating the film in the solution or spin-coating it. Once dried, the film of the organic left on the substrate surface is reminiscent of the type of dirt and grime which accumulates on the surface of windows, walls, etc due to atmospheric pollution.

Figure 5.11. shows the infra red spectrum (recorded over the wavenumber range 3500 to 2500 cm⁻¹) obtained when a stearic acid film is spun-coated on to the surface of a paste film annealed at 450 °C. The peaks observed in the region of 3200-2800 cm⁻¹ are due to stearic acid alone, since any chloroform present following spin-coating is removed by heating, and hence their integrated area can be measured and taken as being representative of the concentration of stearic acid present. Such vibrations correspond to the asymmetric, in-plane C-H stretching mode of the CH₃ group (2957.5 cm⁻¹) and the asymmetric and symmetric C-H stretching modes of the CH₂ group (2922.8 and 2853.4 cm⁻¹ respectively)². As the film is irradiated, we can see from figure 5.11. that the height of such peaks, and hence the integrated area due to stearic acid, decreases as the organic is oxidised, ultimately producing CO₂ and H₂O according to equation 5.4., i.e.



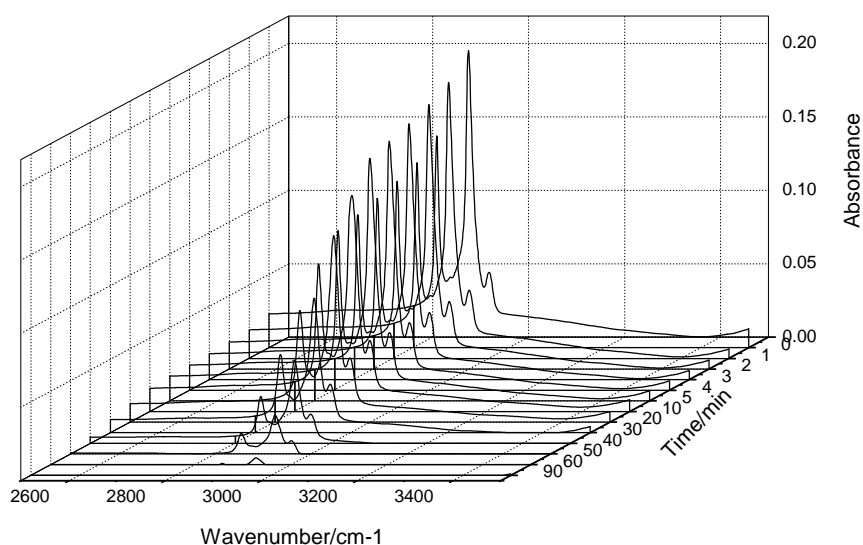


Figure 5.11.: The variation in the infra red absorbance spectrum due to stearic acid with increasing UVA irradiation time on a TiO₂ paste film annealed at 450 °C

Within 90 minutes of UV irradiation at 2.4 mW cm^{-2} , which is ca. 2 times less than the typical output of the summer sun, it can be seen from figure 5.11. that no peaks are visible in the infra red spectrum, suggesting that the stearic acid has been fully oxidised. Figure 5.12. shows the variation in the integrated peak area due to stearic acid with time and from it we infer that the oxidation reaction follows zero order kinetics, in agreement with work conducted elsewhere^{2,23}. Such zero order kinetics are to be anticipated since previous work has suggested that an initial integrated absorbance of $9\text{-}11 \text{ cm}^{-1}$ is equivalent to 61-75 monolayers of stearic acid on a P25 film and ActivTM²⁷. As a result, all TiO₂ surface active sites will be occupied, with plenty more stearic acid ready to occupy sites which become available following the reaction. In this work, the initial integrated absorbance was similar to that reported by Mills et al²⁷. Using the equations highlighted previously in section 2.1.4., the zero order $t_{50\%}$ is calculated to be 30 minutes for this 450 °C paste film.

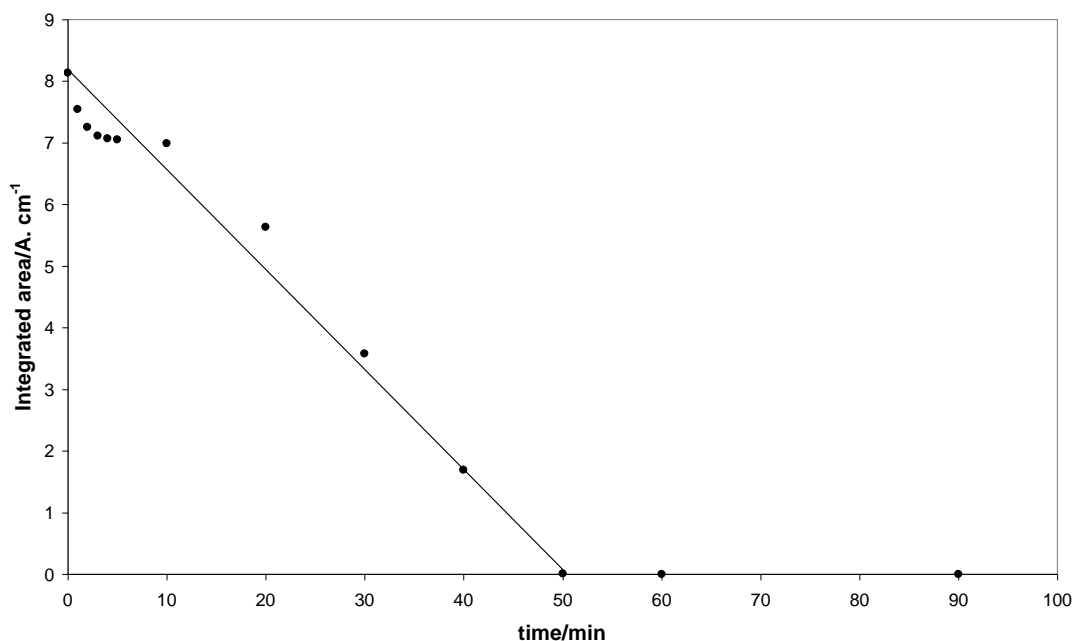


Figure 5.12.: The variation in the integrated peak area due to stearic acid with UVA irradiation on a paste film annealed at 450 °C

In addition to such rapid kinetic behaviour, the film is also observed to give highly reproducible results, as indicated in figure 5.13. The change in the integrated area due to the stearic acid peaks across 5 runs is observed to be strongly consistent, with complete removal of the stearic acid film occurring within ca. 60 minutes UVA irradiation in each instance, despite the slight fluctuation in the initial integrated area of the peaks. The average $t_{50\%}$ across all 5 runs is 29 minutes, with the rate of photooxidation, k_0 , calculated to be $0.151 \text{ A.cm}^{-1} \text{ min}^{-1}$, both assuming zero order kinetics.

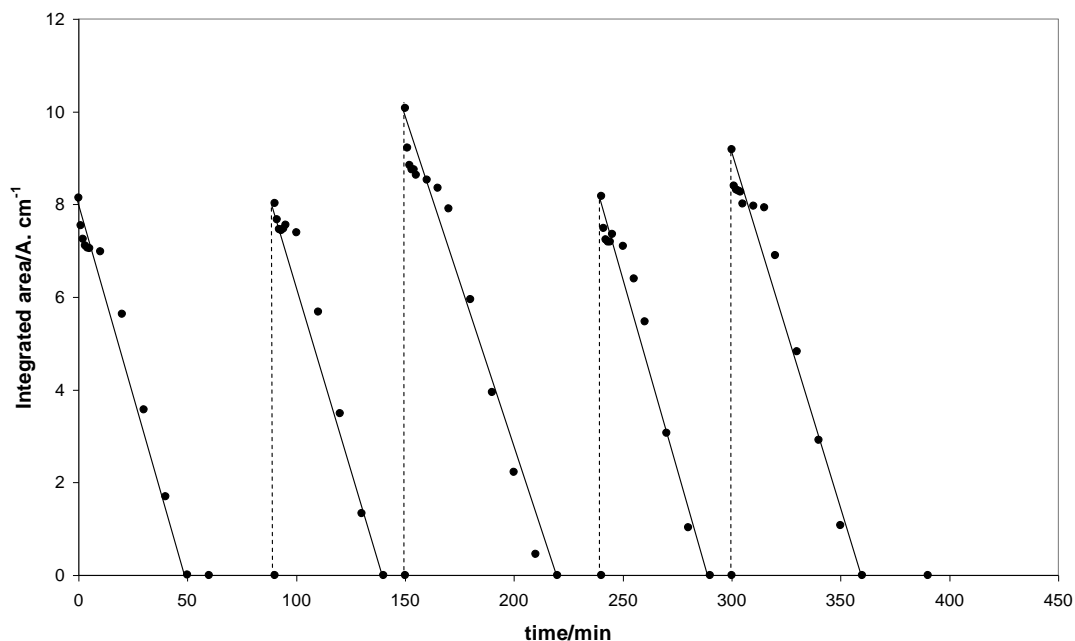


Figure 5.13.: The photooxidation of stearic acid on a paste film annealed at 450 °C over 5 runs

The photooxidation of stearic acid was assessed across the range of paste films annealed at various temperatures and the average rate of degradation, k_0 , extracted from the data obtained across 5 runs. It should be noted, however, that for samples annealed above 900 °C, the rate of photooxidation was so slow that data was only recorded until ca. 20 % of the initial amount of stearic acid present had been oxidised. For such high temperatures, although the rate of photooxidation reported is technically the initial rate obtained, since the reaction has been observed to be zero order even at such low activities it can be assumed that such a rate is indicative of the bulk rate of photooxidation. Figure 5.14. reports the change in the rate of stearic acid photooxidation, k_0 , as the annealing temperature of the underlying paste film is altered over the range 450 – 850 °C.

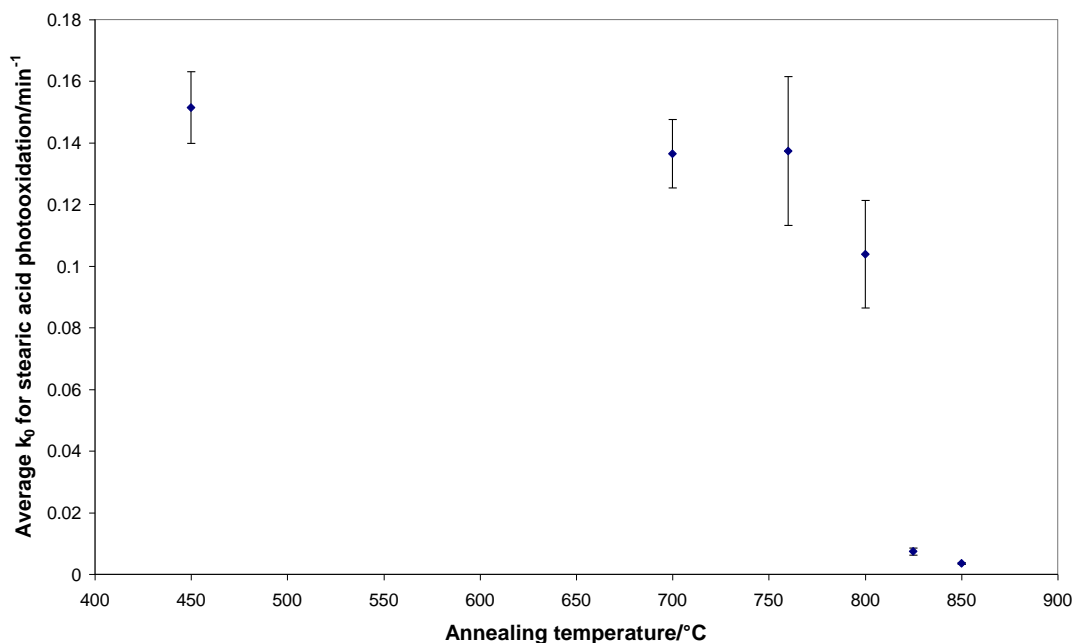


Figure 5.14.: The variation in the zero order rate constant, k_0 , for stearic acid photooxidation with annealing temperature over the range 450-850 °C

As the annealing temperature is increased to 800 °C, there is no significant change in the observed rate of stearic acid photooxidation. However, at 825 °C, the photooxidation rate is seen to drop by a factor of ca. 10 times compared to what is observed at 800 °C. Previously in figures 5.8. and 5.10., we observed that it is around this temperature that the %anatase in the sample falls most sharply, as does the specific surface area, whilst the average particle size increases. Whilst mixed-phase TiO₂ samples such as P25, which has an anatase:rutile ratio of 80:20²⁸, exhibit a high photocatalytic activity, the paste film annealed here at 825 °C has an anatase:rutile ratio of ca. 60:40. Such a result would seem to infer that the synergistic effect which is proposed for many mixed-phase samples has been lost and the sample is now dominated by the poorer photocatalytic activity of rutile TiO₂. The synergistic effect observed for some mixed-phase TiO₂ samples is believed to be a consequence of rutile acting as an ‘electron sink’, whereby the photogenerated e⁻ in the conduction band of anatase can be removed from potential recombination with a photogenerated h⁺. Work by Jing et al postulated that photogenerated e⁻ transfer can also occur from anatase surface states

related to oxygen vacancies, which have an energy between the valence and conduction band for the phase²⁹. As a consequence, both photogenerated species are then free to take part in reactions with surface adsorbed species, i.e. stearic acid.

Returning to figure 5.14., the rate of stearic acid photooxidation is observed to decrease further as the annealing temperature is increased to 850 °C. Such a decrease is to be anticipated since rutile is, overall, the more dominant phase in such a film (from figure 5.8.), and work conducted elsewhere has suggested that rutile is the less active of the two phases owing to its lower surface affinity for organic species and since it has a much higher h^+/e^- recombination rate than anatase³⁰. Evidently, whilst a synergy can exist between the two phases, there maybe a critical composition above which the inactivity of rutile dominates. The combination of two factors, i.e. the decrease in SSA and the increase in rutile content, is thought to be responsible for the major decrease in the rate of stearic acid photooxidation on moving from 800 to 825 °C. However, figure 5.15. below shows how the zero order rate constant varies with the %anatase present in the film.

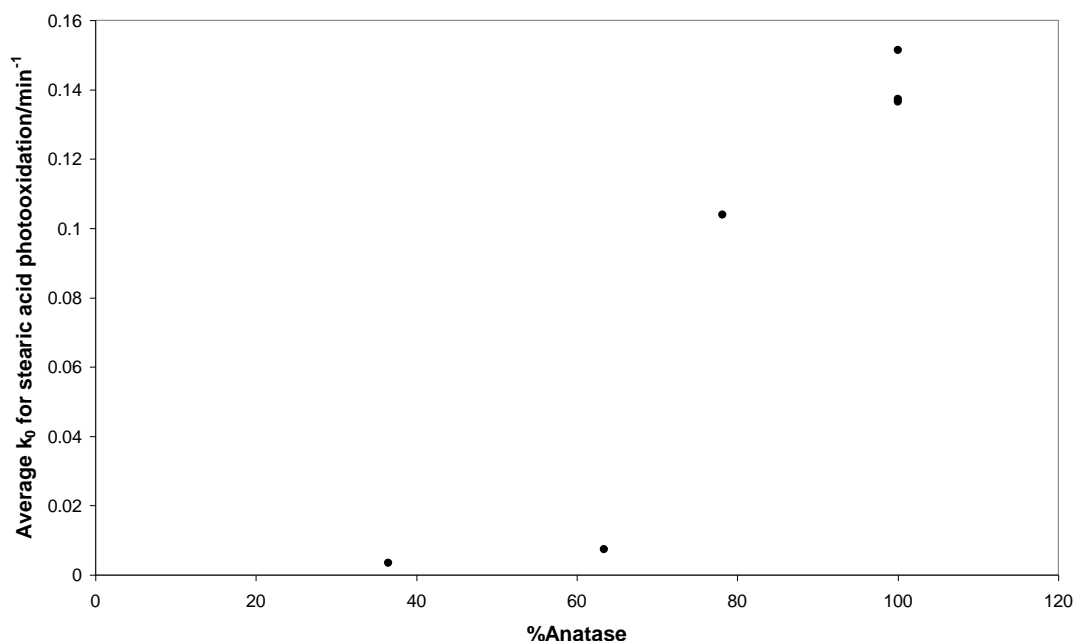


Figure 5.15.: The variation in the rate of stearic acid photooxidation as a function of the anatase level present in the paste films annealed over the temperature range 450-850 °C

A reasonable correlation would appear to exist, suggesting that the emergence of rutile is of greater detriment to the rate of stearic acid removal. Above 850 °C, the time taken for stearic acid to be removed from the paste film surface increased further such that it was not possible to observe complete removal over an appreciable timescale (ca. 1 week). Thus, for such films the initial rate of stearic acid removal, r_i , was calculated over a ca. 20 % decrease in the initial integrated area due to the peaks. The results are shown in figure 5.16.

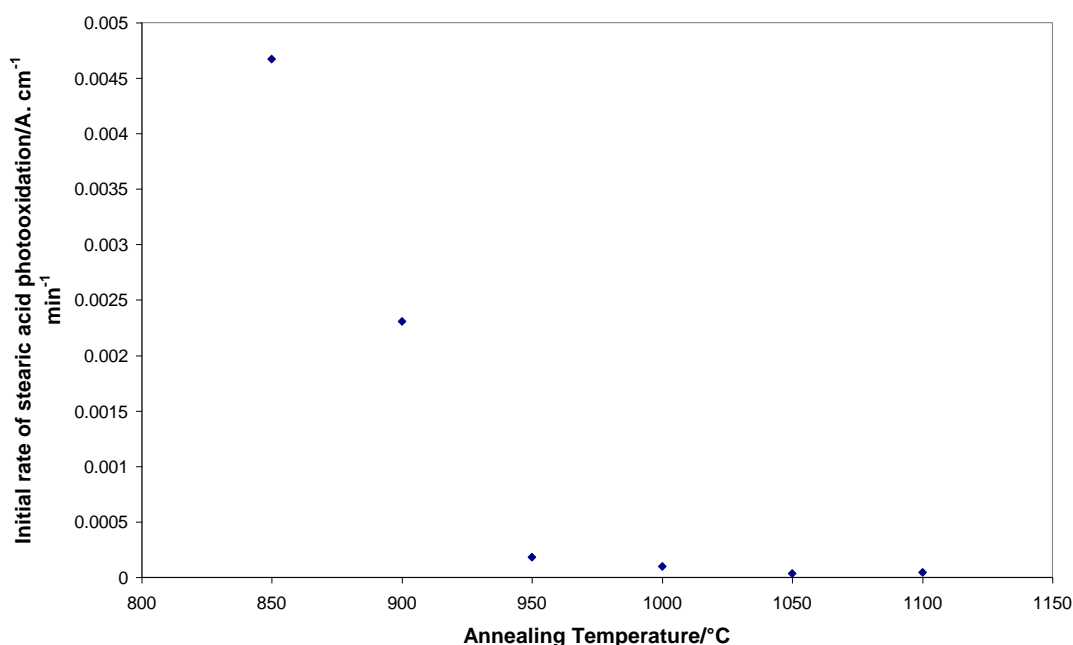


Figure 5.16.: The variation in the initial rate of stearic acid removal with annealing temperature over the range 850-1100 °C

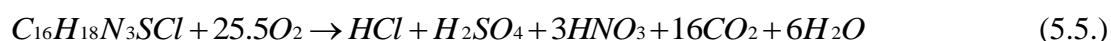
It can be seen that as the temperature increases from 850 to 950 °C, the initial rate of stearic acid removal decreases linearly. Above 950 °C, however, no significant change in the rate of photooxidation is observed. From figure 5.8. previously, we observe that the amount of rutile in the film increases linearly over the range 850-950 °C, and thus it is postulated that its lower photocatalytic activity compared to anatase is responsible for the observed decrease in the photooxidation rate, following on from the results reported

in figure 5.14. Above 950 °C, the films are 100 % rutile in composition, thus no change in the rate of photooxidation is anticipated. Indeed, from figure 5.9. there is also observed to be no further change in the SSA with increasing annealing temperature, and thus our observations in figure 5.16. are to be expected. Interestingly, when no film is present, and hence the stearic acid is subjected to simple UV degradation, the initial rate of removal measured under such conditions is $9.07 \times 10^{-4} \text{ A. cm}^{-1} \text{ min}^{-1}$. Such a rate is greater than the rate of photocatalysis observed on all paste films annealed at temperatures $\geq 950 \text{ }^\circ\text{C}$, implying that the rate of photooxidation we observe is not due to photocatalysis of the organic at all.

5.2.2. The Methylene Blue Test

In addition to stearic acid, the methylene blue (MB) test is a common method for assessing the photocatalytic activity of both photocatalyst films and powders, both laboratory-prepared and commercial. As was described previously, a solution of the dye is placed in contact with the photocatalyst under test and the setup irradiated with UVA light. For films, an aliquot of the solution can simply be extracted at regular intervals and its absorbance measured directly using spectrophotometry.

Figure 5.17. shows the initial spectrum obtained when a 10^{-5} M solution of MB is placed in contact with a 450 °C paste film and left for 15 minutes. Previous work by Xu et al has shown that for powders produced by a sol-gel method, a 10 minute period is required for all of the dye to have been adsorbed on to the surface of the powder³¹, thus saturating all the active sites available for the photocatalytic reaction. As the solution/film combination is then irradiated, the change in the UV/Visible absorbance spectra due to the photomineralisation of the dye is as shown in figure 5.17. Whereas previously in the work on the indicator inks we saw a similar change in spectral profile due to reduction of MB by the photogenerated electrons, the change in MB spectral shape observed here is due to photomineralisation of the dye, i.e. the photogenerated holes are involved directly in the removal of the MB, according to equation 5.5.



In addition, based on the data obtained at λ_{\max} for the dye, by plotting $\ln(\Delta Abs)$ vs. time, in accordance with the first order rate equation, we observe a strong linear fit over a period greater than 2 half-lives, as shown inset in figure 5.17.

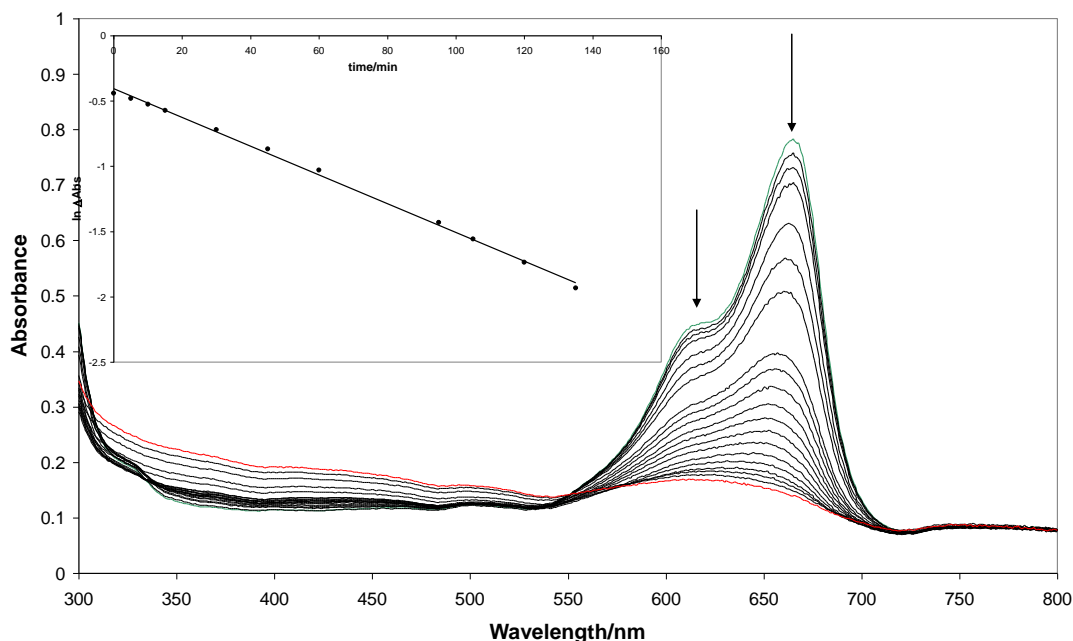


Figure 5.17.: The change in the spectral shape due to MB as the dye is photomineralised when placed in contact with a 450 °C paste film. The green trace shows the initial MB solution spectrum obtained after being placed in contact with the paste film for 15 minutes, whilst the red trace shows the spectrum due to the dye after 270 minutes of UVA irradiation. Spectra were recorded every 5 minutes for 15 minutes, every 15 minutes up to an hour, at 95 and 105 minutes, and then every 15 minutes until completion

Using the first order kinetic model, the $t_{50\%}$ for MB mineralisation by a paste film annealed at 450 °C is calculated to be 51 minutes. In this work, the initial rate was used for assessing the initial rate of photomineralisation, or k_1 , the first-order reaction rate constant, which is calculated using equation 5.6.;

$$k_1 = \frac{r_i}{\Delta Abs} \quad (5.6.)$$

where r_i is the initial rate of photomineralisation and ΔAbs represents the total change in absorbance due to photomineralisation at 665 nm (i.e. λ_{max}). Three kinetic runs were conducted per paste film and an average value of r_i and, where appropriate, k_1 could be calculated for each film. Figure 5.18. shows the variation in the average r_i with annealing temperature up to 1100 °C.

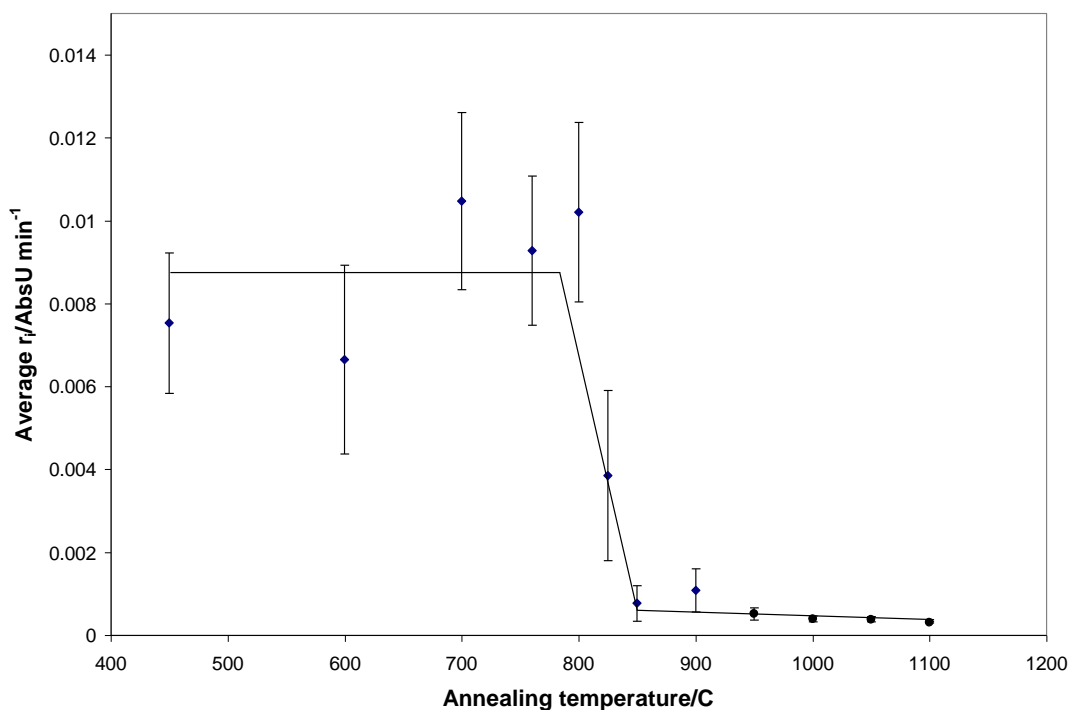


Figure 5.18.: The variation in the initial rate of photomineralisation of MB with increasing film annealing temperature

As would be anticipated from the results obtained with the stearic acid test, the kinetics of MB oxidation exhibit similar trends in the data presented in figure 5.18., despite slight differences noted in the ΔAbs values obtained at different annealing temperatures. Similar to what was observed with the stearic acid test, for MB photomineralisation there appears to be no significant change in the activity of the film over the range 450-800 °C. Above this temperature, however, and again coinciding with the continuing emergence of rutile, the rate of photomineralisation is observed to decrease at 825 °C,

and reduce further still moving to 850 °C. It would appear once again that despite the changes in SSA and average particle size starting to occur at 800 °C, the reaction rate is only adversely affected as the rutile concentration increases beyond ca. 20 % of the film's phase, i.e. the anatase:rutile ratio has a greater effect on the observed kinetics than the variation in the SSA.

Work by Mills and McFarlane³² observed that the initial rate of photomineralisation of MB in the presence of Activ™ was 9×10^{-4} AbsU min⁻¹ using a similar system, which is similar to what we observe here for a paste film annealed at 850 - 900 °C. This suggests that the films annealed above such temperatures exhibit less photocatalytic activity than that observed in the commercial self-cleaning glass, despite their greater thickness.

5.3. The Indicator Ink Test

The final test used to assess the photocatalytic activity of the paste films was based on an indicator ink. As has already been observed using both the methylene blue and stearic acid tests, the paste films produced in this work (typically 1 µm thickness) are much more photocatalytically active than self-cleaning glass films (typically 15 nm thickness) when annealed at low temperatures (i.e. below 825 °C). As a result, it is not possible to use any of the indicator inks described previously in chapters 3 and 4 here, owing to their reduction kinetics being postulated to be too rapid.

5.3.1. The Patent Blue VF Indicator Ink

A new indicator ink was developed for use in the analysis of the photocatalytic activity of low temperature (450-800 °C) paste films based on the dye Patent Blue VF (also known as Acid Blue 1, herein referred to as PB). The structure of the dye and its reduction mechanism is shown in figure 5.19. Patent blue VF is a triphenylmethane dye which has previously been used in, amongst other things, LCDs, inks and detergents³³. Work by Saquib et al has also made use of the dye in a photomineralisation capacity, its degradation kinetics observed as a function of different commercial TiO₂ photocatalyst powders³⁴. The redox potential of the structurally similar dye Patent Blue V is quoted

in one article to be + 750 mV³⁵, ca. 100 times more electropositive than that of MB, implying that PB should be easier to reduce and hence more difficult to re-oxidise. However, as we shall see below, the results observed here would appear to contradict such a redox potential, and thus no formal redox potential is quoted here.

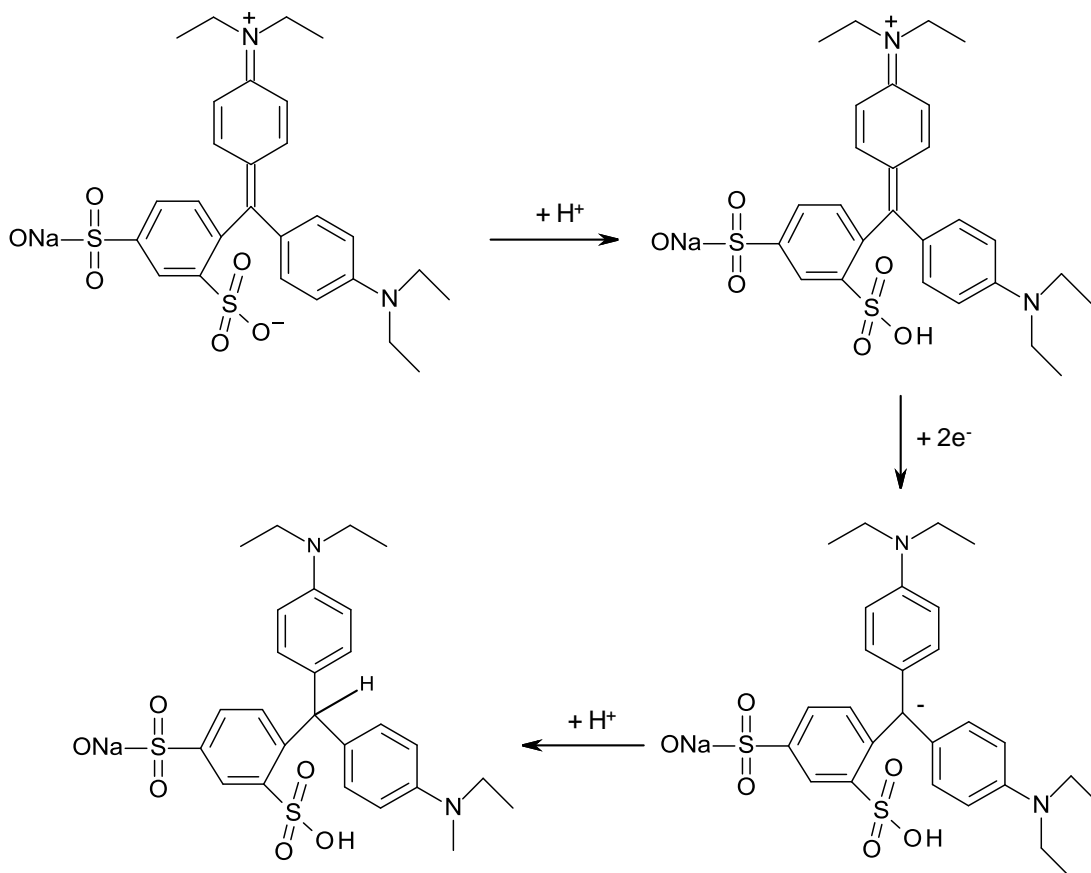


Figure 5.19.: The structure of patent blue VF and its reduction mechanism

The formulation used to produce the indicator ink differed slightly from that used previously to compensate for the increased photocatalytic activity of the underlying substrate(s), the level of glycerol present reduced from 300 mg to 50 mg. Such a move should, theoretically, promote an increase in the rate of electron-hole recombination, since a reduction in the glycerol level reduces the number of available hole scavengers in the formulation, making less electrons available for photoreduction.

The ink was applied to the paste films using a similar method as that outlined previously in chapter 2 for application to Activ™ (i.e. spun-coated at 500 rpm for 15 s then dried in an oven for 10 minutes at 70 °C). Since the low temperature films are reasonably transparent, it is possible to monitor the reduction of the dye using UV-Visible spectroscopy. The initial PB ink spectrum on a 450 °C paste film is shown in figure 5.20., with the subsequent change in spectral shape with increasing UV irradiation time (UV irradiance = 1 mW cm⁻²) indicated.

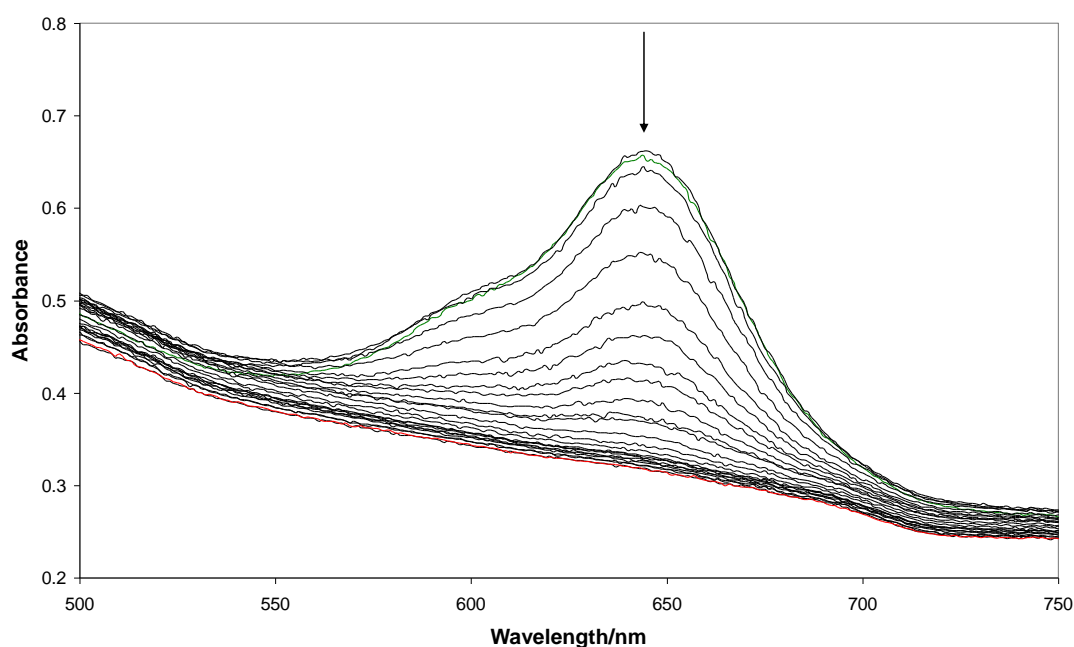


Figure 5.20.: The absorbance spectrum of the PB ink cast on a 450 °C paste film, and the change in spectral shape due to irradiation with UVA light. The green trace indicates the initial ink spectrum whilst the red trace shows the ink spectrum following irradiation. Spectra were recorded every 30 s for 5 minutes, and then every 1 minute up to 18 minutes

As we observed previously for the DCIP, MB and Rf inks, as the PB ink is irradiated on the surface of the paste film, its reduction is indicated by the collapse of the peak ($\lambda_{\text{max}} = 644 \text{ nm}$) due to the dye with increasing irradiation time. The reduction reaction occurs over an 18 minute time period, which would appear relatively slow in comparison to the inks used earlier for Activ™. However, it must be remembered that

the level of glycerol present in the formulation is 6 times less whilst the irradiance used is also much lower than that used under ambient atmospheric conditions; hence there is scope for the reduction rate to be increased.

A zero order kinetic model is adopted for the PB ink since it has been previously demonstrated in chapters 3 and 4, and has been reported by others in this group³⁶, that the inks based on Rz, DCIP and MB obey such a model. This was attributed to all available reactive sites on the film surface being occupied by a dye molecule, with sufficient layers of dye ready to enter the vacancy created following reduction. Using the plot of absorbance at λ_{max} vs. time in figure 5.21., the average $t_{50\%}$ for the process is calculated to be 144 s, whilst the average zero order rate constant, k_0 , is $1.187 \times 10^{-3} \text{ s}^{-1}$.

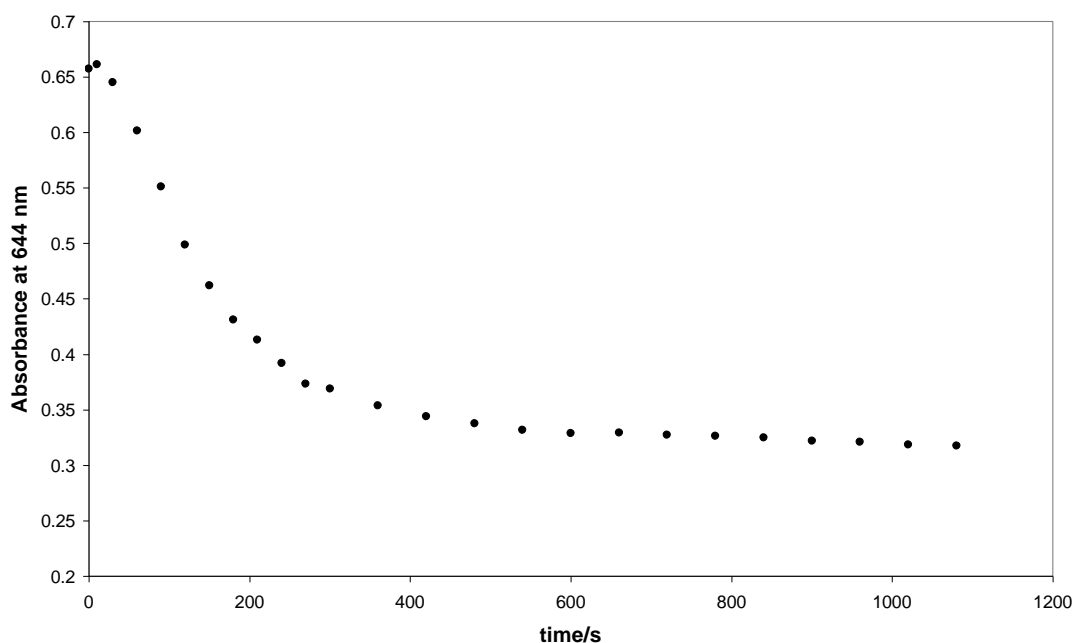


Figure 5.21.: The variation in the absorbance at λ_{max} for the PB ink with irradiation time on a 450 °C paste film

Similar tests were conducted on all paste films up to a maximum annealing temperature of 800 °C. Beyond this annealing temperature, it was not possible to use UV-Visible spectroscopy as a means of monitoring the dye reduction reaction owing to incident

light scattering by the underlying film. The variation in the inverse zero order $t_{50\%}$, which is a measure of k_0 , with annealing temperature is shown in figure 5.22.

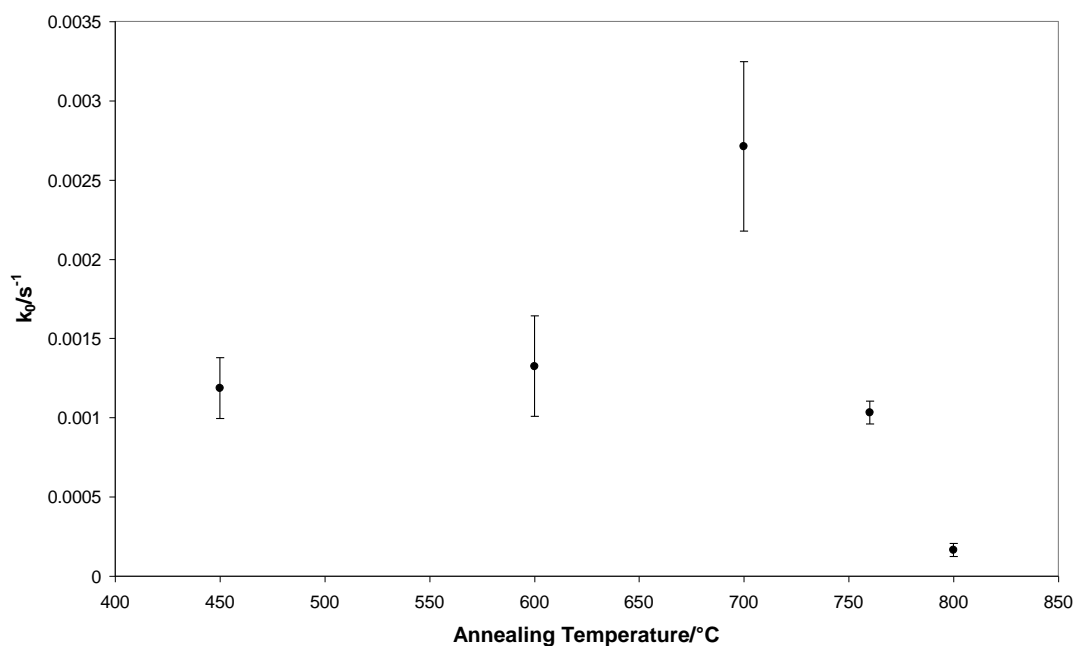


Figure 5.22.: The variation in the average zero order rate constant, k_0 , with annealing temperature for PB reduction

Whereas previously for both the MB and stearic acid tests we observed a sharp reduction in the reaction rate moving from 800 to 825 °C, for the PB indicator ink the most severe change occurs on increasing the annealing temperature from 760 to 800 °C. Indeed, over this 40 °C temperature range, the zero order rate constant is observed to decrease ca. 10-fold. Based on the results reported in figures 5.8. and 5.9., it would appear that the emergence of rutile in the film and/or the reduction in the SSA are responsible for this decrease in reduction rate. Clearly, however, the sensitivity to such changes is greater for the ink reduction test than for both the photomineralisation of MB and the photooxidation of stearic acid.

5.3.2. The DCIP Indicator Ink

As was noted previously, above 800 °C it was not possible to monitor PB reduction using UV-Visible spectroscopy since the underlying paste films annealed above this temperature are too opaque, and thus scatter too much of the incident light. As a result, the peak due to the dye cannot be observed. The films are also very inactive, and hence a more sensitive photocatalyst ink is required. The DCIP indicator ink discussed previously in chapters 3 and 4 is one possible solution. However, owing to the opacity of the films at high temperatures, the photoreduction reaction has to be monitored using diffuse reflectance spectroscopy. As was mentioned previously in section 2.1.4., diffuse reflectance spectroscopy measures the amount of light reflected by a sample, R . The results generated for each sample are referenced to a sintered PTFE standard and then analysed using the Kubelka-Munk equation, i.e. equation 5.7.

$$f(R) = \frac{(1-R)^2}{2R} = \frac{k}{s} \quad (5.7.)$$

where k is the molar absorption coefficient and s the scattering coefficient. According to Julson and Ollis³⁷, for samples which are of low concentration on supports or in media of low absorption in the UV-Vis region, k varies linearly with concentration, i.e.

$$k = 2.303\alpha c \quad (5.8.)$$

where α is the molar absorptivity, providing a link between reflectance spectroscopy and UV-Vis absorbance spectroscopy. Figure 5.23. shows the diffuse reflectance results obtained for the DCIP ink cast on the paste film annealed at 1000 °C.

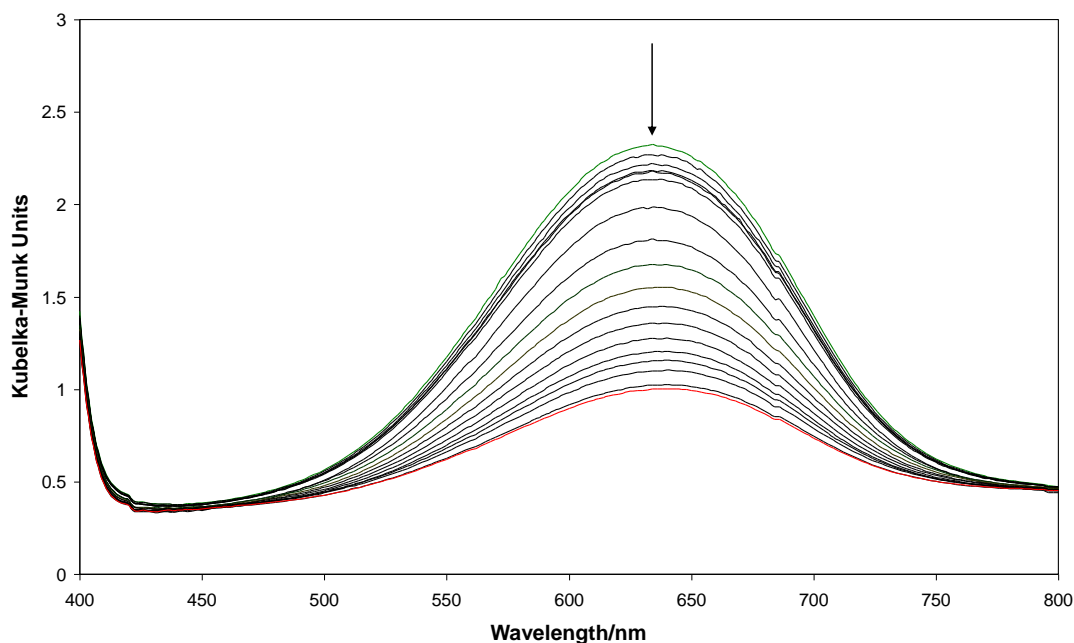


Figure 5.23.: The diffuse reflectance spectrum of a DCIP ink cast on a 1000 °C paste film, and the subsequent spectral changes which occur upon UVA irradiation. The green trace indicates the initial spectrum of the ink whilst the red trace shows that obtained after reduction has ceased. Spectra were recorded at 1 minute intervals for 5 minutes, at 10 minutes, and finally at 10 minute intervals up to 2 hours

As would be anticipated from the discussion above, the diffuse reflectance spectrum of the ink when analysed using the Kubelka-Munk function is indicative of the UV-Visible spectrum that would be observed. Upon irradiation, the spectrum of the dye changes as indicated in figure 5.23.

Similar traces to that observed in figure 5.23. were generated up to and inclusive of the paste film annealed at 1100 °C and figure 5.24. shows how the calculated zero order rate constant, k_0 , varies across the temperature range 800-900 °C, whilst figure 5.25. shows the variation in k_0 , based on initial rate data, for the films annealed at temperatures ≥ 1000 °C.

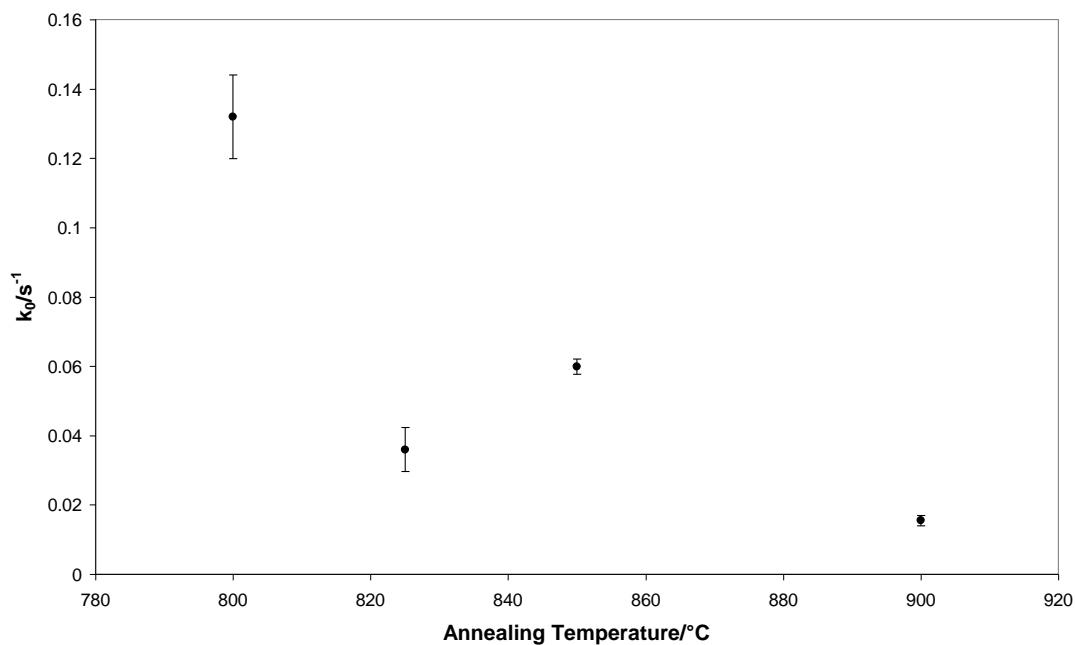


Figure 5.24.: The variation in the average k_0 for DCIP reduction on paste films over the temperature range 800-900 °C

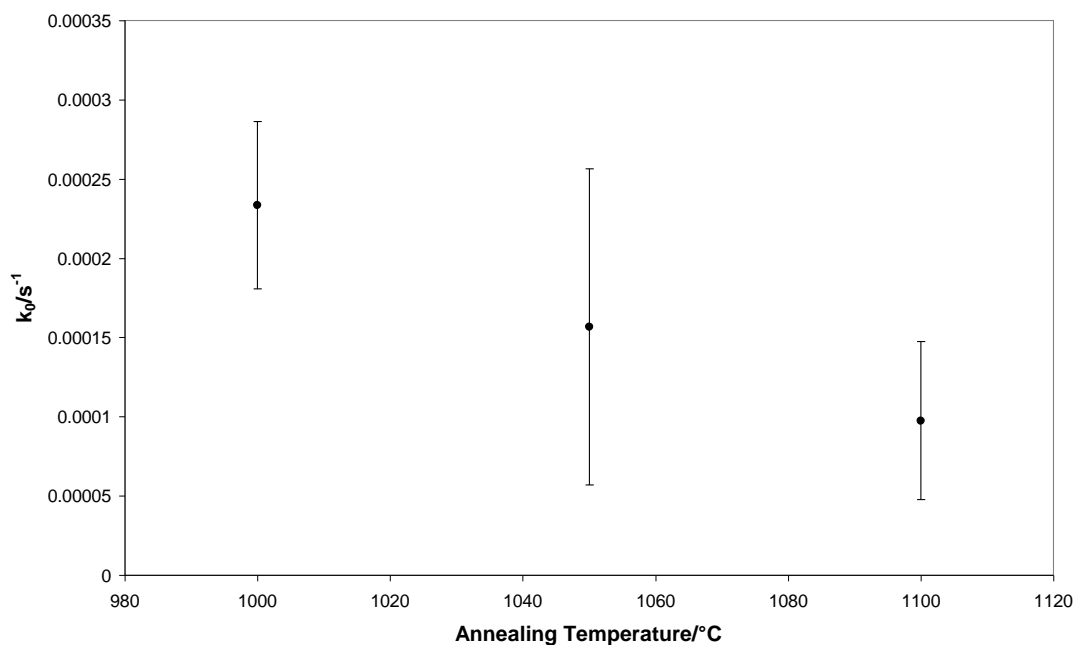


Figure 5.25.: The variation in the average k_0 for DCIP reduction on paste films over the temperature range 1000-1100 °C

As anticipated, a decrease in the value of k_0 is observed, concurring with what we have observed previously for the MB and stearic acid tests that as the annealing temperature increases, the photocatalytic activity decreases. Again, the emergence of rutile as the dominant TiO₂ phase and the drop in the SSA are believed to be responsible for such behaviour. Figure 5.26. plots the change in the average value of k_0 obtained over the annealing temperature range 800-1100 °C for DCIP reduction, utilising the estimated k_0 value for films annealed above 900 °C.

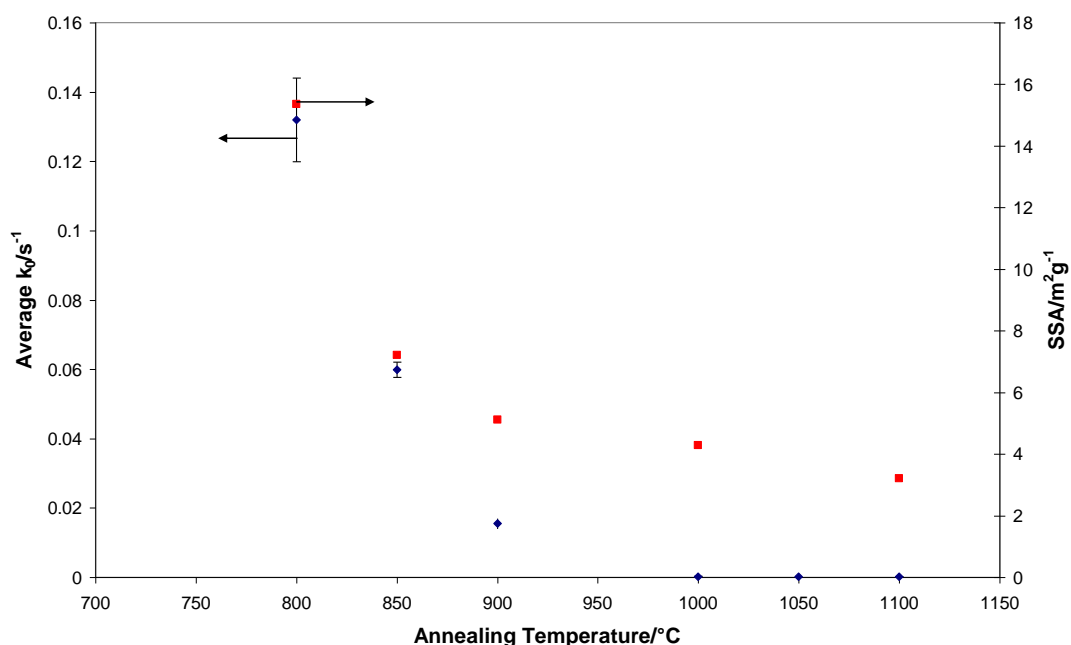


Figure 5.26.: The variation in both the zero order rate constant, k_0 , for DCIP reduction and the SSA with increasing annealing temperature over the range 800-1100 °C

The full extent of the decrease in photocatalytic activity for such samples is now apparent, further corroborated by the data tabulated in table 5.2. By increasing the film annealing temperature from 800 to 1000 °C, the photocatalytic activity drops by a factor of ca. 1000 times. Indeed for the samples annealed at $T > 1000$ °C, it is difficult to ascertain whether photocatalysis is actually occurring or if the changes observed in the DCIP spectrum are indicative of photofading or evaporation of the ink film due to heat

from the lamp. Figure 5.26. also plots the variation in the SSA over the same annealing temperature range. Interestingly, the curve fit of both the DCIP and SSA data are remarkably similar, which would imply that the changes in photocatalytic activity we observe here are indeed related to the SSA of the underlying film.

Annealing Temperature/°C	Zero order rate constant, k_0/s^{-1}
800	0.132
1000	2.33×10^{-4}
1100	2.39×10^{-4}
Blank Hydrotect Tile	4.75×10^{-4}
Indoor Hydrotect Tile	1.57×10^{-3}
Outdoor Hydrotect Tile	7.32×10^{-4}
Standard Bathroom Tile	6.41×10^{-4}

Table 5.2.: The variation in the zero order rate constant for various paste films and commercial tile samples, both photocatalytically active and inactive

Also detailed in table 5.2. are the results obtained for a series of self-cleaning tiles referred to as Hydrotect™ (supplied by Deutsche Steinzeug) and for an ordinary bathroom tile. That referred to as a blank Hydrotect tile is essentially a tile with no added photocatalyst, and thus we would anticipate a similar rate of DCIP reduction to that observed for the standard bathroom tile. The outdoor Hydrotect tile is observed to exhibit a ca. 2-fold increase in the photocatalytic activity compared to its blank counterpart, suggesting that the amount of photocatalyst present is low. Such a tile is observed to be ca. 3x more photocatalytically active than a paste film annealed at 1000 °C. Previously we have suggested that such paste films may be photocatalytically inactive, and that any reduction in the level of MB/stearic acid present, or indeed the reflectance due to DCIP is due to photofading by the intense UVA source.

Of all the tiles tested and detailed in table 5.2., the indoor Hydrotect tile is observed to be the most photocatalytically active. In comparison, its activity is noted to be ca. 10x that obtained with a paste film annealed at 1000 °C, but only 3 times more than that

observed with a blank (i.e. nil photocatalyst) Hydrotect™ tile. Clearly such tiles are of poor activity, with complete reduction of the DCIP ink not observed in a 2 hour irradiation period. However, such indoor and outdoor Hydrotect™ tiles are still marketed as being photocatalytically active despite these findings. Indeed, the only reasonable conclusions which can be drawn from the data presented above is that the paste films annealed at $T \geq 1000$ °C would appear to be photocatalytically inactive in comparison.

5.4. Correlation of Standard Tests

The ultimate aim of this chapter is to assess whether the three methods of measuring the photocatalytic activity outlined above, namely the stearic acid, MB and PB/DCIP indicator ink tests, can be correlated with each other, generating a set of standard tests which researchers could utilise to assess the activity of laboratory-prepared and commercial samples rapidly. Such tests could then be proposed to ISO as being suitable for standardisation purposes.

5.4.1. Low Temperature, ‘High Activity’ Paste Films (450 – 850 °C)

It is necessary to divide the standardisation tests according to the paste films used in this study. Since the PB ink was only used on paste films annealed over the temperature range 450-800 °C, such films must be treated separately. However, since data could be recorded for the MB and stearic acid tests up to and inclusive of 850 °C (i.e. reactions could be run to completion over an appreciable timescale), both the 825 and 850 °C samples are included here in the ‘high activity’ category. Figure 5.27. plots the correlation observed between the MB and stearic acid photomineralisation tests according to their calculated zero and first order rate constants respectively.

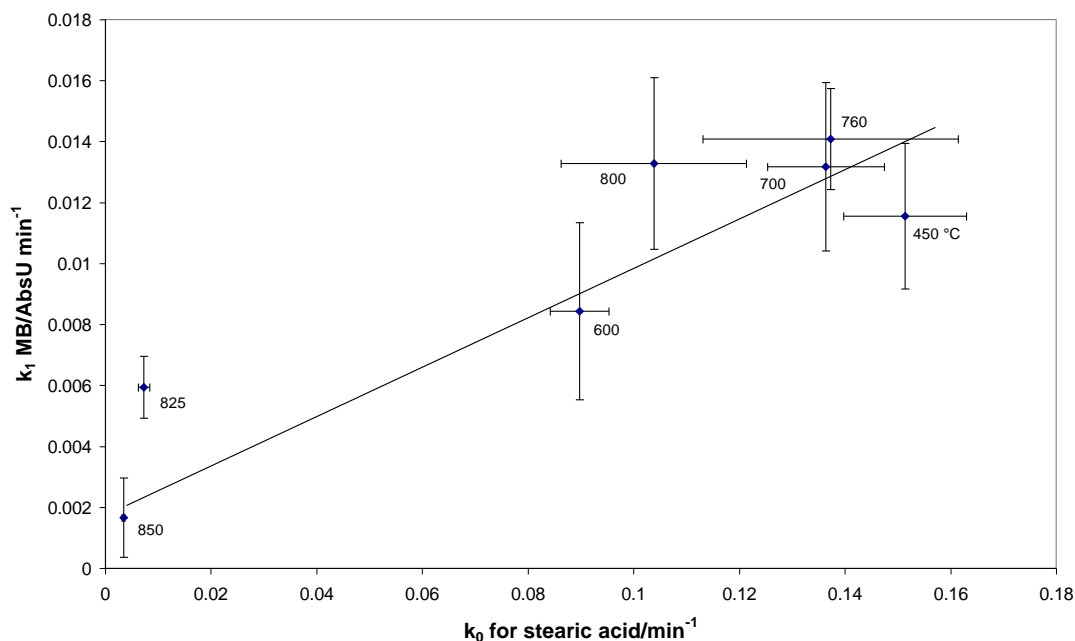


Figure 5.27.: The correlation in the rate of photomineralisation of stearic acid and MB over the temperature range 450-850 °C

In contrast, figure 5.28. shows the comparison between the rate of photoreduction of the PB ink film and the rate of photooxidation of the stearic acid film. It can be immediately seen that for this latter plot, no strong correlation exists, the data appearing randomly distributed over the range shown. Similar results were obtained if the rate of PB photoreduction was compared to the rate of methylene blue photomineralisation over a similar range. Such results were anticipated based on the data generated in figure 5.22. which showed the PB reduction test to be more sensitive to the emergence of rutile than the other tests conducted previously.

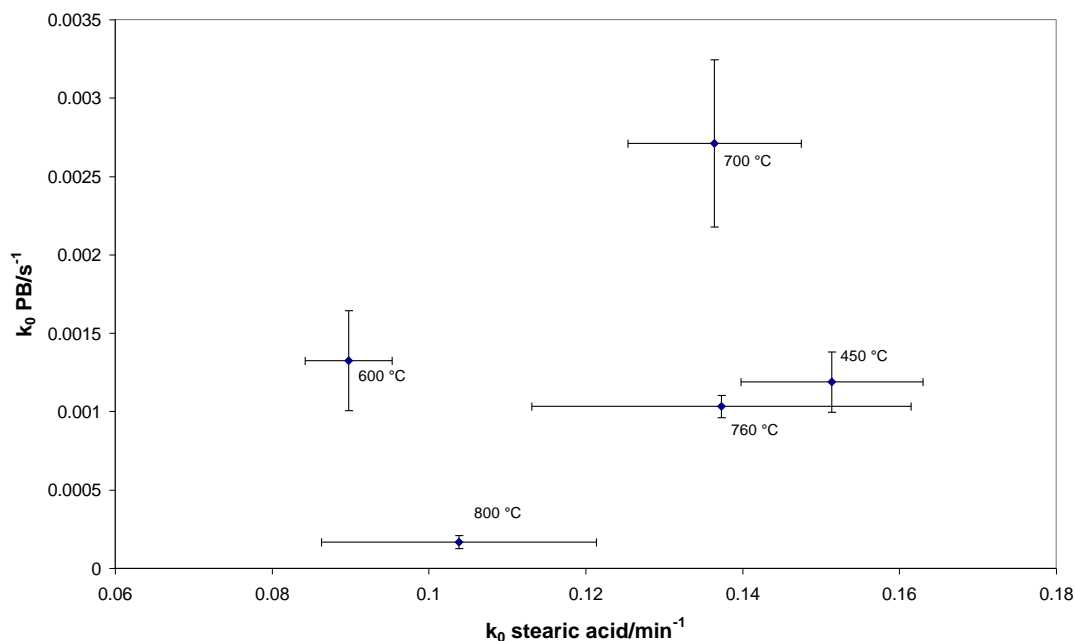


Figure 5.28.: The correlation between the rate of photomineralisation of stearic acid and photoreduction of PB on paste films annealed over the range 450-800 °C

5.4.2. High Temperature, 'Low Activity' Paste Films (800 – 1100 °C)

Whilst there was no marked correlation observed between the ink test and both the stearic acid and methylene blue tests over the temperature range 450-850 °C, we would expect some trends to emerge as the temperature is increased above 800 °C, as it is mainly above this temperature that we begin to observe significant changes in the rate of photomineralisation and photoreduction more substantially. As was alluded to previously, it is necessary to use the data generated from the DCIP ink tests as the indicator ink for standardisation, since the PB ink is too slow to reduce on such low activity films. It must also be noted that owing to the low activity of the paste films, the data used to generate the correlations does not represent complete photomineralisation or photoreduction. Such data is estimated based on the performance of the systems over reasonable time periods; however, owing to the zero order nature of the photomineralisation of stearic acid and the photoreduction of PB, this initial rate is

essentially a measure of the reaction rate constant. For clarity, it is still referred to as the initial rate in both systems.

Figure 5.29. shows the correlation observed between the initial rate of photomineralisation of stearic acid and MB as a log-log plot. Over the temperature range 800-1100 °C, the plot is linear. Using the equation for a straight line, we can therefore infer that $\log_{10} r_{\text{MB}} = m \cdot \log_{10} r_{\text{SA}} + c$, where m is the gradient of the line and c is the y-axis intercept. However, using the equations for logarithms, in order to achieve such a relationship, the two variables must be related by the equation $r_{\text{MB}} = c \cdot r_{\text{SA}}^m$.

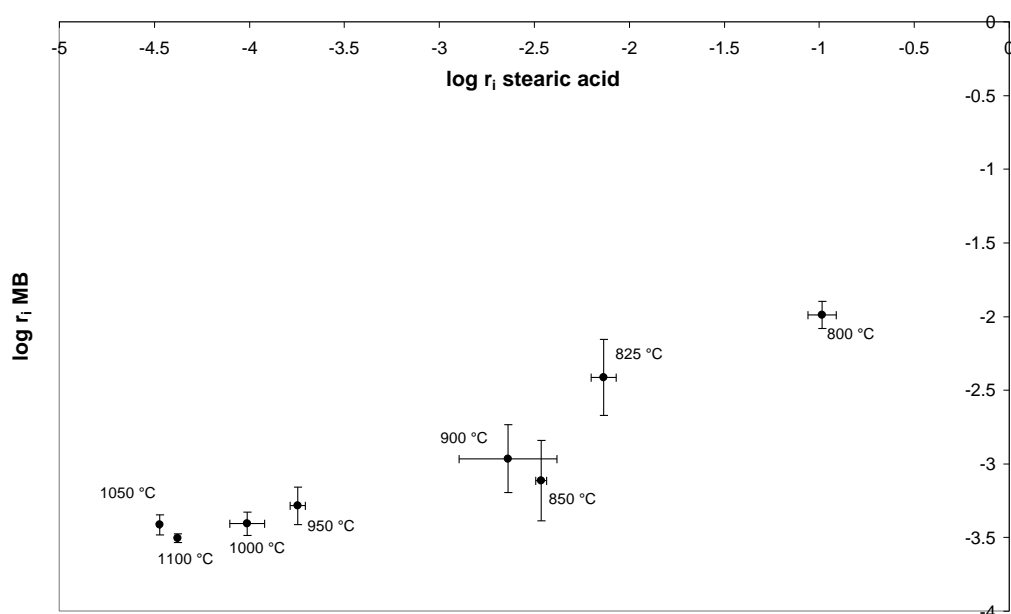


Figure 5.29.: The correlation in the rate of photomineralisation of stearic acid and MB over the temperature range 800-1100 °C

Figures 5.30. and 5.31. compare the rates of photomineralisation of both stearic acid and MB with the rate of photoreduction of the DCIP indicator ink over a similar temperature range. Whereas above in figure 5.29. the linear correlation in the log-log plot is easily observed between the stearic acid and MB tests, both of the figures below show a greater deviation, particularly for the films annealed at 850 °C in figure 5.30., and 850

and 900 °C in figure 5.31. However, a linear plot (and hence a relationship of the form $y = ax^b$) is still believed to exist.

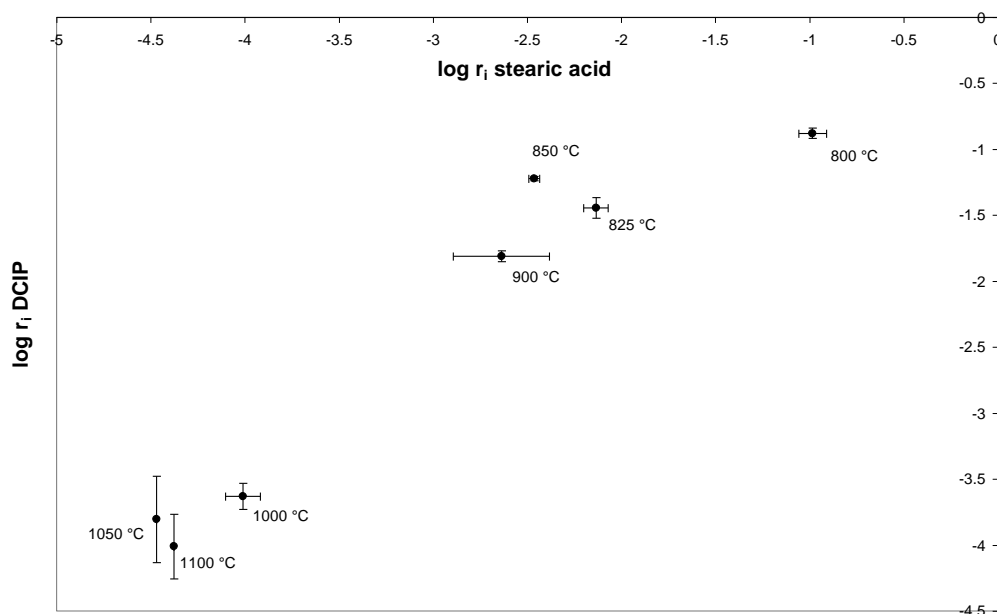


Figure 5.30.: The correlation between the rate of photomineralisation of stearic acid and photoreduction of PB on paste films annealed over the range 800-1100 °C

Table 5.3. details the values of the gradients observed in figures 5.29. – 5.31., since it is this value which ultimately determines the relationship between the tests (i.e. $y = c.x^m$). The values are given from the graphs as observed, whilst a separate column also details the gradients observed when the perceived outlying values at 850 °C are discarded. It can be clearly seen that whilst the R^2 values are poor, in general, they do improve when the data obtained at 850 °C is discarded. The values presented in table 5.3. would seem to suggest that the tests can be correlated to some extent, but that the factor relating such tests, i.e. the gradient, m , varies depending on those test being compared. Of particular interest is the observation that the DCIP and SA tests are linearly correlated (i.e. $m = 1$), which was slightly unexpected since we are comparing photooxidation and photoreduction. However, they are the two tests which are seen to obey a zero order kinetic model, and it may be this which dictates the values observed across all plots.

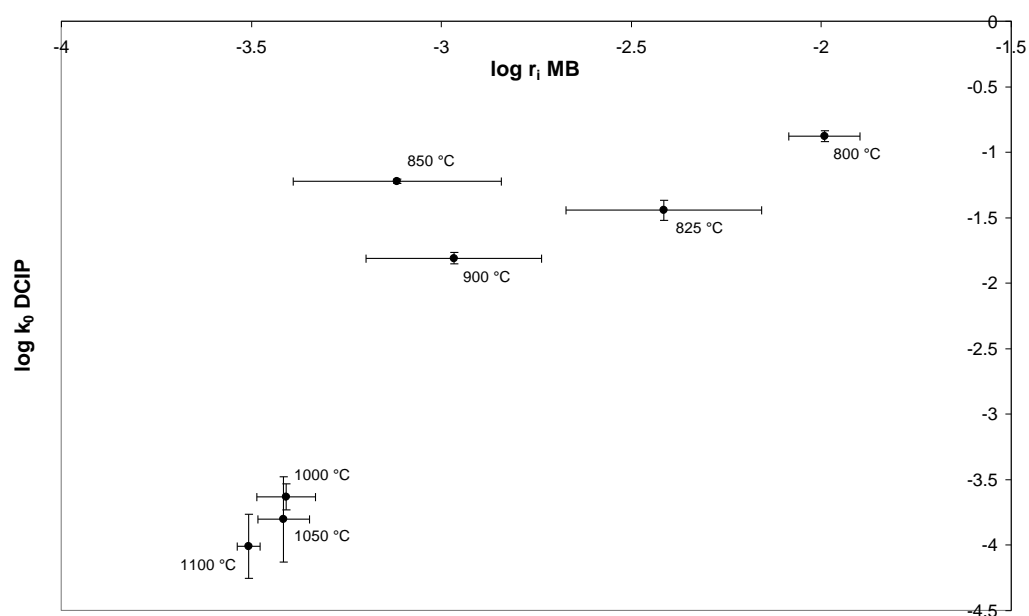


Figure 5.31.: The correlation between the rate of photomineralisation of MB and photoreduction of PB on paste films annealed over the range 800-1100 °C

Figure Number	Calculated Gradient	Adjusted Gradient
5.29. (MB vs. SA)	0.4092 (0.8804)	0.4352 (0.9577)
5.30. (DCIP vs. SA)	0.9956 (0.9257)	0.955 (0.9641)
5.31. (DCIP vs. MB)	1.9728 (0.693)	2.0969 (0.9065)

Table 5.3.: The observed gradients in figures 5.29. – 5.31. The numbers in brackets represent the calculated R^2 values. The second column details the gradients observed if the perceived outlying values for the film annealed at 850 °C are discarded

Such varied findings echo those of Evans et al³⁸, who compared the rate of stearic acid photomineralisation with the rate of photoreduction of the Rz indicator ink described previously. Although the titania films used in such work were created using an atmospheric pressure CVD technique (APCVD), the precursors used to create the film were varied, hence giving rise to films of varying morphology and mean crystallite size.

Although their work on films of varying thickness demonstrates an expected linear response, when new precursors are introduced and compared to films of similar thickness, the trend is less apparent. Interestingly, the authors do not provide further information on characteristics such as SSA or the mean crystallite size for individual samples, although all films are reported to be anatase in nature. It is believed that the added complication of varying such precursors makes the observation of any correlations difficult.

Interestingly, Evans et al³⁸ also correlated the stearic acid and Rz indicator ink tests with the observed change in water contact angle via photoinduced superhydrophilicity (PSH). PSH is a secondary effect exhibited by TiO₂ films whereby the contact angle of a water droplet decreases with increasing UV irradiation. Their findings appear to suggest that the more active a film is, the greater the change in contact angle via PSH, supporting the work of Mills and Crow³⁹ and their theory that PSH is due to oxidation of residual surface organics, thus producing a 'clean' surface. It would be interesting to observe the changes in contact angle for the paste films produced here in order to observe whether a similar trend was apparent.

5.5. Conclusions

By altering the annealing temperature, a range of TiO₂ films of varying morphologies and phase content have been produced using a TiO₂ sol-gel paste. Over the temperature range 450-760 °C, the films appear remarkably similar in composition, the increasing annealing temperature only serving to cause a slight increase in the crystallinity of the anatase phase films. They are noted to be of a relatively similar activity as assessed by three separate tests, namely stearic acid, MB, and an indicator ink based on the dye PB. At annealing temperatures ≥ 800 °C, however, the surface morphology begins to alter, with an apparently linear increase in the average crystallite size and concurrent linear decrease in the calculated SSA up to ca. 1000 °C. In addition to such changes, the higher annealing temperatures permit the emergence of rutile phase TiO₂ through the conversion of existing anatase particles. Such changes in phase alter the photocatalytic

activity of the films. By ca. 1000 °C, the films are completely rutile in nature, with no notable change in the SSA now occurring despite the increasing average crystallite size.

By using three tests of very different properties, the overall aim of having prepared such films was to correlate the rate of photocatalysis observed. Using both the stearic acid (solid:solid interaction) and MB (solid:liquid interaction) tests, similar trends in photocatalytic activity were observed over the temperature range 450-850 °C. Above such temperatures, whilst rates of reaction could still be calculated, the total time for complete mineralisation to occur was observed to increase dramatically, forcing us to rely on initial rates as an indicator of photocatalysis. Both tests suggest that, particularly at temperatures ≥ 1000 °C, the rate of photocatalysis is so slow that it is comparable to what is observed in the absence of an underlying film. Despite this, the tests appear to correlate well over the range 800-1100 °C, where changes in both the phase and surface properties are observed, as evidenced by a log-log plot.

The results obtained using an indicator ink (solid:solid interaction, although reaction involves photoreduction instead of photooxidation, as was the case for the stearic acid and MB tests) differed slightly from those above, with the onset of any change in the rate of photoreduction of PB occurring at 800 °C as opposed to 825 °C. Such a change is concurrent with the emergence of rutile phase TiO₂ and the decrease in the calculated SSA, suggesting a strong dependence on both these factors; for stearic acid and MB, the rate of photocatalysis appears to depend more specifically on the anatase:rutile ratio as opposed to merely the emergence of rutile in the film.

It was also necessary to use two different indicator inks (PB and DCIP), and two different methods of assessment (UV-Visible and diffuse reflectance spectroscopy, respectively) to monitor the photoreduction reaction. Whilst no correlations were observed over the temperature range 450-800 °C using the PB indicator ink, at temperatures ≥ 800 °C it was possible to observe some degree of correlation between the DCIP ink test and MB/SA.

The actual correlation (i.e. the value of m in the equation $y = a \cdot x^m$) using the high temperature films varies depending on the tests being correlated, but even then the R^2 values are no better than ca. 0.96, suggesting some degree of deviation is present. The change in surface morphology and relative phase of the films used in this work is evidently an issue, and requires to be addressed by future researchers prior to touting a single test, let alone a set of such tests, as being a standard for all others to compare and contrast generated results to. However, the initial results shown here are pleasing and could possibly be developed further before any proposals to ISO are made.

5.6. References

- (1) A. Mills; N. Elliott; G. Hill; D. Fallis; J. R. Durrant; R. L. Willis *Photochem. Photobiol. Sci.* **2003**, *2*, 591.
- (2) A. Mills; G. Hill; M. Crow; S. Hodgen *Journal of Applied Electrochemistry* **2005**, *35*, 641.
- (3) J. Yu; J. C. Yu; M. K.-P. Leung; W. Ho; B. Cheng; X. Zhao; J. Zhao *Journal of Catalysis* **2003**, *217*, 69.
- (4) K. Y. Jung; S. B. Park; S.-K. Ihm *Applied Catalysis A: General* **2002**, *224*, 229.
- (5) K. Baba; R. Hatada *Surface and Coatings Technology* **2001**, *136*, 241.
- (6) V. Puddu; H. Choi; D. D. Dionysiou; G. L. Puma *Applied Catalysis B: Environmental* **2010**, *94*, 211.
- (7) Y. Chen; D. D. Dionysiou *Journal of Molecular Catalysis A: Chemical* **2006**, *244*, 73.
- (8) S. Bakardjieva; J. Šubrt; V. Štengl; M. J. Dianez; M. J. Sayagues *Applied Catalysis B: Environmental* **2005**, *58*, 193.
- (9) D. Reyes-Coronado; G. Rodriguez-Gattorno; M. E. Espinosa-Pesqueira; C. Cab; R. d. Coss; G. Oskam *Nanotechnology* **2008**, *19*, 1.
- (10) JCPDS Powder Diffraction File, Card No. 21-1272 Swarthmore, PA
- (11) K. V. Baiju; S. Shukla; K. S. Sandhya; J. James; K. G. K. Warriar *J. Phys. Chem. C* **2007**, *111*, 7612.
- (12) JCPDS Powder Diffraction File, Card No. 21-1276 Swarthmore, PA

-
- (13) P. Górska; A. Zaleska; E. Kowalska; T. Klimczuk; J. W. Sobczak; E. Skwarek; W. Janusz; J. Hupka *Applied Catalysis B: Environmental* **2008**, *84*, 440.
- (14) D. H. Kim; M. A. Anderson; W. A. Zeltner *Journal of Environmental Engineering* **1995**, 590.
- (15) R. A. Spurr; H. Myers *Analytical Chemistry* **1957**, *29*, 760.
- (16) G. Colón; M. C. Hidalgo; J. A. Navío *Applied Catalysis A: General* **2002**, *231*, 185.
- (17) N. R. C. F. Machado; V. S. Santana *Catalysis Today* **2005**, *107-108*, 595.
- (18) T. Ohno; K. Tokieda; S. Higashida; M. Matsumura *Applied Catalysis A: General* **2003**, *244*, 383.
- (19) Y. Tanaka; M. Suganuma *Journal of Sol-Gel Science and Technology* **2001**, *22*, 83.
- (20) S.-J. Tsai; S. Cheng *Catalysis Today* **1997**, *33*, 227.
- (21) H. Wang; Z. Wu; Y. Liu *Journal of Hazardous Materials* **2009**, *164*, 600.
- (22) R. Fretwell; P. Douglas *Journal of Photochemistry and Photobiology A: Chemistry* **2001**, *143*, 229.
- (23) T. Minabe; D. A. Tryk; P. Sawunyama; Y. Kikuchi; K. Hashimoto; A. Fujishima *Journal of Photochemistry and Photobiology A: Chemistry* **2000**, *137*, 53.
- (24) P. Sawunyama; L. Jiang; A. Fujishima; K. Hashimoto *J. Phys. Chem. B* **1997**, *101*, 11000.
- (25) L. Peruchon; E. Puzenat; A. Girard-Egrot; L. Blum; J. M. Herrmann; C. Guillard *Journal of Photochemistry and Photobiology A: Chemistry* **2008**, *197*, 170.
- (26) A. Mills; N. Elliott; I. P. Parkin; S. A. O'Neill; R. J. Clark *Journal of Photochemistry and Photobiology A: Chemistry* **2002**, *151*, 171.
- (27) A. Mills; A. Lepre; N. Elliott; S. Bhopal; I. P. Parkin; S. A. O'Neill *Journal of Photochemistry and Photobiology A: Chemistry* **2003**, *160*, 213.
- (28) G. Colón; M. C. Hidalgo; J. A. Navío *Journal of Photochemistry and Photobiology A: Chemistry* **2001**, *138*, 79.
- (29) L. Jing; S. Li; S. Song; L. Xue; H. Fu *Solar Energy Materials and Solar Cells* **2008**, *92*, 1030.
- (30) D. C. Hurum; A. G. Agrios; S. E. Crist; K. A. Gray; T. Rajh; M. C. Thurnauer *Journal of Electron Spectroscopy and Related Phenomena* **2006**, *150*, 155.

- (31) N. Xu; Z. Shi; Y. Fan; J. Dong; J. Shi; M. Z.-C. Hu *Ind. Eng. Chem. Res.* **1999**, *38*, 373.
- (32) A. Mills; M. McFarlane *Catalysis Today* **2007**, *129*, 22.
- (33) R. W. Sabnis *Handbook of Acid-Base Indicators*; CRC Press, 2008.
- (34) M. Saquib; M. A. Tariq; M. Faisal; M. Muneer *Desalination* **2008**, *219*, 301.
- (35) J. H. Yoe; G. R. B. Jr. *Ind. Eng. Chem. Res. Anal. Ed.* **1939**, *11*, 492.
- (36) A. Cusick The Kinetics of Dye Photocatalysis Univeristy of Strathclyde, Glasgow 2009.
- (37) A. J. Julson; D. F. Ollis *Applied Catalysis B: Environmental* **2006**, *65*, 315.
- (38) P. Evans; S. Mantke; A. Mills; A. Robinson; D. W. Sheel *Journal of Photochemistry and Photobiology A: Chemistry* **2007**, *188*, 387.
- (39) A. Mills; M. Crow *International Journal of Photoenergy* **2008**, *2008*, 1.

6 Acidic Photocatalyst Indicator Inks and Reversible Redox Dyes

As discussed previously in chapter 4, of the four inks tested for their suitability in the indicator ink formulation under anaerobic conditions, the ink based on MB is one of the fastest. Indeed, only the Rz ink is comparable in terms of rate of reduction under such conditions. Whilst the Rz ink is unsuitable for use in the field simply owing to its colour change, however, the MB ink suffers from a more serious problem; namely that reduction does not occur under ambient atmospheric conditions, owing to the high O₂-sensitivity of the reduced product of MB, leuco-MB¹. Despite this, the ink would still appear to be the most attractive option to use under anaerobic conditions, since a colourless leuco- product is generated; Rz, on the other hand, generates a pink, intermediate product (Rf) before reducing further to colourless dihydro-Rf.

Recent work by Mills et al² has demonstrated that if the standard MB ink described previously in chapter 4 is acidified, the ink reduction kinetics are observed to be faster than that of both the standard DCIP and Rz inks. More importantly, the rate of recovery of such an acidified ink is slowed significantly under ambient atmospheric conditions compared to what is observed for the standard ink. It is postulated that by lowering the pH of the ink to ca. pH 2, the overall driving force for the re-oxidation of LMB back to MB by atmospheric O₂ is smaller than at pH 5.2., the standard MB ink pH². Such a change in redox behaviour is not unusual for dyes since many exhibit a variation in their formal redox potential with pH. Quantitatively, the t_{50 %} for this acidic MB ink is quoted as 17 s, whilst that reported for the standard Rz and DCIP inks is 132 and 56 s respectively². Whilst such results for Rz and DCIP differ with what has been quoted previously here in chapter 4, probably due to the batch of Activ™ used, the main focal point of the results generated by Mills et al is that the acidic MB ink reduces ca. 3 times faster than its nearest rival².

The aim of the work described in this chapter is to confirm the reported observations made about the acidic MB ink and then compare it to the performance of other acid-based inks. Such inks will contain dyes from the oxazine, thiazine and phenazine

families which, if encapsulated in the standard indicator ink formulation as used in chapters 3 and 4, would be anticipated to be unsuitable according to their standard redox potentials. Whilst the acidification of such inks may permit reduction of the dye to occur, possibly of greater interest is the recovery kinetics observed, since these also dictate the suitability of such inks for use in the field.

6.1. Dye Families and the Dyes Used

The dyes used in this work derive from three dye families, namely;

- Thiazines (Methylene Blue (MB), Toluidine Blue (TB) and Thionine (Th));
- Phenazines (Neutral Red (NR) and Safranin O (SO)), and;
- Oxazines (Brilliant Cresyl Blue (BCB) and Nile Blue (NB))

The structures of the dyes listed above and their postulated reduced products, along with their standard redox potentials, are given in table 6.1. Whilst we have previously detailed the performance of MB in a non-acidic formulation in chapter 4, the other dyes examined here are novel indicator ink components. In all instances, the dyes were assessed in a non-acidic formulation initially, although the majority of the data generated is not shown here.

Of the other thiazines tested for their suitability in both indicator ink formulations, namely TB and Th, both are observed to have a slightly more positive redox potential than MB, implying that such dyes should be easier to reduce in comparison. Conversely, the reduced forms of such dyes should be more difficult to re-oxidise than leuco-MB. From table 6.1., both phenazines to be tested have relatively large, negative redox potentials, and so it would be anticipated that these would be much more difficult to reduce than any of the other dyes in the non-acidic formulation, whilst their reduced forms will be more O₂-sensitive. The two oxazine dyes that were assessed have markedly different redox potentials, implying that their behaviour will differ not only from that of the other dye families, but between themselves too.

Dye Family	Dye	Oxidised indicator dye (D_{ox})	Reduced indicator dye (D_{red})	$E^\circ(D_{ox}/D_{red})/V$ at pH 7 vs. SHE ³
Thiazines	MB			+ 0.011
	TB			+ 0.034
	Th			+ 0.056
Oxazines	NB			- 0.119
	BCB			+ 0.032*
Phenazines	NR			- 0.330
	SO			- 0.289*

Table 6.1.: The dyes tested for their suitability in both a non-acidic and acidic indicator ink formulation. * denotes that the values of the redox potential quoted are for the structurally similar compounds cresyl blue and safranin T respectively, since the reference which provides all other values of the redox potential does not quote them for the compounds as shown

Since an acidic MB ink has been successfully tested by Mills et al², the results generated in this chapter for it will be used as the benchmark. In all instances, it is assumed that the reduced form of the dye, as shown in table 6.1., is the final product of the dye in the indicator ink formulation following complete photoreduction on Activ™.

6.2. Thiazines

6.2.1. Methylene Blue Under Anaerobic Conditions

The performance of MB in a standard indicator ink on an ‘older’ batch of Activ™ was documented previously in chapter 4. In summary, the dye was observed to respond rapidly under anaerobic conditions, outperforming both the DCIP and Rf indicator inks and comparable to what was observed using Rz. However, upon exposure of the reduced form of the dye, leuco-MB, to air/ambient atmospheric conditions, rapid re-oxidation occurred. Indeed, such is the O₂-sensitivity of leuco-MB that it was not possible to reduce the dye to any significant extent under ambient atmospheric conditions, as shown in figure 6.1.

The recent results reported by Mills et al for the acidic MB ink² were obtained using a new batch of Activ™, supplied again by Pilkington Glass. This new batch is promoted as having a higher photocatalytic activity than its predecessor, which was used here in chapters 3 and 4. As a result, the new batch used by Mills et al² is used as the substrate in this chapter since it is more likely that consumers currently purchasing the product will be provided with this newer, more active form of Activ™.

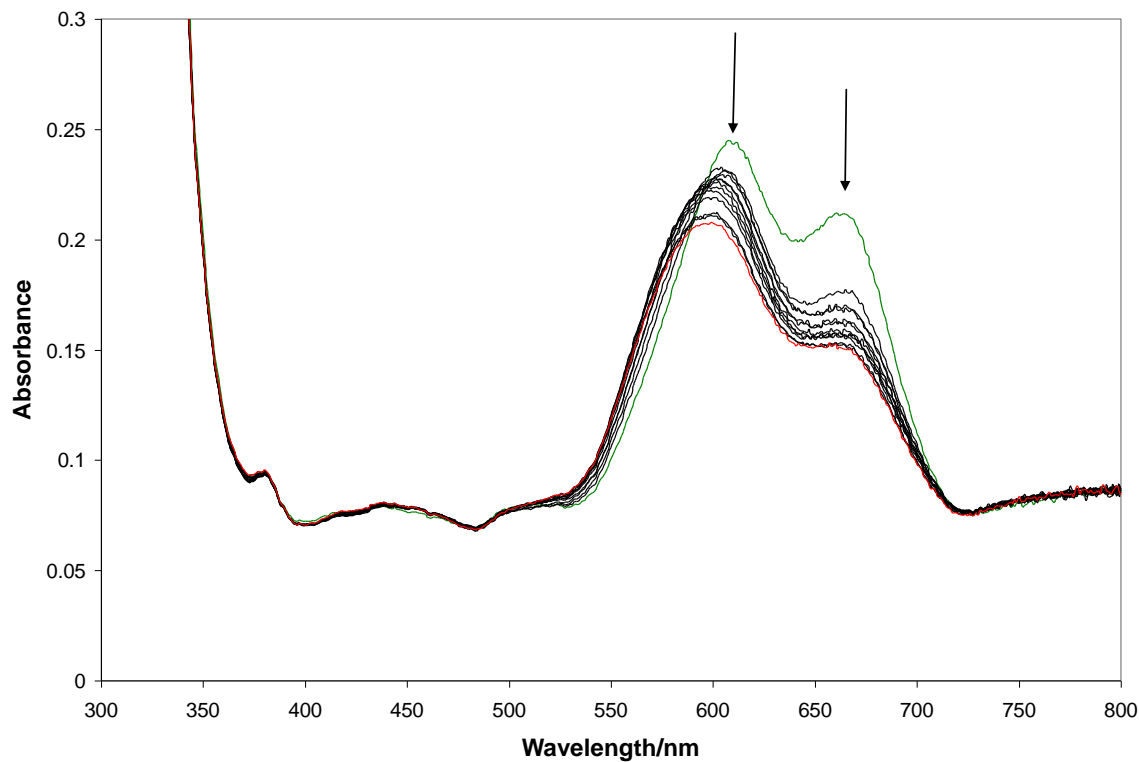


Figure 6.1.: The change in spectral shape for a MB ink as it is irradiated under ambient atmospheric conditions. The green trace shows the initial spectrum of the ink, whilst the red trace shows the ink spectrum 1 hour later. Spectra were recorded at 1 minute intervals for 4 minutes, at 2 minute intervals up to 10 minutes, and finally at 10 minute intervals up to 1 hour

Figure 6.2. shows the performance of the standard MB ink under anaerobic conditions on this new batch of ActivTM. Once again we observe the collapse of the peaks with increasing irradiation time as MB is reduced to leuco-MB. Figure 6.3. shows how the absorbance at λ_{\max} for the dye varies with time based on the results shown in figure 6.2.

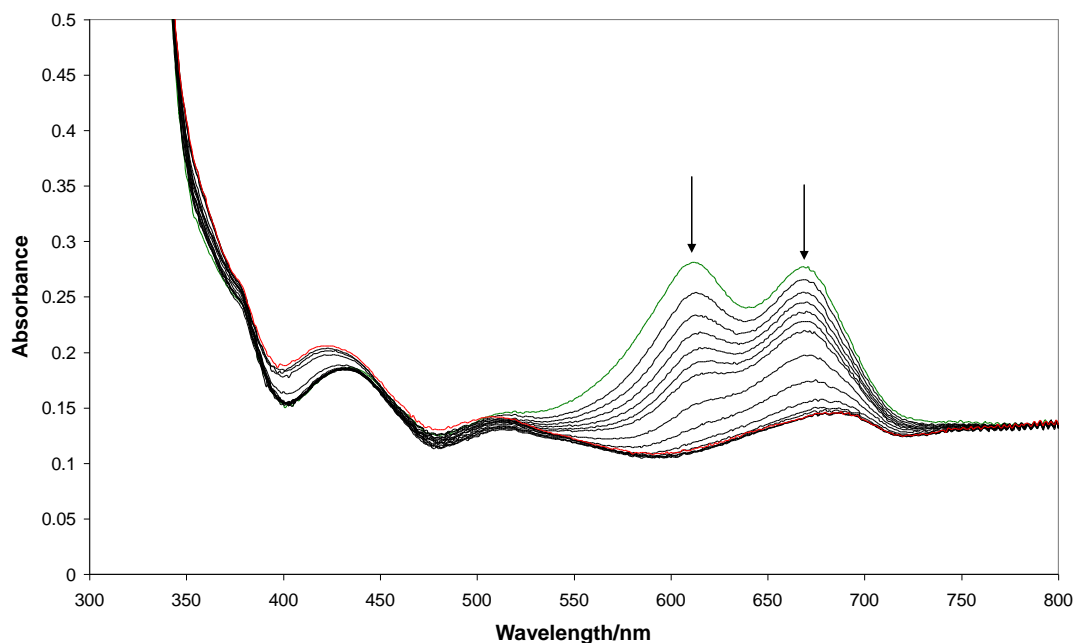


Figure 6.2.: The variation in the spectral shape due to MB as it is reduced on the surface of ‘new’ Activ™ under anaerobic conditions. The green trace shows the initial ink spectrum whilst the red trace shows that obtained upon complete reduction. Spectra were recorded every 10 s for 1 minute, then at 30 s intervals up to 5 minutes, and finally after 10 minutes UVA irradiation

Whereas previously in chapter 4 the majority of the reduction reaction occurred over ca. 20 minutes, we now observe complete reduction of the dye in ca. 3 minutes under similar conditions. Such a finding implies that the ‘new’ batch of Activ™ used in this work is some 5-10 times more potent than its predecessor that was used previously. The zero order $t_{50\%}$ is calculated to be 59 s, whereas previously in chapter 4 it was quoted as ca. 340 s, reaffirming the observation above that this new batch of Activ™ is 5-10 times more photocatalytically active. The results shown in figure 6.3. would also appear to further confirm a zero order kinetic model for dye reduction in such indicator inks as postulated in chapters 3 and 4 here, and by others elsewhere⁴.

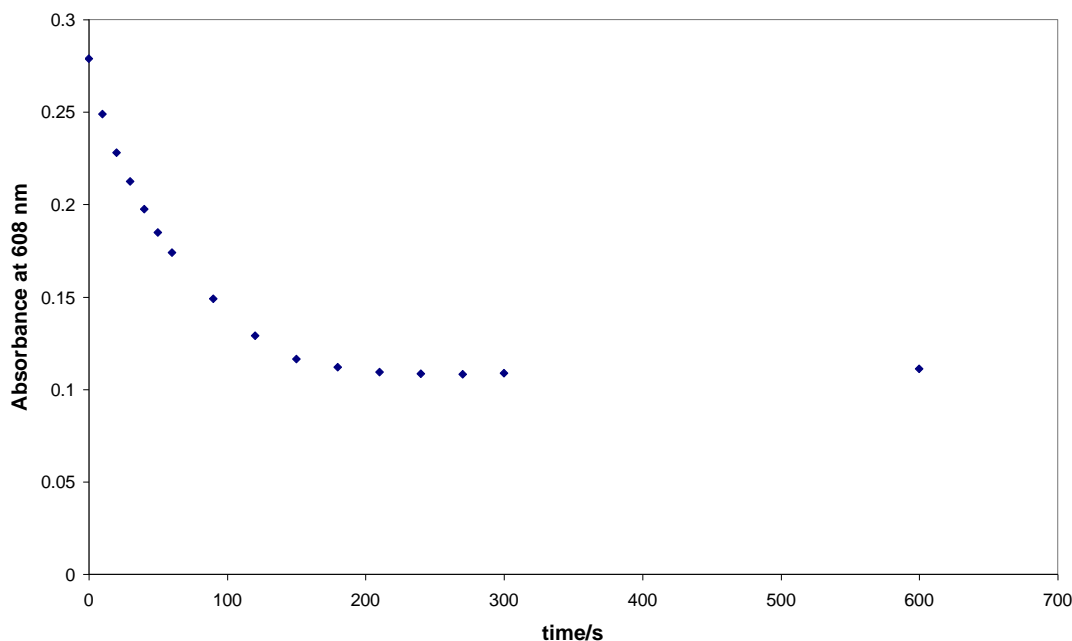


Figure 6.3.: The variation in the absorbance at λ_{\max} due to MB with irradiation time as the dye is reduced in the indicator ink formulation on ‘new’ ActivTM under anaerobic conditions

Following reduction, the recovery of the ink was then assessed under ambient atmospheric conditions. As anticipated from the work previously in chapter 4, the ink recovers ca. 90 % of its initial blue colour, and does so rapidly (i.e. within 5 minutes) upon exposure to such conditions (data not shown here). Such results imply that the recovery kinetics for the standard MB ink are unaffected by changing the batch of ActivTM used here, which was expected since the properties of both the dye and its reduced form, leuco-MB, should remain largely unaffected by the change in activity of the substrate.

The acidic MB ink was then tested under similar conditions, and the variation in the spectral shape due to the dye, and the dye’s peak absorbance with increasing irradiation time, are shown in figures 6.4. and 6.5. respectively. Immediately from figure 6.4. we note that the λ_{\max} for the dye has now blue-shifted down to 608 nm, most likely due to a solvatochromic effect. Whilst the decrease in the absorbance of the peaks we have now come to associate with the reduction of the dye in the indicator ink formulation is still

observed, from both figures 6.4. and 6.5., the time taken for complete reduction to occur appears to be much slower (ca. 5 times) than what is observed for the non-acidic ink under similar conditions above in figures 6.2. and 6.3. Assuming zero order kinetics, the $t_{50\%}$ for the acidified ink is calculated from figure 6.5. to be 115 s, which is ca. 2 times slower than that observed above for its non-acidic counterpart under similar conditions.

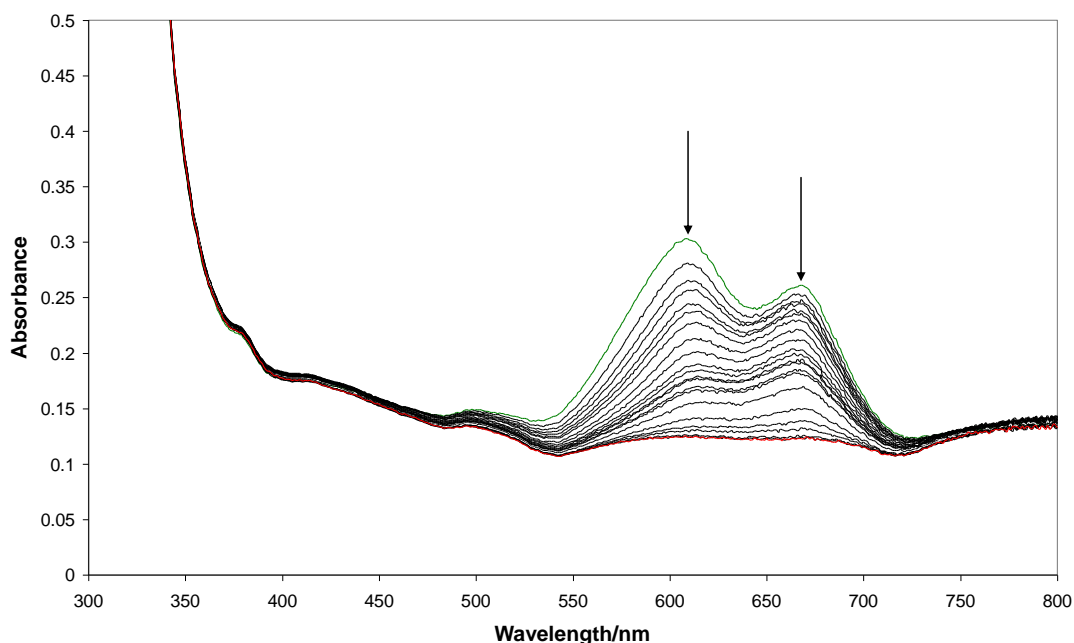


Figure 6.4.: The variation in the spectral shape of the acidified MB ink with increasing irradiation time under anaerobic conditions. The green trace shows the initial ink spectrum obtained on Activ™ whilst the red trace shows that obtained after complete reduction. Spectra were recorded at 10 s intervals for 1 minute, then at 30 s intervals up to 5 minutes, and finally at 5 minute intervals up to 50 minutes

The results generated in figures 6.2.-6.5. would therefore appear to imply that upon acidifying the ink, the rate of reduction is retarded somewhat. Since it is generally accepted that acidification will alter the redox potential of the MB/leuco-MB couple², the observed decrease in reaction rate would appear to suggest that the redox potential has been made less positive, or indeed negative, by such a process. However, others

have reported that the redox potential for the MB/LMB couple increases from + 0.011 V to + 0.532 V upon moving from pH 7 to pH 0¹. Therefore, we would anticipate an increase in the rate of reduction upon moving to acidic conditions, since a more positive redox potential implies a greater tendency to reduce.

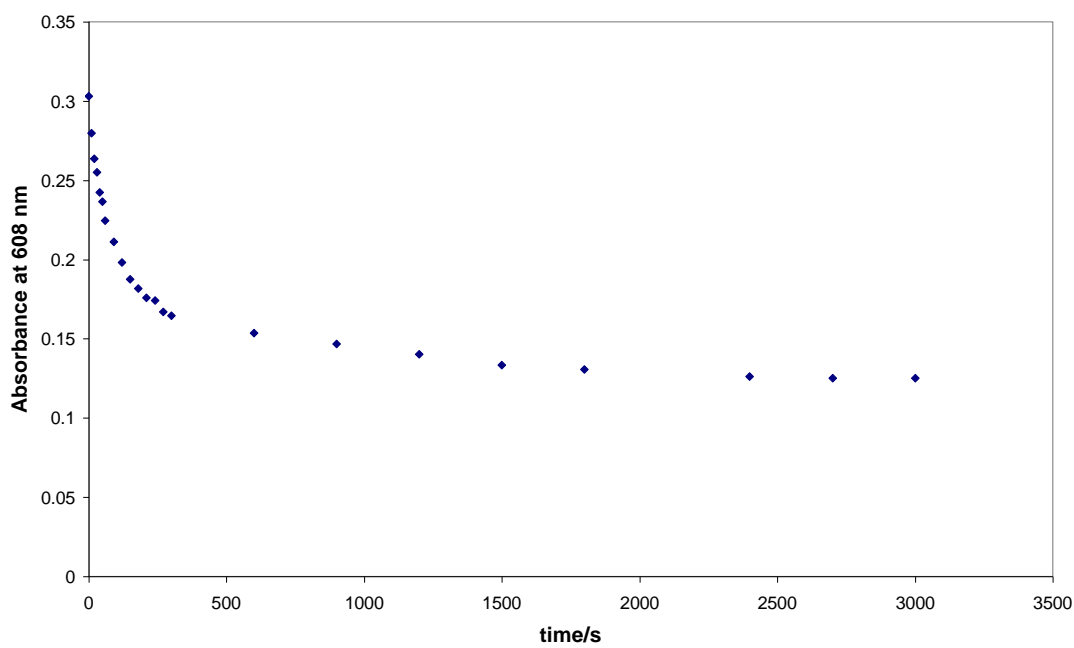


Figure 6.5.: The variation in the absorbance at λ_{\max} due to MB with increasing irradiation time as the acidified ink is reduced on ActivTM

It is postulated that the increased time for reduction observed here upon acidification is due to the stability of the MB radical, $\text{MB}^{\cdot+}$, with increasing acidity, as suggested by Mills and Wang¹. If such a species becomes more stable with increasing acidity, it is possible that its longevity slows the reduction reaction to LMB. In addition, the change in reaction pH may also be detrimental to reduction since, as highlighted by Carp et al⁵, the interaction of charged electron donors and acceptors for reaction with the photocatalyst is strongly influenced by the pH. Although the pH of zero point charge for ActivTM is not known, it would be anticipated that the pH of the ink is less than this value. According to Carp et al⁵, such conditions would thus favour the adsorption of anionic electron donors and acceptors. Within the ink, MB is cationic whilst glycerol,

the SED, is uncharged. With the TiO_2 surface also exhibiting a positive charge, this may also be detrimental to the reduction of the cationic MB dye.

Following reduction, the acidified ink was then allowed to recover in the presence of O_2 . Initially, a stream of air from a bench tap was flowed into the system for 30 minutes, after which time the ink was then exposed to ambient atmospheric conditions. Figure 6.6. shows the variation in the absorbance at λ_{max} for MB during both the reduction and recovery periods.

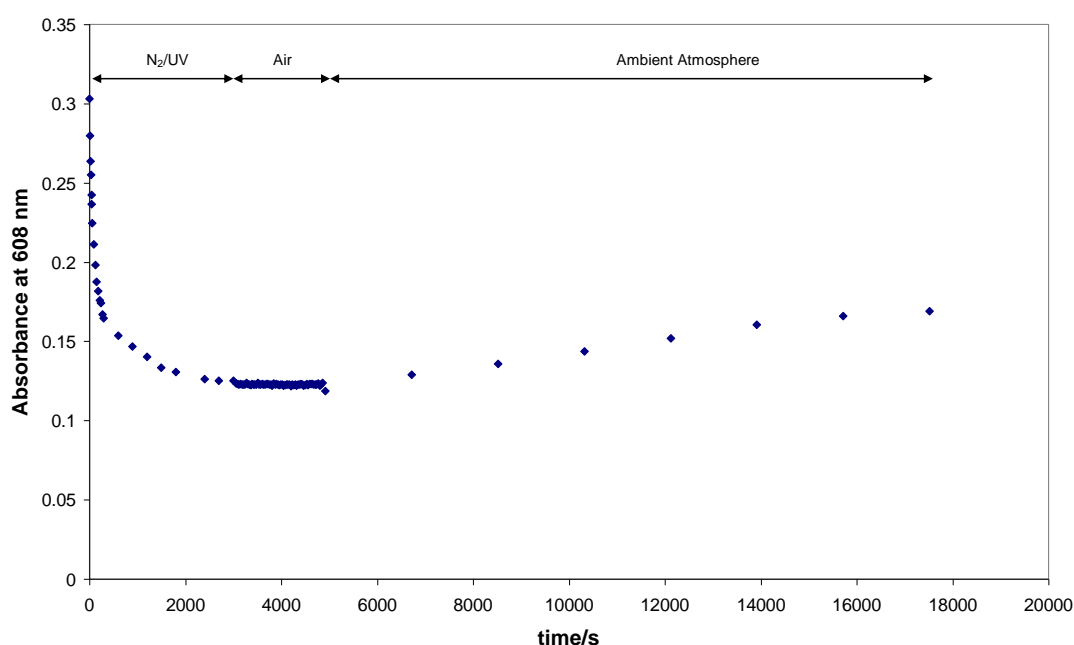


Figure 6.6.: The variation in the absorbance at λ_{max} for MB with time in the acidified ink formulation as it is initially reduced under anaerobic conditions on Activ™ before being allowed to recover, initially using air from a bench tap, and then when subjected to ambient atmospheric conditions

Despite saturating the system with air from a tap, no increase in the peak absorbance is observed over the initial 30 minute recovery period. It is only upon exposure to ambient atmospheric conditions that any recovery is noted. However, even then, the film is observed to recover slowly to a maximum of 25% of its original colour over a

period of 3.5 hours. Beyond this time, the absorbance was then observed to plateau before a slight decrease occurred (data not shown). In chapter 4, we observed a 90% increase in the absorbance at λ_{\max} almost immediately in the standard ink formulation upon exposure to ambient atmospheric conditions. Evidently, acidification appears to stabilise leuco-MB to some degree in the work conducted here. The lack of recovery in the dry air atmosphere initially is attributed to the low relative humidity in such a gas stream, water acting as a plasticizer for the ink and thus facilitating movement of the dye molecules and/or O_2 through the film, resulting in re-oxidation.

Such retardation in the rate of MB recovery is important for the ink's potential use in the field, since it implies less susceptibility to the level of O_2 present. Previous work by Impert et al⁶ has observed that by altering the pH of a leuco-MB solution from ca. pH 8 to pH 0, the LMB is protonated, making it less reactive to atmospheric O_2 owing to the higher redox potential of the MB/LMB couple ($E_{\text{MB/LMB}}^0$ (pH 0) = 0.532 V vs. 0.011 V at pH 7). Such an observation would explain the observed decrease in the rate of recovery observed here compared to that for the standard ink in chapter 4.

The retardation in the recovery may also be due to a phenomenon that has previously been noted by Pennarun et al in their work on a micro-optical ring electrode⁷. They postulated that LMB may be electrogenerated on the surface of their electrode due to the following reaction;



where $LMB^{+\cdot}$ is a cationic radical of LMB. According to the authors, such a layer of LMB produced by this reaction acts as insulation, preventing the diffusion of counter ions to the electrode surface. It is postulated, therefore, that the LMB photocatalytically generated in this work may deposit as a layer on the ActivTM surface, making it more resistant to re-oxidation, and hence giving the appearance that the re-oxidation kinetics have slowed in comparison.

6.2.2. The Acidic Methylene Blue Ink Under Ambient Atmospheric Conditions

The true test of such an ink, however, is its performance under ambient atmospheric conditions. Figure 6.7. plots the change in spectral shape observed for the acidic ink, whilst the change in the absorbance at λ_{\max} due to MB with increasing irradiation time is shown in figure 6.8. under such conditions.

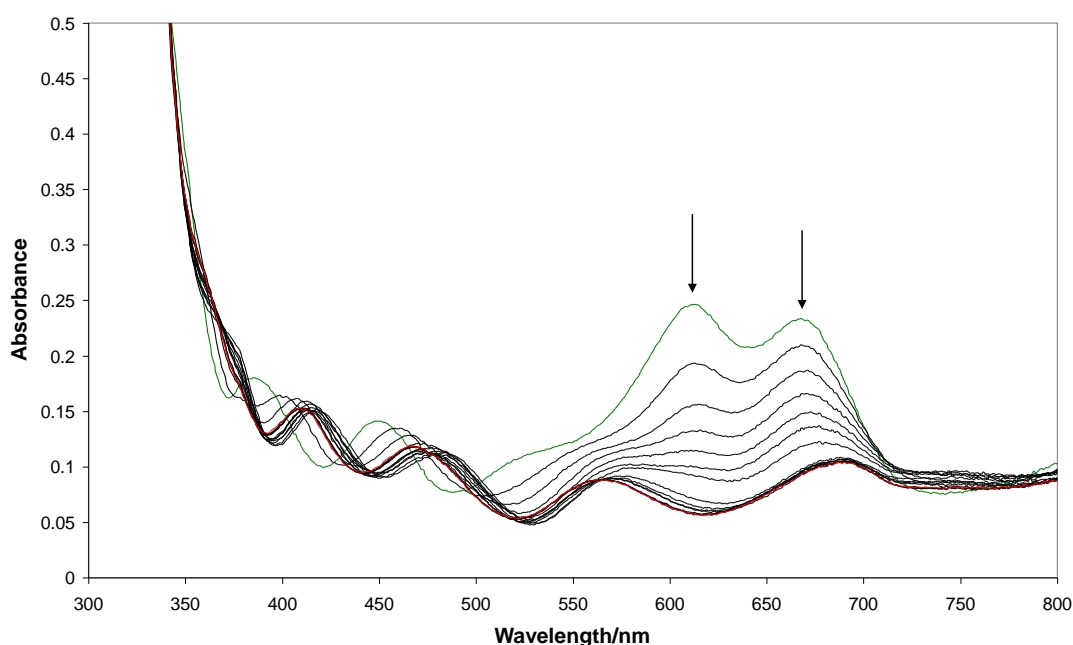


Figure 6.7.: The variation in spectral shape of the acidic MB indicator ink as it is reduced on the surface of Activ™ under ambient atmospheric conditions. The green trace shows the initial ink spectrum whilst the red trace shows that after 5 minutes UVA irradiation. Spectra were recorded at 10 s intervals for 1 minute, then at 30 s intervals up to 5 minutes

As was observed under anaerobic conditions, the λ_{\max} is blue-shifted in the initial ink spectrum to 608 nm compared to the non-acidic ink. Of greater interest, however, is the fact that the ink appears to reduce at all under such conditions. Evidently acidification of the ink formulation invokes such a change in the chemistry of the dye that not only is reduction possible under ambient atmospheric conditions, it appears to be unhindered by re-oxidation of leuco-MB over the timescale of the experiment.

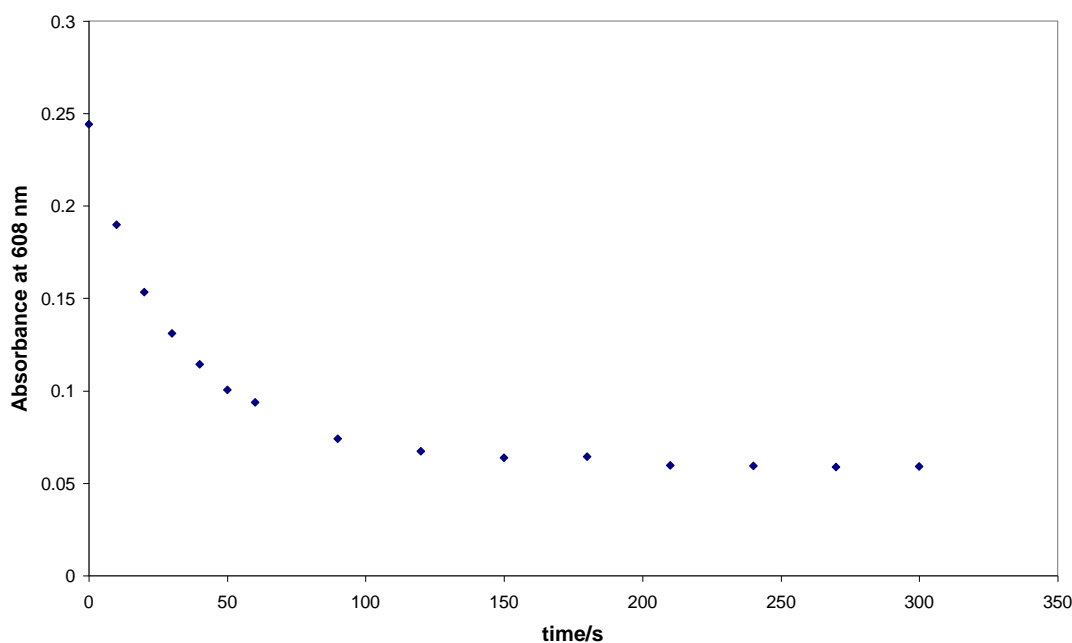


Figure 6.8.: The variation in the absorbance at λ_{\max} of the acidic MB ink with irradiation time under ambient atmospheric conditions

This observation is most likely due to acidification increasing the redox potential for the system as noted previously by Mills and Wang¹ and Impert et al⁶. In figure 6.7., the spectra observed for the MB film as it is reduced is seen to exhibit a strong interference pattern. Such patterns indeed appear to be present when using all the acidic indicator inks tested here, and are thought to be a consequence of the cleaning protocol used between tests. They can be eliminated simply by washing the substrate with deionised water prior to casting the ink film; however, whether present or not, similar $t_{50\%}$ values are observed, hence they do not appear to affect the reduction kinetics. Such interference patterns are usually attributed to the presence of a film on the substrate surface. In this instance, it is impossible to say whether what is being observed is the TiO₂ film, the ink film, or even some residual ethanol from the cleaning protocol. The latter of these would appear to be the most unlikely, given the vigorous cleaning protocol; however, the fact that washing the substrate seems to eliminate the pattern suggests it is worth considering. Since the source of the interference pattern is

unknown, it is therefore impossible to calculate the thickness of the film which is causing it, as such a calculation involves knowledge of the refractive index.

We also note from figures 6.7. and 6.8. that the reduction reaction is complete in 5 minutes, ca. 10 times faster than what is observed for the same ink under anaerobic conditions in figure 6.4. This overall decrease in the time taken for complete reduction is confirmed in figure 6.8., the data shown yielding a calculated zero order $t_{50\%}$ of 25 s, which is ca. 4 times faster than what we observed previously under anaerobic conditions in figure 6.5. This apparent increase may simply be due to the higher incident UV irradiance used under ambient atmospheric conditions (ca. 4.5 mW cm^{-2} compared to ca. 1.3 mW cm^{-2} under a N_2 atmosphere). However, the relative humidity may also be a factor. Under ambient atmospheric conditions, the relative humidity is ca. 60%, and thus there is sufficient moisture present to act as a source of H^+ ions. However, under anaerobic conditions, the relative humidity is ca. 10 %. Such levels, although providing the system with some moisture, may not be high enough to provide enough H^+ ions for the reduction reaction. In addition, water is an excellent plasticizer, and thus its presence should hydrate the film sufficiently to allow movement of the dye molecules to the photocatalyst surface.

Interestingly, Mills et al quote the $t_{50\%}$ for the same system to be 17 s, which is very similar to what is observed here². Although these are only 2 samples, such results would appear to suggest that the reproducibility of the new batch of Activ™ is high. The ink was then allowed to recover under ambient atmospheric conditions for 1 hour, and the variation in the peak absorbance due to MB with time is shown in figure 6.9.

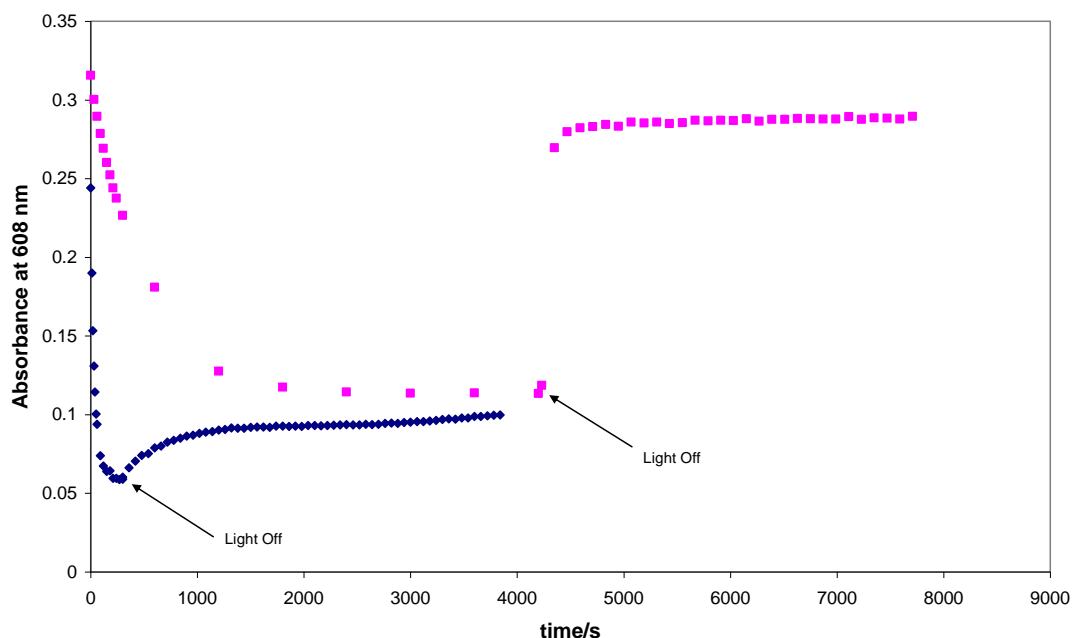


Figure 6.9.: The variation in the peak absorbance due to MB as the acidic indicator ink is reduced and then allowed to recover under ambient atmospheric conditions (blue trace). The pink trace shows the variation in the peak absorbance for a ‘neutral’ MB film irradiated under N_2 and allowed to recover under ambient atmospheric conditions on the old batch of ActivTM

The ink is observed to recover ca. 25 % of its original blue colour over the first 25 minutes before plateau. Such a recovery is similar to what was observed for the same ink following reduction under anaerobic conditions, although the increase does occur more rapidly. This increase in rapidity is thought to be due to the slightly different recovery conditions used here, with no initial exposure to dry air used in the latter test. Most importantly, however, is that the noted recovery is much less than what is observed for the non-acidic MB ink in chapter 4 following reduction under anaerobic conditions, as indicated by the pink trace in figure 6.9. Whether this is simply due to acidification altering the dye redox potential, or inhibition of LMB re-oxidation by the formation of an insulating layer on the ActivTM surface is, however, unclear.

Acidification would therefore not only appear to promote bleaching of the ink under ambient atmospheric conditions, but it also appears to limit the amount of recovery

which then occurs, either due to the stability of LMB via protonation as suggested by Impert et al⁶, or due to its insulative properties when formed as a layer on the Activ™ surface as was observed by Pennarun et al⁷ for their electrode. Compared to what was observed in chapter 4 for the Rz ink under ambient atmospheric conditions, the rate of photoreduction of this acidified MB ink is comparable. Although it could be argued that the Rz ink does not recover as significantly, thus making it more attractive for use in the field, the acidified MB ink does reduce to a colourless product, making it competitive, at least, to the original technology in this area. It also bleaches faster than the DCIP ink characterised in chapter 3.

6.2.3. Thionine (Th) and Toluidine Blue (TB)

Similar experiments to those detailed above were conducted for both Th and TB, the other thiazines tested here. Figure 6.10. shows the structure and reduction mechanism for Th, whilst figure 4.11 shows the same for TB.

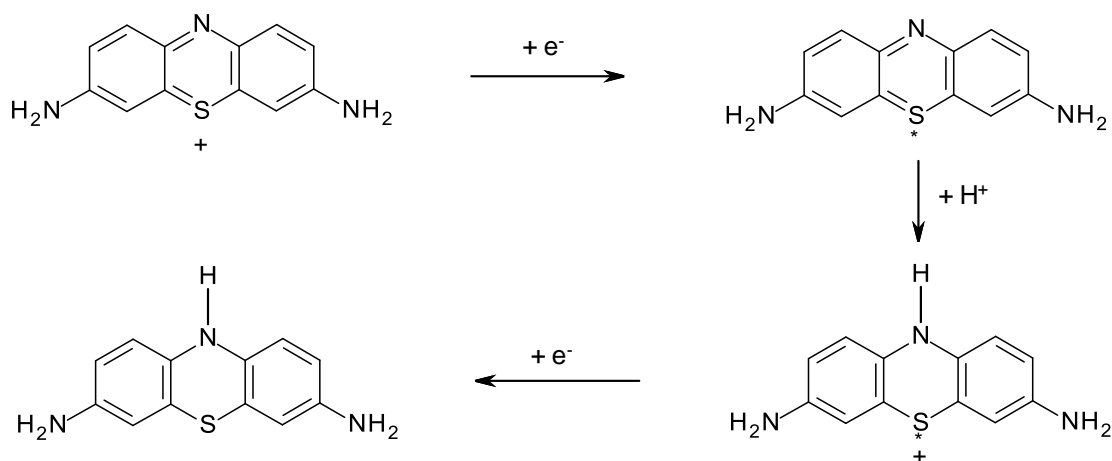


Figure 6.10.: The structure of Th and its reduction mechanism

Table 6.2. details the recovery and reduction results generated, compared to those detailed above for MB, whilst figures 6.12. and 6.13. show the change in spectral shape which occurs when such dyes are placed in the acidic indicator ink formulation and reduced under ambient atmospheric conditions.

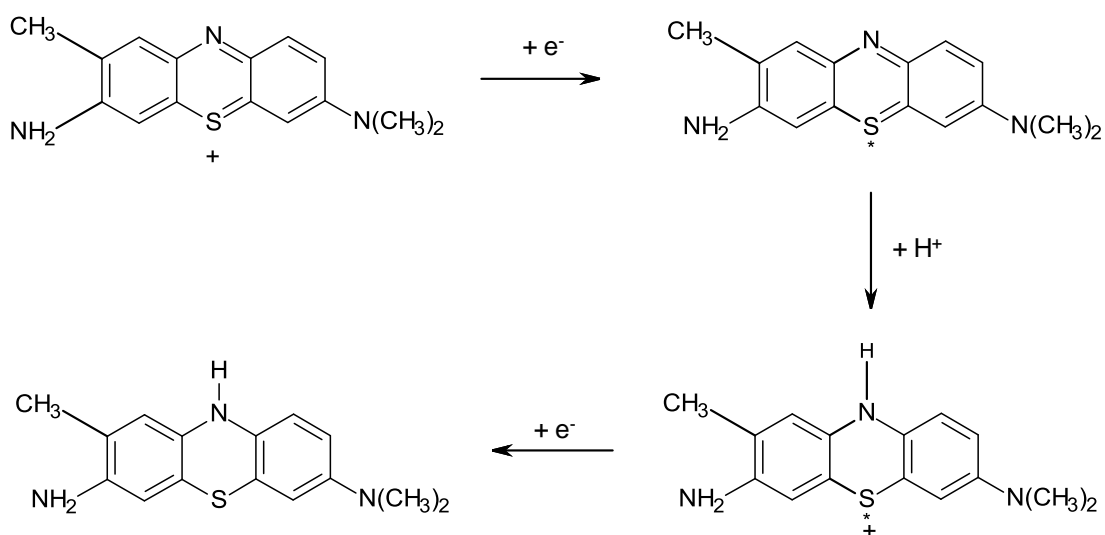


Figure 6.11.: The structure of, and the reduction mechanism for TB

Dye	Non-acidic		Acidic			
	Anaerobic		Anaerobic		Ambient Atmospheric	
	$t_{50\%}/s$	% recovery in air	$t_{50\%}/s$	% recovery in air	$t_{50\%}/s$	% recovery in air
MB	59	90 (5)	115	25 (210)	25	25 (25)
Th	478	82 (30)	402	10 (30)	122	9 (60)
TB	191	87 (30)	192	5 (60)	38	25 (60)

Table 6.2.: A comparison of the results obtained for the thiazine dyes. Note that the numbers in brackets represent the time (in minutes) taken for the quoted % recovery to be achieved

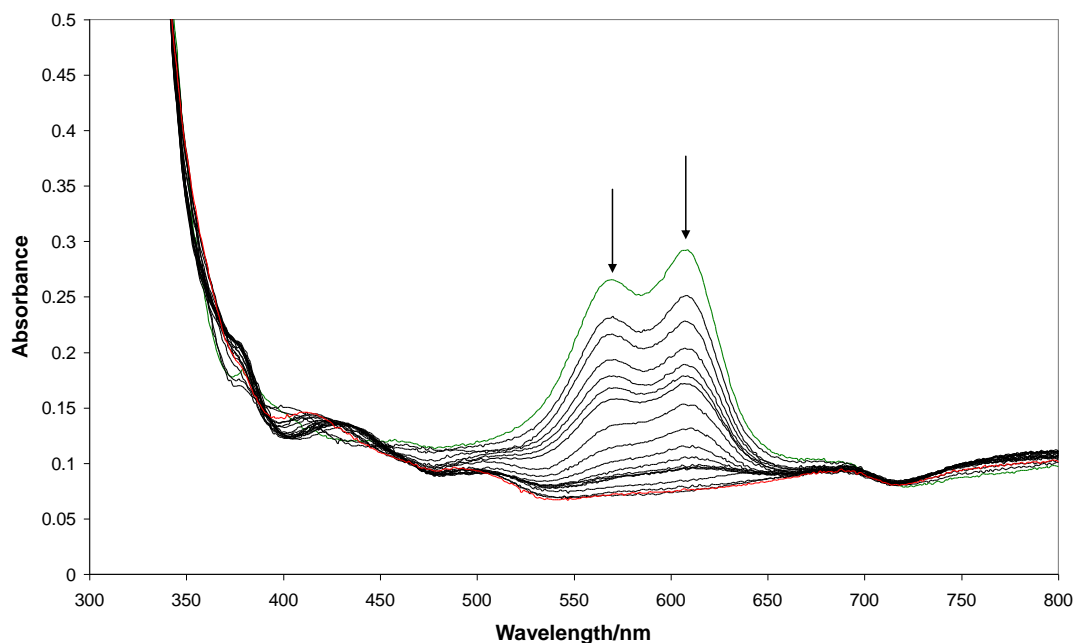


Figure 6.12.: The change in spectral shape which occurs as the acidic Th ink is reduced on Activ™. The green trace shows the initial ink spectrum prior to reduction, whilst the red trace shows that obtained after 25 minutes of UVA irradiation. Spectra were recorded every 10 s for 1 minute, then every 30 s up to 5 minutes, and finally every 5 minutes up to 25 minutes

In both instances, if the dye is placed directly into the standard (i.e. non-acidic) indicator ink formulation, no reduction is observed under ambient atmospheric conditions. Under anaerobic conditions, however, such systems are observed to bleach, albeit at a slower rate than that for MB according to the data reported in table 6.2. Based on the redox potentials of the dyes quoted previously in table 6.1., we would anticipate that the ease with which the dyes can be reduced should be of the order $\text{Th} > \text{TB} > \text{MB}$. However, what we actually observe in the indicator inks is a complete reversal, i.e. $\text{MB} > \text{TB} > \text{Th}$. Indeed, even for the acidic inks, where the redox potential of each dye is expected to differ from that quoted previously in table 6.1., we observe similar trends under both anaerobic and ambient atmospheric conditions.

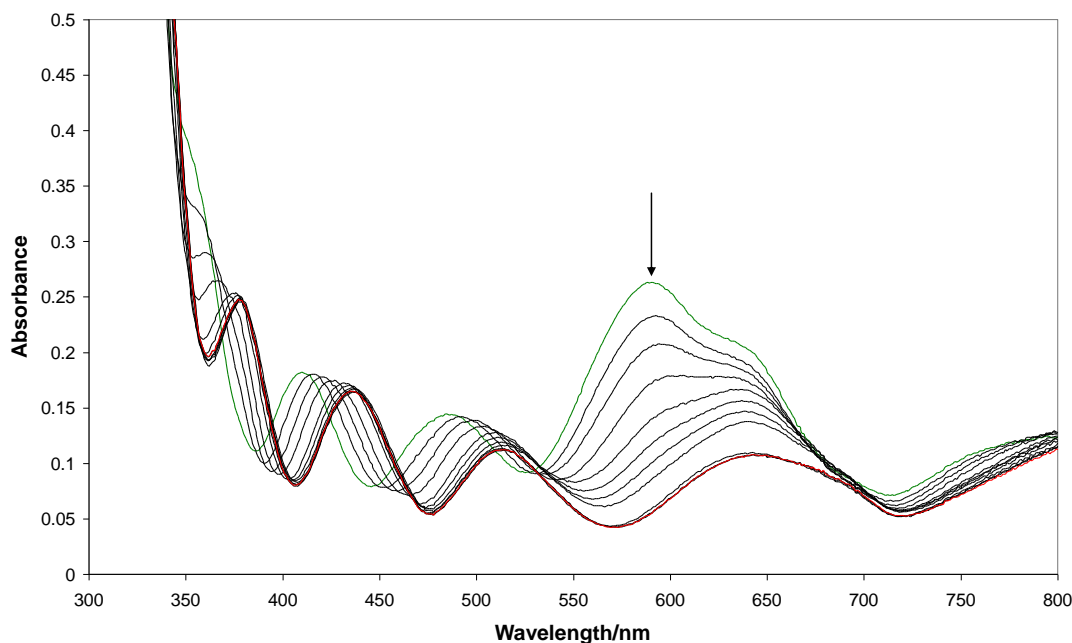


Figure 6.13.: The change in spectral shape which occurs as the acidic TB ink is reduced on Activ™. The green trace shows the initial ink spectrum prior to reduction, whilst the red trace shows that obtained after 2.5 minutes of UVA irradiation. Spectra were recorded at 5 s, 10 s, then every 10 s up to 1 minute, and finally every 30 s up to 2.5 minutes

Bishop⁸ and Clark⁹ have reported the pKa values for each dye, which are tabulated in table 6.3. below. The terms K_{r1} and K_{r2} refer to the basic ionisation of a hydrogen ion at each of the amino groups on the dyes, whilst K_{O1} is the dissociation constant for a hydrogen ion at the polar amino group in the oxidised form. For MB, the latter is negligible and thus a value of pK_{O1} cannot be quantified. The values for Th and TB, however, are remarkably similar, suggesting that the dissociation constant for a hydrogen ion on both dyes, and hence they're ability to reduce, would be comparable. From table 6.2., this is clearly not the case, TB seemingly easier to reduce than Th. Similarly, the values quoted for pK_{r1} would suggest that Th should be the easiest to re-oxidise, since it has the lowest value quoted for the three dyes. A quick glance at table 6.2. would appear to disagree with this suggestion. It can thus be inferred that the variation in the reduction/recovery profiles is not due to the pKa values for the different redox processes.

Dye	E°/V at pH 7 vs. SHE	pK_{O1}	pK_{r1}	pK_{r2}
MB	0.011	-	4.52	5.85
Th	0.056	11.0	4.38	5.30
TB	0.034	11.04	4.81	5.41

Table 6.3.: A comparison of the redox potentials and pK_a values for the thiazine dyes MB, Th and TB

One possible explanation for this apparent anomaly in reduction rate could lie in Marcus Theory¹⁰⁻¹¹. Marcus developed a theory which described the rate at which electron transfer reactions occur. According to this theory, for redox reactions, much like in Eyring's Transition State theory, the reactants come together to form a precursor complex, undergo electron transfer to the successor complex, and dissociate as the products. It therefore seems logical that despite the thiazines tested above having the same basic structural framework, their rate of reduction will be impacted by the substituents present on the nitrogen units. Figure 6.14. shows a diagram of potential energy, $P(E)$ as a function of potential, E .

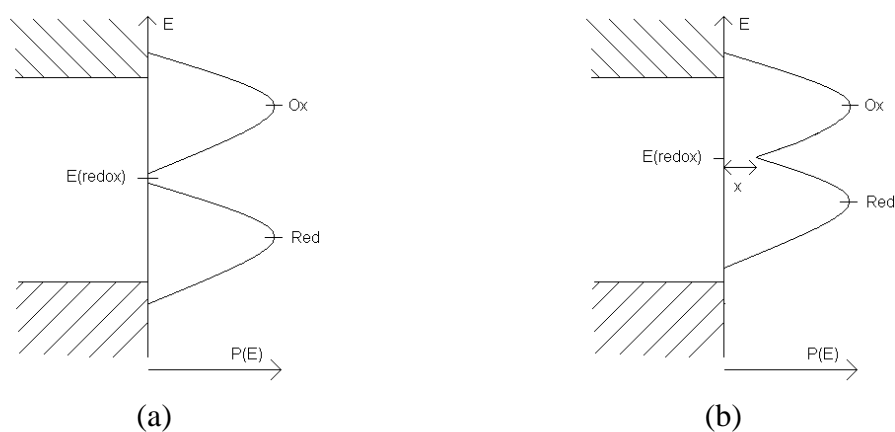


Figure 6.14.: Diagrams showing how potential energy, $P(E)$ varies with redox potential. The diagram on the left, (a), shows what might be anticipated, whilst (b) shows the overlap in parabolas which occurs. The degree of overlap of these parabolas is indicated by x

It might be anticipated that the population of molecules in the oxidised and reduced states at potentials around the redox potential, $E(\text{redox})$, would vary as shown in (a). However, in truth, what is observed is an overlap of the oxidised and reduced parabolas, as shown in (b). The degree of overlap, represented by x , is a measure of the reorganisation energy. It may well be, therefore, that this energy is less for MB than for Th/TB, implying that the oxidised and reduced states for MB interchange easier at potentials around $E(\text{redox})$, thus explaining the faster rate of reduction observed here. Such overlap could be mistakenly construed as a shift in redox potential, making it appear as though the MB redox potential has shifted to a more positive value than that for Th.

Despite this apparent anomaly, the other thiazine dyes tested do exhibit some similar traits to the MB ink. Both reduction reactions shown in figures 6.12. and 6.13. exhibit the interference pattern observed earlier for the acidic MB ink, although once again this can be removed through modification of the substrate cleaning protocol and does not appear to impact on the rate of reduction observed. In addition, when both Th and TB are encapsulated in the standard formulation and reduced under anaerobic conditions, the percentage recovery upon exposure to ambient atmospheric conditions is similar to that for MB, albeit at a slower rate, in agreement with the values of the redox potentials quoted previously in table 6.1. Since Th and TB have a more positive redox potential compared to MB, they should be more difficult to re-oxidise in comparison.

For the acidic Th and TB formulations, reduction occurs under both anaerobic and ambient atmospheric conditions. The % recovery of such inks is also much lower than what is observed for their non-acidic counterparts. In addition, the reduction reaction under ambient atmospheric conditions is ca. 4 times faster than that observed under anaerobic conditions, although this is again attributed to an increase in UVA irradiance and relative humidity. Such results cannot be explained based on the redox and pKa data. However, the explanation based on Marcus Theory may be at work in this formulation also. Overall, the acidified MB ink would still seem to be the most suitable from the thiazine family for thin, low activity films.

6.3. Phenazines

Similar to the thiazines described above, the two phenazine dyes used in this work, namely neutral red (NR) and safranin O (SO), were also assessed for their suitability in both the standard and acidic indicator ink formulations. The structures of the dyes and their reduction mechanisms are shown in figures 6.15. and 6.16., whilst the main results are detailed in table 6.4.

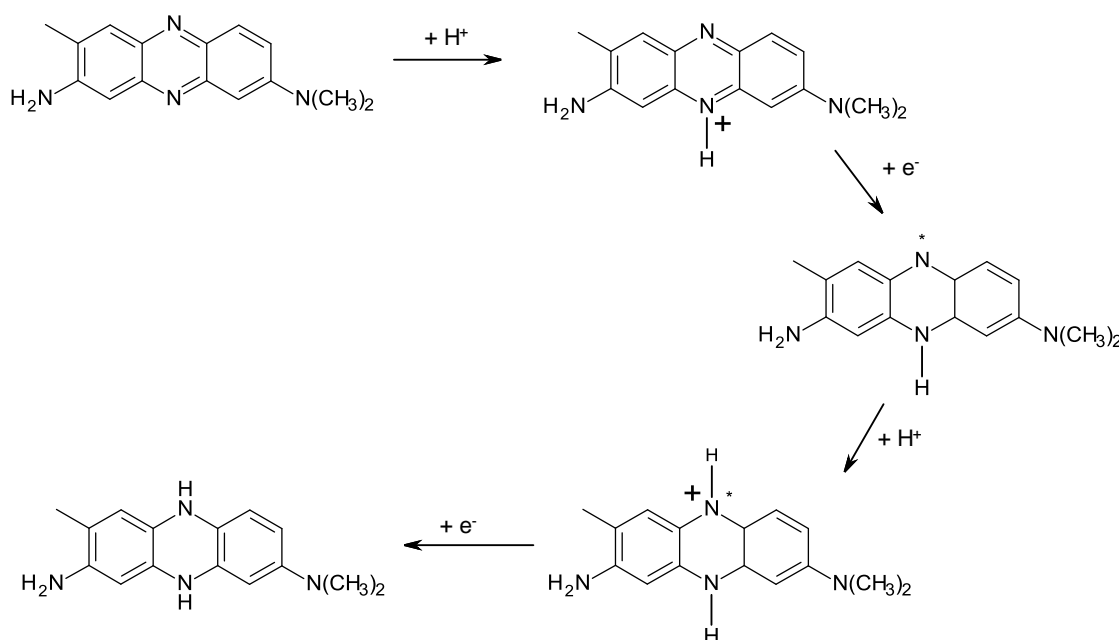


Figure 6.15.: The structure of NR and its subsequent reduction mechanism

Once again, no reduction was observed for either dye in the standard formulation under ambient atmospheric conditions, as anticipated from the redox potentials tabulated previously in table 6.1. Indeed, for NR, only partial reduction was observed even under anaerobic conditions. Worse still, upon moving to an acidic formulation, the dye was observed to be insoluble in the indicator ink.

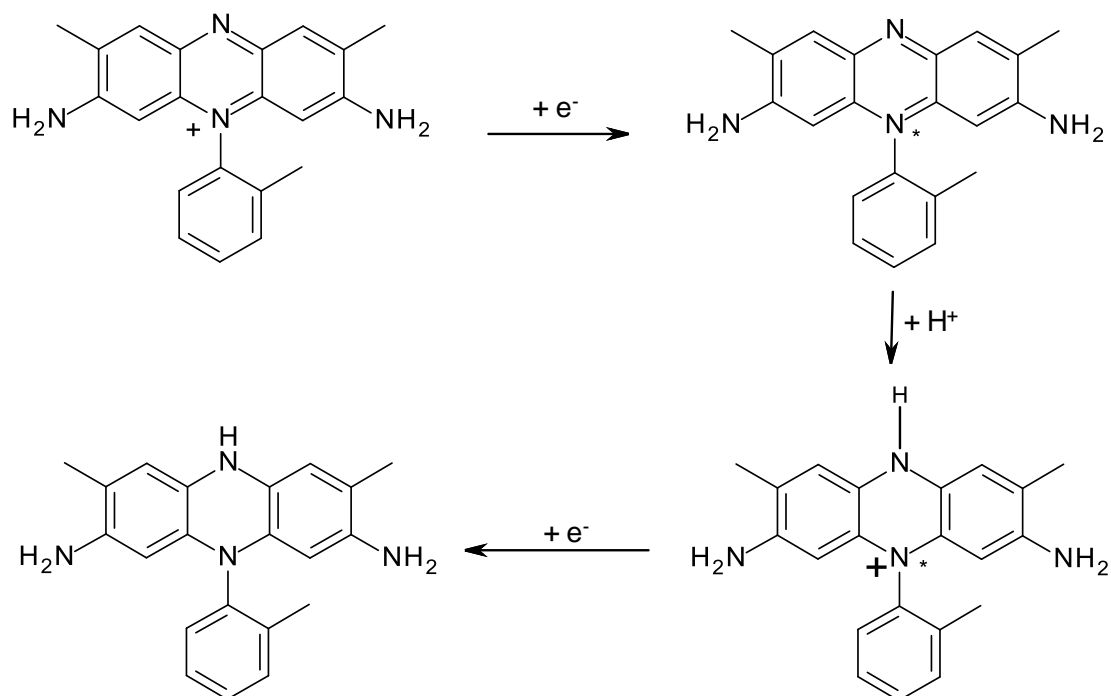


Figure 6.16.: The structure of SO and its subsequent reduction mechanism

Dye	Non-acidic		Acidic			
	Anaerobic		Anaerobic		Ambient Atmospheric	
	$t_{50} \text{ %/s}$	% recovery in air	$t_{50} \text{ %/s}$	% recovery in air	$t_{50} \text{ %/s}$	% recovery in air
NR	N/A	N/A	N/A	N/A	N/A	N/A
SO	101	80 (30)	165	84 (30)	N/A	N/A

Table 6.4.: A comparison of the results obtained for the phenazine dyes. Note that the numbers in brackets represent the time (in minutes) taken for the quoted % recovery to be achieved

Using SO, it is possible to reduce both the acidic and non-acidic ink under anaerobic conditions, with the change in spectral shape observed for the acidic version shown in figure 6.17. However, although the reduction of the dye is again indicated by a collapse of the main peak, as the reaction progresses a minor peak is observed to emerge at ca. 452 nm. Given that the dye generates a red ink initially, as indicated by the main peak

at 503 nm, it comes as no surprise that the emergence of this second peak with reduction causes the film to develop a slight red/pink colour. As a result, what is observed over the course of the reduction reaction is more of a fading of the initial ink colour than a bleaching. This is obviously undesirable; what is sought is an ink which reduces to a colourless product, or which at least undergoes a striking colour change.

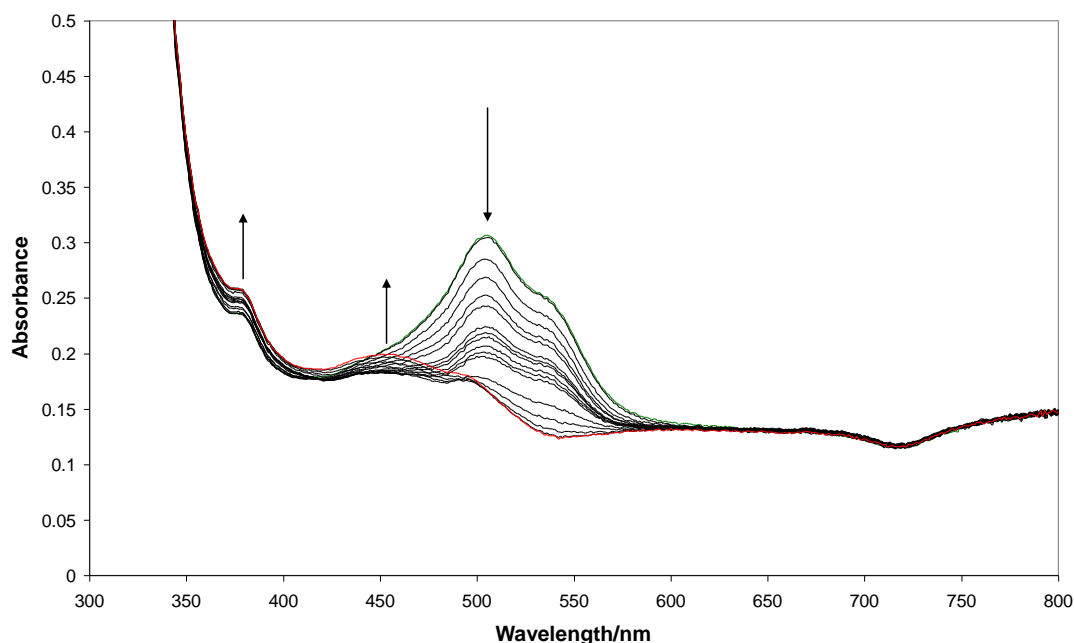


Figure 6.17.: The variation in the spectra of the acidic SO ink as it is reduced under anaerobic conditions on Activ™. The green trace indicates the initial ink spectrum obtained whilst the red trace shows that observed after 35 minutes. Spectra were recorded at 10 s, 1 minute, then at 1 minute intervals up to 10 minutes, and finally at 5 minute intervals up to 35 minutes

In addition to this, when the experiment is repeated under ambient atmospheric conditions, no significant reduction is observed (data not shown). It is believed that despite altering the pH, the highly negative redox potential of the dye (-0.289 V)³ is not altered sufficiently so as to facilitate reduction under such conditions, with re-oxidation by atmospheric O_2 being the dominant process. Coupled with the emergence of a secondary peak during reduction, when possible, which imparts a red colour to the ink, such an ink is clearly unsuitable for use in the field.

6.4. Oxazines

The final two dyes assessed for their suitability in the acidic indicator ink formulation, namely nile blue (NB) and brilliant cresyl blue (BCB), are derived from the oxazine family. Figure 6.18. gives the structures of NB and its subsequent reduction mechanism, whilst figure 6.19. shows the same for BCB. Table 6.5. details the key findings on their performance.

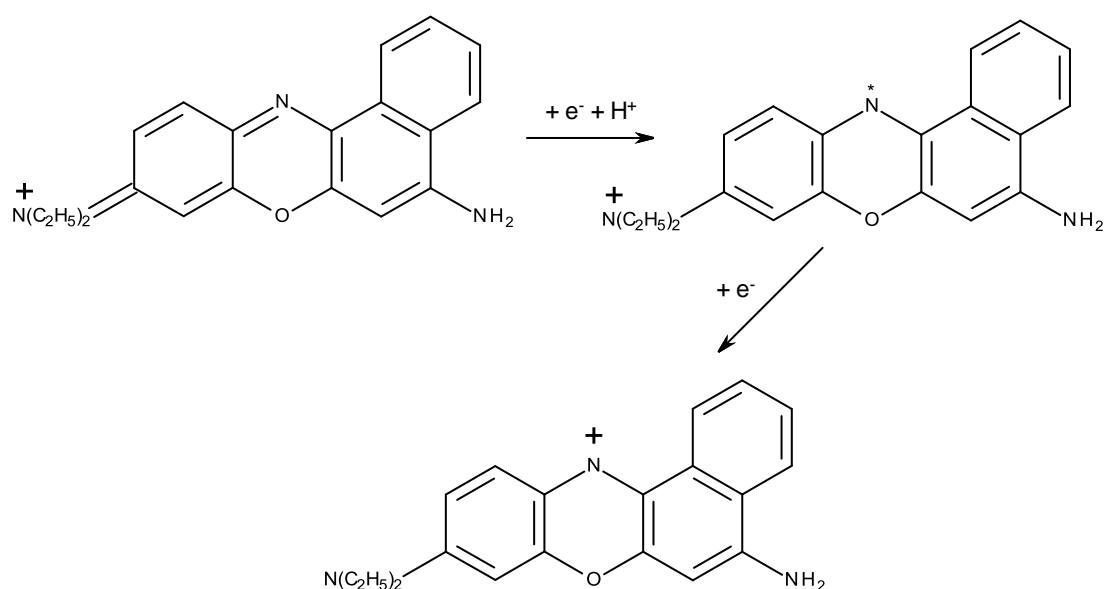


Figure 6.18.: The structure of NB and its subsequent reduction mechanism

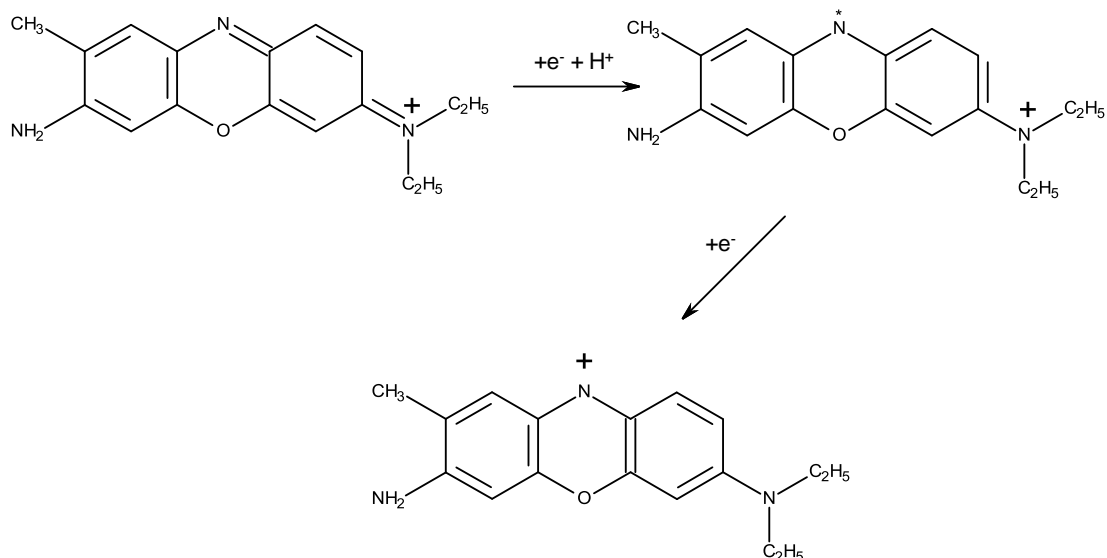


Figure 6.19.: The structure of BCB and its subsequent reduction mechanism

Dye	Non-acidic		Acidic			
	Anaerobic		Anaerobic		Ambient Atmospheric	
	t ₅₀ %/s	% recovery in air	t ₅₀ %/s	% recovery in air	t ₅₀ %/s	% recovery in air
NB	60	75 (5)	N/A	N/A	N/A	N/A
BCB	282	70 (30)	238	20 (30)	30	55 (60)

Table 6.5.: A comparison of the results obtained for the oxazine dyes. Note that the numbers in brackets represent the time (in minutes) taken for the quoted % recovery to be achieved

Once again, no reduction was observed for the non-acidic inks under ambient atmospheric conditions. Whilst it was possible to reduce the NB ink under anaerobic conditions, at a rate comparable to that of the MB ink under similar conditions, no data could be generated for an acidic version of the ink since the dye was found to be insoluble in the formulation. BCB, on the other hand, is observed to not only reduce in the standard formulation, but it is also capable of reducing when placed in the acidic formulation under both anaerobic and ambient atmospheric conditions. Figure 6.20.

shows the change in the spectra of the acidic ink observed as it is reduced under ambient atmospheric conditions.

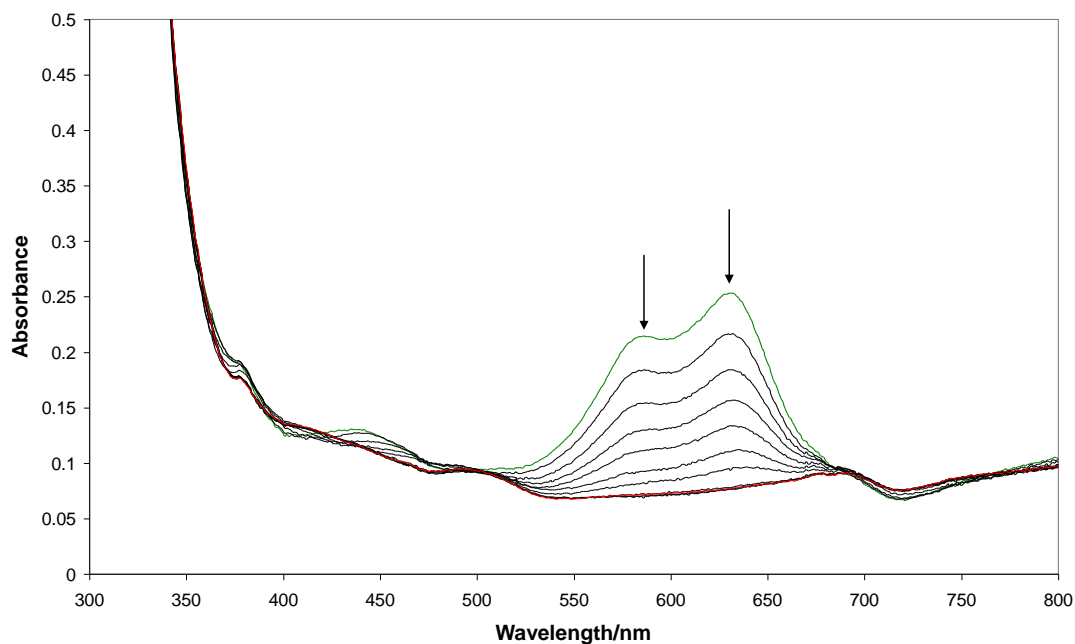


Figure 6.20.: The variation in the spectral shape of the acidic BCB ink as it is reduced under ambient atmospheric conditions on Activ™. The green trace indicates the initial ink spectrum whilst the red trace shows that following 3 minutes UVA irradiation. Spectra were recorded every 10 s for 1 minute, and then at 30 s intervals up to 3 minutes

As was observed for the thiazine dyes tested here, upon moving from anaerobic to ambient atmospheric conditions, the rate of reduction of the acidic BCB ink increases. Such an increase is of the factor of ca. 8 times, suggesting that it is not attributable solely to the increase in irradiance that comes with using ambient atmospheric conditions. Indeed, the rate of reduction of the acidic BCB ink under such conditions is comparable to that observed previously for MB and TB, and hence faster than what is observed for Th. It is postulated therefore that, as was the case with MB, the increase in the relative humidity upon moving to ambient atmospheric conditions is sufficient to increase the amount of H^+ ions available for the reduction reaction. In addition, BCB is noted to have a pK_a of 9.9¹², implying it is ca. 10 times more likely to dissociate than

the thiazine dyes, which would increase the reduction rate. However, whilst such a rate of reduction is impressive, the ink does recover a maximum of half of its original colour over the course of 1 hour, whereas none of the thiazines presented previously exceed a maximum of 25 % over a similar time period.

Of all the dyes tested here, based on the results presented in tables 6.2., 6.4. and 6.5., the thiazine dyes would appear to be the most suitable for use in the acidic indicator ink formulation for very different reasons. Indeed, the choice of which dye is best essentially comes down to one question – is the user looking for the most rapid indicator ink or that which generates the longest, reduced dye lifetime? If it is a question of rapidity, the acidic MB ink is the clear favourite, since it reduces ca. 4 times faster in comparison to that of Th. However, the reduced form of Th does last longer than that of MB (Th recovers only 9 % of its original blue colour whereas MB recovers 25 % of its original blue colour in 25 minutes). Hence if the user is looking for the ink which will remain colourless the longest then Th is the more attractive option.

Whilst NB, NR and SO are totally unsuitable for use in the acidic indicator ink under ambient atmospheric conditions, the acidic BCB ink can be considered as an intermediate option. Whilst it produces a suitable, acidic indicator ink which reduces to a colourless product under ambient atmospheric conditions, the % recovery over 1 hour is high (55 %) compared to what we observe for the thiazine dyes. In addition, it is not the fastest dye to reduce in the indicator ink formulation, although it is faster than others.

6.5. Conclusions

When MB is placed in an acidic indicator ink formulation, not only is reduction under ambient atmospheric conditions facilitated, but the recovery of the ink is less rapid than what we have observed previously for its non-acidic counterpart. It is believed that such observations are owed somewhat to an altering of the electrochemical potential of the MB/leuco-MB redox couple with pH. The behaviour of two other thiazine dyes, namely toluidine blue and thionine, mimic that of MB in such a formulation. However,

based on the redox potential of all three dyes, the trends observed in terms of the rate of reduction and the degree of recovery are the reverse of what would be anticipated. Such results do not appear to be a function of the dye pKa, but are postulated to be derived from Marcus Theory. The findings would appear to imply that the reorganisation energy between the oxidised and reduced forms of MB is lower than for its thiazine counterparts at potentials around $E(\text{redox})$, thus upsetting the anticipated trends for rate of oxidation/recovery.

Dyes from both the oxazine and phenazine families were also assessed for their suitability in this acidic formulation, with only that based on BCB giving a favourable performance compared to that of the thiazines. Both NB and NR were observed to be insoluble, apparently due to the pH of the ink, whilst SO produced an ink which, upon reduction under anaerobic conditions, did not fully photobleach. Instead, owing to the emergence of a peak at ca. 450 nm during reduction, the ink was observed merely to fade in colour on the photocatalyst surface as the reduction reaction proceeded. Worse still, when the acidic ink is irradiated under ambient atmospheric conditions, no significant reduction is observed.

Of all the dyes tested, all of the thiazines would appear suitable for use in an indicator ink formulation, with discretion required on the part of the analyst as to whether rapidity of reduction or longevity of the reduced state is the most important factor. Personally, despite its greater recovery compared to Th, MB appears to present the greatest formulation since its reduction kinetics are the most rapid. BCB, despite its rapid reduction kinetics, would appear unsuitable on the basis that it recovers over half of its original colour within an hour.

6.6. References

- (1) A. Mills; J. Wang *Journal of Photochemistry and Photobiology A: Chemistry* **1999**, *127*, 123.
- (2) A. Mills; J. Hepburn; M. McFarlane *ACS Applied Materials and Interfaces* **2009**, *1*, 1163.

-
- (3) M. S. Chan; J. R. Bolton *Solar Energy* **1980**, 24, 561.
 - (4) A. Cusick *The Kinetics of Dye Photocatalysis* Univeristy of Strathclyde, Glasgow 2009.
 - (5) O. Carp; C. L. Huisman; A. Reller *Progress in Solid State Chemistry* **2004**, 32, 33.
 - (6) O. Impert; A. Katafias; P. Kita; A. Mills; A. Pietkiewicz-Graczyk; G. Wrzeszcz *Dalton Transactions* **2003**, 348.
 - (7) G. I. Pennarun; C. Boxall; D. O'Hare *The Analyst* **1996**, 121, 1779.
 - (8) E. Bishop *Indicators*; Pergamon Press, 1972.
 - (9) W. M. Clark *Oxidation Reduction Potentials of Organic Systems*; Williams and Wilkens, 1960.
 - (10) http://en.wikipedia.org/wiki/Marcus_theory 23/12/2011
 - (11) A. J. Bard; L. R. Faulkner *Electrochemical Methods: Fundamentals and Applications*; Wiley, 2001.
 - (12) S. Woislowski *Journal of the American Chemical Society* **1953**, 75, 5201.

Summary

The aim of this work was to initially develop an indicator ink test suitable for use in the field, and to compare and contrast its performance with that of other indicator inks, including that based on resazurin, which is the forerunner in the literature. By comparing the indicator ink performance with that of standard tests involving the photooxidation of both methylene blue and stearic acid, it was hoped that the three tests could be correlated and thus allow us to promote them to other researchers as standardisation tools. In order to do this, it was necessary to prepare a set of films of varying photocatalytic activity in-house, and thus part of the work described here characterises these films, particularly with respect to the effect of temperature on composition. Finally the work on the indicator inks was revisited, with a view to developing a new generation based on an acidic formulation.

An ink based on the dye 2,6-dichloroindophenol was presented and characterised initially. Despite reducing at a rate slower than that of the resazurin-based ink, it still reduces rapidly on the surface of Activ™, and has the additional advantage of reducing to a colourless product. Unfortunately some recovery of the ink is observed under dark conditions, but of greater concern is the observation that the ink formulation is stable for a maximum of one month; the resazurin ink lasts three times longer.

The ink was then characterised as a function of many factors, including dye and SED level, irradiance, etc., with comparisons being drawn with the resazurin ink where appropriate. Despite the similarities in formulation, the ink presented here is observed to be more sensitive to the level of SED present and does not suffer from undesirable multimer formation as the dye level is increased, which for the resazurin ink has a negative impact on the rate of reduction. The kinetics of dye reduction are zero order in nature, which is in agreement with work conducted by others within this laboratory on this and other indicator inks, including that based on resazurin.

The standard 2,6-dichloroindophenol ink formulation was then compared to other inks based on resazurin, methylene blue and resorufin under similar conditions, with a view

to ultimately determining the most suitable for use in the field, and hence to be used in standardisation testing here. Whilst the methylene blue and resazurin inks are the fastest to reduce under anaerobic conditions, the former cannot be used under ambient atmospheric conditions owing to the high sensitivity of its reduced product, leuco-methylene blue, to oxygen. The resorufin ink is also unsuitable in comparison since its rate of colour change is observed to be the slowest for all inks examined here.

Although the resazurin ink is observed to reduce faster than the 2,6-dichloroindophenol ink in both the presence and absence of oxygen, of greater interest is the observation that the resazurin ink is affected by the level of oxygen present in the atmosphere. Owing to the dye's electrochemical irreversibility, such an observation is highly unexpected and attributed to the reaction or increased lifetime of an intermediate (e.g. a radical) on the reduction pathway with oxygen. The ink based on 2,6-dichloroindophenol, despite being a redox dye, is observed to be unaffected by the level of O₂ present. Incorporation into a felt-tipped pen is thus possible, with the increased dye level required to generate a striking blue colour on self-cleaning surfaces only partially compromised by the zero order nature of the ink.

A series of films were then prepared of varying photocatalytic activity with a view to using them to correlate three standard tests of activity, namely the indicator inks, stearic acid and methylene blue. The films were initially characterised using a variety of techniques, including atomic force microscopy and x-ray diffraction. As the annealing temperature of such films was increased, the phase of such films changed from photoactive anatase to inactive rutile, accompanied by an increase in particle size and a decrease in the specific surface area. Of greatest interest are the films annealed over the range ca. 760-950 °C, since it is in this region where the films are a mix of anatase and rutile, and thus we observe changes in photocatalytic activity.

All three tests exhibit a similar trend over the annealing temperature range; namely that as the rutile content increases, the photocatalytic activity decreases. For the indicator ink test, however, the decrease in the photocatalytic activity also appears to be affected by the decrease in the specific surface area. Attempts to correlate all three tests have

shown to be of limited success, which is thought to be due to the changes in the surface morphology that accompany the change in photocatalytic activity. What is needed is a method of preparing a set of films whereby the rutile:anatase ratio changes, yet the surface morphology is unaffected.

Finally, as an aside, the methylene blue ink observed to be unsuitable earlier was revisited following recent research which suggested that acidification of the formulation promoted longevity of the reduced dye product, leuco-methylene blue. Such results were confirmed here, and are attributed to an alteration of the dye's electrochemical potential with acidification. Similar results were observed for other thiazine dyes, although the trends in the rate of reduction and re-oxidation could not be explained using the electrochemical potential or pKa alone.

Other dyes from the phenazine and oxazine families were assessed in a similar capacity, but none with the exception of brilliant cresyl blue matched the performance of the thiazines. Indeed the choice of which dye is the most suitable for use comes down to a simple question: is the operator looking for the fastest reducing dye in the formulation, or the one which generates the most stable leuco- product? Personally, the methylene blue ink is the most preferable owing to its rapid reduction kinetics and reasonable reduced product longevity.

Further Work

Although this thesis has successfully answered many questions with regards to the development of the indicator inks, there are questions that still remain. More importantly, the work has also generated new questions which require to be probed before the 2,6-dichloroindophenol and, to a lesser extent, the acidic methylene blue inks can feasibly be rolled out for use in the field. Within each chapter, there would certainly appear to be at least one major question which requires to be addressed before a complete understanding is achieved.

Of greatest interest in the characterisation of the indicator ink based on 2,6-dichloroindophenol is the observed shelf-life of the formulation. Evidently such a product is not entirely viable if every month a new set of pens has to be created for operators to use. Indeed, the dye is observed to be unstable after a short period of time even when simply dissolved in water. The root cause of this instability is unknown and merits further exploration. If the issue could be isolated, it may be possible to screen a range of products which could be added to the formulation to preserve the dye's lifetime, e.g. if the dye is susceptible to hydrolysis at the position of the chloride groups as suggested here, then theoretically addition of an agent to reduce the amount of free hydroxide present could increase the ink lifetime.

The effect of SED level and type on the rate of reduction of the ink is also interesting, in particular when compared to the resazurin ink. Why is it that for the ink described here, the level of SED can be reduced ca. 10 times with no adverse effect on reduction rate, whilst the same cannot be said for the resazurin ink? Is it simply owing to the ease of reduction of 2,6-dichloroindophenol? In addition, the type of SED is clearly very important, with longer chain and cyclic polyols observed to generate a slower reduction rate or be totally unsuitable for use. However, surely such molecules would generate radicals with a higher degree of stability? Thus what influences whether a molecule can form a stable radical, and why does increasing chain length appear to inhibit their formation?

The observation that the resazurin and 2,6-dichloroindophenol inks are the most suitable for use in the field in chapter 4 is not entirely unexpected, since leuco-methylene blue is known to be oxygen sensitive and resorufin has a more negative electrochemical potential in comparison. However, the observation of the oxygen sensitivity of the resazurin ink was a major surprise. Since reduction of the dye is electrochemically irreversible, no formal redox potential exists for the dye, and hence the observed oxygen sensitivity cannot be formally attributed to re-oxidation of resorufin. It is postulated here that a short-lived radical with high oxygen sensitivity is responsible, but this would certainly be an area worth investigating further, possibly through a flash photolysis study. In addition, the effect of humidity on the reduction rate may also be attributed to the same species, so a thorough investigation into the effect of atmospheric conditions on the dye's reduction may prove useful in understanding this phenomenon.

Throughout the work on the standardisation testing, it would appear that one of the major factors in determining the activity of the photocatalyst films is the surface morphology. In our attempts to produce a series of films of varying photocatalytic activity, the effect of increasing annealing temperature on the surface characteristics was overlooked. What is needed is a method of producing films with no significant difference in, or which have a very narrow range of particle sizes/specific surface areas, but with varying activity. Only then can a true correlation study be conducted. Better still, if the phase of the films were constant then the synergistic effect of anatase/rutile blends could also be neglected.

It may also prove interesting to take the sol-gel paste films produced here and attempt to generate a range of self-cleaning tiles. It would appear that the commercial Hydrotect tiles are of a fairly low activity, and it has been demonstrated that white, opaque films can be produced of a higher photocatalytic activity in comparison. The main focus of such research would undoubtedly be the sourcing of a suitable substrate to support the film, since many tiles will be highly porous, but beyond that it would appear a viable route to a novel, more active generation of tiles.

The acidic methylene blue ink, although not yet characterised to the same extent as that of the resazurin or 2,6-dichloroindophenol inks, seems to combine their positive features (namely a long shelf-life and a colourless leuco-product, respectively) and thus represents a new way forward in this field. However, within the context of the study presented here, the preliminary work appears to have yielded more questions than answers. In particular, the effect of acidification on the reduction and re-oxidation rates is interesting, particularly when the results for the inks based on thionine and toluidine blue are also considered. Based on the redox potentials and pKa for the dyes, such trends cannot be explained. So what is controlling the trends observed? Is it an effect of Marcus Theory, as postulated? And does the extent of acidification of the ink formulation influence the trends at all? It may well be that simply changing the concentration of acid in the formulation may allow us to probe further the reduction kinetics observed and possibly extend the lifetime of the reduced species generated by the photocatalytic reaction.